Enzyme catalyzed perhydrolysis, molecular basis and application

A DISSERTATION
SUBMITTED TO THE FACULTY OF THE GRADUATE SCHOOL
OF THE UNIVERSITY OF MINNESOTA
BY

Delu (Tyler) Yin

IN PARTIAL FULFILLMENT OF THE REQUIREMENTS
FOR THE DEGREE OF
DOCTOR OF PHILOSOPHY

Adviser: Romas J. Kazlauskas

October 2011

Acknowledgements

I owe a great deal of gratitude to a number of people who have supported me while in graduate school. First and foremost, I'd like to thank my advisor Dr. Romas Kazlauskas for his mentoring and guidance throughout my research and writing endeavors. In particular, Romas encouraged me to test my ideas but also challenged me to tackle my experiments and results logically. I also thank Dr. Robert DiCosimo and Dr. Mark Payne for accepting me to their lab at Dupont de Nemours and company for a summer internship. The summer internship was insightful on how scientists bring a product from development to commercialization. While working at Dupont, I had the pleasure of meeting Kelly Petrillo, Eugene Hann and other personnel who graciously devoted some of their time to helping me get established at the company. I thank all of the wonderful collaborators who made this work possible; their contributions are mentioned in page ii.

I am indebted to Edward Hoeffner at the Khalert Structural Biology Lab for his advice on how to grow protein crystals. I thank Dr. LeeAnn Higgins and Dr. Bruce Witthuhn at the University of Minnesota Mass Spectrometry Consortium for their assistance with mass spectrometry. I also thank Dr. Yuk Sham and Nicholas Labello at the Minnesota Supercomputing Institute for their advice and assistance at molecular modeling.

I thank all of the Kazlauskas lab members past and present for their scientific and nonscientific discussions and for sharing a few laughs; in particular Dr. Peter Bernhardt for starting the perhydrolase project by engineering the L29P PFE mutant. Last but not least, I thank my family for their support and understanding, especially my brother George for the yearly birthday greetings.

Abstract

Enzyme catalyzed perhydrolysis converts a carboxylic acid or ester to a peracid. In the former reaction, the amount of peracid generated is thermodynamically controlled (K_{eq} = 3) – while in the latter, the reaction is kinetically controlled, thus a higher concentration of peracid can be generated. Enzymes that catalyze perhydrolysis of carboxylic acids share high sequence similarity and are thought to use an esterase-like mechanism. Alternatively, carboxylic acids can also use a non-covalent mechanism, such as those used by hydroxynitrile lyases.

To test whether carboxylic acid perhydrolases use an esterase-like mechanism, we identify a key covalent intermediate by mass spectrometry that can be attributed to an esterase-like mechanism but not a non-covalent mechanism. We also find that carboxylic acid perhydrolases are good catalysts for hydrolysis of peracetic acid, suggesting that their natural role is to degrade peracids generated as by-products in a living organism. Next, we determine how perhydrolases increase the rate of perhydrolysis.

Carboxylic acid perhydrolases increase the rate of perhydrolysis by either increasing the selectivity for hydrogen peroxide or lower the activation barrier towards acyl-enzyme formation. We measure the selectivity of hydrogen peroxide using wild-type *Pseudomonas fluorescens* esterase (PFE) and L29P PFE (a model carboxylic acid perhydrolase). The L29P PFE variant is less selective for hydrogen peroxide than the wild-type despite having higher perhydrolysis activity. We measure the rate of acyl-enzyme formation using isotope exchange of acetic acid in $H_2{}^{18}O/H_2{}^{16}O$. The L29P PFE variant catalyzes the isotope exchange rate faster than the wild-type. Thus, carboxylic acid perhydrolases favor the formation of acyl-enzyme from carboxylic acids.

We find that carboxylic acid perhydrolase (L29P PFE) does not catalyze ester perhydrolysis for accumulating high concentrations of peracetic acid. Instead, wild-type PFE and a new variant, F162L PFE accumulate up to 130 mM of peracetic acid. We measure kinetic parameters and show that hydrolysis of peracetic acid limits maximum accumulation. The F162L PFE variant minimizes hydrolysis of peracetic acid by lower-

ing the K_m and increasing the k_{cat} for ethyl acetate hydrolysis. The kinetic parameters are also used to predict the maximum amount of peracetic acid that can be accumulated.

The F162L PFE variant is used to improve the efficiency of lignocellulose pretreatment from a previously published result using wild-type PFE. Enzymatically generated peracetic acid reacts converts lignin into smaller and more soluble lignin pieces. The chemoenzymatic process is further improved by forming peracetic acid in a biphasic layer which allows the reuse of enzyme. The pretreatment reaction conditions were also optimized by increasing the temperature to 60 ˚C and reducing the reaction time to 6 hours.

Table of Contents

List of Tables

List of Figures

Contribution of authors

This thesis contains one introduction, three publications (chapter 2, 5, and 6) and two drafts (chapter 3 and 4) that will be submitted for publication. The work described in these chapters were done as part of my research for the degree of Doctor of Philosophy.

Professor Romas Kazlauskas was my supervisor throughout my doctoral degree, and therefore is a coauthor in each manuscript. Dr. Kazlauskas reviewed, and edited each of the chapters.

Chapter 2: Dr. Bernhardt constructed the L29P PFE mutant and measured the initial perhydrolysis activity. Dr. Morley and Dr. Cheeseman purified and crystalized the apo-L29P enzyme. Dr. Schrag and Dr. Purpero refined the diffraction data of the apo-L29P and L29P/acetate respectively. I measured the steady-state kinetics for perhydrolysis and hydrolysis, measured the pH-rate profile, performed the mass spectrometry, grew the crystals of L29P/acetate and wrote the manuscript.

Chapter 3. Dr. Jing measured the L29X peracetic acid/acetate concentration mentioned in the supplemental information. Dr. Fujii constructed the L29X mutants. Dr. Purpero refined the diffraction data for the apo-L29I and L29I/acetate. I measured the steady-state kinetics for perhydrolysis/hydrolysis, screened the L29X variants, measured the selectivity parameters, grew the crystals for apo-L29I and L29I/acetate, and wrote the manuscript.

Chapter 4. Dr. Dicosimo made significant intellectual contributions on how to measure the absolute amount of peracetic acid. I performed all experiments and wrote the manuscript.

Chapter 5. Dr. Jing pretreated several lignocellulose samples with enzyme generated peracetic acid, and optimized the reaction time and temperature. Dr. Duncan and Dr. AlDajani measured the amount of sugar released from pretreated lignocellulose and edited the manuscript. Dr. Tschirner and Dr. Schilling made intellectual contributions as well as revised and edited the manuscript. I optimized the enzymatic conditions and de-

veloped the biphasic experiments to generate peracetic acid, pretreated lignocellulose on a large scale using the biphasic method, and wrote the corresponding results and methods.

Chapter 6. Dr. Colton is the primary author who synthesized the inhibitors, grew the crystals of CRL and wrote the corresponding results and methods section. Dr. Grochulski refined the diffraction data for the CRL-inhibitor. I modeled the (R)-CRL intermediate performed the molecular dynamics simulations and wrote the corresponding results and methods.

Chapter 1
Introduction
1.1 Biocatalysis from past to present.

Biocatalysis is the use of enzymes or whole-cell catalysts to transform organic compounds. The application of biocatalysis dates back to antiquity, where it was applied fermenting foods and beverages such as the transformation of carbohydrates to ethanol. It was not until 1857 that yeast (*Saccharomyces cerevisiae*) was discovered to be the principal catalyst by Louis Pasteur. It took another 42 years before it was deduced that enzymes (zymases) were the machinery that's responsible for ethanol fermentation. Today, scientists use biocatalysis to benefit humanity, but with a better understanding of how enzymes and whole-cell catalysts work.

Industrial chemists have traditionally used harsh reagents such as concentrated acids and or organic solvents to make useful products. Often, undesired by-products are generated which increases the overall cost and causes environmental concerns. The use of enzymes has the advantage that they can enhance the rate of chemical reactions up to 10^{17} over the uncatalyzed rate[1] and under mild conditions. Additionally, enzymes have undergone evolutionary pressure to be chemoselective, regioselective, and or enantioselective. A broadly used example is the application of cellulases, an enzyme that hydrolyzes sugar polymers, to the detergent, food and textile industry[2]. Cellulases are added to detergents for brightening the color of clothes and to create a stone-wash appearance in denim jeans. More recently, a major effort has gone into modifying cellulases for biofuels production. The degradation of cellulose represents a key step in making biofuels[3].

The chemical industry is interested in usies enzymes for substituting chemical steps to save costs and or to reduce waste. For example, Panova and coworkers used a nitrilase to generate ammonium glycolate, which was then converted to glycolic acid using ion exchange chromatography, Figure 1.1a. This process bypassed the traditional synthesis route of using high-pressure and temperature[4]. Another example is cyanation of ethyl (*S*)-3-hydroxybutyrate to (*R*)-4-cyano-3-hydroxybutyrate where the chemical proc-

ess can result in mixed enantiomers because the process is non-selective[5]. Not surprising, chemists use enzymes to catalyze reactions under mild conditions and generate fewer by-products. In the previous example, a halohydrin dehalogenase catalyzed the cyanation reaction to prevent the formation of the (*S*)-enantiomer [6], Figure 1.1b. Enzymes have become important for pharmaceutical companies to either increase the enantiomeric purity of the product (less waste) or bypass chemical steps. For example, Savile and coworkers modified a transaminase to synthesize sitagliptin which increased enantioselectivity from 97% e.e. to 99.95% e.e. and bypassed several steps involving high pressure[7], Figure 1.1c. One caveat to these examples is that the enzymes used here were designed and engineered to improve the activity and or enantioselectivity.

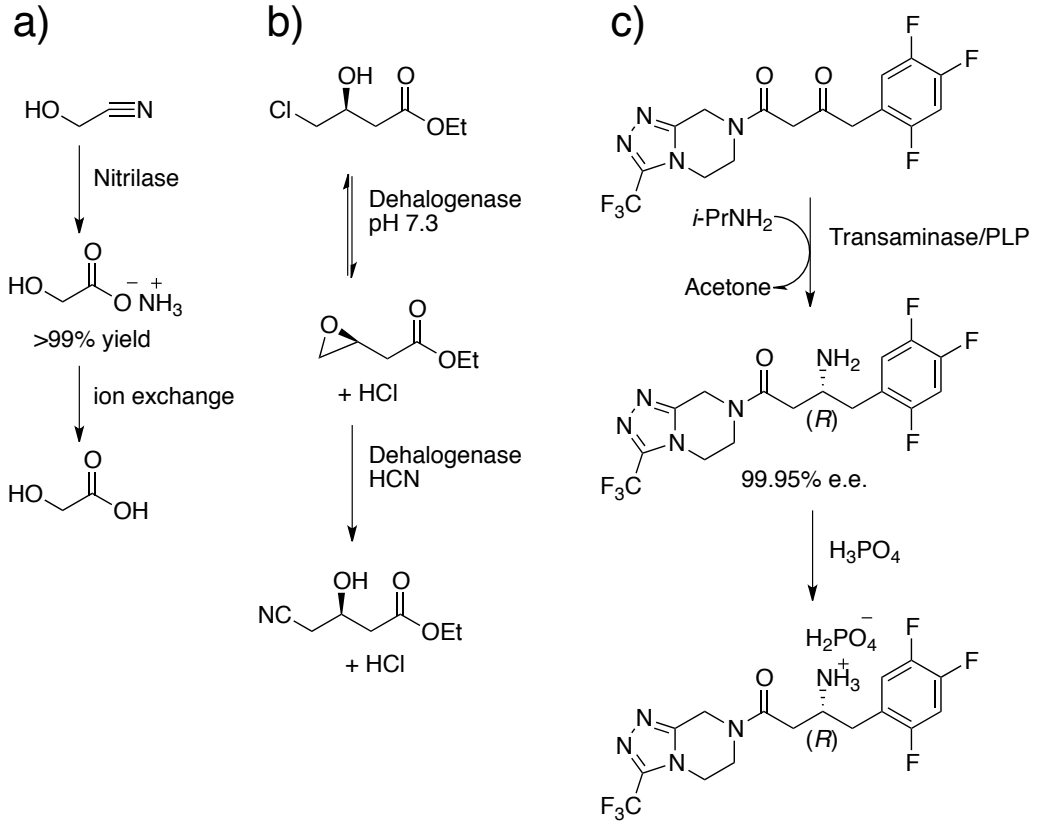

Figure 1.1. Examples of enzymes used in chemoenzymatic processes. a) The use of nitrilase to generate ammonia glycolate, adopted from Panova *et* al.[4] b) Halohydrin dehalogenase used to catalyze the formation of (*R*)-4-cyano-3-hydroxybutyrate, adopted from Huisman *et* al.[6] c) Transaminase (PLP as a cofactor) used to catalyze the formation of sitagliptin, adopted from Savile *et* al.[7].

1.2 Chemical and industrial applications of peracetic acid

Peracids are useful reagents for chemists and industrial applications. Peracids, or peroxycarboxylic acids are used to add oxygen to olefins, ketones, aldehydes, organic sulfur, phosphorus and organic-metals; chemists commonly use *meta*-chloroperbenzoic acid to form lactones from cyclic ketones and to form epoxides from alkenes.

In industrial peracetic acid (PAA) is used to in a wide range of applications from disinfection to wastewater decontamination. PAA is more efficacious as a broad spectrum antimicrobial agent[8] than hydrogen peroxide. Catalase synthesized by microbes break-down hydrogen peroxide to oxygen but is not known to decompose peracetic acid. Thus, the amount of peracetic acid required to destroy microbes is less than hydrogen peroxide. The breakdown product of PAA is acetic acid and hydrogen peroxide, which further decomposes to oxygen – O_2 and acetic acid are harmless at very dilute amounts. PAA is also highly applicable to environmental waste water treatment[9] and decontamination after animal processing[10]. PAA can also be used to remove lignin from lignocellulose. PAA decomposes lignin to lower molecular weights fragments that are water soluble. The cellulose and hemi-cellulose remain water insoluble and can be used for downstream fermentation processes.

1.2.1 Chemical synthesis of peracetic acid

There are four ways to chemically synthesize peracetic acid. In the first method hydrogen peroxide is used with acetic acid to form peracetic acid, Figure 2a. The reaction is thermodynamically controlled, where the equilibrium is only slightly favorable for the formation of peracetic acid (Keq ~ 3)[11]. The rate of peracetic acid formation can be increased by using sulfuric acid as a catalyst[12]. The amount of peracetic acid can also be increased by distillation. To generate higher amounts without distillation, chemists use esters (Figure 1.2b), acetyl chloride (Figure 1.2c), or acetic anhydride (not shown) where the reaction is kinetically controlled. These methods share a common mechanism, where the acid, ester or acetyl chloride undergoes nucleophilic attack by hydrogen peroxide.

The fourth method of chemically generating peracetic acid is the oxidation of acetaldehyde at low temperatures[13], Figure 1.2d. The reaction is attractive because it uses oxygen in place of hydrogen peroxide and the absence of water, but is outweighed by requirement that the reaction needs to be performed at 0 ˚C and the possible formation of peracetic acid crystals which are unstable at higher temperatures.

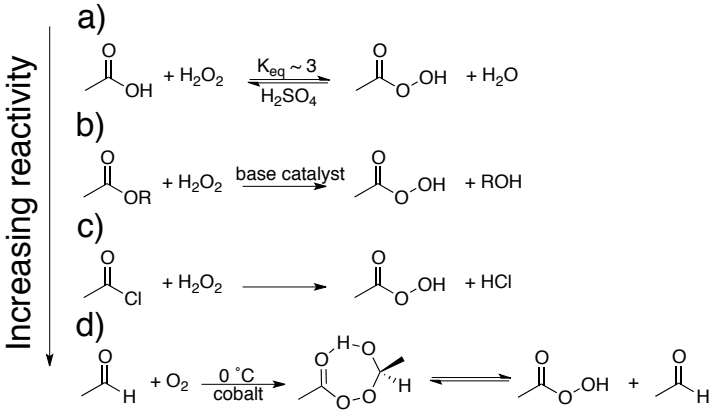

Figure 1.2. Chemical methods to synthesize peracetic acid. a) Formation of peracetic acid from acetic acid is thermodynamically controlled and is the slowest. b) Perhydrolysis of an ester is kinetically controlled and can be made faster by addition of a base such as sodium hydroxide. c) Generation of peracetic acid from acetyl chloride is even faster and does not require addition of base or a catalyst. d) Oxidation of acetaldehyde can generate peracetic acid but the temperature must be below 0 ˚C to prevent an explosion.

Despite the advantages of using peracids for industrial applications and as a useful reagent for chemists, the cost limits its use. Compared to hypochlorite, PAA is 4 times more expensive. One reason for the increased cost is that PAA is explosive in high (>70%) concentrations, therefore the reagent must first be diluted before transport. In-situ generation of dilute peracetic acid would bypass transportation hazards and associated costs. Some of the chemical methods above can be adapted to generate peracetic acid in-situ but at the cost of creating other hazards such as high acid content. Alternatively, hydrolases can be adapted to catalyze perhydrolysis of acetic acid or acetate ester in-situ which would be more environmentally friendly than the use of harsh chemicals.

1.3 α/β hydrolases, their structure and mechanism

Hydrolases are enzymes that cleave chemical bonds by the addition of water. Hydrolases are classified E.C 3 according to the enzyme classification system. There are over 1,500 enzymes that belong to E.C 3, according to BRENDA, an online database[14]. Examples of hydrolases are eseterases and lipases which cleave ester bonds, peptidases which cleave amide bonds, and glycosidases which cleave glycosidic bonds.

1.3.1 General description of esterases and lipases

Esterases and lipases are classified as carboxylic ester hydrolases (E.C 3.1.1). Esterases and lipases belong to a family of enzymes that are structurally classified as α/β hydrolases. The key structural criteria of an α/β hydrolase fold is the presence of eight beta strands and five alpha helixes[15], Figure 1.3a. The beta strands are parallel except for b2, which is anti-parallel to the others. The alpha helixes are connected between each beta strand except for beta strands 1 and 2. Another similarity shared among α/β hydrolases is the presence of a catalytic triad (Ser [or Asp or Cys]-His-Asp), Figure 1.3b. In some hydrolases, the serine is substituted for a cysteine or aspartate, while in others a glutamate is found in place of an aspartate. Naturally occurring substitutions change the substrate selectivity and in some cases the mechanism.

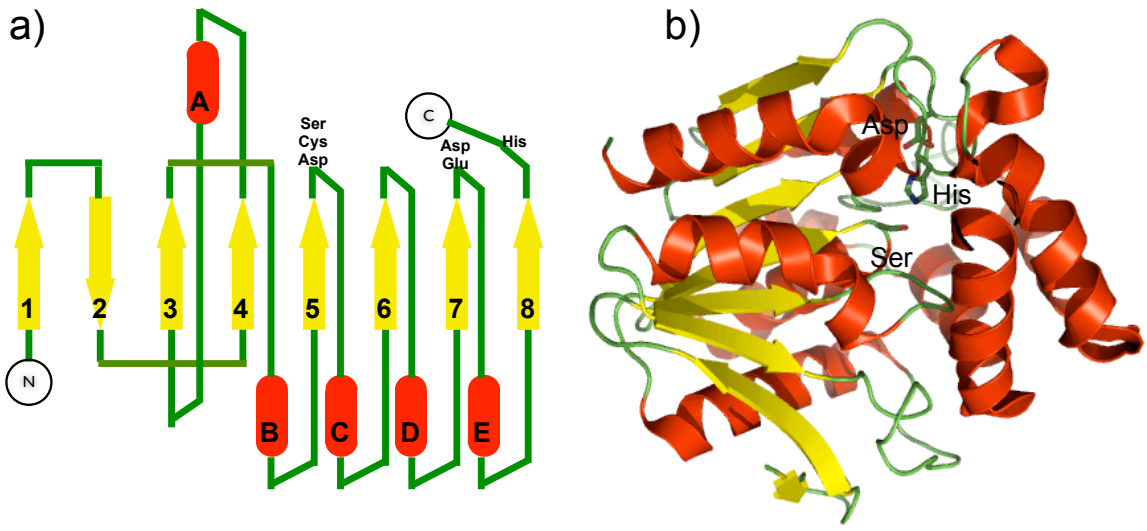

Figure 1.3. Topology and three dimension structure of an α/β hydrolase. a) A canonical α/β hydrolase topology map, adapted from Carr *et* al.[15]. b) A crystal structure of *Pseudomonas fluorescens* esterase that exhibits a typical α/β hydrolase (Protein data bank accession: 1VA4).

1.3.2 Mechanism of selected α/β hydrolases

Esterases are α/β hydrolases which cleave ester bonds by the addition of water. The free enzymes bind and react with an ester to form the first tetrahedral intermediate (Td1)[16], Figure 1.4a. Collapse of Td1 followed by the liberation of alcohol forms the acyl-enzyme intermediate. The acyl-enzyme intermediate binds and reacts with water to form the second tetrahedral intermediate (Td2). Collapse of the Td2 intermediate liberates a carboxylic acid and the free enzyme. Although epoxide hydrolases contain an α/β hydrolase fold, these enzymes contain an aspartate instead of a serine. This allows the catalyst to react with epoxides to form diols. Another example are dienolactone hydrolases, that cleave C-C bonds. These enzymes also have an α/β hydrolase fold, but contain a cysteine in place of the catalytic serine. The catalytic cysteine reacts with dienelactone to form a covalent intermediate. An arginine residues forms hydrogen bonds with the carboxylate group of dienelactone to position the substrate in a productive orientation[17]. Unlike the previous two examples, hydroxy nitrile lyases are α/β hydrolase fold enzymes that do not use the catalytic nucleophile to form covalent intermediates[18]. Instead, the free enzyme binds the cyanohydrin and uses the catalytic serine, threonine and lysine to position the substrate in a catalytically productive orientation, Figure 1.4b. The role of the catalytic histidine act as a acid/base catalyst. Throughout the reaction mechanism, no covalent intermediate is formed.

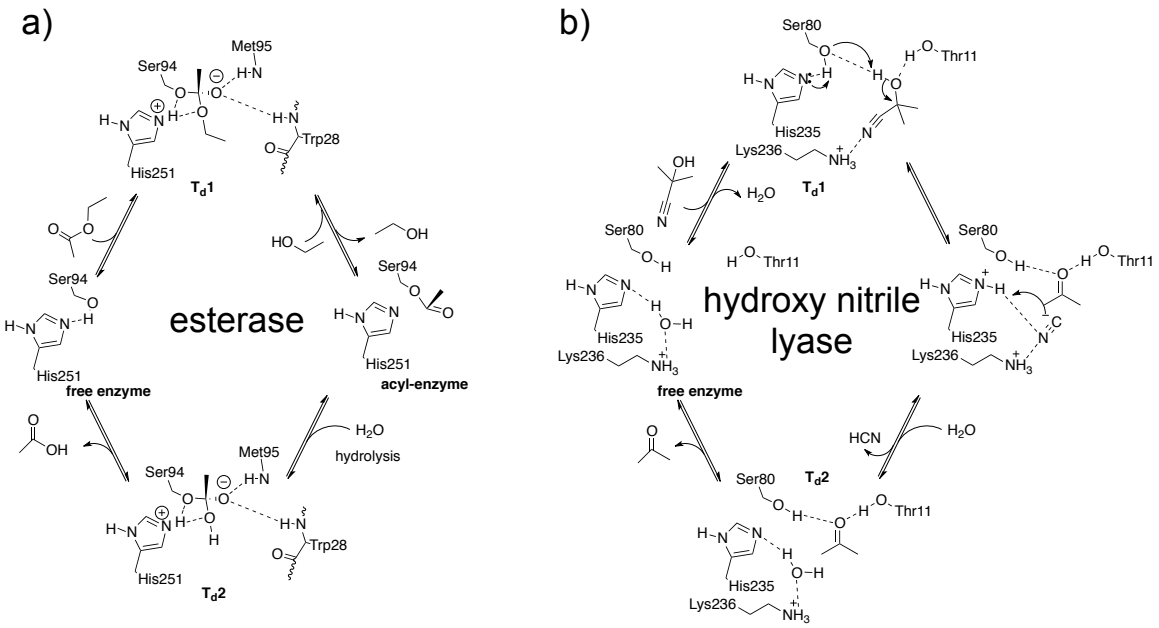

Figure 1.4. Mechanism examples of an esterase and hydroxynitrile lyase. a) Esterases use a ping pong bibi mechanism, which is typified by *Pseudomonas fluorescens* esterase[16]. b) Hydroxy nitrile lyases use the ordered uni bi mechanism, which is typified by HNL from *Hevea brasiliensis*[18].

These examples show that the α/β hydrolase fold is amiable to modifications for creating new activity using an existing scaffold. Not surprisingly, hydrolases have been already used extensively in chemoenzymatic or enzymatic industrial processes, such as the kinetic resolution of chiral esters[19]. In particular, lipases have been used in the food industry[20] to catalyze acyl-transfer, the transfer of the acyl-enzyme to an alcohol instead of water. Lipases are used to change the molecular weight of triglycerides by exchanging with other alcohols. Researchers interested in generating peracetic acid using enzymes have looked towards lipases and esterase to catalyze perhydrolysis. The mechanism for perhydrolysis is expected to be similar to ester hydrolysis because the similarity of water and hydrogen peroxide.

1.4 Naturally occurring perhydrolases

Naturally occurring perhydrolases catalyze the perhydrolysis of acetic acid. Perhydrolase activity is likely a side-reaction, since the formation of peracetic acid is destructive in living cells.

Bromoperoxidase from *Streptomyces aureofaciens* Tü 24 was the first perhydrolase to be purified and characterized[21]. These researchers were not interested in perhydrolysis, rather halogenation of organic compounds. Thus, the assay they used at the time was the bromination of monochlorodimedone, Figure 1.5a. At the time, it was known that peroxidases predominately used metal-heme to halogenate compounds, but the bromoperoxidase from *Streptomyces aureofaciens* lacked a characteristic *Soret* peak[21]. Since they lacked a heme catalytic center, and the three-dimensional structure was unknown, Haag and coworkers proposed that a methionine could be involved in the oxidation of monochlorodimedone to bromochlorodimedone[22]. In 1994, the x-ray crystal structure of bromoperoxidase A2 (2.05 Å resolution) from *Streptomyces aureofaciens* (ATCC 10762) was elucidate[23]. The topology belonged to the α/β hydrolase superfamily and that it contained a canonical Ser-His-Asp catalytic triad. The observation of a catalytic triad was strong evidence against a catalytic role for methionine . Subsequently, Picard and coworkers proposed an esterase-like mechanism for perhydrolases which involves a nucleophilic serine[24]. Evidence favoring a serine nucleophile came from the absence of activity without acetate (Figure 1.5b) and the racemic mixture of bromohydrin products which suggests a chemoenzymatic process.

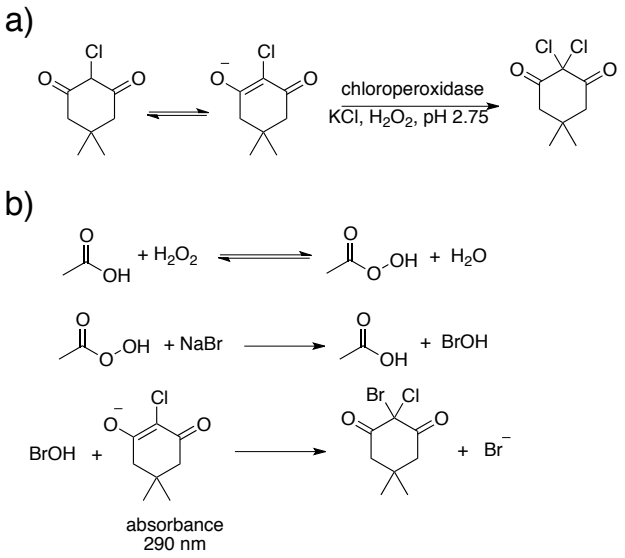

Figure 1.5. Variations of the monochlordimedone assay. a) The monochlorodimedone assay as described by Morris and Hager[25] intended for heme containing peroxidases. The absorbance at 278 nm is likely caused by the enolate tautomer. The colorimetric assay is based on the loss of absorbance at 278 nm. b) The monochlorodimedone assay adapted for perhydrolases. The presence of acetic acid at pH 5.0 - 5.5 is essential for activity.

Further evidence of an esterase-like mechanism came from the crystal structure of additional non-heme chloroperoxidases, some complexed with benzoate or propionate[26]. Picard and coworkers also suggested that perhydrolases were more selective for hydrogen peroxide than other hydrolases by comparing trypsin, elastase, alkaline protease and acetylcholine esterase. Thus, perhydrolases should be classified separately from esterases because they're selective for the formation of peracetic acid. Acetylcholine esterase showed perhydrolase activity equivalent to chloroperoxidase-T, but it was irreversibly inactivated by hydrogen peroxide[24].

The hypothesis that chloroperoxidases were unique in having perhydrolase activity was challenged by Kirk and Conrad[27]. Using several lipases including Cal-B, the authors showed significant formation of peroxyhexanoic acid (147 μM for Cal-B). Kirk and Conrad concluded that perhydrolysis is a common side-activity for hydrolases. The ability of some lipases to form peracids showed that perhydrolysis is not unique to chlor-

peroxidases, but it did not reveal why some hydrolases catalyzed perhydrolysis faster than others.

1.5 *Pseudomonas fluorescens* esterase (PFE)

1.5.1 Activity of PFE

In 1990, an aryl-esterase from *Pseudomonas fluorescens* (PFE) was cloned and purified[28]. The enzyme prefers to hydrolyze *para*-nitrophenyl acetate over straight chain esters. Krebsfanger and coworkers[29] showed that PFE is highly enantioselective toward α-phenyl ethanol (enantioselectivity >100) and is stable at temperatures up to 60 ˚C. Liu and coworkers tested additional esters with different acyl chain lengths and with better leaving groups[30]. The ester acyl chain length for PFE was optimal up to four carbons, but attaching vinyl or propenyl to the alcohol group gave 10 to 100 fold higher activity over unactivated straight chain esters[30], Figure 1.6.

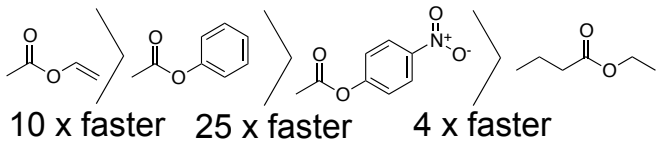

Figure 1.6. Substrate preference for PFE hydrolysis. PFE hydrolyzes vinyl acetate 10 times faster than phenyl acetate; phenyl acetate is 25-times faster than p-nitrophenyl acetate; p-nitrophenyl acetate is 4 times faster ethyl butyrate. Data from Liu *et* al.[30] and from Choi *et* al.[28].

1.5.2 Structure of PFE

Hofmann and coworkers[26] first noted the sequence similarity between PFE and other chloroperoxidases. Cheeseman and coworkers solved the structure of PFE by x-ray crystallography (1.8 Å resolution) which showed a canonical α/β hydrolase fold[16] with a Ser-His-Asp catalytic triad. The authors also observed a modest perhydrolase activity towards acetate despite having a high structural similarity to the closest perhydrolase (chloroperoxidase-T[26]) (r.m.s.d of 0.8 Å)[16]. The absence of some conserved perhydrolase residues in PFE made this enzyme a good candidate to study the molecular basis of naturally occurring perhydrolases.

1.5.3 Engineering PFE into a perhydrolase

Bernhardt and coworkers constructed a Venn diagram of the sequence alignment between PFE with closely related esterases and perhydrolases[31]. The authors identified 14 conserved residues within the amino acid sequences shared among perhydrolases but not with esters or PFE. The authors substituted PFE amino acid sequence with conserved residues of perhydrolases step-wise[31]. The variant L29P drastically improved perhydrolase activity while decreasing hydrolysis. Molecular modeling suggested that the Pro mutation caused a switch in the backbone configuration from trans to cis. In turn, this caused the main-chain carbonyl in the oxyanion loop to move closer to the active-site serine. The authors hypothesize that perhydrolases use the main-chain carbonyl to form an extra hydrogen bond that is not possible for esterases. Chapters 2 and 3 of this thesis test this hypothesis.

1.6 Protein engineering of enzymes

Protein engineering is the design and construction of new proteins by modifying the amino acid sequence. Protein engineers use a variety of strategies and techniques to identify and alter the amino acid sequence. These modifications can result in changes to the activity, stability, and selectivity of an enzyme. In addition, researchers must avoid making deleterious effects to properties where the enzyme is already efficient while trying to improve another. For example, engineering an enzyme to improve its catalytic efficiency (k_{cat}/K_m) should not come at the cost of lowering its thermal stable and activity, Figure 1.7.

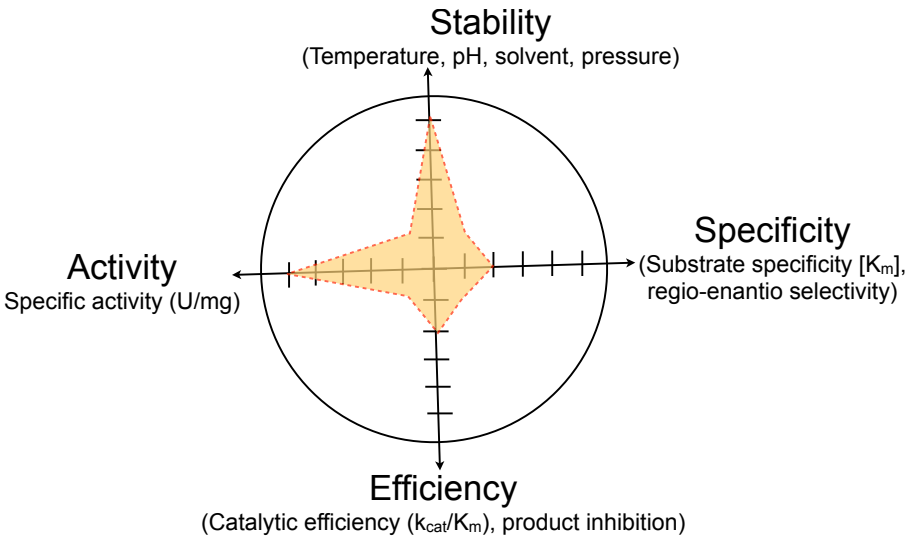

Figure 1.7. Multiple parameters of an enzyme. This hypothetical enzyme has high activity and is very stable. However, the specificity and efficiency is low. Improvements to the efficiency and or specificity should not come at the cost of activity or stability. This figure was adapted from Lorenz and Eck[32].

The strategy researchers choose depends largely on what information is on hand about the enzyme. Researchers must use a directed evolution (the mimic of natural selection) approach if the only information available is the amino acid sequence. A well characterized enzyme (kinetics, crystal/NMR structure) allows researcher to use computer aided modeling to limit the variants to a few dozen. In some cases both strategies are needed; computer aided modeling can identify the position where mutations might be most beneficial, but random mutagenesis and screening identifies which amino acid works best at that position. Thus, directed evolution and computer aided design are not mutually exclusive, but a continuum where the choice depends upon the amount of information available[33].

1.6.1 Directed evolution strategies

Directed evolution is an iterative approach to introducing mutations and screening for variants. Mutations are introduced in the form of substitutions, insertions or deletions within the DNA sequence. Several techniques to introduce mutations exist such as error-prone polymerase chain reaction (PCR) and DNA shuffling. Mutations exists in a collec-

tion known as a library, some variants are beneficial while most others are not. Screening for variants involves retaining mutants with improved properties based on selection criteria which removes beneficial variants from deleterious ones.

1.6.1.1 Error-prone PCR

The most widely used technique to introduce random mutations is error-prone PCR (ePCR)[34], where the amount of DNA is doubled in each cycle using a heat-stable form of DNA polymerase, Figure 1.8a. In ePCR, magnesium is supplemented with manganese which causes DNA polymerase to become more prone to substituting the wrong nucleotide, either by transition (purine for purine, or pyrimidine for pyrimidine) or transversion (purine for pyrimidine or pyrimidine for purine) or to cause insertions and deletions. The main advantage to this method is relative simplicity and rapid turn-around time, one to two days in the hands of an experienced researcher. The mutations can be subject to several additional rounds of ePCR to improve the desired phenotype. Thus, the assumption to this technique is that mutations cause an additive effect and the trajectory of mutations does not matter. Another assumption is that multiple solutions exist because the technique does not sample all of the possibilities.

In one example, the thermostability of a phytase from E.coli was enhanced using ePCR[35]. Phytases are enzymes that degrade phytate, a class of compounds that bind to phosphate. In animal feed, the majority of phosphate is bound to phytate, which goes undigested. Microbes in the soil readily degrade phytate which contributes to downstream phosphate run-offs. Animal feed is usually processed into pellets which are subject to high temperatures, up to 80 ˚C. Thus, to incorporate phytase into animal feed the thermastability of the enzyme must be improved. Kim and Lei used ePCR to generate variants of phytase, which were then screened for improved thermastability. They found a single mutation K46E as well as a variant containing triple mutations (K65E/K97M/S209G) which improved the thermostability at 80 ˚C by 20% and increased the melting temperature by 6-7 ˚C. The catalytic activity of both mutations were improved by 52% and 152% respectively.

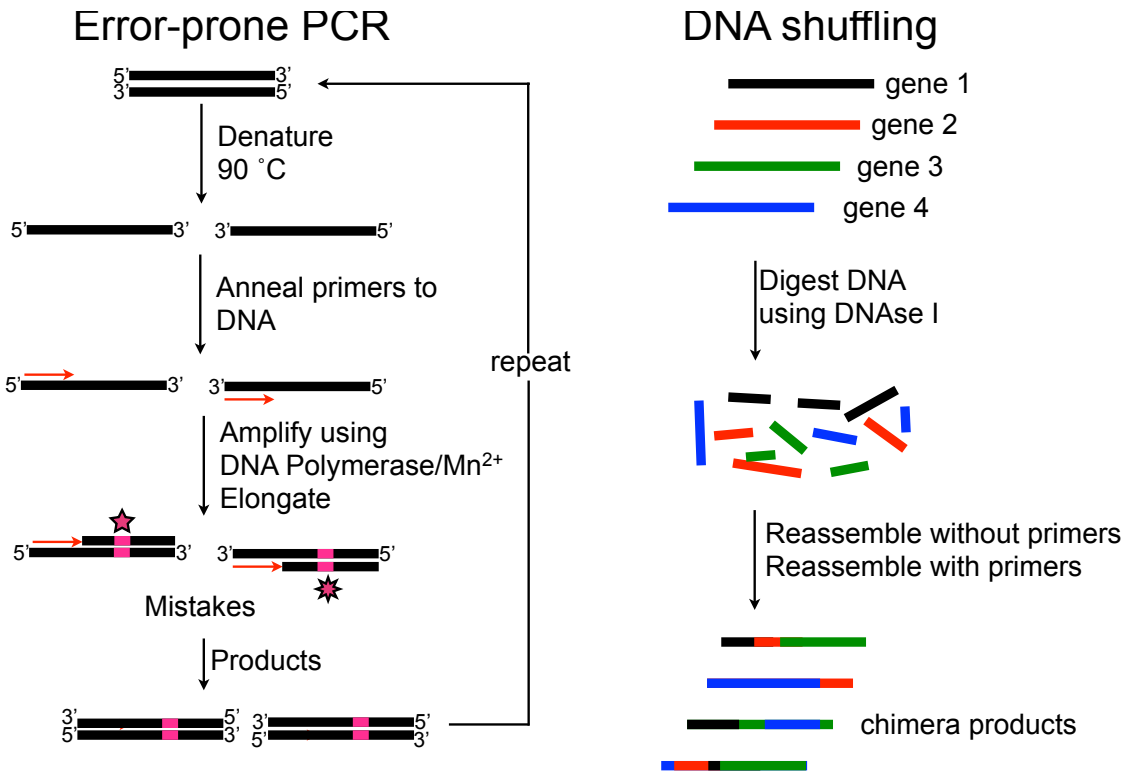

Figure 1.8. Schematic diagram of methods to introduce mutations onto DNA sequence. a) Error-prone PCR substitutes manganese for magnesium to cause DNA polymerase to create transitions, transversions or insertions/deletions. The amount of manganese or the number of cycles and be used to control the numbers of mutations created. b) DNA shuffling uses homologous recombination of related genes to create chimeras, where segments of DNA are identical to the parent gene.

1.6.1.2 DNA shuffling

DNA shuffling is a technique that makes chimeras of several related DNA sequences. This technique requires that the user has a minimum of two to three homologous sequences to work with. The parental DNA is fragmented by DNAse I, an endonclease specific for DNA to generate 50 to 100 base pairs (bp), Figure 1.8b. The fragmented pieces are used as self-priming templates in several rounds of PCR until the [36]. An additional round of PCR using primers insures that the products are similar in size to the parental genes. The products are chimeras which contains pieces of DNA from all parental

strands used. In principle, a chimera gene can receive beneficial traits from both parents. The requirement for high specificity is the main drawback of this technique.

The first successful example of DNA shuffling was increasing the minimum inhibitory concentration of TIM-β-lactamase by 64-fold over the best mutation reported for cefotaxime[37]. Stemmer took six related β-lactamase genes and subjected them to three rounds of DNA shuffling, keeping the variant which required the highest concentration of cefotaxime to kill the host organism. To remove neutral or "non-beneficial" mutations, Sterner performed an additional round of DNA shuffling with the wild-type. The best variant of β-lactamase contained six mutations, only two of these mutations were identified by error-prone PCR. Thus, recombination of homologous genes can create beneficial variants that may be missed by error-prone PCR because the improved β-lactamase requires simultaneous multiple mutations.

1.6.2 Computer modeling of enzymes

Computational modeling is a strategy to predict modifications to improve the parameters of an enzyme. Successful modeling can be as simple as overlaying similar protein structures and analyzing structural differences. More complicated modeling requires researchers to analyze the tertiary structure of the protein and then build intermediates that are likely to be the rate-limiting step, and to make models of modified proteins. Similar to directed evolution, this method is iterative – predicted mutations must be experimentally determined then modeled once more if further improvements are needed.

1.6.2.1 Molecular mechanics

Researchers use molecular mechanics to analyze chemical intermediates. Molecular mechanics uses force fields to model large molecular systems such as proteins. A typical force field contain functional forms which account for the potential energy of bond stretching, angles, torsions, and nonbonded terms such as electrostatic and van der Waals effects, Figure 1.9a. Functional forms of force fields are further simplified to cater at specific tasks and to reduce computation time. For example, the potential for bond distances

is treated as a simple harmonic oscillator for the AMBER force field[38]. The ideal treatment for bond distances is to use the Morse potential[39], which includes treatment for bond breaking, Figure 1.9b. The simple harmonic treatment for AMBER forcefield is valid, because it's designed to model protein structures, which are usually at a ground state conformation. More complex force fields such as MM2 forcefield[40] add cubic and quartet terms to account for strained molecules. However, the cubic term reaches a maximum and at longer distances the potential energy reaches a negative value. Therefore, a quartet term is added to prevent the potential energy from reaching physically impossible values.

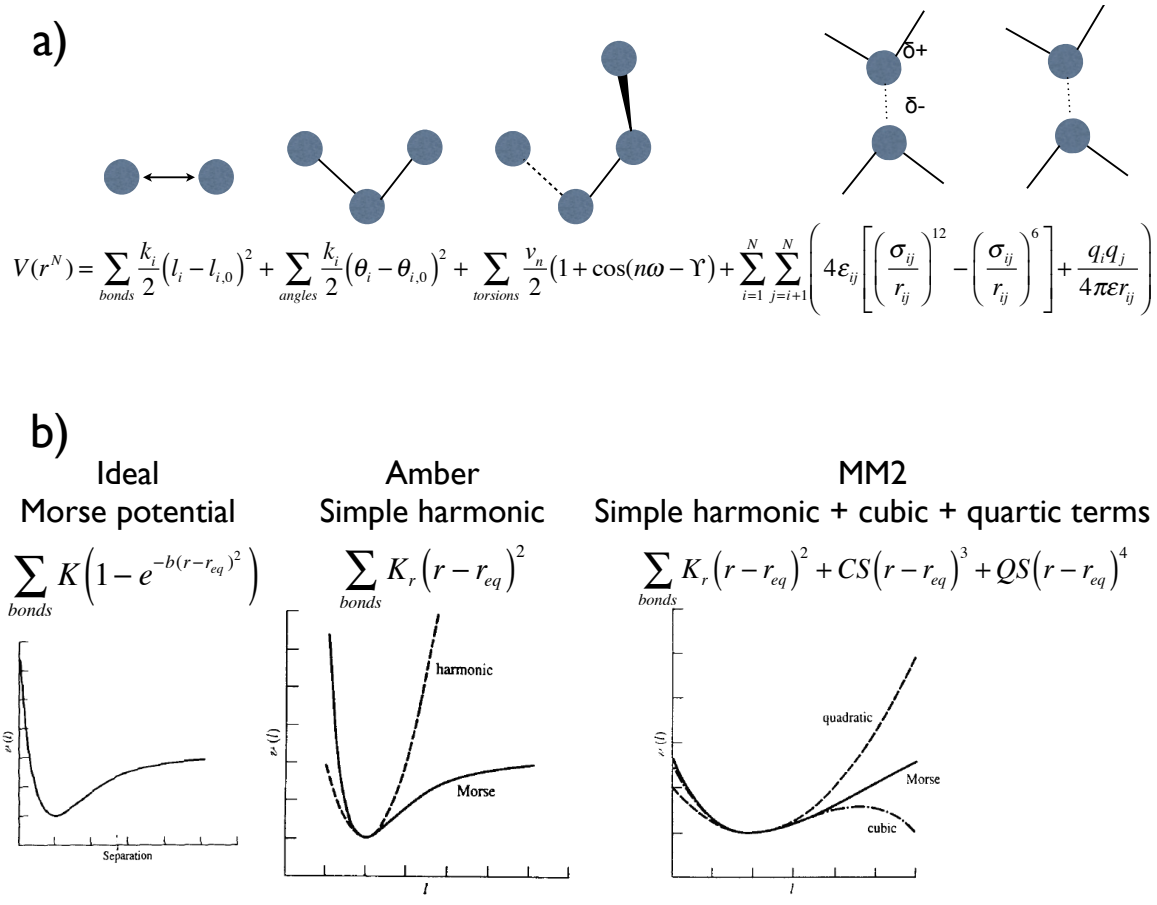

Figure 1.9. General equation for a forcefield and modifications. a) The potential energy of the molecule is described as the sum of intermolecular and intramolecular interactions. The top of the equation are cartoon representations of each term. b) The amber forcefield is most accurate for simple molecules near the ground state. More complex forcefields

such as MM2 include cubic and quartic terms. This figure was adapted from Leach *et al*[41].

Molecular mechanics give accurate structures since it has been parameterized with experimental data. It does not work when bond breaking or making occurs because it does not model electrons. For an accurate descriptions, quantum mechanical treatment is needed, which at present is limited to modeling a few dozen atoms.

Molecular mechanics can be used to optimize the energy of an intermediate by adjusting the bond length, angle, and dihedral angles. Energy optimization is a method to reach a local minimum for a given structure. The inherent drawback with energy optimization is that researchers will get a static low energy structure of the protein molecule. Proteins in aqueous solution are dynamic, the side-chains and the main-chain of flexible loops can adopt different orientations. Therefore, high energy conformations of intermediates that may be important for catalysis may be missed using molecular mechanics alone. Molecular dynamics uses molecular mechanics to determine the trajectory of atoms in a protein structure. This would allow the sampling of different conformations but at the cost of increased computation time. Despite these drawbacks, researchers have successfully modeled enzymes to improve their properties.

1.6.2.2 Examples of computer modeling to engineer enzymes

Computer modeling can be used to identify residues that can improve the binding efficiency of enzymes. Savile and coworkers used a combination of computer modeling and directed evolution to improve a transaminase to form from prositagliptin ketone to sitagliptin[7]. The researchers modeled prostagliptin into the transaminase to find that the substrate does not fit into the active site. The modeling allowed the researchers to identify potential residues that could be altered to fit the substrate. Using this approach, they identified a mutation with modest activity. Directed evolution of the new variant allowed for increased activity and selectivity, Figure 1.10.

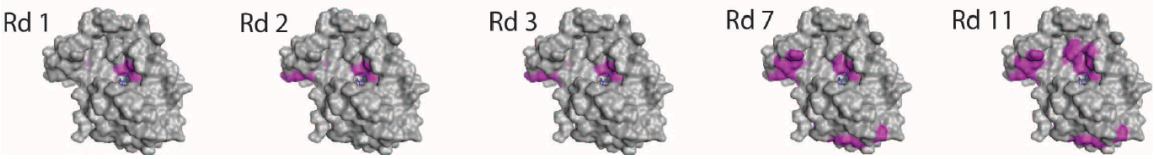

Figure 1.10. Location of residues that improve transaminase activity and enantioselectivity. Molecular modeling identified residues within the active site for modification (Rd1 = round 1). Further improvements came from several rounds (Rd x) of directed evolution. The transaminase exists as a dimer, but the figure shows a monomer. Thus, The front-left facing side of the molecular model represent the active site. This figure was reproduced from Savile and coworkers[7].

Computer modeling can also identify missing critical residues among diverged enzyme families. Padhi and coworkers superimposed the structure of an esterase and hydroxynitrile lyase to identify missing residues which prevent the esterase from catalyzing the lysis of mandelonitrile[42], Figure 1.11. The researchers showed that a double mutant, G12T/M239K, could abolish esterase activity while increasing hydroxynitrile lyase activity by 13,000-fold faster than the uncatalyzed reaction. The high sequence similarity (45%) and identical structural scaffold between the esterase and hydroxy nitrile lyases aided the researchers to focus on differences in the active site. Previous kinetic studies on hydroxynitrile lyases confirm that both threonine and lysine at the active site are essential for activity. The combined knowledge of computer modeling and kinetic mechanism allowed the researchers to test a small number of variants to identify the desired property.

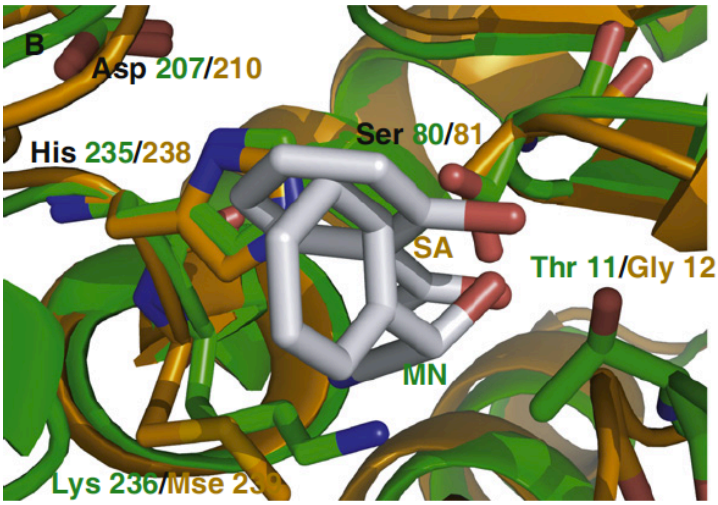

Figure 1.11. Superimposed structure of hydroxy nitrile lyase (mandelonitrile as a substrate, green structure) with SABP2 esterase (salicylic acid as a substrate, orange structure). Both structures have the same fold, but differ in the side-chain residues. In the active site, hydroxynitrile lyase contains a lysine and threonine, while at the same position, the esterase contains a methionine and glycine. This figure was reproduced from Padhi and coworkers[42].

1.7 Enzyme kinetics

Enzyme kinetics is the study of how enzymes catalyze chemical reactions by measuring their reaction rate. The reaction rate is used to determine the catalytic mechanism based on mathematical models. Enzymes increase the rate of chemical reactions by lowering the activation barrier without changing the equilibrium constant. The activation barrier is the transition state from reactant to product. The transition state represents the smallest fraction of the population for the reactant and product because it's highest in energy. Linus Pauling was the first to describe how enzymes increase the rate of chemical reactions by lower the activation energy[43]. For example, the chemical interconversion of S, a substrate to P, a product is slow, Figure 1.12.

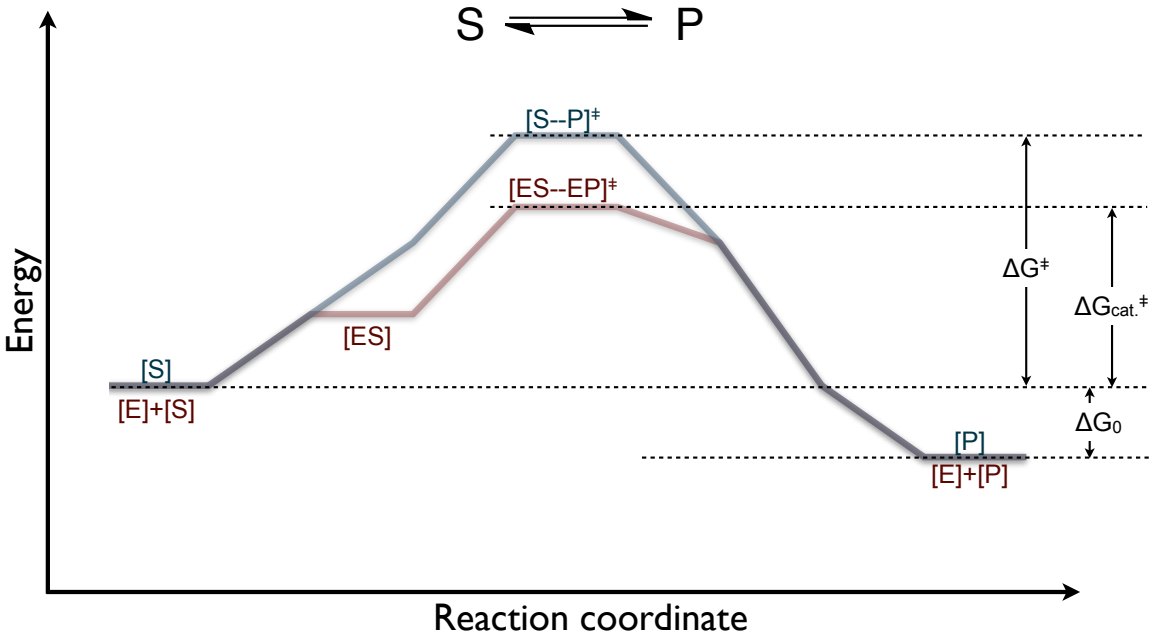

Figure 1.12. Reaction coordinate of a unimolecular interconversion. The uncatalyzed reaction must overcome an activation barrier before proceeding to form the product. In the enzyme catalyzed reaction, the enzyme lowers the activation barrier to speed up the reaction. The overall Gibbs free energy does not change.

The enzyme is able to bind and react with S in way to lower the activation barrier ($\Delta G_{cat.}^{\ddagger}$). The equilibrium constant does not change because the change in Gibbs free energy (ΔG_0) is the same for the uncatalyzed and catalyzed reaction. The relationship between the equilibrium constant and Gibbs free energy is:

$$K_{eq} = e^{-\Delta G_0 / RT} \qquad \text{equation (1)}$$

R is the gas constant (8.31 J/(mol*K)) and T is the temperature in Kelvin.

1.7.1 Kinetic model for a simple interconversion reaction

Enzymologists use mathematical models to describe the behavior of enzymes. The models provide a hypothesis to test a proposed mechanism for an enzyme. For example, the enzyme catalyzed interconversion reaction of S to P with one intermediate, [ES], Figure 1.13. The enzymes binds and reacts with S to form an enzyme intermediate complex [ES]. Formation of this [ES] complex can either rapidly equilibrate, or be in a steady-state, the net concentration of [ES] does not change[44].

$$E + S \underset{k_{-1}}{\overset{Ks\ k_1}{\rightleftharpoons}} [ES] \xrightarrow{k_2} E + P$$

Figure 1.13. Reaction mechanism of an enzyme catalyzed interconversion reaction.

The change of product, P over time is dependent upon the rate constant k_2 and [ES] concentration, Figure 1.14 (eq. 1). The total amount of enzyme in a simple interconversion reaction is [E] and [ES]. Thus, dividing eq.1 by eq.2 in Figure 1.14 gives rate equation as a fraction of the total enzyme concentration. At this juncture, either the rapid equilibrium assumption or stead state assumption can be applied to eq. 3.

In the rapid equilibrium assumption developed by Henri-Michaelis-Menten, the free enzyme and substrate are in equilibrium with the enzyme substrate complex. Thus, substituting eq. 4a into eq. 3 gives the velocity equation with K_S. This velocity equation can be simplified by letting the product of k_2 (the rate limiting limiting step) and enzyme total, $[E]_T$ to be equivalent to the maximum velocity, V_{max}. Further simplification can be done by multiplying the right hand side of eq. 5a by $(K_S/[E]_T)$. Equation 6a is valid for enzymes that rapidly equilibrate to the Michaelis complex, ([ES]). The rate of the enzyme catalyzed reaction will not increase when substrate concentration is much greater than the equilibrium constant.

Alternatively, the relationship between [E], [S] and [ES] can be thought of as being in a steady-state, the net concentration of [ES] is zero. Formation and reduction of the [ES] complex are equivalent, and can be reduced to eq. 4b. Substituting eq. 4b into eq. 3 gives the velocity equation that's dependent on individual kinetic constants. Similar to the approach in the rapid equilibrium step, V_{max} is equivalent to the product of k_2 and $[E]_T$. A new term, Km is introduced to be equivalent to $(k_2/(k_1+k_{-1}))$. The physical meaning of K_m is the affinity for a substrate and how fast the product is formed. Substituting Km into eq. 5b and multiplying the right hand side by $(K_m/[E]_T)$ gives the simplified velocity equation in eq. 6b.

$$\frac{d[P]}{dt} = v = k_2[ES] \quad \text{eq.1}$$

$$[E]_t = [E] + [ES] \quad \text{eq. 2}$$

$$\frac{v}{[E]_t} = \frac{k_2[ES]}{[E] + [ES]} \quad \text{eq. 3}$$

rapid equilibrium

$$K_S = \frac{[E][S]}{[ES]}$$

$$[ES] = \frac{[E][S]}{K_S} \quad \text{eq. 4a}$$

$$\frac{v}{[E]_t} = \frac{k_2 \frac{[S]}{K_S}[E]}{[E] + \frac{[S]}{K_S}[E]} \quad \text{eq. 5a}$$

substitute V_{max}

$$V_{max} = [E]_t k_2$$

multiply right side by:

$$\frac{K_S}{[E]}$$

$$\frac{v}{V_{max}} = \frac{[S]}{K_S + [S]} \quad \text{eq. 6a}$$

steady state

$$\left(+\frac{d[ES]}{dt}\right) = [E][S]k_1$$

$$\left(-\frac{d[ES]}{dt}\right) = [ES]k_{-1} + [ES]k_2 = [ES](k_{-1} + k_2)$$

$$\left(+\frac{d[ES]}{dt}\right) = \left(-\frac{d[ES]}{dt}\right) \therefore [E][S]k_1 = [ES](k_{-1} + k_2)$$

$$[ES] = \frac{[E][S]k_1}{(k_{-1} + k_2)} \quad \text{eq. 4b}$$

$$\frac{v}{[E]_t} = \frac{k_2 \frac{[E][S]k_1}{(k_{-1} + k_2)}}{[E] + \frac{[E][S]k_1}{(k_{-1} + k_2)}} \quad \text{eq. 5b}$$

substitute V_{max}

$$V_{max} = [E]_t k_2$$

substitute K_m

$$K_m = \frac{k_1}{(k_{-1} + k_2)}$$

multiply right side by:

$$\frac{K_m}{[E]}$$

$$\frac{v}{V_{max}} = \frac{[S]}{K_m + [S]} \quad \text{eq. 6b}$$

Figure 1.14. Derivation of the Henri-Michaelis-Menten equation. Velocity of product formation is dependent on [ES] concentration and k_2. Following the correction for a mass balance, the velocity equation can either follow the rapid equilibrium assumption (left path) or the steady state assumption (right path).

1.7.2 Kinetic model for bi-substrate reactions

Most enzymes catalyze reactions involving multiple substrates and products. For example, transaminases, acyl-transferases, and esterases use the ping pong bi-bi mechanism. The free enzyme binds and reacts with [A], the first substrate to form an enzyme substrate complex [EA], Figure 1.15a. Next, the first product, [P] to form an enzyme-substrate intermediate, [F]. For esterases, this form is called the acyl-enzyme intermediate. Another substrate, [B] binds and reacts with the enzyme-intermediate to form another enzyme substrate intermediate, [FB]. Subsequently, the second product, [Q] and the free enzyme is released. The ping pong bi-bi mechanism can be derived using the King-Altman method[45] and Cleland notations[46]. The King-Altman method is a way to organize and group the rate constants (k_1, k_2, k_{-1}, etc...) with substrate and or product concentrations. The Cleland notations convert the grouped rate constants into physically meaningful kinetic constants (V_{max}, K_m). Thus, the initial forward velocity equation contains an additional substrate term and also the K_m terms for substrates [A] and [B], Figure 1.15b. The initial forward velocity equation can be simplified by isolating either the first or second substrate concentration. When either substrate is saturated, the velocity equation becomes identical to Henri-Michaelis-Menten equation.

a)

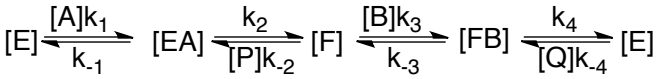

b)

$$\frac{v}{V_{\max}} = \frac{[A][B]}{K_{m_B}[A] + K_{m_A}[B] + [A][B]}$$

Multiply right side by (1/[B])/(1/[B])

$$\frac{v}{V_{\max}} = \frac{[A]}{K_{m_A} + [A]\left(1 + \frac{K_{m_B}}{[B]}\right)}$$

When [B] is saturated

$$\frac{v}{V_{\max}} = \frac{[A]}{K_{m_A} + [A]}$$

Figure 1.15. Ping pong bi-bi mechanism. General scheme for a ping pong bi-bi mechanism. Initial forward velocity equation for a ping pong bi-bi mechanism adapted from Segel[44].

1.7.2 Kinetic model for reactions with multiple competing substrates

The ping pong bi-bi mechanism can be further complicated if an alternative substrate is present which can result in a branch point. For example, α-chymotrypsin is a serine protease that hydrolyzes peptide bonds using the ping pong bi-bi mechanism. The enzyme can also catalyze hydrolysis of esters as a side reaction. Bender and coworkers tested several alcohols to probe the kinetic mechanism of α-chymotrypsin[47]. In the presence of an alcohol, α-chymotrypsin also catalyzes acyl-transfer. The authors measured the rate of acyl-transfer to hydrolysis and showed that the enzyme partitions according to the amount of alcohol present. Thus, their model predicts that the ratio of acyl-transfer to hydrolysis is linearly dependent on the concentration of alcohol. Fink and Bender measured the ratio of acyl-transfer to hydrolysis dependence on alcohol concentration using papain[48]. Unlike α-chymotrypsin, the authors found that the ratio of acyl-transfer to water reached a plateau – while a similar finding was found between the competition of amine

nucleophile and water for penicillin acylase[49]. Fink and Bender proposed a more complex model, where water can outcompete the enzyme-substrate complex.

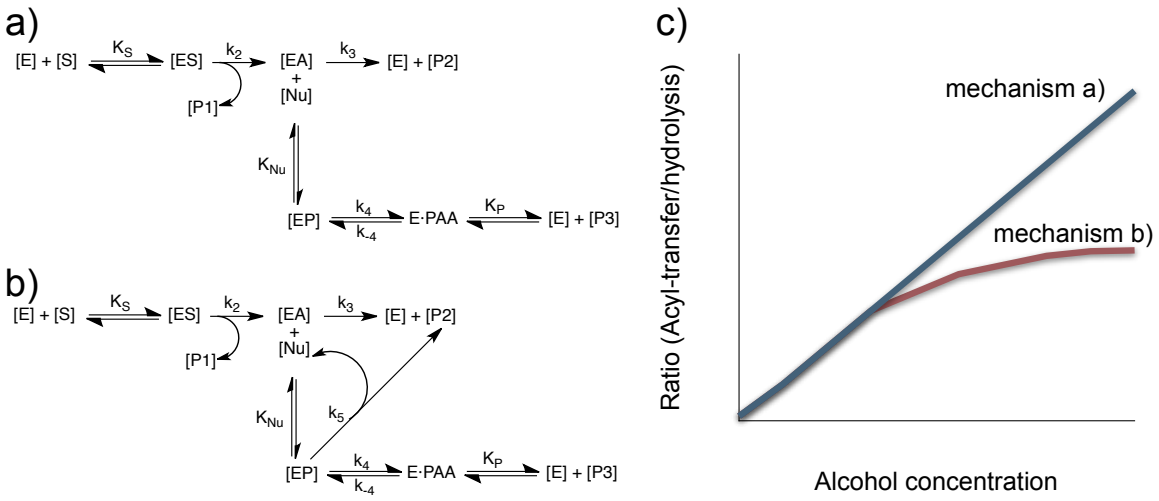

Figure 1.16. Acyl transfer mechanisms. a) Acyl-transfer mechanism proposed by Bender and coworkers[47]. b) Amended Acyl-transfer proposed by Fink and Bender[48]. c) The mechanism in a) predicts that the dependence of acyl-transfer/hydrolysis to alcohol concentration is linear. The mechanism in b) predicts that the dependence of acyl-transfer/hydrolysis to alcohol concentration will reach a plateau.

Enzyme catalyzed perhydrolysis could use either mechanism. For perhydrolases, hydrogen peroxide must compete for the same enzyme for as water. This results in a similar branch point as seen in penicillin acylase and papain. Which mechanism perhydrolases use is currently unknown and is addressed in this thesis.

The study of mechanism and kinetics is important to perhydrolases in order to determine how the rate and kinetic constants contribute to perhydrolysis and to identify the rate-limiting step. Understanding of the mechanism will aid the design and engineering of improved perhydrolases that have higher nucleophile selectivity and activity towards perhydrolysis.

Chapter 2

To engineer a better perhydrolase using computer modeling, the kinetics and mechanism of perhydrolysis must be understood. The kinetics of ester and peracetic acid hydrolysis is measured using wild-type and L29P PFE. L29P PFE efficiently catalyze peracetic acid hydrolysis near diffusion control, and is also a good enzyme for lactone hydrolysis. Perhydrolases either use an esterase-like mechanism or a non-covalent mechanism. This chapter contains evidence which supports the former.*

*This chapter is a copy of a published article and is reproduced with permission from Biochemistry, Vol. 49, Yin, D.L.T.; Bernhardt, P.; Morley, K.L.; Jiang, Y.; Cheeseman, J.D.; Purpero, V.; Schrag, J.D.; Kazlauskas, R.J., "Switching catalysis from hydrolysis to perhydrolysis in *Pseudomonas fluorescens* esterase", 1931-1942, Copyright 2010, American Chemical Society (See Appendix for reprint).

Switching catalysis from hydrolysis to perhydrolysis in *P. fluorescens* esterase

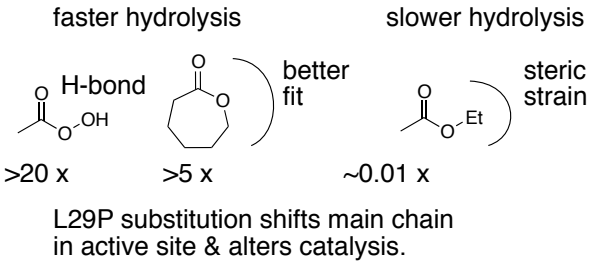

Many serine hydrolases catalyze perhydrolysis – the reversible formation of peracids from carboxylic acids and hydrogen peroxide. Recently we showed that a single amino acid substitution in the alcohol binding pocket - L29P - in *Pseudomonas fluorescens* (SIK WI) aryl esterase (PFE) increased the specificity constant of PFE for peracetic acid formation >100-fold [Bernhardt *et al. Angew. Chem. Intl. Ed.* **2005**, *44*, 2742]. In this paper, we extend this work to address the three following questions. First, what is the molecular basis of the increase in perhydrolysis activity? We previously proposed that the L29P substitution creates a hydrogen bond between the enzyme and hydrogen peroxide in the transition state. Here we report two x-ray structures of L29P PFE that support this proposal. Both structures show a main chain carbonyl oxygen closer to the active-site serine as expected. One structure further shows acetate in the active site in an orientation consistent with reaction by an acyl-enzyme mechanism. We also detected an acyl-enzyme intermediate in the hydrolysis of ε-caprolactone by mass spectrometry. Second, can we further increase perhydrolysis activity? We discovered that the reverse reaction – hydrolysis of peracetic acid to acetic acid and hydrogen peroxide – occurs at nearly the diffusion limited rate. Since the reverse reaction cannot increase further, neither can the forward reaction. Consistent with this prediction, two variants with additional amino acid substitutions showed two fold higher k_{cat}, but K_m also increased so the specificity constant, k_{cat}/K_m, remained similar. Third, how does the L29P substitution change the esterase activity? Ester hydrolysis decreased for most esters (75-fold for ethyl acetate), but not for methyl esters. In contrast, L29P PFE catalyzed hydrolysis of ε-caprolactone five times more efficiently than wild-type PFE. Molecular modeling suggests that moving the car-

bonyl group closer to the active site blocks access for larger alcohol moieties, but binds ε-caprolactone more tightly. These results are consistent with the natural function of perhydrolases being either hydrolysis of peroxycarboxylic acids or hydrolysis of lactones.

2.1 Introduction

Many serine hydrolases catalyze perhydrolysis – the reversible formation of peroxycarboxylic acids from carboxylic acids and hydrogen peroxide[1-3]. Enhancing this reactivity could offer new catalysts for organic synthesis and industry. Peracids can introduce oxygen into olefins, cyclic ketones, amines, and organic sulfur compounds, making them essential oxidants for organic synthesis[4, 5]. Industry uses peracids for disinfecting, waste water treatment, de-staining of fabrics, pulp bleaching, and removal of lignin from biomass. Unfortunately, concentrated peracids are explosive and corrosive, but the *in situ* generation of dilute peracids minimizes these hazards. Chemical *in situ* generation of peracids often involves two steps or harsh reaction conditions or hazardous catalysts, or a combination thereof[5]. Enzyme-catalyzed reactions are an environmentally friendly alternative that avoid harsh reaction conditions and hazardous catalysts.

Perhydrolases are a subgroup of serine hydrolases that are particularly efficient at catalyzing perhydrolysis. Perhydrolases have an α/β-hydrolase fold[6] and use a Ser-His-Asp catalytic triad[7-9]. Perhydrolysis likely takes place with a ping-pong bi-bi mechanism[9, 10], Figure 2.1A. The catalytic serine attacks the carbonyl carbon of a carboxylic acid and displaces water to form an acyl-enzyme intermediate. Next, hydrogen peroxide reacts with this acyl enzyme to form the peracid product and to regenerate the catalyst. Hydrogen bonds from two main-chain amides, called the oxyanion hole, activate the carbonyl group for attack and stabilize the tetrahedral intermediate.

Some reactions catalyzed by α/β-hydrolases do not involve a covalent acyl-enzyme intermediate[11]. For example, hydroxynitrile lyases catalyze the direct attack of cyanide on the aldehyde to form a cyanohydrin[12]. Bugg proposed that perhydrolysis could also occur by direct attack by hydrogen peroxide on acetic acid without the formation of an acetyl-enzyme intermediate[11], Figure 2.1B. Support for this mechanism was

an x-ray crystal structure of propionate bound to the active site of a perhydrolase in the orientation suggested in Figure 2.1B.

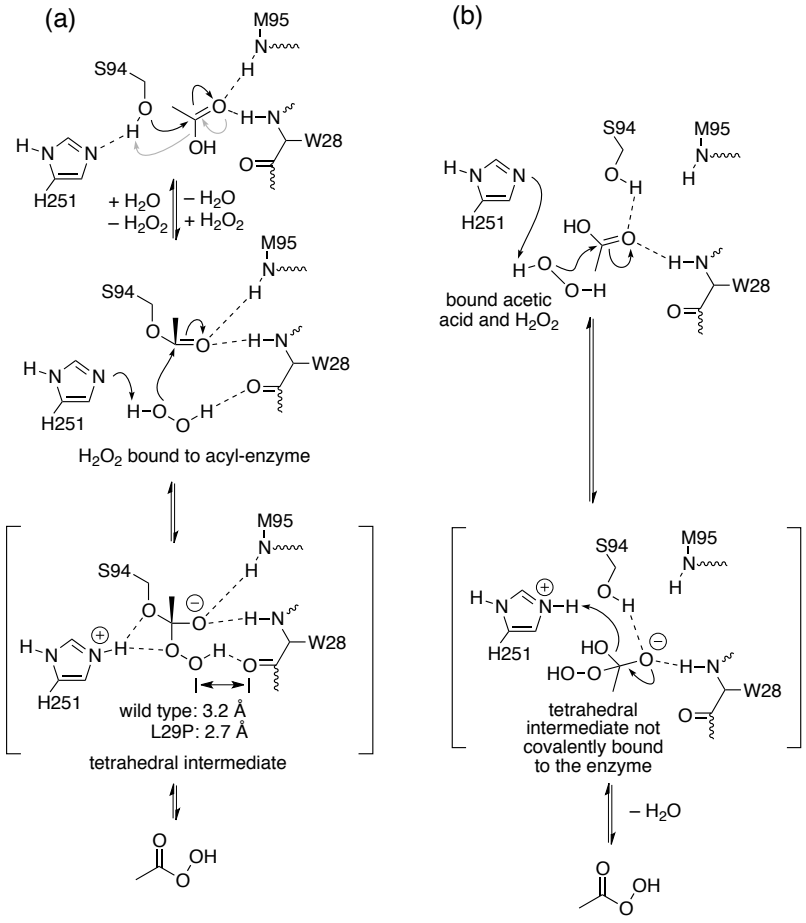

Figure 2.1 Proposed mechanisms for perhydrolysis of acetic acid. The numbering corresponds to the active site of PFE. **a)** The ping-pong bi-bi mechanism involves an acetyl-enzyme intermediate. The first diagram shows the enzyme-acetic acid complex. The γ-hydroxyl group of active site serine 94 is a nucleophile that attacks the carbonyl group of acetic acid to form a tetrahedral intermediate (not shown) via the black curved arrows. Next, this tetrahedral intermediate collapses via the release of water (gray curved arrows) to form an acetyl-enzyme intermediate. Finally hydrogen peroxide binds to yield the complex shown in the second diagram. The N–H's of M95 and W28, called the oxyanion hole, donate hydrogen bonds to the carbonyl oxygen. Nucleophilic attack of hydrogen peroxide on the acyl enzyme forms a second tetrahedral intermediate. In wild-type PFE, the carbonyl oxygen of W28 is too far from the hydrogen peroxide to form a hydrogen bond. The L29P substitution moves this carbonyl 0.5 Å closer to the catalytic serine side-

chain allowing a hydrogen bond to form and stabilize the tetrahedral intermediate. **b)** The ordered bi-bi noncovalent mechanism proposed by Bugg (*11*) does not form an acyl-enzyme intermediate. Both acetic acid and hydrogen peroxide bind the enzyme simultaneously. In this mechanism, acetic acid does not bind to the oxyanion hole, but the γ-hydroxyl group of active site S94 and N–H of W28 donate a hydrogen bond to the carbonyl oxygen of acetic acid. Hydrogen peroxide attacks the bound acetic acid to form a tetrahedral intermediate without covalent links to the enzyme.

Pseudomonas fluorescens esterase (PFE) is a hydrolase, but its amino acid sequence most closely resembles perhydrolases. The amino acid sequence of PFE is 54% identical and 69% similar to that for a perhydrolase from *P. fluorescens* (CPO-F). However, CPO-F is a good perhydrolase (k_{cat} = 1.9 s^{-1}), while PFE is a poor one (k_{cat} = 0.12 s^{-1}). The x-ray structures of the active sites showed subtle differences, but it was unclear which ones were responsible for the different catalytic activities[*9*]. Recently, we reported a single amino acid substitution, L29P in PFE that increased the perhydrolase activity 28-fold to 3.5 s^{-1}[*13*], which is higher than that for CPO-F[*14*]. We attributed the increased catalytic efficiency to a new hydrogen bond between a carbonyl oxygen of W28 and the peroxy group of the second tetrahedral intermediate (C=O...O distance 2.7 Å) using molecular modeling, Figure 1A. The wild-type enzyme could not form this hydrogen bond because the carbonyl group was 0.5 Å further away from the active site (C=O...O distance 3.2 Å). In this paper we confirm the structure of the L29P variant by crystallography and the ping-pong bi-bi mechanism for this enzyme by characterization of an enzyme-acetate complex by x-ray crystallography and by detection of an acyl-enzyme intermediate by mass spectrometry. Further kinetic characterization of the L29P PFE shows that it is as nearly efficient for perhydrolysis as physically possible because it catalyzes the reverse reaction – hydrolysis of peracetic acid – at a nearly diffusion controlled rate. The L29P substitution also decreases the efficiency of ester hydrolysis, but increases the efficiency of lactone hydrolysis.

2.2 Results

Previously, we used computer modeling to predict the structure of the L29P PFE variant. The predicted structure indicated a change from a trans orientation along the peptide bond for the wild-type protein (L29) to a cis conformation in the variant due to the introduction of proline at position 29. This change in the peptide bond orientation moved the protein main chain, and in particular the carbonyl oxygen of W28 closer to the active site. Now we solved an x-ray crystal structure that confirms the predicted structure. In addition, we solved a crystal structure of L29P PFE with substrate acetate bound to the active site to gain further insight into the mechanism.

2.2.1 Crystal structures of L29P PFE. Two crystal structures of L29P PFE variants both show a similar orientation of the proline at position 29, Figure 2.2. L29P PFE (PDB ID: 3hea) shows the apo enzyme, while L29P PFE /acetate (PDB ID: 3hi4) was soaked in acetate and contains a single acetate in the active site. Both forms of L29P crystallized under similar conditions as wild type and were refined using the $P3_2$ space group with six near-identical monomers comprising the dimer of trimers. Molecular replacement with the wild-type structure solved both structure and allowed the refinement of the model to a final resolution of 1.90 Å for L29P and 2.25 Å for L29P/acetate. Table 2.6 in the Materials and Methods section summarizes the statistics for both data sets and the final refinement. The L29P structure contained additional electron density in the active site which could not be identified as glycerol, buffer or water.

The L29P PFE structure superimposed onto the wild-type structure (PDB ID: 1VA4 [19]) with an $RMSD_{all\text{-}atom}$ of 0.16 Å for the best monomer fit (chain A of L29P PFE and chain A of WT PFE), Figure 2.2A. The largest difference with an $RMSD_{backbone}$ of 0.64 Å is in the oxyanion-stabilizing loop containing residues 27-30 between β-strand 1 and α-helix 1. In contrast to the wild-type W28-L29 trans peptide bond, the mutant W28-P29 peptide bond adopts a cis conformation, Figure 2.2A. This conformational change directs the carbonyl oxygen of the W28 peptide bond towards the catalytic serine residue (W28-C=O...S94-Oγ distances: 6.3 Å and 5.2 Å for wild-type PFE and L29P PFE, respectively). Another, less significant, change was a shift in the indole ring of W28 side-

chain. The 7-position of the indole ring is shifted by 1.3 Å as compared to the wild-type enzyme. The structure of L29P PFE/acetate shows the same cis conformation of the W28-P29 peptide bond and the protein conformation is otherwise also similar to L29P PFE.

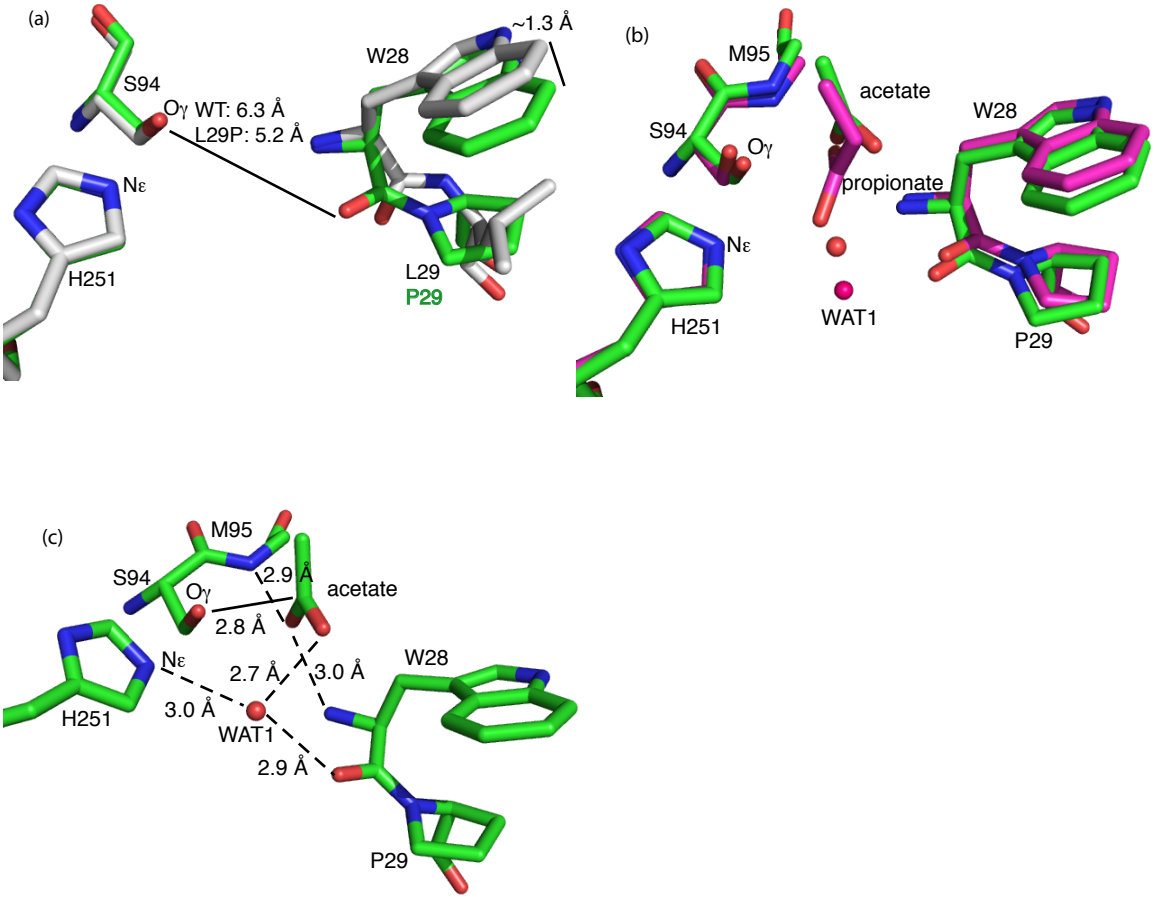

Figure 2.2 Active site x-ray crystal structures of L29P PFE and L29P PFE/acetate. **A**) Superposition of L29P PFE (green CPK colors, PDB ID: 3hea) and wild-type PFE (white CPK colors, PDB ID: 1va4) show similar conformations of the catalytic triad residues. (Only H251 and S94 are shown.) The leucine 29 to proline substitution changes the W28 to L29 peptide bond conformation from trans to cis thereby shifting the main chain carbonyl group of W28 closer to the active site serine by 1.1 Å. A second difference is a shift in the indole ring of the W28 residue by ~1.3 Å for the 7 position. **B)** Superposition of the structures of L29P PFE/acetate (green CPK colors, PDB ID: 3hi4) and perhydrolase CPO-F soaked with propionate (magenta CPK colors, PDB ID: 1a8s). Both show a similar orientations of the W28 carbonyl group and indole ring, but the acetate, propanoate

and active site water molecules (WAT1, orange for L29P, magenta for CPO-F) have different orientations. **C**) L29P PFE/acetate (PDB ID: 3hi4) shows the substrate acetate in an orientation consistent with formation of an acetyl-enzyme intermediate. The acetate carbonyl oxygen accept hydrogen bonds from the two amide N-H's that form the oxyanion hole (M95, W28). The carbonyl carbon of acetate is 2.8 Å from S94-Oγ in this monomer and ranges from 2.8 to 3.1 Å in the six monomers in the asymmetric unit.

These changes in the active site make L29P PFE similar to a naturally occurring perhydrolase (CPO-F, the perhydrolase from *P. fluorescens*). Superposition of the x-ray crystal structure of L29P PFE/acetate with that of CPO-F/propionate (PDB ID: 1A8S[9]) shows a good overall fit of protein ($RMSD_{all\text{-}atom}$ of 0.68 Å when aligning backbone atoms of chain A of L29P PFE with CPO-F) and nearly identical conformations near the active site, including the W-*cis*-P peptide bond and the position of the tryptophan side chain, Figure 2.2B. One exception to the similarity is that the orientation of the propanoate molecule in CPO-F differs significantly from the orientation of acetate in L29P PFE, see below.

The active site of L29P PFE soaked in acetate (pH 5) contains an acetate and a water molecule in each monomer of the asymmetric unit, Figure 2.2C. In each monomer, the C=O of acetate accepts hydrogen bonds from the two N-H's in the oxyanion hole. The distances from the oxygen to the αN of M95 and W28 range from 2.8 to 3.1 Å. The methyl group points towards the acyl pocket while the carboxylic hydroxyl oxygen points towards the alcohol pocket. Since the crystal soak solution was at pH of 5, the ionization form of acetic acid may be acetate or acetic acid. (The pK_a of 4.8 for acetic acid predicts 61% is in the acetate form and 39% is acetic acid.) The substrate for the reaction is likely acetic acid. Distance between the C=O of acetate and S94-Oγ ranges between 2.8 to 3.1 Å. The single water molecule, "WAT1" observed in the alcohol pocket of PFE makes a hydrogen bond between C=O of W28 (2.9 Å) and C-O (2.7 Å) of acetate. The orientation of the acetate is consistent with the formation of an acetyl-enzyme intermediate. The next mechanistic step could be attack of the active site serine on the acetate carbonyl carbon.

The previous x-ray crystal structure of propanoate bound to CPO-F had a different orientation, which was not consistent with the next step being formation of a propanoyl

enzyme intermediate. These crystals of CPO-F were soaked in propanoate at pH 6.6[9], where propanoate, not propanoic acid, predominates. The pK_a of 4.9 for propanoic acid predicts that 98% is in the propanoate form. The carboxylate anion of propanoate is hydrogen bonded to Nε of H251, which prevents the histidine from acting as a base to deprotonate Oγ of the serine. The catalytically nonproductive orientation of the propanoate is consistent with very low catalytic activity at pH 6.6.

2.2.2 Mass spectrometry of the acyl-enzyme intermediate. Electrospray ionization mass spectrometry showed an acyl enzyme during the PFE-L29P-catalyzed hydrolysis of ε-caprolactone at pH ~5.5, Figure 2.3. The enzyme appeared at the expected mass of 30,912 Da and, in the presence of 25 mM ε-caprolactone, an additional peak appeared at 31,026 Da. The 114 Da increase in mass is consistent with the formation of an acyl-enzyme intermediate. The observation of the acyl-enzyme intermediate with L29P PFE is consistent with a covalent mechanism and thus, strongly supports the ping-pong bi-bi mechanism. Further, the x-ray structure of acetate bound to L29P PFE supports the ping-pong bi-bi mechanism. Other serine hydrolases that follow a ping-pong bi-bi mechanism, e.g, porcine pancreatic elastase[32, 33] also show an acyl-enzyme intermediate at low pH.

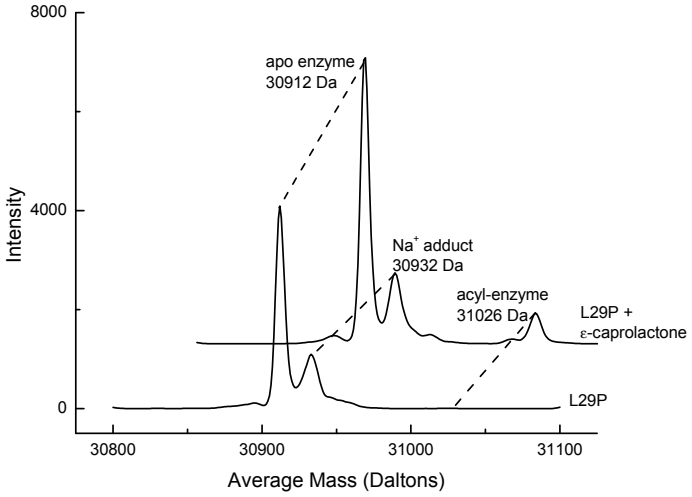

Figure 2.3 Deconvoluted electrospray-ionization spectra show an acyl-enzyme intermediate during the PFE-L29P-catalyzed hydrolysis of ε-caprolactone in citrate/formate buffer pH ~5.5. Without substrate shows the major peak at 30,912 Da, which is consistent with the calculated value of 30,911.9 Da using ProtParam[15]. Addition of 25 mM ε-caprolactone shows an additional peak at 31,026 Da, which is 114 Da higher that the free enzyme. This peak is assigned as the covalent acyl-enzyme intermediate. Peaks at lower mass are present in both spectra and are not identified.

Attempts to detect the acetyl-enzyme intermediate in L29P PFE in 0.5 M acetate at pH 5.5 were inconclusive. The high concentration of acetate in this solution yielded gave mono-, di- and trisodium adducts of the enzyme. The disodium adduct (expected at M+44 Da) and any acetyl enzyme (expected at M+42 Da) overlap and could not be distinguished. The formation of an ester from an acid is thermodynamically uphill, so the amount of acetyl enzyme formed from acetate is expected to be small. On the other hand, converting one ester into another can be thermodynamically neutral, so ε-caprolactone should form more acyl-enzyme intermediate.

Is it possible to further increase the rate of L29P PFE-catalyzed perhydrolysis? Below we measured the kinetics for the reverse reaction and found that it is near the diffusion limit. Since the reverse reaction cannot be much faster, then the forward rate (k_{cat}/K_m) also cannot be much faster either. The ratio of the forward and reverse reactions is fixed by the equilibrium constant.

2.2.3 Hydrolysis of peracetic acid. Perhydrolases catalyze the hydrolysis of peracetic acid to acetic acid and hydrogen peroxide, the reverse of the reaction in Figure 2.1 above. We monitored the rate of hydrolysis with a pHstat, which controls the addition of base. Peracetic acid (pK_a 8.20[34]) is >99% protonated at pH 5.5, while 85% of the product acetic acid (pK_a 4.75) dissociates to form acetate. Thus, hydrolysis of one mole of peracetic acid at pH 5.5 releases 0.85 moles of protons. The observed rates were corrected for the incomplete ionization of acetic acid at pH 5.5 to give the true rates listed in Table 2.1.

Table 2.1 Steady state kinetic constants for hydrolysis of peracetic acid catalyzed by wild-type PFE and L29P PFE.[a]

Enzyme	k_{cat} [s^{-1}]	K_m [mM]	k_{cat}/K_m [s^{-1} M^{-1}]
Wild-type PFE	100 ± 3	0.041 ± 0.005	2 x 10^6
L29P PFE	139 ± 2	<0.003 [b]	>5 x 10^7

[a] Initial rates were measured at 23 °C by pHstat, which controlled the addition of 0.0100 N NaOH to keep the pH at 5.5. [b] The K_m value for peracetic acid with L29P PFE could not be measured accurately because the pHstat method could not detect hydrolysis of peracetic acid below 0.01 mM. The rate of hydrolysis decreased only when the concentration of peracetic acid was below 0.03 mM. From this value we estimated the K_m to be < 0.003 mM.

Both wild-type PFE and L29P PFE were excellent catalysts for the hydrolysis of peracetic acid. The k_{cat} values were similar (100 and 139 s^{-1}, respectively), but the K_m for peracetic acid was >14-fold lower for L29P PFE than for the wild-type enzyme (<0.003 versus 0.041 mM). The value of K_m for L29P PFE is only an upper limit because the pHstat method could detect hydrolysis of peracetic acid only above 0.01 mM. The rate of hydrolysis decreased slightly below 0.03 mM peracetic acid, so we estimated that K_m is < 0.003 mM. Due to this lower K_m for peracetic acid, the specificity constant is >20-fold higher for L29P PFE than for wild-type PFE. We expect that the true specificity constant is ~100-fold higher for L29P PFE than for wild-type PFE because the specificity constant for the forward reaction is ~100-fold higher for L29P PFE than for wild-type PFE. The Haldane relationship[35] requires that the ratio of forward and reverse reactions to equal the equilibrium constant. The lower K_m for peracetic acid for L29P PFE is consistent with the hypothesis that this amino acid substitution stabilizes the peroxy intermediate. Peracetic acid is structurally closer to the peroxy intermediate than either acetic acid or hydrogen peroxide and its binding to the active site may be favored by the shifted carbonyl group of W28.

This specificity constant for the L29P PFE-catalyzed hydrolysis of ~10^8 s^{-1} M^{-1} approaches the value for bimolecular rate constants of a diffusion controlled enzyme-

catalyzed reaction: 4 x 10^8 s^{-1} M^{-1} for triose phosphate isomerase [36]. This high specificity constant indicates that L29P PFE is a highly efficient catalyst for the reaction in Figure 2.1 and catalyzes hydrolysis of peracetic acid at close to the diffusion limit.

2.2.4 Mutants with higher k_{cat} for perhydrolysis. Previously, we compared the amino acid sequences of hydrolases and perhydrolases to identify residues responsible for perhydrolase versus esterase activities in α/β hydrolases. This comparison and subsequent experimentation identified the single amino acid substitution variant L29P PFE[13]. In this paper, we attempted to further improve L29P PFE by aligning its amino acid sequence with not all perhydrolases, but with the perhydrolases that have the highest specific activity: BPO-A1, a perhydrolase from *Streptomyces aureofaciens* ATCC 10762 (previously called a nonheme bromoperoxidase), CPO-T, a perhydrolase from *Streptomyces aureofaciens* Tü24 (previously called a nonheme chloroperoxidase), and CPO-L, a perhydrolase from *Streptomyces lividans* TK64 (previously called a nonheme chloroperoxidase)[37]. Seventeen residues were conserved in BPO-A1 and CPO-L but not with L29P PFE. We chose H57 and H93 for mutagenesis because they were closest to the active site. We also enlarged the acyl binding pocket of L29P PFE by replacing F125 with Ala. Starting with L29P PFE, additional site directed mutagenesis yielded the three double mutants - L29P/F93H PFE, L29P/F125A PFE, L29P/F57H PFE. (See Methods and Materials for details.)

Michaelis-Menten kinetic constants for the ping-pong bi-bi reaction were measured by keeping the acetate concentration constant and varying hydrogen peroxide and then by keeping hydrogen peroxide constant and varying acetate. This approach yields apparent kinetic constants for the varied substrate. The Michaelis constants for acetate and hydrogen peroxide are expected to differ, but the k_{cat} values should be the same when the concentration of the constant substrate is high enough to saturate the enzyme.

Initial rates were monitored spectrophotometrically using an indirect assay. Enzyme-generated peracetic acid oxidized bromide ion to bromonium, which reacted with monochlorodimedone to form bromochlorodimedone. The decrease in monochlorodimedone concentration causes a decrease in absorbance at 290 nm[16]. Reaction rates

were measured at five or more different substrate concentrations. The data was fit to the Michaelis-Menten equation using a nonlinear regression and gave a close fit ($R^2 > 0.97$).

The value of k_{cat} improved for L29P PFE ~44-fold for perhydrolysis of acetic acid as compared to wild-type PFE (42-fold higher with acetic acid as the varied substrate - 0.12 to 5.1 s^{-1} and 47-fold higher with hydrogen peroxide as the varied substrate 0.094 to 4.4 s^{-1}), Table 2.2. The value of k_{cat} would be the same in both cases if the enzyme were completely saturated with the constant substrate. The K_m value for acetic acid was high (210 mM) so the acetate concentration of 500 mM did not completely saturate the enzyme. For this reason the value of k_{cat} measured when acetic acid is the constant substrate was slightly lower than when hydrogen peroxide was the constant substrate. The K_m values decreased for L29P PFE as compared to wild-type PFE, but only approximately two fold. The K_m for hydrogen peroxide decreased 1.8-fold (3.3 to 1.8 mM) and the K_m for acetic acid decreased 2.4-fold (500 to 210 mM). The combined improvements in both k_{cat} and K_m gave a specificity constant (k_{cat}/K_m) improvement 70-100-fold, Table 2.2.

Table 2.2 Apparent steady state kinetic constants for perhydrolysis of acetic acid catalyzed by wild-type PFE, L29P PFE and double mutants.[a]

Enzyme	Varied substrate	k_{cat} [s^{-1}]	K_m^{app} [mM]	k_{cat}/K_m^{app} [s^{-1} M^{-1}]
Wild-type PFE	Acetic acid[b]	0.12 ± 0.02	500 ± 100	0.2
	Hydrogen peroxide	0.094 ± 0.002	3.3 ± 0.2	28
L29P PFE	Acetic acid	5.1 ± 0.4	210 ± 60	20
	Hydrogen peroxide	4.4 ± 0.2	1.8 ± 0.2	2000
L29P/F93H PFE	Acetic acid	11 ± 1	610 ± 120	20
	Hydrogen peroxide	9 ± 1	2.7 ± 0.6	3000
L29P/F125A PFE	Acetic acid	10 ± 1	340 ± 80	30
	Hydrogen peroxide	13 ± 1	4.8 ± 0.7	3000
L29P/F57H PFE	Acetic acid	3.3 ± 0.2	380 ± 40	10
	Hydrogen peroxide	6.8 ± 0.2	3.3 ± 0.4	1000

[a] Kinetic constants were obtained at 23 °C by varying each substrate independently. The fixed acetic acid concentration was 1.4 M except for L29P PFE where it was 500 mM. The fixed hydrogen peroxide concentration was 9.9 mM, which saturates the active site and therefore yields higher values of k_{cat}. [b] Acetic acid is the likely substrate for the en-

zyme, so we refer to the substrate as acetic acid even though at pH 5.5 approximately 85 mol% is in the acetate form. The concentrations refer to the sum of both acetic acid and acetate.

Two of the double mutants - L29P/F93H PFE and L29P/F125A PFE - showed an additional two fold improvement in k_{cat}, but the K_m values increased by a similar amount, so the specificity constants did not change as compared to the single mutant L29P PFE. The k_{cat} values were 11 and 9 s^{-1} for L29P/F93H PFE and 10 and 13 s^{-1} for L29P/F125A PFE, both approximately a twofold increase over 5.1 and 4.4 s^{-1} for L29P PFE using acetic acid or hydrogen peroxide as the varied substrate, respectively. The K_m values increased approximately two fold. The molecular basis of the improvements in k_{cat} are not clear. Although the F93H substitution is next to the active site serine, molecular modeling of L29P/F93H PFE shows that the Nε of H93 is too far away to hydrogen bond to either H251 (4.4 Å) or S94 (4.9 Å).

The third double mutant - L29P/F57H PFE - showed an approximately 1.5-fold decrease in k_{cat} and a similar increase in K_m, so the overall specificity constant decreased approximately two fold as compared to L29P PFE: 20 and 2000 s^{-1} M^{-1} as compared to 10 and 1000 s^{-1} M^{-1} for L29P PFE using acetic acid or hydrogen peroxide as the varied substrate, respectively. These results suggest that the histidine at position 57 in perhydrolases does not contribute to catalysis. The pH-rate profiles of these enzymes are in Figure 2.6 of the Supporting Information.

Above, we examined the increase in perhydrolysis activity upon making the L29P substitution PFE. This increase is accompanied by a decrease in esterase activity. Below we examine the esterase activity of this variant and suggest that steric hindrance created by the L29P substitution causes the decrease. In contrast, the rate of hydrolysis of lactones, which have a different shape from esters, increases in L29P PFE.

2.2.5 Hydrolysis of esters. Wild-type PFE catalyzes hydrolysis of a wide range of esters[38], but L29P PFE catalyzes hydrolysis of only methyl esters efficiently, Table 2.3. For methyl acetate, both wild-type PFE and L29P PFE show similar kinetic constants. For ethyl acetate, the kinetic constants for wild-type PFE remain similar, but the k_{cat} for

L29P PFE decreased 11-fold and the specificity constant decreased 50-fold as compared to methyl acetate. We previously reported similar results for propanoate esters and *p*-nitrophenyl acetate, but without k_{cat} and K_m data[13]. Both wild-type PFE and L29P PFE catalyze hydrolysis of methyl propanoate at similar rates, but L29P PFE is 5-fold slower that wild-type PFE for propyl propanoate. L29P PFE catalyzes hydrolysis of *p*-nitrophenyl acetate 100-fold slower than wild-type PFE. Poor water solubility of these substrates prevented measurement of the kinetic constants. Thus, esters with an alcohol group larger than methyl appear to be poor substrates for L29P PFE, but the size of the alcohol group has little effect for wild-type PFE.

Table 2.3 Steady state kinetic constants for hydrolysis of acetate esters and ε-caprolactone by wild-type PFE and L29P PFE.[a]

Enzyme	substrate	k_{cat} [s^{-1}]	K_m [mM]	k_{cat}/K_m [s^{-1} M^{-1}]
Wild-type PFE	methyl acetate	25 ± 1	43 ± 3	600
Wild-type PFE	ethyl acetate	9 ± 1	33 ± 1	300
Wild-type PFE	ε-caprolactone	>140	>2000	50[b]
L29P PFE	methyl acetate	7.7 ± 0.2	50 ± 5	200
L29P PFE	ethyl acetate	0.67 ± 0.05	160 ± 30	4
L29P PFE	ε-caprolactone	11 ± 1	39 ± 1	280

[a]Rates of hydrolysis were measured at 23 °C using the pH indicator *p*-nitrophenol at pH 7.2 in 5.0 mM BES buffer. [b] Determined from the initial slope of rate versus substrate concentration, $R^2 = 0.996$.

2.2.6 Molecular modeling of ester hydrolysis. Molecular modeling suggests that as the carbonyl group of W28 moves closer to the catalytic serine in L29P PFE, it creates steric hindrance for alcohol moieties larger than methyl. We modeled the tetrahedral intermediate that forms upon attack of the active site serine on the ester, Figure 2.4. Key interactions include two hydrogen bonds to the oxyanion oxygen from the backbone amides of M95 and W28 and two hydrogen bonds formed from Nε of H251 to Oγ of S94 and to the alcohol oxygen, Table 2.4. For the wild-type PFE, hydrogen bond distances ranged from

2.7-2.9 Å for both methyl acetate and ethyl acetate, which indicate a strong hydrogen bonds. For L29P PFE, all four hydrogen bond distances were 2.8 Å for methyl acetate, but for ethyl acetate the distance between Nε of H251 and the alcohol group was 3.5 Å, which is too far away to make a hydrogen bond. This missing hydrogen bond likely accounts for the 50-fold lower reaction rate.

Table 2.4 Key hydrogen bond distances (Å) in the modeled first tetrahedral intermediate for hydrolysis of acetate esters and ε-caprolactone by wild-type PFE and L29P PFE [a].

Enzyme (substrate model)	oxyanion O to M95 Nα	oxyanion O to W28 Nα	His251Nε to S94Oγ	H251Nε to alcohol oxygen
Wt PFE (methyl acetate)	2.9	2.7	2.6	2.8
Wt PFE (ethyl acetate)	2.9	2.7	2.7	2.7
L29P PFE (methyl acetate)	2.8	2.8	2.8	2.8
L29P PFE (ethyl acetate)	2.7	2.7	2.7	**3.5**

[a] The program suite Maestro was used for visualization and distance measurements. Macromodel using OPLS-2005 force field was used to optimize the geometry of all models using conjugate gradient algorithm to an RMSD of ≤ 0.05 Å. The distance in bold is too far to be a hydrogen bond which indicates a catalytically non productive model.

Consistent with these modeling results, the water-accessible regions in the active site shows a smaller alcohol-binding region in L29P PFE as compared to wild-type PFE. Wild-type PFE shows a single solvent-accessible region in the active site that fits the tetrahedral intermediate for hydrolysis of ethyl acetate, Figure 2.5. In contrast, the shift of the W28 C=O moves closer to the active site in L29P PFE and separates the alcohol pocket into two regions. For this smaller pocket to fit a larger alcohol group, the alcohol moiety must twist into a different conformation, thereby breaking a key hydrogen bond. The smaller alcohol-binding region of L29P PFE supports observation of the 50-fold lower specificity constant for ethyl acetate in L29P PFE as compared to wild-type PFE. In addition, L29P causes a shift in the indole ring of W28 that enlarges the acyl pocket.

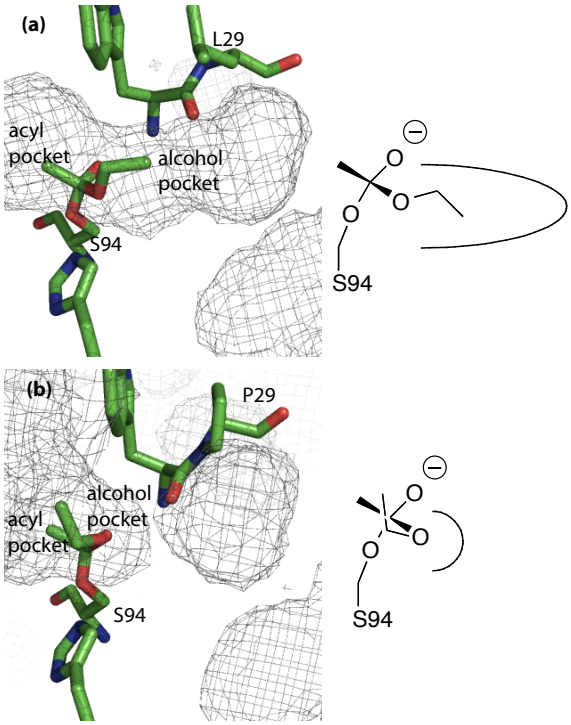

Figure 2.4 Mesh showing water-accessible regions in the active sites of wild-type PFE and L29P with the modeled tetrahedral intermediate for the acetylation of active site serine by ethyl acetate (T_d1). (A) The alcohol pocket accommodates the ethyl group of the tetrahedral intermediate and could also accept a longer alcohol, but not larger acyl groups. The acyl pocket of wild-type PFE is small while the alcohol pocket is larger, as shown on the diagram on the right side. (B) The leucine to proline substitution shifts the main chain W28 carbonyl which pinches off the alcohol pocket. The ethyl group is forced to adopt an unfavorable conformation in the enlarged acyl pocket caused by a shift in the indole ring of W28. A diagram on the right shows that the acyl pocket of L29P is larger than the alcohol pocket. The mesh shows regions accessible to a sphere with a radius of 1.4 Å, which models a water molecule. Water molecules were removed before modeling the mesh regions.

2.2.7 Hydrolysis of ε-caprolactone. Several lactonases and lactamases show perhydrolysis activity[39, 40]. For this reason, we also measured the ability of PFE and L29P PFE to catalyze the hydrolysis of ε-caprolactone. Steady state kinetics shows that L29P PFE is an approximately five fold better catalyst than wild-type PFE for hydrolysis of ε-caprolactone, due to a higher affinity towards the lactone, Table 2.3. The kinetic data for L29P PFE fit the Michaelis-Menten equation and yield a K_m of 39 mM and a k_{cat} of 11 s^{-1},

which corresponds to a k_{cat}/K_m of 280 s^{-1} M^{-1}. For wild-type PFE, the rate of hydrolysis increased linearly with increasing ε-caprolactone concentration even at 500 mM (approaching the solubility limit), so we could not fit the data to the Michaelis-Menten equation. The slope of this line was used to estimate the k_{cat}/K_m value of 50 s^{-1} M^{-1}. We estimate that K_m must be >2000 mM (at least four times the highest value tested) and that k_{cat} must be >140 s^{-1} (at least five times the value seen at a substrate concentration of $<k_{cat}/2$). In spite of the higher k_{cat} value for wild-type PFE, L29P PFE would be an approximately five fold better catalyst for hydrolysis of ε-caprolactone at the low concentrations expected *in vivo* because it binds ε-caprolactone more tightly. Unlike esters which adopt a trans conformation, lactones adopt a cisoid conformation up to 7-membered rings.

2.2.8 Molecular modeling of ε-caprolactone hydrolysis and binding. Molecular modeling of the tetrahedral intermediates for hydrolysis of ε-caprolactone yielded hydrogen bond distances of less than 3.0 Å between the Nε of H251 to Oγ of S94 and to the alcohol oxygen for both wild-type PFE and L29P PFE. (Data not shown.) However, the substrate ε-caprolactone bound better to L29P PFE than to wild-type PFE, consistent with the lower K_m of ε-caprolactone with L29P. Docking ε-caprolactone using GLIDE[41] found eight different orientations bound to the active site of L29P but only one to wild type. The larger acyl pocket in L29P accommodates the lactone better than does wild-type PFE and can account for the at least fifty-fold higher affinity for L29P PFE.

2.3 Materials and Methods

General. Water was 18-ohm purity using Milli-Q Water System (Millipore, Billerica, MA). All chemicals including acetic acid, hydrogen peroxide and peracetic acid were bought from Sigma Aldrich. Specific activity measurements were done using Costar 3635 96-well plates (Corning, Lowell, MA) and read using SpectraMax plus-384 plate reader (Molecular Devices, Sunnyvale, CA). Kinetic constants were determined by measuring the specific activity as a function of change in substrate concentration. Data was fit to the Michaelis-Menten equation: rate = V_{max} * [S] / (K_m + [S]) using software from either

OriginPro 7.5 (Origin Lab, Northampton, MA) or Kaleidagraph 4 (Synergy Software, Reading, PA). R^2 values were >0.97 for both mutants and wild-type PFE.

2.3.1 Mutagenesis. Plasmid pJOE2792 (*13*), which is an *E. coli* expression vector, has the PFE gene from *P. fluorescens* SIK WI inserted as an NdeI/BamHI fragment. Expression is regulated by a rhamnose-inducible promoter. Previously, the L29P variant of PFE was made using polymerase chain reaction (PCR)-based site-directed mutagenesis[*13*]. In this paper, the plasmid containing the L29P PFE plasmid (pL29P) was used as the template for the new mutants. Mutagenic primers, Table 2.5, were designed using PrimerX (http://bioinformatics.org/primerx/) and synthesized by Integrated DNA Technologies (IDT, Coralville, IA). A typical PCR reaction (50 µL) for mutagenesis, using *Pfu Turbo* polymerase kit (Stratagene, La Jolla, CA), was performed by initially heating the mixture of pL29P, dNTPs, primers, and 1X buffer to 95 °C for 30 s, followed by 16 cycles of 95 °C for 30 s, 55 °C for 1 min and 68 °C for 5 min 30. The amplified PCR product was treated with *Dpn*I (1 U for 1 h at 37 °C), an endonuclease that cleaves template DNA, which is methylated, but not the amplified product DNA. Next, the PCR product was transformed into *E. coli* DH5α−T1 competent cells (Invitrogen) by the heat-shock method. Transformed cells were plated on LB (Luria-Bertani broth)-agar containing ampicillin (0.1 mg/mL) and grown for 17 h at 37 °C. Individual colonies were picked and inoculated into 15-mL sterile tubes containing LB (5 mL with 0.1 mg/mL ampicillin) and grown for 17 h at 37 °C. Plasmids were isolated from the 17-h culture using a plasmid mini-prep kit (Qiagen, Valencia, CA). The mutations were confirmed DNA sequencing using sequencing primers in both the forward (64 bp upstream from the start codon, ATG) and reverse (15 bp downstream from the stop codon, TGA) by the Biomedical Genomics Center (U. of Minnesota) using ABI BigDye Terminator version 3.1 chemistry. The 17-h grown culture of *E. coli* were mixed with glycerol (20% *v*/*v*), then frozen at −80 °C for long-term storage.

Table 2.5 Nucleotide sequences of primers for mutagenesis and sequencing of pL29P[a]

Primer name	5' to 3' forward sequence	5' to 3' reverse sequence
sequencing primers	CGAGAAGGTCG-CGAATTC	CTCTCATCCGCCAAAAC A
L29P/F93H	AAGGAGGT-GACCCTGGTGGGC**CAT**T CCATGGGCGGC	GCCGCCCATGGA**ATG**GC CCACCAGGGT-CACCTCCTT
L29P/F57H	ACCGCCGCGGC**CAT**GGC CGCTCGG	CCGAGCGGCC**ATG**GCCG CGGCGGT

[a]Mutation sites in the primers are marked in bold.

2.3.2 Protein expression and purification. Typically, LB media (5 mL containing 0.1 mg/mL ampicillin) was inoculated with a single colony, then grown overnight at 37 °C. The overnight grown culture was diluted (1:100) with fresh LB media (100 mL containing 0.1 mg/mL ampicillin) and grown at 37 °C until the absorbance at 600 nm reached 0.6. Filter-sterilized rhamnose (20% w/v) was added to a concentration of 2% (w/v) to induce protein expression and the culture was incubated for an additional 3 h at 37 °C. The induced culture was centrifuged (4,000 x g, 15 min) and the cell paste was resuspended in buffer A (50 mM NaH_2PO_4, 300 mM NaCl, 10 mM imidazole) to a concentration of 20% (w/v). The resuspended culture was flash frozen in liquid nitrogen, thawed to room temperature, lysozyme added (final concentration of 1 mg/mL) and incubated on ice for 30 min. The cell lysate was centrifuged (10,000 x g, 60 min) and the supernatant was poured onto a column of Ni-NTA agarose resin (5 mL, Invitrogen) pre-equilibrated with buffer A (25 mL). The column was washed with buffer B (50 mL, 50 mM NaH_2PO_4, 300 mM NaCl, 20 mM imidazole) and the protein was eluted with buffer C (10 mL, 50 mM NaH_2PO_4, 300 mM NaCl, 250 mM imidazole). Typical yield was 10-15 mg protein or 100-150 mg/L of culture broth. Protein concentrations were measured by absorbance at 280 nm using the calculated extinction coefficient of PFE (35,410 M^{-1} cm^{-1})[15].

2.3.3 Detection of acyl-enzyme intermediate by ESI mass spectrometry. A solution of ε-caprolactone substrate (100 mM in 2 mM citrate buffer, pH 5.5, 10 μL) was mixed with enzyme PFE-L29P (9 mg/mL, 10 μL) at 4 ˚C. Water: acetonitrile (50:50 with 0.1% formic acid, 20 μL) was added immediately, the sample was loaded in a 50-μL syringe and injected into a 10-μL loop. Addition of formic acid did not significantly alter the pH (pH paper). The reaction likely occurred in the syringe as the solution warmed to room temperature, 23 ˚C. Electrospray ionization (ESI) mass spectrometry was analyzed using Qstar Pulsar (Applied Biosystems, Foster City, CA) using a Turbo Ionspray as the nebulizer. Bayesian protein reconstruction was used to deconvolute the multiply charged spectra (see Figure 2.5 in the supporting information) to yield the spectra shown in Figure 2.3.

2.3.4 Steady-state kinetic constants for perhydrolysis of acetic acid. Kinetic constants for perhydrolysis were determined using the monochlorodimedone (MCD) assay[16], where the amount of enzyme added was adjusted to give a linear dependence of the reaction rate to enzyme concentration at 23 ˚C. All reactions contained MCD (0.047 mM) and sodium bromide (149 mM). The concentrations of hydrogen peroxide and acetate were varied to give evenly spaced data points on both sides of apparent K_m, solubility limited acetate concentrations to <1.5 M, and enzyme stability limited hydrogen peroxide concentrations to <150 mM. When varying the concentration of hydrogen peroxide, the concentration of acetate was 1.00 M, when varying the concentration of acetate, the concentration of hydrogen peroxide was 9.9 mM. Some of the kinetic constants in this paper differ slightly from those in the preliminary communication[13]. The current values are believed to be accurate, but we do not clearly understand why they differ.

2.3.5 pH activity profiles for perhydrolysis of acetic acid. The initial rate of PFE-catalyzed perhydrolysis was measured with near saturating amount of acetate (1.00 M) and hydrogen peroxide (9.9 mM) while varying the pH with either NaOH (1.00 N) or HCl (1.00 N) at 23 ˚C. Acetic acid served as both a substrate and buffer, which was adjusted to the desired pH immediately before the reaction was initiated with enzyme. The amount of enzyme used varied from 0.050 to 5 μg depending on the mutant being tested and the pH. The data were fit to the equation for a doubly ionizing system using the

Solver function of Microsoft Excel. The equation used is: rate = $C[H^+]K_1/(K_1K_2 + [H^+]K_1 + [H^+]^2)$, where K_1 is the first acid ionization constant and K_2 is the second acid ionization constant[17]. C is an arbitrary constant. This equation assumes that only the singly ionized form contributes to catalysis.

2.3.6 Steady-state kinetic constants for hydrolysis of peracetic acid. Initial rates of peracetic acid hydrolysis were measured using a pHstat at pH 5.5 at 23 ˚C. A typical assay (50 mL) contained peracetic acid (0.03 to 1 mM), enzyme (typically 3.2 μg for L29P PFE and 11.6 μg for wild-type PFE) constantly mixed with a magnetic stirring bar while monitoring the amount of NaOH (0.01 N) added. The pHstat could not detect hydrolysis below 0.03 mM peracetic acid. To account for the incomplete ionization of acetic acid at pH 5.5, the k_{cat}^{app} value was increased according to the equation below, which was derived from the Hendersen-Hasselbach equation.

$rate_{true} = rate_{observed}/[10^{pH-pKa}/(10^{pH-pKa} + 1)] = rate_{observed}/0.834$

2.3.7 Steady state kinetics of L29P PFE-catalyzed hydrolysis of ε-caprolactone. Hydrolysis of ε-caprolactone was monitored colorimetrically by measuring acid release using *p*-nitrophenol as the pH indicator (*18*). Reactions were run at room temperature by mixing ε-caprolactone stock solution (19 μL in acetonitrile), 171 μL buffer (4.0 mM *N*, *N*-bis[2-hydroxyethyl]-2-aminoethanesulfonic acid (BES), pH 7.2, 0.50 mM *p*-nitrophenol, 0.33 mM Triton X-100) and 10 μL enzyme (in 4 mM BES buffer, pH 7.2). The hydrolysis rates were determined from the decrease in absorbance at 404 nm as a function of time. The extinction coefficient for *p*-nitrophenoxide is 16600 M^{-1} cm^{-1}. The ratio of [BES]: [*p*-nitrophenol] is 8.47:1 so the protonation of one *p*-nitrophenol molecule indicated the release of 9.47 protons. Each reaction was run in triplicate and the average values were used for calculations. The formula for the rate calculation is

$$v\ \left(mmol\ \ s^{-1}\right) = \frac{1000 \times \Delta A/\Delta \min}{16600\ \ M\ \ cm^{-1} \times 0.58\ \ cm} \times 9.47 \times 0.0002\ \ L$$

2.3.8 Steady-state kinetic constants for hydrolysis of methyl and ethyl acetate. Initial rates were measured using a pH indicator assay which monitors the decrease in absorption of *p*-nitrophenoxide upon protonation to the phenol (pNP) (ε_{404} = 16.6 x 10^3 M^{-1} cm^{-}

^{1}) at pH = 7.2 (*18*) at 23 ˚C. To stabilize the pH, the assay mixture contained a small amount of buffer (5 mM *N, N*-bis(2-hydroxyethyl)-2-aminoethanesulfonic acid (BES), so the initial rates were adjusted to include the protons that were buffered by BES: $v_{true} = v_{obs.}$*(1 + 5 mM BES)/(0.81 mM pNP). A typical reaction mixture contained 50 to 500 mM of either methyl or ethyl acetate with 0.81 mM pNP, 5 mM BES and 0.050 to 5 μg enzyme.

2.3.9 Crystallization, data collection and structure determination of L29P PFE. Initial crystallization screens were performed using the hanging-drop vapor-diffusion method in a 24-well plate. The precipitant solutions ranged in pH from 5.0-7.5 and contained between 1 and 2 M $(NH_4)_2SO_4$ and 0-2% polyethylene glycol. Drops contained 3 μL protein solution (10 mg/mL) and 5 μL precipitant solution. The best crystallization conditions were 1.7 M $(NH_4)_2SO_4$, 0.1 M $NaKH_2PO_4$ pH 7.5, which are similar to the best ones for wild-type PFE[*19*]. Crystals were flash-frozen to 93 K after brief immersion in a cryoprotectant solution consisting of precipitant solution with glycerol (25% *v*/*v*) added. Data for L29P PFE was collected at beam line X29 at the National Synchrotron Light Source, Brookhaven National Laboratory (Upton, NY) using an ADSC (San Diego, CA) Quantum-315 CCD detector. Data were reduced using d*TREK[*20*]. Crystals of the L29P PFE were isomorphous with crystals from wild-type PFE (PDB ID: 1VA4). Models of the mutant protein were generated from wild-type PFE using the software O[*21*]. Refinements were performed using Refmac version 5 of the CCP4 Suite of crystallographic programs (1994)[*22*], summarized in Table 2.6. Rigid body refinements allowing each of the six polypeptide chains in the asymmetric unit to move independently were followed by restrained maximum likelihood refinement. Medium or loose NCS restraints were used throughout the refinement. Water molecules were placed using ARP/WARP[*23*]. Final fitting of the models was done in O using SigmaA weighted $2F_o$-F_c maps[*24*] The structures were validated using PROCHECK[*25*]. The L29P PFE protein crystallized as a dimer of trimers and had no significant deviation from the main-chain conformation of the wild-type protein, except at the oxyanion loop close to the active site. Each monomer of the asymmetric unit contained a continuous density from the S94 side chain, which could not

be unambiguously identified as glycerol, water or buffer. Our best guess was a tetrahedral intermediate for hydrolysis of ethyl acetate, which is a poor substrate for L29P PFE. Ethyl acetate was not present in the crystallization buffer, so this assignment is speculative and this adduct in not shown in Figure 2.2. The refined structure of L29P PFE was deposited in RCSB Protein Data Bank (www.rcsb.org), PDB ID: 3hea. X-ray structures of wild type and L29P and of CPO-F with L29P PFE were superimposed using the software Chimera[26] or Pymol[27].

2.3.10 Crystallization, data collection and structure determination of L29P PFE/ acetate. Crystals of L29P were immersed in mother liquor solution containing glycerol (25% *v*/*v*) for 1 min, then transferred to a drop (10 μL) containing mother liquor solution with glycerol (25% *v*/*v*) and 250 mM acetate at pH 5.0 ("soak solution") for 30 s. The crystal was then transferred 2 more times into fresh soak solutions for a total soak time of 90 s, then the soaked crystals were quickly flash-frozen to 77 K. Data for L29P PFE was collected at The Kahlert Structural Biology Laboratory of the University of Minnesota using Rigaku MSC Micromax 007 X-ray generators with R-axis IV++ image plates. Data was collected using Crystal Clear. Crystals of the L29P PFE were isomorphous with crystals from wild-type PFE (PDB ID: 1VA4). The structure was solved by molecular replacement using MOLREP[28] in the CCP4 Suite of crystallographic programs (1994). Models of the mutant protein were generated from wild-type PFE using the software Coot[29]. Refinements were performed using Refmac version 5 of the CCP4 Suite of crystallographic programs (1994)[22], summarized in Table 2.6. Rigid body refinements allowing each of the six polypeptide chains in the asymmetric unit to move independently were followed by restrained maximum likelihood refinement. Medium or loose NCS restraints were used throughout the refinement. Water molecules were placed using ARP/WARP[23] from CCP4 and Find Waters/Solvate in Coot. Final fitting of the models was done in Coot using SigmaA weighted $2F_o$-F_c maps. The structures were validated using PROCHECK[25] and Molprobity[30]. The L29P PFE soaked with acetate shows a single acetate molecule in the active site. In addition, the *cis*-Pro 29 bond adopts the same orientation as in L29P PFE. The structure has been deposited in the RSCB Protein Data Bank

(www.rcsb.org) as structure 3hi4.

Table 2.6 Data-collection and refinement statistics for L29P PFE, and L29P PFE with acetate.

	L29P PFE (3hea)	L29P PFE/ acetate (3hi4)
Data Collection		
Space Group	$P3_2$	$P3_2$
Unit-cell parameters		
$a = b$ (Å)	145.59	145.49
c (Å)	128.20	129.99
$\alpha = \beta$ (°)	90	90
γ (°)	120	120
No. reflections		
Observed	604510	228713
Unique	231042	138751
R_{sym} (%)		
Overall	5.6	7.9
Highest Shell	31.3 (1.99-1.9 Å)	26.5 (2.29-2.25 Å)
Completeness (%)		
Overall	96.5 (93.5)	99.6(98.8)
I/σ (I)		
Overall	10.5 (3.0)	12.3 (2.15)
Refinement		
Resolution range (Å)	48.11-1.90	39.97-2.25
R_{work} (highest shell) (%)	19.0 (28.9)	16.6 (26.5)
R_{free} (highest shell) (%)	21.2 (30.8)	20.3 (30.7)
R.m.s deviations from ideality		
Bond lengths (Å)	0.006	0.03
Bond angles (°)	0.930	1.97
Ramachandran analysis		
Most favored (%)	91.3	97.03
Allowed (%)	8.3	2.57
Generously Allowed (%)	0.4	0.4

Disallowed (%)	0.0	
Final model		
No. of atoms		
Protein	12924	12802
Solvent (H_2O and glycerol)	1271	1192
Mean *B* factor (Å^2)		
Main chain	22.25	27.96
Side chain	23.21	29.59
Solvent	31.68	35.69

2.3.11 Molecular modeling. Modeling and visualization of wild type and L29P PFE were done using Maestro (Schrödinger, Portland, Oregon) at the Minnesota Supercomputing Institute (U. of Minnesota). Macromodel using OPLS-2005[31] force field and the conjugate gradient algorithm were used to optimize the geometry of all structures until the root mean square deviation was ≤ 0.05 Å. First, hydrogens were added to the backbone and side chains of a single subunit of either L29P PFE or wild-type PFE. The ε nitrogen of the catalytic histidine, His251 was protonated for modeling of the first tetrahedral intermediate. The geometry of the hydrogens attached to the subunit were optimized to minimize the energy of the whole structure. Next, the first tetrahedral intermediate for either methyl, ethyl acetate, or ε-caprolactone was built on the catalytic serine 94, and its geometry was optimized. Finally, the geometry of the entire structure and intermediate was optimized.

2.3.12 Docking ε-caprolactone into PFE using GLIDE. Structures of PFE wild type and L29P PFE were prepared using Protein Wizard Prep in Maestro, which added missing hydrogen atoms and optimized bond angles and distances. Separately, the structure of ε-caprolactone was prepared and optimized using OPLS-2005. The ε-caprolactone was positioned in the active site such that the carbonyl oxygen of the substrate was within hydrogen bond distance (2.5 Å to 3.0 Å) of αN of M95 and W28 while the carbonyl carbon is positioned ~1.5 Å from S94 Oγ. The outer boundary box was set to 20 Å, which covers

>95% of the protein, while the inner boundary box (ε-caprolactone) was set to a maximum of 14 x 14 x 14 Å. A standard precision model was used to generate all poses.

2.4 Discussion

Two experiments support the acyl-enzyme mechanism: the detection of the acyl-enzyme intermediate by mass spectrometry and the observation of an acetate complex by x-ray crystallography that is consistent with an enzyme-substrate complex that reacts via an acyl enzyme. The molecular weight observed for the acyl-enzyme intermediate is also consistent with a noncovalent enzyme-ε-caprolactone complex since the molecular weight is the same as that for the acyl-enzyme intermediate. An example of a noncovalent complex observed by mass spectrometry is phosphoenolpyruvate complexed to 3-deoxy-D-manno-octulosonate 8-phosphate (DO8P) synthase[42]. This enzyme binds phosphoenolpyruvate tightly (K_m = 3.1 μM), which allows the complex to persist during mass spectrometry. In our case, L29P PFE binds ε-caprolactone 10,000 times less tightly (K_m = 39 mM), so a noncovalent complex is unlikely. Therefore, the acyl-enzyme intermediate is the most likely assignment. The X-ray crystal structure of the substrate (acetate) complex with PFE favors the acyl-enzyme mechanism because the acetate orientation is consistent with attack of the active site serine at the carbonyl. Importantly, these crystals formed at pH 5.0, near the optimum of 5.5 for perhydrolysis. This structure likely contains the substrate in its reactive form as acetic acid. The pH-activity profiles (see Supporting Information) show that acetic acid not acetate is the reactive form of the substrate. Previous experiments to distinguish the acyl-enzyme mechanism from the noncovalent mechanism for PFE yielded ambiguous results; see discussion in the Supporting Information.

Modeling based on the x-ray structure of L29P PFE and the acyl-enzyme mechanism can explain the observed increase in perhydrolysis[13]. Molecular modeling of the second tetrahedral intermediate for perhydrolysis using molecular mechanics showed an additional hydrogen bond from hydrogen peroxide to the C=O of W28 of L29P PFE, but the same distance is too far way for wild-type PFE. This hydrogen bond can stabilize the

transition state for perhydrolysis and is the molecular basis for the increased perhydrolysis activity. Lee and coworkers[43] did additional modeling that agrees with this proposal. They used quantum mechanics to calculate the charges, bond distances, and angles for the second tetrahedral intermediate to create a more accurate model of the second tetrahedral intermediate. Modeling of this tetrahedral intermediate with a molecular mechanics force field showed the same hydrogen bond between hydrogen peroxide and the C=O of W28 of L29P PFE. Further, this hydrogen bond persisted during a molecular dynamics simulation of 5 ns as the conformation of the protein and tetrahedral intermediate changed. This stability of this hydrogen bond supports the notion that it is an important contribution to catalysis. A similar simulation of using wild-type PFE showed no hydrogen bond, even during the molecular dynamic simulation where the C=O of W28 could move closer to the active site. The authors did not model the Michaelis complexes for these reactions, but we hypothesize that this hydrogen bond could also form in the Michaelis complex and account for the increase in k_{cat} by eliminating nonproductive binding of hydrogen peroxide. In wild-type PFE, the hydrogen peroxide binds with a similar affinity, but, we hypothesize, in a nonproductive orientation, which hinders catalysis and lowers k_{cat}. Shifting this nonproductive orientation to a productive orientation in L29P PFE increases k_{cat}.

The increase in the specificity constant for reverse reaction – hydrolysis of peracetic acid – is mainly due to decrease in K_m and not an increase in k_{cat} as in perhydrolysis of acetic acid. The substrate is peracetic acid, which is a more complex structure than hydrogen peroxide. It does not bind tightly to wild-type PFE, but adding a hydrogen bond between the carbonyl oxygen of W28 and peracetic acid increases the affinity of the enzyme for this substrate. We hypothesize that nonproductive binding is not significant for this substrate. The new hydrogen bond also accounts for this decrease in K_m.

The high rate of the reverse reaction shows that L29P PFE is a very efficient catalyst near the diffusion limit. For this reason, the specificity constant for the forward reaction cannot be significantly improved. Biocatalysis normally occurs in solutions containing substrate concentrations well above K_m, so k_{cat} is the more important constant. It may

be possible to increase k_{cat} at the expense of increasing K_m. Consistent with this expectation, two double mutants – L29P/F125A PFE and L29P/F93H PFE – enhanced the k_{cat} for perhydrolysis of acetic acid two fold, but at the cost of increasing K_m as compared to L29P PFE. Bugg and coworkers made a N109H mutation in a C-C hydrolase, which is analogous to the F93H substitution above[44]. The N109H substitution increased the specific activity of ester aminolysis by hydroxylamine approximately four fold. These researchers hypothesized that the substitution may help orient the hydroxylamine. In our case, the F93H substitution in the L29P PFE increased k_{cat} approximately two fold, but the K_m for hydrogen peroxide increased, making it unlikely that this substitution contributes to the binding of hydrogen peroxide. This different explanation for the effects of analogous substitution is consistent with the different proposed mechanism for the two enzymes.

Steric hindrance within the alcohol binding site created by the L29P mutation decreases the esterase activity. The specificity constant for L29P PFE towards hydrolysis of ethyl acetate is 75-fold lower than in the wild-type enzyme. A model of the first tetrahedral intermediate using ethyl acetate shows that the distance between the catalytic H251 and the alcohol group is too far away (3.5 Å) to make a hydrogen bond. In addition, the model reveals a dihedral twist of the alcohol group that resembles the structure of lactones. Consistent with this rationale, the k_{cat}/K_m value for ε-caprolactone increased five fold in L29P PFE as compared to wild-type PFE.

One possible biological role for perhydrolases is lactone hydrolysis. L29P PFE, and presumably CPO-F, shows higher lactonase activity than esterases. *Pseudomonas fluorescens* strains can degrade four-ring polynuclear aromatic hydrocarbons[45], which can involve lactone intermediates, so there is a biological role for the lactonase activity. In addition, at least two other lactonases[39] and a lactamase[40] show perhydrolase activity.

Another biological role of perhydrolases may be to detoxify peracetic acid as suggested previously by Shimizu and coworkers[46]. Perhydrolases, including L29P PFE, catalyze the hydrolysis of peracetic acid to hydrogen peroxide and acetic acid. Catalase

can further detoxify the hydrogen peroxide. The L29P substitution in PFE decreased the K_m for peracetic acid to less than 0.003 mM as compared to wild type of 41 mM. The k_{cat} increased modestly. These kinetic constants would enable the enzyme to detoxify very low concentrations of peracetic acid to protect the cell. Disruption of the perhydrolase gene in a soil bacterium increased its sensitivity to peracetic acid and conversely, expressing a perhydrolase in *E. coli* increased its resistance to peracetic acid[46]. The biological role of perhydrolases is unlikely the formation of peracetic acid because the *in vivo* concentrations of acetic acid and hydrogen peroxide are too low to make appreciable amounts peracid. For example, an *in vivo* concentration of 7 mM acetic acid and 7 mM hydrogen peroxide would yield only ~ 0.02 μM peracetic acid at pH 7. This value is based on an equilibrium constant of 2 for the perhydrolysis of unionized acetic acid and accounts for the predominantly ionized form of acetic acid at pH 7[47]. In contrast, Shimizu and coworkers used a 30,000-fold higher amount – 600 μM peracetic acid – to inhibit bacterial growth[46]. A natural source of peracetic acid is the oxidative decarboxylation of pyruvate by thiamin pyrophosphate dependent acetolactate synthases[48]. This side reaction causes the oxygen sensitivity of some anaerobic organisms and perhydrolases may reduce this sensitivity. For biocatalysis, however, the synthesis of peracetic acid is a very useful reaction.

These results reported herein also provide insight into mechanisms of divergent evolution of new catalytic activities. The catalytic mechanisms of ester hydrolysis, lactone hydrolysis, and perhydrolysis are similar, so that the wild-type enzyme can catalyze all three of these reactions. The single amino acid substitution L29P dramatically changes the relative efficiency of these reactions by changing the substrate binding. Hydrogen peroxide and lactones bind better, ethyl esters bind worse. Modern divergent enzymes, like the esterase and perhydrolase from *Pseudomonas fluorescens*, typically differ by tens or even hundreds of amino acid substitutions. Mechanistic analysis suggests that the new catalytic reaction mechanisms require only a few substitutions. The experiments in this paper show how and why a single amino acid substitution dramatically changes catalytic activity.

2.5 Supporting Information.

2.5.1 Electrospray mass spectra of acyl enzyme intermediate. Figure 2.5 shows the actual spectra showing the multicharged ions observed in the electrospray mass spectra. This figure is the data from which the doconvoluted spectra shown in Figure 2.3 of the paper are based.

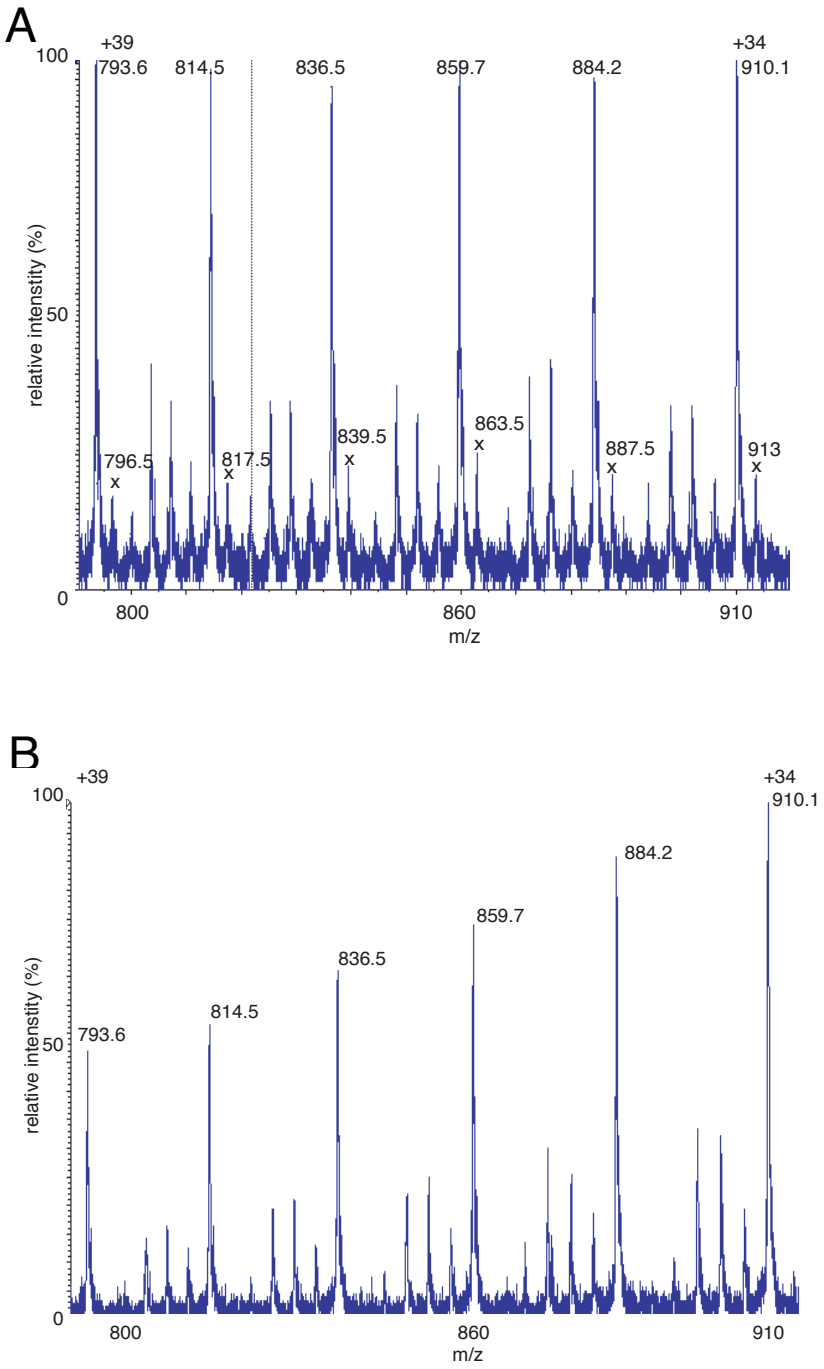

Figure 2.5. Electrospray ionization mass spectra for the +34 to +39 charged ions of L29P PFE with and without ε-caprolactone. A) L29P with ε-caprolactone in citrate/ formate at pH ~5.5 forms the acyl-enzyme intermediate. The peaks that are assigned to the intermediate are denoted with an "x" and the corresponding m/z. B) L29P PFE only in citrate/formate at pH ~5.5.

2.5.2 pH-rate profile of perhydrolysis catalyzed by mutants and wild-type PFE. The pH rate profile for enzyme-catalyzed perhydrolysis is a bell-shaped curve, Figure 2.6, in contrast to a rise at pH 5 and a plateau for hydrolysis of esters[38]. The bell-shaped curve for perhydrolysis indicates that catalysis requires one group to be deprotonated and another to be deprotonated. We propose that the rise at at pH 4-5 corresponds to the deprotonation of the active site histidine (same as for ester hydrolysis) and the decrease at pH 6-7 corresponds to the ionization of acetic acid. The mechanism requires that the active site histidine act as a base to deprotonate the active site Oγ hydroxyl of serine. The mechanism also requires acetic acid to be in the protonated form because formation of an acetyl enzyme from acetate is unlikely or impossible. There is no corresponding decrease in activity for ester hydrolysis because the ester does not ionize.

The experimental data were fit to a doubly ionizing system giving the curves in Figure 2.6. The rise at pH 4-5 corresponded to a pK_a of 5.4 to 6.9 (range for different enzymes), which is similar the 6.5 expected for the imidazoyl moiety of histidine. The decrease at pH 6-7 corresponded to a pK_a of 4.0-5.7 (range for different enzymes), which is similar to the value of 4.8 for free acetic acid. The location of the rise or decrease does not directly indicate the pK_a; it must be calculated from a best fit of the data to a doubly ionizing system. The maximum activity occurs at pH 5.5 where the predominant species are not the catalytically active ones. Most of the imidazoyl side chain is still protonated (inactive form) and most of the acetic acid is deprotonated (inactive form). This pH of 5.5 is value where the largest concentration of both active forms coexist. The pH optimum for perhydrolysis is approximately 5.5 for four enzymes, but one - L29P/F93H PFE - shows a lower pH optimum near 5.3 due to a shift in the rise at pH 5 to lower pH. This shift may be due to a decrease in the pK_a of the active site histidine. The F93H mutation adds another histidine in the active site. Protonation of this histidine adds a positive charge and likely makes it easier to convert the active site histidine to the catalytically active, deprotonated form.

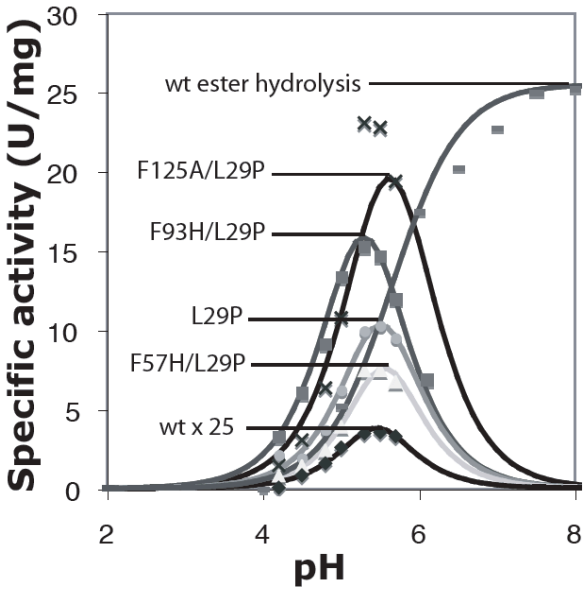

Figure 2.6. The pH-rate profile for perhydrolysis of acetic acid is a bell-shaped curve, while the profile for hydrolysis of esters reaches a plateau. Deprotonation of the active site histidine likely accounts for the increase in activity at pH 4-5 for both perhydrolysis and ester hydrolysis, since the mechanism requires the histidine to act as a base. Deprotonation of the perhydrolysis substrate acetic acid likely accounts for the decrease in perhydrolysis activity at pH 5-6. Formation of the acetyl enzyme intermediate is impossible from acetate. The shift in the pH optimum for L29P/F93H PFE may be due to a shift in the pK_a of the active site histidine. The lines are a best fit to a doubly ionizing system using a pKa of 5.4-6.9 for the rise at pH 4-5 and a pKa of 4.0-5.6 for the decrease at pH 6-7. The location of the rise and decrease does not directly indicate the pK_a. Initial rates for perhydrolysis of acetic acid were measured using the monochlorodimedone assay (1.0 M acetic acid, 9.9 mM H_2O_2, see Experimental Section). Data for hydrolysis of ethyl acetate are from reference 22, which did not report specific activity. Our measured specific activity at pH 7.2 was 18 U/mg, Table 2.2, so the data are normalized to this value.

2.5.3 Discussion of previous experiments to distinguish acyl enzyme versus a noncovalent mechanisms for PFE.

Previous attempts to distinguish betwen an acyl enzyme mechanism and a non covalent mechanism for PFE[11] did not yield a clear answer. Presteady state kinetics of PFE-catalyzed hydrolysis of *p*-nitrophenyl acetate do not show burst kinetics, but this also does not rule out either mechanism. Bugg and coworkers measured the pre-steady-state kinetics for hydrolysis of *p*-nitrophenyl acetate for several enzymes. Two enzymes (CAL-B and acetylcholine esterase) showed burst kinetics – a initial fast release of *p*-

nitrophenol ($k = 7\ s^{-1}$) followed by a slow constant release ($k = 0.03\ s^{-1}$ and $0.006\ s^{-1}$, respectively). This observation is consistent with a fast initial formation of an acetyl enzyme intermediate followed by a slower rate-limiting deacylation. Thus, the slow step in these enzymes is the release of the acetyl enzyme intermediate. PFE did not show burst kinetics; *p*-nitrophenol was released at a constant rate of $38\ s^{-1}$, which is 1200 to 6000 faster than the rate for the other two enzymes. This result means either 1) PFE catalyzes this faster hydrolysis of *p*-nitrophenyl acetate without forming an acetyl enzyme intermediate or 2) PFE still forms an acetyl enzyme intermediate, but is faster because both the acetylation step and the deacetylation step are fast. Thus, the observation of burst kinetics demonstrates an acyl enzyme intermediate, but the absence of burst kinetics is an ambiguous result. It may indicate a fast deacylation step.

Bugg and coworkers also measured the Hammett reaction parameter, ρ, for PFE-catalyzed p-nitrophenyl benzoate hydrolysis as 0.0, indicating that substituents on the benzoate do not influence the rate-determining step of the reaction. The transition state for both mechanisms involves nucleophilic attack at the carbonyl by water. Reaction of p-nitrophenyl benzoates with hydroxide shows ρ values of 2.21 indicating that electron withdrawing groups speed up the reaction. Both the non covalent mechanism and the acyl enzyme mechanism predict a positive value for ρ. Indeed, BphD, a C–C hydrolase that likely follows a non covalent mechanism, showed $\rho = +0.98$ and CALB, a hydrolase that follow an acyl enzyme mechanism, showed $\rho = +0.56$. One possible explanation is that an enzyme conformational change may be rate limiting in PFE-catalyzed hydrolysis of p-nitrophenyl benzoates. Previous work showed that benzoates are very poor substrates for PFE and the x-ray structure shows that acyl binding site is too small for the benzoate phenyl group. Thus, we hypothesize that the enzyme conformation must change before the p-nitrophenyl benzoates can react. If this change is rate-determining, it will not change with different substituents on the benzoate.

The pH-activity profiles also do not distinguish the two mechanisms. Both mechanisms require the active site histidine to act as a base to deprotonate the nucleophile hydrogen peroxide. Protonation of this histidine accounts for the drop in activity a

low pH. Both mechanisms also involve nucleophilic attack at the carbonyl and thus require the carboxylic acid form of the substrate. Deprotonation of the substrate accounts for the drop in activity at high pH. Nucleophilic attack on the carboxylate form of the substrate is impossible.

Chapter 3

Carboxylic acid perhydrolases catalyze a substitution in carboxylic acids with hydrogen peroxide to form peroxycarboxylic acids. In chapter 2, L29P PFE, the model carboxylic acid perhydrolase, catalyze the perhydrolysis of acetic acid 43-fold faster than wild-type PFE in terms of k_{cat}. The increase in activity was attributed to higher hydrogen peroxide selectivity. The mutation causes a main-chain carbonyl to move closer to the active site. We hypothesized that the main-chain carbonyl increase hydrogen peroxide selectivity by forming a hydrogen bond. In this chapter, we test the first hypothesis by measuring the nucleophile selectivity of L29P and wild-type PFE. We also generate a site-saturation library at the 29 position to test whether proline is an essential residue for perhydrolysis.

New structural motif and revised molecular basis of the promiscuous carboxylic acid perhydrolase activity in serine hydrolases

Carboxylic acid perhydrolases catalyze a substitution in carboxylic acids with hydrogen peroxide to form peroxycarboxylic acids. The five x-ray crystal structures of carboxylic acid perhydrolases all show a proline residue in the oxyanion loop, which moves a main chain carbonyl oxygen closer to the active site. Previously, we hypothesized that the closer carbonyl group increases the selectivity of the enzyme for hydrogen peroxide over water[1]. In this paper, we test this hypothesis, focusing on L29P PFE, which is a 43-fold faster perhydrolase for acetic acid that wild type PFE, and show that this hypothesis is incorrect. First, L29P PFE catalyzes hydrolysis of methyl acetate faster (k_{cat}/K_m = 200 $s^{-1}M^{-1}$) than perhydrolysis of methyl acetate ((k_{cat}/K_m = 20 $s^{-1}M^{-1}$), suggesting lower selectivity for hydrogen peroxide. Second, wild type PFE is already highly selective for hydrogen peroxide over water (β_0 = 430), but selectivity *decreases* slightly for L29P PFE (β_0 = 220). This decrease is opposite to the prediction from the hypothesis. Third, the rate of acetyl enzyme formation measured by monitoring ^{18}O-water exchange into acetic acid, was 26-fold faster in L29P PFE (62 U/mg) than in wild type PFE (2.4 U/mg), which matches is similar to the 43-fold faster perhydrolysis in L29P PFE. Fourth, saturation mutagenesis at the 29 position of PFE identified six other amino acid substitutions beside proline that increase perhydrolysis of acetic acid at least four fold over wild type. The best variant, Leu29Ile PFE, catalyzed perhydrolysis 83 times faster that wild type PFE, which is 2-fold better than L29P PFE. A 1.8-Å resolution x-ray crystal structure of L29I PFE shows the oxyanion loop conformation is mixture of type I and II β turns, which differs from the type II β turn in L29P PFE and the other known carboxylic acid perhydrolases. This new structural motif for a perhydrolase makes the previous hypothesis for the perhydrolysis mechanism impossible. We propose a new molecular basis for carboxylic acid pehydrolysis that is consistent with the kinetics and both structural motifs. A hydrogen bond acceptor (water for one structural motif, acetate in the other) orients that acetic

acid and promotes loss of water from the tetrahedral intermediate leading to faster formation of the acetyl enzyme intermediate.

3.1 Introduction

Peroxycarboxylic acids such as peracetic acid are important reagents to add oxygen to olefins, ketones, aldehydes, transition metals, and organic sulfur and phosphorus[[2], [3], [4], [5]]. Peracids are useful disinfectants because they kill microorganisms and inactivate viruses[[6], [7]]. Peracids also remove lignin from lignocellulose to brighten pulp for paper making or pretreat biomass for biofuel production[[8], [9], [10]]. The oxidizing power of peracids is the same as for hydrogen peroxide; their advantage is that they are much faster oxidants than hydrogen peroxide. The hydroxide leaving group in hydrogen peroxide is replaced by the better acetate leaving group in peracetic acid. One disadvantage of peracids is that concentrated solutions (>70 vol%) can explode[11]. This hazard makes them hard to store and expensive to transport. In-situ formation of peracids avoids these problems.

Perhydrolysis is the formation of peracids from carboxylic acids or carboxylic acid esters and hydrogen peroxide. Perhydrolases (initially called metal-free haloperoxidases[12]) are enzymes that catalyze either of these reactions, Figure 3.1. Perhydrolysis of carboxylic acids and perhydrolysis of carboxylic acid esters have different requirements, so perhydrolases are usually efficient for only one of these reactions. The focus of this paper is perhydrolysis of carboxylic acids. All perhydrolases identified so far resemble esterases since they have an α/β hydrolase fold and contain a Ser-His-Asp catalytic triad in their active site. Given the reactive nature of peracids and low natural concentrations of hydrogen peroxide, it is highly unlikely that perhydrolysis is the natural function of these enzymes. Instead, perhydrolysis is an accidental (promiscuous) function of these enzymes. Understanding the molecular basis of perhydrolysis is an important step to the design of more efficient enzymes for this reaction and to understand how new, unnatural functions occur in enzymes.

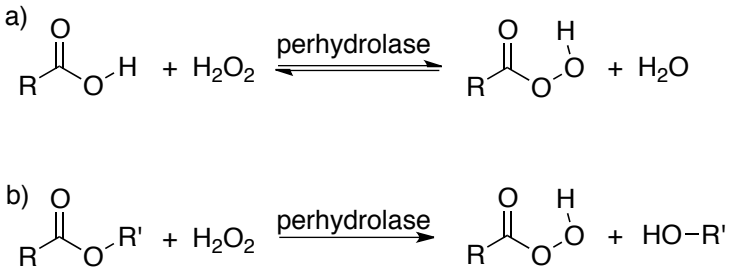

Figure 3.1. Perhydrolases catalyze the reaction of hydrogen peroxide with a) carboxylic acids or b) carboxylic acid esters to make peroxycarboxylic acids. This paper focuses on the perhydrolysis of acetic acid to make peracetic acid.

The essential structural feature of carboxylic acid perhydrolases is a conserved proline in the oxyanion loop that places this loop closer to the active site serine than in hydrolases, Figure 3.2. The five x-ray crystal structures of carboxylic acid perhydrolases all show a proline residue with a cis conformation of its amide bond in the oxyanion loop. Comparing these structures to the structure of a related esterase (*Pseudomonas fluorescens* esterase, PFE) shows that this proline residue moves the oxyanion loop closer to the active site. In a typical esterase like PFE, the distance between carbonyl oxygen of amino acid after proline and the active site Ser-Oγ is 6.2 Å. For perhydrolases this distance is ~1 Å closer: 5.1 Å bromoperoxidase A1[13], 4.7 ((-) γ-lactamase)[14], 5.6 Å chloroperoxidase-T[13], 5.2 Å chloroperoxidase-L[13], and 5.3 Å dihydrocoumarin hydrolase[15]. Site-directed mutagenesis of PFE to introduce this proline increased its perhydrolysis activity 43-fold and, as in other perhydrolases, moved the carbonyl oxygen of W28 closer to the active site: Trp28 carbonyl oxygen to the active site Ser-Oγ is 5.5 Å . How this structural difference between esterases and carboxylic acid perhydrolases accounts for their different reactivity is the focus of this paper.

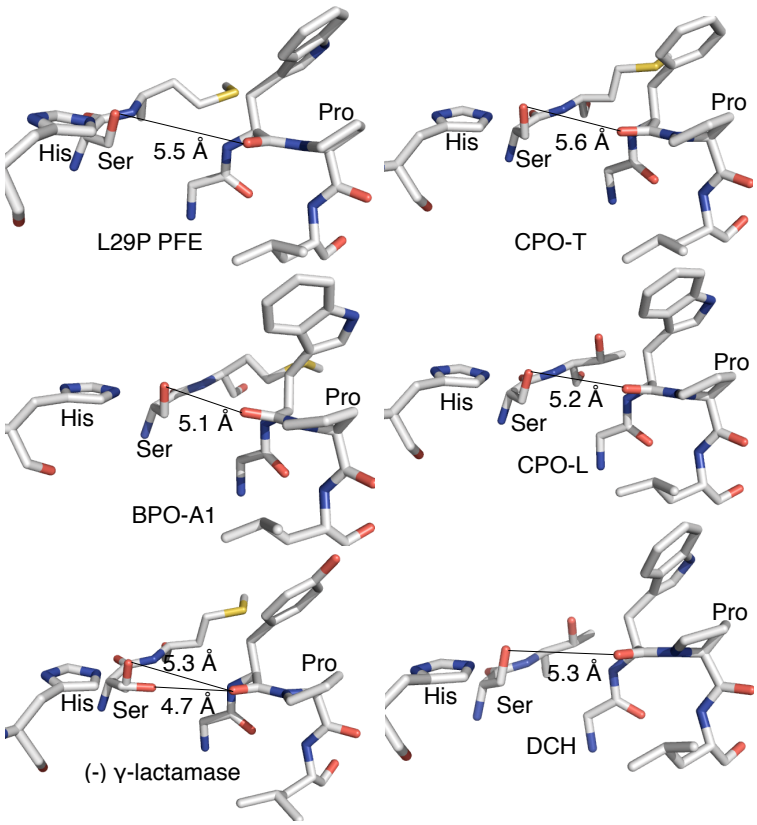

Figure 3.2. A shortened distance (5.1 - 5.5 Å) between Ser Oγ and a carbonyl oxygen adjacent proline in the oxyanion loop is the key structural feature of carboxylic acid perhydrolases. In typical esterases, this distance is 6.2 Å. Site-directed mutagenesis in an esterase (PFE, *Pseudomonas fluorescens* esterase) to introduce a proline in the oxyanion loop created a similar distance; moreover, it increased perhydrolysis activity 28-fold. (-) γ-lactamase contains two measurements because the crystal structure shows two conformations of the Ser-Oγ. The conformation corresponding to the 5.3 Å distance is likely the catalytic one since it is similar to the one in the other perhydrolases. Abbreviations: bromoperoxidase-A1, BPO-A1; chloroperoxidase-T or L, CPO-T or L; dihydrocoumarin hydrolase, DCH.

The catalytic mechanism for serine-hydrolase catalyzed perhydrolysis is similar to that for hydrolysis, Figure 3.3a. The catalytic serine reacts with acetic acid to form an acetyl-enzyme intermediate[1]. This first step involves a tetrahedral intermediate, T_d1; the transition state resembles this intermediate. In the second step, water reacts with acetyl enzyme via a second tetrahedral intermediate, T_d2, to form the product peracetic acid. The overall kinetic mechanism is ping pong bi bi where the first substrate, acetic acid,

reacts with the enzyme to form the acetyl enzyme intermediate, and then the second substrate, hydrogen peroxide, reacts with this intermediate to form the product peracetic acid. The catalytic histidine acts is a base or acid during the reaction and the oxyanion hole (two main chain N–H's) donates hydrogen bonds to stabilize the tetrahedral intermediates and transition states.

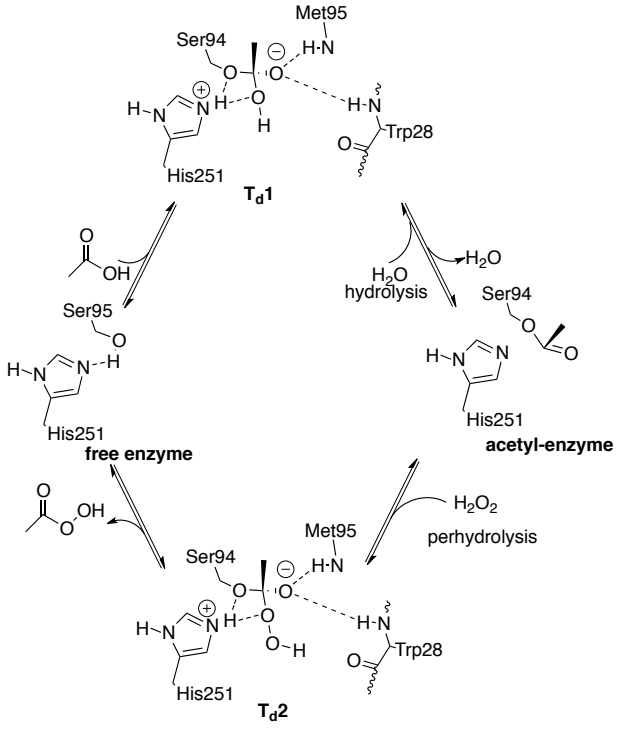

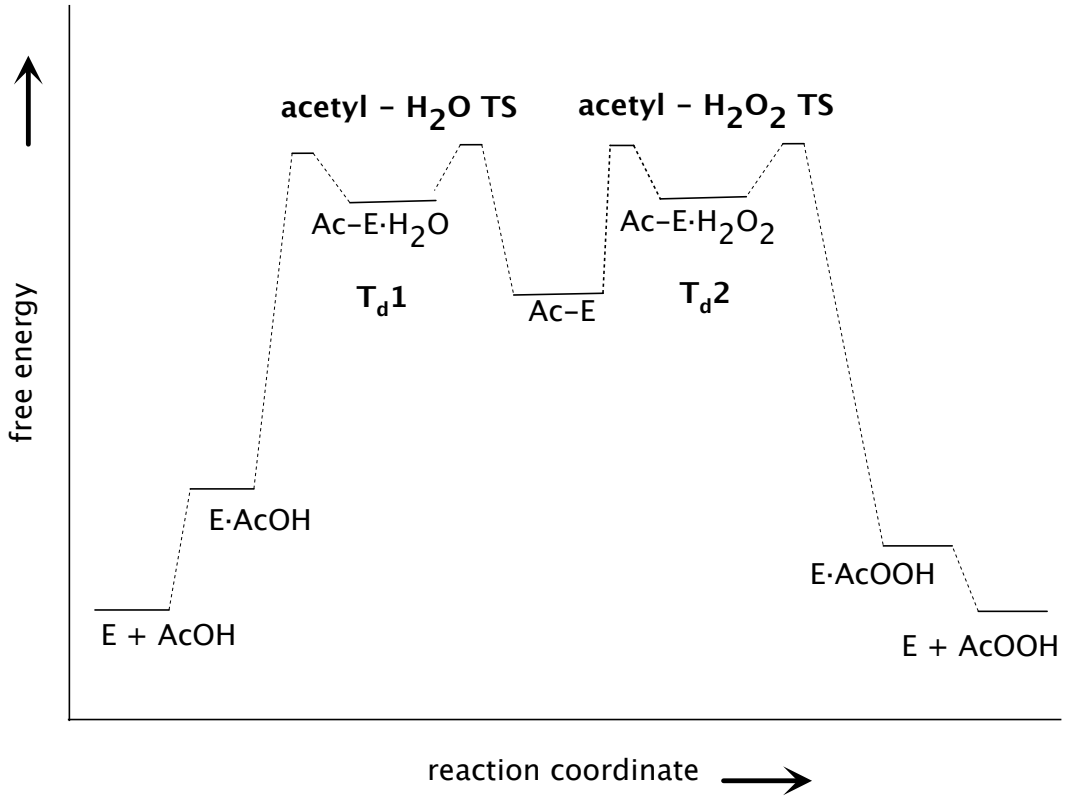

Figure 3.3. Serine-hydrolase-catalyzed perhydrolysis of acetic acid. a) Perhydrolysis of acetic acid follow the ping-pong bi bi mechanism where the first substrate (acetic acid) binds and reacts with the enzyme to form an acetyl enzyme intermediate. Next, the second substrate (hydrogen peroxide) reacts with acetyl enzyme to form the product peracetic acid. Formation of the acetyl enzyme involves attack of S94-Oγ on acetic acid to form a tetrahedral intermediate, T_d1, which releases water. Release of the acetyl enzyme involves a second tetrahedral intermediate, T_d2, which adds hydrogen peroxide. The amino acid numbering corresponds to the amino acids in PFE. The third member of the catalytic triad, Asp222, is not shown for clarity. b) Approximate free energy diagram for perhydrolysis of acetic acid involves and acetyl enzyme inter mediate (Ac–E) and two high energy tetrahedral intermediates (T_d1 and T_d2). Nucleophilic attack of the active site serine on acetic acid leads to a high energy transition state (acetyl - H_2O TS) and a corresponding tetrahedral intermediate (T_d1). Collapse of T_d1 and the release of water forms the acetyl enzyme intermediate. The binding of hydrogen peroxide forms another high energy transition state (acetyl-H_2O_2 TS) and the corresponding tetrahedral intermediate (T_d2). The release of peracetic acid results in a slightly lower energy than the starting materials because the overall equilibrium constant slightly favors peracetic acid ($K_{eq} \sim 3$).

The free energy profile of this reaction involves the multiple transition states, two tetrahedral intermediates and an acetyl-enzyme intermediate, Figure 3.3b. Nucleophilic

attack of the active site serine on acetic acid via a transition state forms the first tetrahedral intermediate (T_d1). Loss of water via another transition state forms the acetyl-enzyme intermediate. Reaction of the acetyl enzyme with hydrogen peroxide forms the second second tetrahedral intermediate (T_d2), which is similar in energy to the first one. If the acetyl-enzyme intermediate reacts with water, then reaction path is in the reverse direction back to acetic acid via T_d1.

There are two ways to change this free energy profile to increase the rate of perhydrolysis. Hypothesis 1 is to increase the proportion of acetyl enzyme that goes on to peracetic acid rather than reverts to starting acetic acid. The selectivity of hydrogen peroxide over water should be ~43-fold higher in a perhydrolase like L29P PFE than in an esterase like PFE because perhydrolysis is 43-fold faster for L29P PFE compared to PFE.

A second way to increase the rate of perhydrolysis is to increase the rate of formation of the acetyl enzyme intermediate (Hypothesis 2). The rate limiting step for perhydrolysis of acetic acid is likely the formation of the acetyl-enzyme intermediate. Formation of the an ester link in the acetyl-enzyme from acetic acid and the active site serine hydroxyl has an unfavorable equilibrium. Increasing the rate of formation of the acetyl enzyme will increase the overall rate of the reaction. If hypothesis 2 is correct, then the rate of acetyl enzyme formation should be 43 times faster for L29P PFE than for wild type PFE.

In this paper, we test both hypotheses using kinetic measurements, which rule out hypothesis 1 and support hypothesis 2. In addition, we report a new structural motif for a carboxylic acid perhydrolase in the L29I variant of PFE. This new motif is also inconsistent with hypothesis 1. Finally, we propose a new molecular basis for carboxylic acid perhydrolases that is consistent with the kinetics and with x-ray crystal structures of both types of carboxylic acid perhydrolases.

3.2 Results

3.2.1 L29P PFE is a 10-fold better hydrolase than perhydrolase for methyl acetate. L29P PFE catalyzes perhydrolysis of acetic acid 43-fold faster than wild type PFE[1]. The old hypothesis - that L29P PFE is more selective for hydrogen peroxide over water than wild-type - predicts that L29P should also catalyze perhydrolysis of esters faster than wild type PFE. Below we test this prediction and find that it is incorrect.

To measure perhydrolysis, we use the monochlorodimedone (MCD) assay[16]. Perhydrolysis was measured using the monochlorodimedone (MCD) assay. Monochlorodimedone favors the enol tautomer, which absorbs light at 290 nm. Peracid generated either chemically or enzymatically reacts with bromide ion to form hypobromous acid, which brominates MCD. This bromination prevents formation of the enol tautomer and thus decreases the absorbance at 290 nm.

Wild-type PFE (k_{cat}/K_m = 300 $s^{-1}M^{-1}$) is 15-fold more efficient than L29P PFE (20 $s^{-1}M^{-1}$) for perhydrolysis of methyl acetate, Table 1. The K_m for methyl acetate makes at 7-fold contribution to this difference, wild-type PFE (K_m = 60 mM) vs. L29P (420 mM), while k_{cat} makes a 1.7-fold contribution, wild-type PFE (15 s^{-1}) is 1.7-fold faster than L29P PFE (8.7 s^{-1}). Thus, even though L29P PFE is 100-fold better perhydrolase than PFE for acetic acid, it is a 15-fold worse perhydrolase than PFE for methyl acetate.

Table 3.1. Apparent steady state kinetic parameters for perhydrolysis and hydrolysis (in parenthesis) of methyl acetate catalyzed by wild-type PFE and L29P PFE.[a]

Enzyme	k_{cat}^{app} [s^{-1}]	K_m^{app} [mM]	k_{cat}/K_M^{app} [s^{-1} M^{-1}]
Wild-type PFE (hydrolysis)	15 ± 0.5 (25 ± 0.47)	60 ± 6.1 (43 ± 2.9)	300 (600)
L29P PFE (hydrolysis)	8.7 ± 0.5 (7.7 ± 0.21)	420 ± 70 (50 ± 4.8)	20 (200)

[a] Perhydrolysis of methyl acetate was measured at 23 °C in 100 mM citrate buffer (pH 6.5) by monitoring the absorbance at 290 nm. The concentration of methyl acetate was varied while the concentration of hydrogen peroxide was constant at 10 mM.
[b]Hydrolysis methyl acetates was measured colorimetrically using 0.45 mM p-nitrophenol as the pH indicator at pH 7.2 with 5 mM BES buffer.

To measure hydrolysis, we use *p*-nitrophenol (pNP) at pH 7.2 as a pH indicator[17]. Hydrolysis of methyl acetate forms acetic acid, which protonates pNP and reduces its absorbance at 404 nm. The apparent steady-state kinetic constants for wild-type and L29P PFE were found by fitting the initial rates data to the Michaelis-Menten formula with the Briggs-Haldane assumption of pseudo-steady-state kinetics.

Wild-type PFE (k_{cat}/K_m = 600 $s^{-1}M^{-1}$) is 3-fold more efficient than L29P PFE (200 $s^{-1}M^{-1}$) for hydrolysis of methyl acetate. The K_m of methyl acetate for both catalysts are similar, wild-type PFE (43 mM) and L29P (50 mM), but the kcat values is 3-fold higher for wild-type PFE (25 s^{-1}) over L29P PFE (7.7 s^{-1}).

Comparing hydrolysis and perhydrolysis catalyzed by L29P PFE shows that L29P PFE is a 10-fold better hydrolase than perhydrolase. The k_{cat} for perhydrolysis versus hydrolysis are similar, but the K_m towards methyl acetate shows tighter binding when water is the nucleophile as compared to hydrogen peroxide. Wild-type PFE is 2-fold more efficient at hydrolysis than perhydrolysis, so the relative hydrolysis ability is also higher for L29P PFE. This result that L29P PFE remains a better hydrolase than perhydrolase for methyl acetate contradicts the prediction that it should be a better perhydrolase due to higher selectivity for hydrogen peroxide.

One reason for this contradiction may be that measuring perhydrolysis and hydrolysis separately does not reveal the selectivity of the enzyme for the two nucleophiles. Therefore, measured the selectivity of both enzymes for hydrogen peroxide versus water.

3.2.2 Wild-type PFE is more selective than L29P PFE for hydrogen peroxide versus water. Selectivity for water and hydrogen peroxide by wild-type and L29P PFE were measured for methyl acetate as the substrate. This use of an ester substrate rather than a carboxylic acid allows measure of the initial rates of hydrolysis and perhydrolysis by detecting the release of protons, Figure 3.4. Hydrolysis of methyl acetate releases one proton due to the ionization of acetic acid. Perhydrolysis of methyl acetate does not release significant amounts of proton because peracetic acid remains mostly protonated at pH 7.2. When the solution contains NaBr, additional reactions of peracetic acid occur that

result in the release of one proton. Peracetic acid oxidizes bromide to bromonium, which reacts with additional bromide to form bromine. (An equivalent alternative is that bromonium may first react with water to form hypobromous acid and next react with bromide to form bromine.) The bromine oxidizes hydrogen peroxide to form oxygen and hydrogen bromide[18]. The overall reaction releases one proton for each peracetic acid.

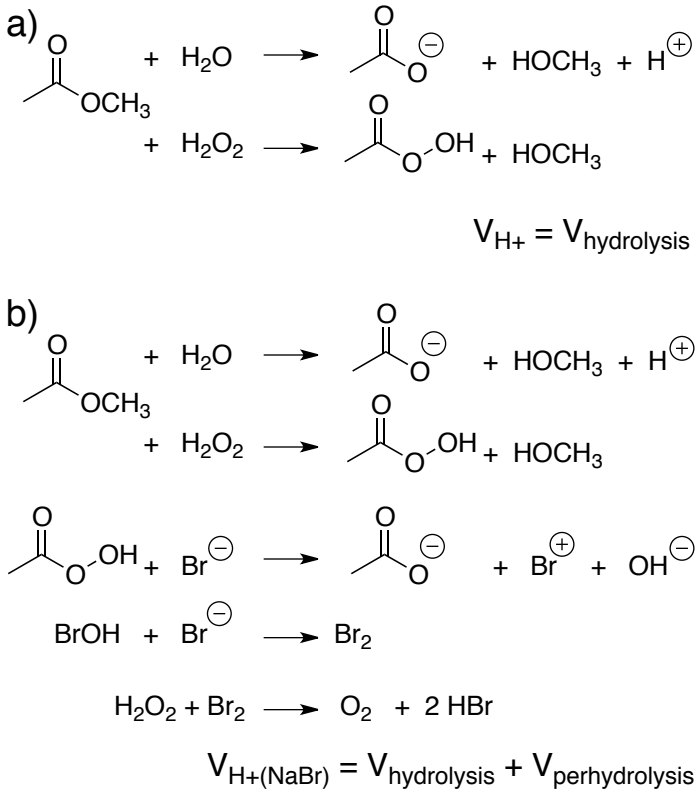

Figure 3.4. Measuring the relative amounts of perhydrolysis and hydrolysis of methyl acetate using a pHstat. a) Hydrolysis of methyl acetate at pH 7.2 releases a proton, but the accompanying perhydrolysis of methyl acetate does not release significant amounts of proton because peracetic acid (pK_a = 8.2) remain mainly protonated. b) In the presence of sodium bromide, peracetic acid reacts with bromide to also generate a proton after several steps.

Measuring the rate of proton release without NaBr reveals the rates of hydrolysis, while measuring the rate of proton release with NaBr reveals the sum of hydrolysis and perhydrolyis. The rate of perhydrolysis is the difference between the two rates, eq. 1. A plot of the rate

$$V_{perhydrolysis} = V_{H^+(NaBr)} - V_{H^+} \quad (1)$$

of perhydrolysis relative to hydrolysis (the selectivity for perhydrolysis) as a function of hydrogen peroxide concentration shows a hyperbolic saturation curve, Figure 3.5. The relative amount of perhydrolysis increases with increasing hydrogen peroxide concentration and then reaches a plateau.

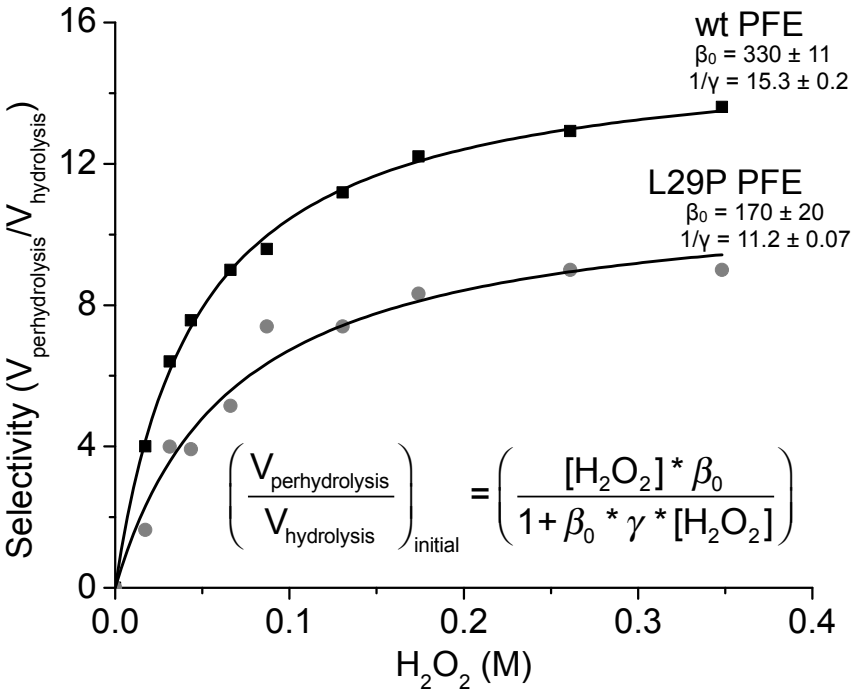

Figure 3.5. Relative initial rates of perhydrolysis to hydrolysis of methyl acetate for wild-type and L29P PFE initially increase with increasing hydrogen peroxide concentration and then reach a plateau. The initial rates of perhydrolysis and hydrolysis were determined by pH-stat. Selectivity parameters for the model in Figure 6b were determined by fitting data to the formula shown. The parameter β_0 is the perhydrolysis over hydrolysis ratio at low nucleophile concentrations and $1/\gamma$ is the perhydrolysis over hydrolysis ratio at saturating nucleophile concentrations.

To interpret this behavior, we consider two kinetic schemes for the hydrolysis and perhydrolysis reactions, Figure 3.6. The simplest kinetic scheme involves formation of the acetyl enzyme followed by competition between water and hydrogen peroxide for this acetyl enzyme, Figure 3.6a. The product ratio depends on the relative reactivity of the enzyme with each nucleophile and the relative concentrations of the two nucleophiles. The relative amount of peracid should increase linearly with increasing concentrations of

hydrogen peroxide. This simple kinetic scheme is analogous to that proposed by Bender and coworkers for the competition of the acyl enzyme in chymotrypsin for water and an alcohol nucleophile[19]. The data for both wild-type PFE and L29P PFE show a curve that flattens to a plateau at high hydrogen peroxide concentration; thus this simple model does not fit the experimental data. In previous similar cases – competition between water and alcohol nucleophile for the acyl enzyme in papain[20] and the competition between water and amine nucleophile in penicillin acylase[21] – researchers also measured a similar plateau.

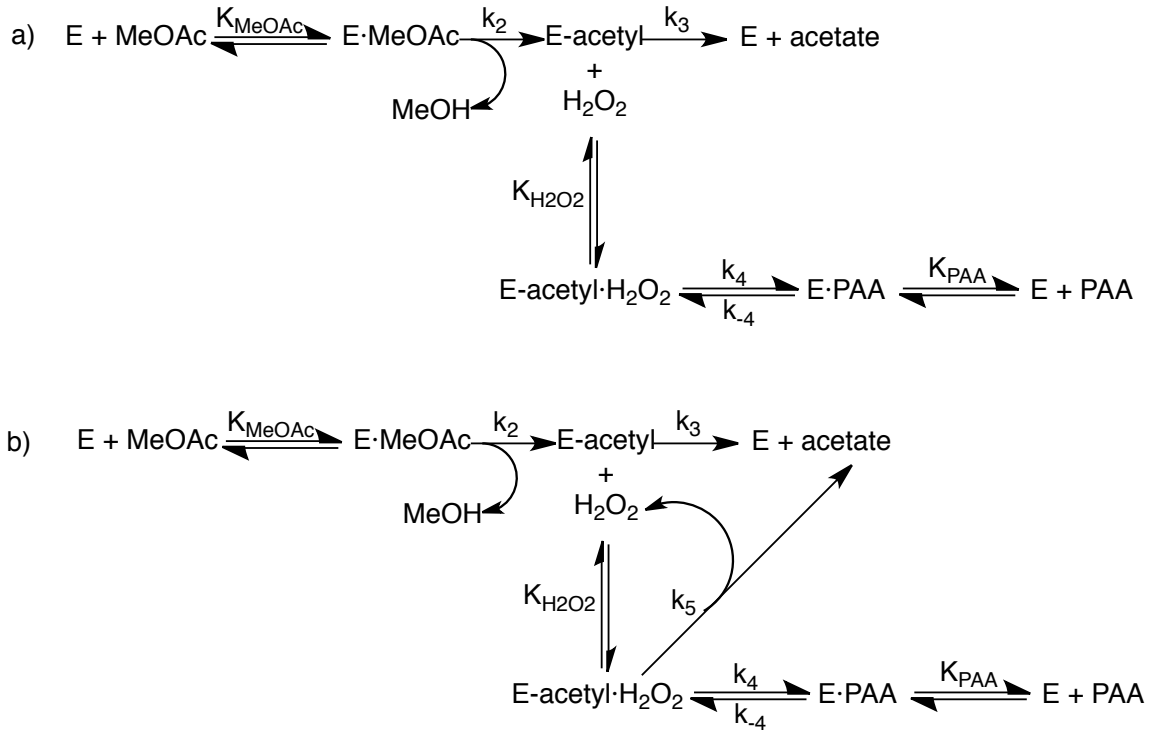

Figure 3.6. Kinetic schemes for enzyme-catalyzed perhydrolysis of methyl acetate. a) Simple scheme involving direct competition of water and hydrogen peroxide for the acetyl enzyme intermediate. This scheme predicts that ratio of peracid to acid formed depends linearly on the concentration of hydrogen peroxide. b) More complex scheme where acetyl-enzyme•hydrogen peroxide complex may also undergo hydrolysis. At low hydrogen peroxide concentrations, water and hydrogen peroxide compete for the acetyl enzyme intermediate and the relative amount of perhydrolysis increases with increasing hydrogen peroxide concentrations. At saturating hydrogen peroxide concentrations, higher hydrogen peroxide concentrations will not increase the amount of perhydrolysis.

Fink and Bender introduced a more complex model, Figure 3.6b, to account for poor fit of the data to the simple model. The more complex kinetic model provides two hydrolysis paths - at low concentrations of hydrogen peroxide, water competes directly with hydrogen peroxide for the acetyl enzyme as above, while at high concentrations of hydrogen peroxide, water can react with the acetyl-enzyme·H_2O_2 complex. This second path allows hydrolysis even when the acetyl enzyme is saturated with hydrogen peroxide. This model predicts that the ratio of perhydrolysis/hydrolysis reach a plateau once the enzyme is saturated with hydrogen peroxide.

Based on this more complex kinetic model, Youshko and coworkers[21] derived three measures of selectivity, two of which are discussed here. Their work focused on penicillin-acylase-catalyzed aminolysis of esters, but the same kinetic form applies to perhydrolysis. The parameter β_0 measures the selectivity for nucleophile over water at low nucleophile concentration, eq. 2, while the parameter $1/\gamma$ measures the selectivity for nucleophile over water at saturating nucleophile concentrations, eq. 3. Youshko and co-workers further showed that the values of β_0 and $1/\gamma$ can be determined by fitting data in similar to that in Figure 3.5 to equation 4.

$$\beta_0 = \left(\frac{k_4}{k_3 K_{H_2O_2}} \right) \tag{2}$$

$$\gamma = \frac{k_4}{k_5} \tag{3}$$

$$\left(\frac{V_{perhydrolysis}}{V_{hydrolysis}} \right)_{initial} = \left(\frac{[H_2O_2] * \beta_0}{1 + \beta_0 * \gamma * [H_2O_2]} \right) \tag{4}$$

The fit of equation 4 to the experimental data is excellent for both wild-type PFE and for L29P PFE, Figure 3.5. The fit indicates that L29P PFE is not more selective for hydrogen peroxide than wild type PFE. At low hydrogen peroxide concentration, wild-

type PFE (β_0 = 330±11) is twice as selective as L29P PFE (β_0 = 170±20) for hydrogen peroxide and at saturating hydrogen peroxide concentrations, wild-type PFE ($1/\gamma$ = 15.3±0.2) is ~40% more selective than L29P PFE ($1/\gamma$ = 11.2 ± 0.1) for hydrogen peroxide. This finding contradicts the prediction from hypothesis 1 that L29P PFE is more selective for hydrogen peroxide than wild type PFE.

3.2.3 Differences in acetyl enzyme formation measured using $H_2{}^{18}O$ exchange. The alternative hypothesis (hypothesis 2) is that L29P-PFE catalyzes perhydrolysis faster because the acetyl enzyme forms faster. To test this hypothesis, we measured the initial rate of isotope exchange of ^{18}O-water with acetic acid at pH 5.0 using gas chromatography combined with ion trap mass spectrometry. The relative abundance of ^{18}O-acetate to ^{16}O-acetate was detected at 47 and 45 atomic mass units, which corresponds to the loss of a methyl group in the ion trap. Isotope exchange involves formation of the acetyl enzyme intermediate, so faster isotope exchange indicates faster acetyl enzyme formation.

The initial rate of isotope exchange of ^{18}O-water with acetic acid catalyzed by L29P was 26-fold faster than wild-type PFE, Table 3.2. This rate increase is similar to the rate increase for perhydrolysis of acetic acid, thus, this kinetic experiment is consistent with hypothesis 2.

Table 3.2. Wild-type PFE and variants catalyzed isotope exchange.[a]

Enzyme	Isotope exchange rate,specific activity [U/mg] (rate relative to wild type PFE)	Perhydrolysis of acetic acid, specific activity [U/mg] (rate relative to wild type PFE)
Wild-type PFE	2.4 (1)	0.23 (1)
L29P PFE	62 (26)	9.9 (43)
L29I PFE	140 (58)	19 (83)

[a] The reaction mixture consisted of enzyme (0.08 mg/mL to 1mg/mL), 45 mol%, ^{18}O-water, and 1 M acetate pH 5.0. Aliquots (1 μL) were taken at different time intervals between 0 and 60 minutes, then flash frozen with liquid nitrogen. The frozen aliquots were diluted with 1.5 mL of 2.5 mM phosphoric acid buffer and immediately analyzed by GC/MS. The initial rate was adjusted to account for the 55% unobserved rate of ^{16}O-water.

A new structure motif for carboxylic acid perhydrolases

3.2.4 Saturation mutagenesis at Leu29 of PFE. The design of the L29P mutation in PFE came from sequence comparisons with carboxylic acid perhydrolases, which all have a proline in the corresponding location in the oxyanion loop. To look for other possible structures that also catalyze perhydrolysis, we used saturation mutagenesis at the 29 position of PFE to create other variants.

All seventeen L29X variants catalyzed hydrolysis of *p*-nitrophenyl acetate, but the specific activity was lower than that of wild type, Table S1. Both L29F (6.9 U/mg) and L29I (5.1 U/mg) showed almost half the activity of the wild type (14 U/mg). Variants L29P (0.10 U/mg) and L29D (0.098 U/mg) showed the lowest activity, more than 100-fold lower than wild-type PFE. We previously suggested that steric hindrance accounts for the drop in hydrolysis activity for L29P[1].

Six of the seventeen L29X variants catalyzed perhydrolysis of acetic acid at least four times faster than wild type: L29I PFE (14 U/mg), L29P PFE (9.9 U/mg), L29S PFE (1.1 U/mg), L29V PFE (0.96 U/mg), L29A PFE (0.91 U/mg) and L29E PFE (0.65 U/mg), Table 3.6. This value for L29I PFE is almost 100-fold higher than wild type PFE (0.15 U/mg). This result is surprising first because the natural perhydrolases contain a proline at position 29, not isoleucine and second because the apparently minor change of leucine to isoleucine caused a >100-fold change in perhydrolysis activity. Nine other variants (L29D, W, N, C, F, Y, H, K, Q) showed up to >20-fold decreases in perhydrolysis, seven other variants (L29S, V, A, E, G, M, T) showed 2 to 7-fold increased perhydrolysis over wild-type, and two variants (L29W, D) showed no detectable activity. The ability to change perhydrolysis over a >2000-fold range by amino acid substitutions at this position identifies this location as a key position for perhydrolysis.

3.2.5 L29I PFE is kinetically similar to L29P PFE for hydrolysis and perhydrolysis. Kinetic constants for perhydrolysis of acetic acid were determined using the monochlorodimedone assay. Steady state kinetic constants for acetic acid were obtained by varying acetic acid concentration at a constant H_2O_2 concentration of 10 mM (approximately 2 x K_m). Steady state kinetic constants for hydrogen peroxide were obtained by varying H_2O_2

concentration at a constant acetic acid concentration of 2 M (approximately 4 x K_m). The turnover number k_{cat} shows a 2-fold improvement for L29I (10 s^{-1}) over L29P (5 s^{-1}) PFE. The K_m for acetic acid increased 2-fold for L29I compared to L29P (400 vs. 200 mM) while an approximate 1.7-fold increase for hydrogen peroxide (5.7 vs. 1.8 mM) was observed. Despite an increase in k_{cat} for L29I, the overall efficiency for acetic acid and hydrogen peroxide remained the same.

Table 3.3. Apparent steady state kinetic parameters for hydrolysis of methyl acetate, ethyl acetate and ε-caprolactone and perhydrolysis of acetic acid catalyzed by wild-type, L29P- and L29I-PFE.[a]

Reaction	Enzyme	substrate	k_{cat} [s^{-1}]	K_m [mM]	k_{cat}/K_m [s^{-1} M^{-1}]
Hydrolysis[b]					
	Wild-type PFE[c]	methyl acetate	25 ± 0.47	43 ± 2.9	600
	Wild-type PFE[c]	ethyl acetate	8.8 ± 1.1	33 ± 1.0	300
	Wild-type PFE[c]	ε-caprolactone	>140	>2000	50
	Wild-type PFE[c]	peracetic acid	100 ± 3	0.041 ± 0.005	2 x 10^6
	L29P PFE[c]	methyl acetate	7.7 ± 0.21	50 ± 4.8	200
	L29P PFE[c]	ethyl acetate	0.67 ± 0.048	160 ± 29	4
	L29P PFE[c]	ε-caprolactone	11 ± 1	39 ± 0.7	280
	L29P PFE[c]	peracetic acid	139 ± 2	<0.003	5 x 10^7
	L29I PFE	methyl acetate	17 ± 0.56	64 ± 7	270
	L29I PFE	ethyl acetate	16 ± 2.6	29 ± 1.3	550
	L29I PFE	ε-caprolactone	8.0 ± 0.15	79 ± 4.3	100
	L29I PFE	peracetic acid	240 ± 2	<0.003	8 x 10^7
Perhydrolysis					
	Wild-type PFE	Acetic acid[a]	0.12 ± 0.02	500 ± 140	0.2
		Hydrogen peroxide	0.094 ± 0.002	3.3 ± 0.2	28
	L29P PFE	Acetic acid	5.1 ± 0.4	210 ± 60	20
		Hydrogen peroxide	4.4 ± 0.2	1.8 ± 0.2	2000

L29I PFE	Acetic acid	10 ± 1	400 ± 52	25
	Hydrogen peroxide	11 ± 1	5.7 ± 0.90	2000

[a] Acetic acid is the substrate for the enzyme, so we refer to the substrate as acetic acid even though at pH 5.5 approximately 85 mol% is in the acetate form. The concentrations refer to the sum of both acetic acid and acetate. Kinetic parameters for L29I were obtained by first vary acetic acid concentrations and keeping hydrogen peroxide concentration to 10 mM. Then, 2M acetic acid was held constant to vary hydrogen peroxide concentration. The pH of the reaction was held constant at 5.5. [b] Rate of hydrolysis was measured using a pH indicator assay at pH 7.2. The solutions contained 0.9 mM p-nitrophenol in 5.0 mM BES buffer and were monitored spectrophotometrically at 404 nm. Hydrolysis of peracetic acid was measured at 23 ˚C using a pHstat at pH 5.5. [c] From Yin et al.[1].

This catalytic activity of this new perhydrolase is comparable to some natural perhydrolases, but less than that of others. The first order rate constant for L29I PFE (10 s^{-1}) is faster than BPO-A2[23] (7.5 s^{-1}), nearly as fast as CPO-L (19 s^{-1})[24] and BPO-A1[23] (22 s^{-1}), but much slower than DCH[15] (100 s^{-1}). These first order rate constants were calculated from the reported specific activities (U/mg) of these perhydrolases.

Measuring the initial rate of hydrolysis and perhydrolysis of methyl acetate catalyzed by L29I PFE followed by fitting to equation 4 revealed its selectivity of for hydrogen peroxide over water. The selectivity of L29I PFE at both low and saturating concentrations of hydrogen peroxide were, within experimental error, the same as those for L29P PFE: L29I PFE: β_0 = 160± 19, $1/\gamma$ = 10±0.5; L29P PFE: β_0 = 170±20, $1/\gamma$ = 11±0.07. A plot of perhydrolysis/hydrolysis ratio as a function of hydrogen peroxide concentration is shown in Figure 3.15 of the supplemental material. This data should be shown somewhere; either in Figure 5 or in the supporting information.

The hydrolysis abilities of L29I-PFE are sometimes comparable to L29P PFE while other times comparable to wild type PFE. For methyl acetate, L29I PFE is similar to both L29P PFE and wild type PFE: 3-fold less efficient than wild-type PFE, and comparable in efficiency to L29P PFE. For ethyl acetate, L29I is 1.6-fold more efficient than wild-type PFE, and 140-fold higher than L29P PFE. L29P PFE is a poor catalyst for ethyl

and larger esters due to steric hindrance caused by moving the carbonyl of Trp29 closer to the active site serine. L29I PFE is a good catalyst for ethyl acetate because the active site remains more open as in wild type. For ε-caprolactone, L29I PFE is 2-fold more efficient than wild-type, but 3-fold worse than L29P PFE. For hydrolysis of peracetic acid, L29I PFE is 40-fold more efficient than wild type PFE and 1.6-fold more efficient than L29P PFE. For both L29I PFE and L29P PFE, the K_m was below the detection limit of the pH-stat and the high efficiency is near the diffusion limit for an enzyme-catalyzed reaction.

L29I PFE (140 U/mg) catalyzed isotope exchange between 18O-water and acetic acid is 2-fold faster than L29P PFE (62 U/mg). This increase is similar to the 2-fold increase observed for perhydrolysis of acetic acid over the L29P PFE variant. Thus, the rate limiting step for carboxylic acid perhydrolysis of L29I is the same as L29P PFE. two sentences on the 18O-exchange experiment.

3.2.6 X-ray crystal structure of L29I PFE. X-ray crystallography revealed an unusual structure of the oxyanion loop of L29I PFE. Crystals of L29I PFE formed under conditions similar to wild-type PFE. L29I/Ac was briefly immersed in mother liquor with 0.5 M acetate at pH 5.0, then mounted on a cryo-loop and frozen in liquid nitrogen. The wild-type structure served as the model to solve both L29I and L29I/Ac PFE structures by molecular replacement. The unit cell contains six nearly identical polypeptide chains having an α/β fold[25]. Superposition of the L29I and the wild-type structures show little difference: average rmsd of 0.14 Å; chain B of both structures matched most closely with an rmsd of 0.11 Å.

The major difference between L29I and wild-type PFE is in the oxyanion loop, which contains the L29I substitution. This loop occurs after strand β3 in the α/β-hydrolase fold and contains Trp28, whose main chain N–H donates a hydrogen bond to the oxyanion intermediate during catalysis, see Figure 3.3 above. In wild-type PFE this loop adopts a type II β-turn conformation, while in L29I-PFE this loop is an approximately equal mixture of a type II and a type I β-turn conformation, Figure 3.7.

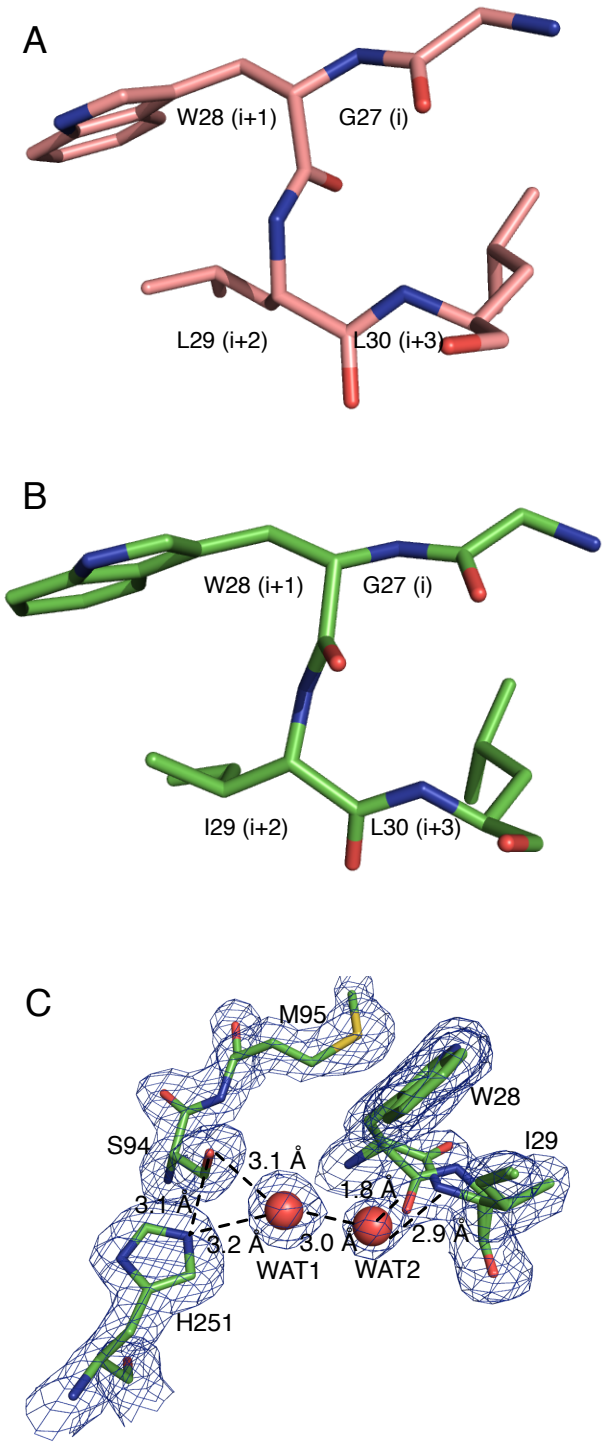

Figure 3.7. Structure of the oxyanion loop in wild-type PFE and L29I PFE. The 'i' notation refers to the β-turn starting with Gly (i) and ending with Leu (i+3). (a) The oxyanion loop in wild-type PFE (PDB code: 1VA4) is a type II β-turn where the carbonyl group of W28 (i+1) points into the plane of the paper, which is toward the active site. (b) The oxyanion loop in L29I PFE contains an approximately equal mixture of type I and II β-turns.

In the type I conformation shown, the carbonyl group of W28 (i+1) points out of the plane of the paper, which is to away from the active site. (c) Model of the active site of L29I PFE showing both type I and II β-turns overlaid with $2F_o$-F_c. Two water molecules in the active site form hydrogen bond networks, but likely only for the type I turn. For the type II turn, the water molecule WAT2 is too close to the carbonyl oxygen, so it is either missing or in a different location.

β-Turns reverse the direction of the peptide chain and consist of four amino acid residues where the first and last residues (*i* and *i* + 3) form a hydrogen bond between C=O (*i*) to N–H (*i* + 3)[[26], [27]]. This hydrogen bond is similar to the one between adjacent antiparallel beta strands; hence the name β-turn. The two central residues in a β turn (second and third residues called *i* + 1 and *i* + 2, respectively) lack hydrogen bonds between the main chain carbonyl and N–H groups. This lack of hydrogen bond is critical for catalysis in ester hydrolysis and acyl transfer since the *i* + 1 N–H group stabilizes the oxyanion intermediate by donating a hydrogen bond.

The central residues in a β turn can adopt different conformations. The type I β turn contains $\Phi_{i+1} = -60°$, $\psi_{i+1} = -30°$, $\Phi_{i+2} = -90°$, $\psi_{i+2} = 0°$, while the type II β turn contains $\Phi_{i+1} = -60°$, $\psi_{i+1} = 120°$, $\Phi_{i+2} = 80°$, $\psi_{i+2} = 0°$. Variations of ±30° from these ideal values are still classified with these conformations. In PFE these angles are –66°, 135°, 87°, –21° and thus correspond to a type II turn (*i* + 1 = Trp28, *i* + 2 = Leu29). In the type I conformation of L29I, these angles are –71°, –93°, –89°, 60° and correspond to a type I turn (*i* + 1 = W28, *i* + 2 = I29). In the type II conformation of L29I, these angles are -96˚, 137˚, 54˚, 50˚. The consequence of this difference is that the carbonyl groups of wild-type PFE W28 and L29I W28 point in opposite directions: wild-type PFE W28 points into the active site and L29I W28 points away from the active site.

The type II β turn orientation of the oxyanion loop does not differ significantly from wild-type and is therefore unlikely to cause the increase in perhydrolysis. The type I β turn orientation of the oxyanion loop is the most likely cause of the higher perhydrolysis. However, the type I β turn orientation makes it impossible for the main-chain carbonyl to accept a hydrogen bond with hydrogen peroxide because the carbonyl points

away from the active site. Thus, the molecular basis for the higher perhydrolysis must differ from that for L29P PFE.

3.2.7 X-ray structure of L29I PFE acetic acid complex. To solve the x-ray structure of L29I-PFE with acetic acid, crystals of L29I-PFE were briefly immersed in mother liquor with 0.5 M acetate at pH 5.0, then mounted on a cryo-loop and frozen in liquid nitrogen. After data collection, the structure was solved by molecular replacement using the wild-type PFE structure as the model. Like the oxyanion loop of L29I-PFE, the oxyanion loop of L29I/Ac showed a mixture of type I and II β turns. The structure of L29I/Ac also revealed two acetic acid or acetate molecules in the active site, Figure 3.8. The first acetate, ACT1 is most likely in the acid form since it is in a productive orientation for attack by the S94-Oγ. The C=O of ACT1 accepts hydrogen bonds from the oxyanion hole amides of W28 (3.7 Å) and M95 (3.5 Å). distance and angle from serine The distance from the S94-Oγ to C=O of ACT1 is 2.9 Å at an angle of 150˚. The second acetate, ACT2 is positioned near the oxyanion loop and forms a hydrogen bond (2.5 Å) with ACT1. explain why the catalytic role of the acetate is unclear. The catalytic role of ACT2 is unclear because the distance between methyl group of ACT2 and main chain carbonyl are likely much further in solution due to nonpolar-polar repulsion. The L29I structure complexed with acetate also shows a different rotamer of I29 than the apo L29I structure, Supplemental Information. This new rotomer relieves the internal steric clash caused by the apo structure but adds different steric strains such as a syn-pentane interaction.

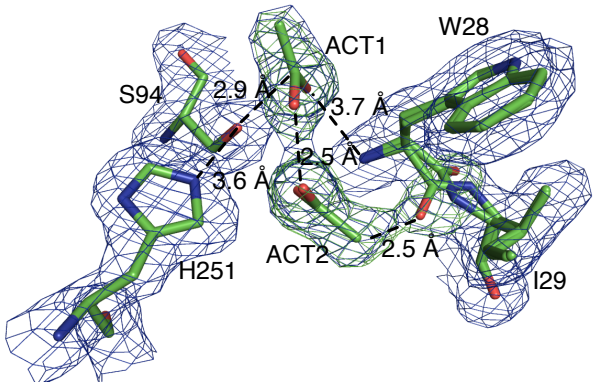

Figure 3.8. Proposed mechanism for L29I perhydrolysis of acetate. Active site of L29I/Ac showing 2Fo-Fc (blue) overlaid with Fo-Fc (green). ACT1 is an acetate in orientation ready for nucleophilic attack by the catalytic serine. ACT2 is a second acetate, which hydrogen bonds to ACT1. The methyl group of ACT2 is positioned too close to the carbonyl oxygen (2.8 Å) which suggests that the type I turn is preferred.

3.2.8 Molecular modeling of the acetate complex of L29I PFE. To identify a catalytic role for the type I β turn orientation of the oxyanion loop, we modeled the tetrahedral intermediate for formation of the acetyl enzyme (T_d1 in Figure 3.3). An acetate, acetic acid or water molecule were added in a location similar to that seen in the x-ray structure. The geometry of these complexes were optimized using the OPLS_2005 forcefield until an R.M.S.D $\leq$ 0.05 Å is reached.

The type I turn of L29I-T_d1 intermediate with acetate (Figure 3.9a) shows the acetate stabilizes the T_d1 intermediate. The T_d1 intermediate retains all of the catalytically important hydrogen bonds; the histidine forming hydrogen bond with Ser-Oγ and OH, while the oxyanion forms hydrogen bonds to the two amides (M95 and W28). In addition, the acetate forms a H-bond with the OH of T_d1 and is held in place by two amides (I29 and L30). The other structures which were modeled showed that acetic acid disrupted a critical hydrogen bond in the oxyanion hole, Figure 3.14. In the case where the T_d1 intermediate with a type II turn was modeled with acetate, the hydrogen bond between OH of T_d1 and acetate was present but without a network to hold the acetate in place. Thus, this hydrogen bond is unlikely to be stable.

The L29P-T_d1 intermediate (Figure 3.9b) uses a water molecule to form a hydrogen bond network between the OH of T_d1 and the main-chain carbonyl. The orientation of the main-chain carbonyl likely precludes a second acetate from binding to the active site. The water used in this model comes from the crystal structure of L29P soaked with acetate (PDB: 3Hi4).

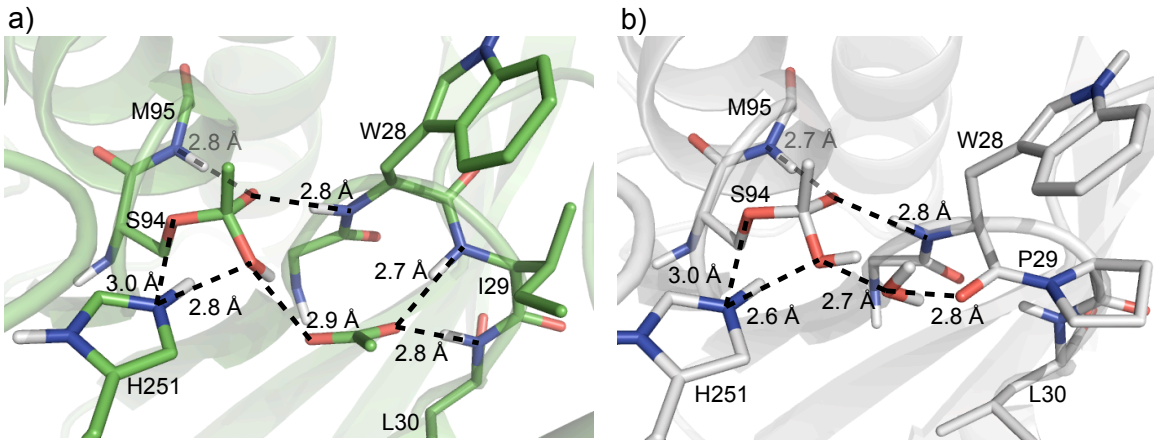

Figure 3.9. Modeling of T_d1 in PFE variants. The geometry optimized structure of L29P-T_d1 intermediate a) shows a hydrogen bond network between OH of T_d1 to water and main-chain carbonyl. Similarly, the geometry optimized structure of L29I-T_d1 intermediate b) shows an additional hydrogen bond similar to the water molecule in L29P-T_d1 intermediate. However, this hydrogen bond network uses the extra acetate nearest to the alcohol pocket. The acetate is held in place by the amide backbone of I29 and L30.

The model for L29P and L29I T_d1 intermediate shows that a stable structure can be made using water or acetate respectively. This model explains why L29I PFE is a good acetic acid perhydrolase despite the absence of the proline residue at the oxyanion hole. Additionally, the model leaves the possibility of a general base molecule that could substitute either water or acetate to stabilize the tetrahedral intermediate.

3.3 Experimental Section

3.3.1 General. Water used in all experiments was 18-ohm purity using Milli-Q Water System (Millipore, Billerica, MA). Chemicals were from Sigma Aldrich; *E. coli* DH5a-T1 competent cells were from Invitrogen (Invitrogen, Carlsbad, CA). All primers were from Integrated DNA Technologies (IDT, Coralville, IA). Enzyme activity was measured in 96-well plates using a diode-array microplate reader. Kinetic constants (V_{max} and K_M) were determined by measuring the specific activity as a function of substrate concentration. Data was fit to the Michaelis-Menten equation: rate = V_{max} * [S] / (K_M + [S]) using software from OriginLab v. 8.0 (OriginLab, Massachusetts, USA). R^2 values were >0.97 for both mutants and wild-type PFE.

3.3.2 General. Saturation mutagenesis of PFE at the 29 position. Plasmid pL29P[1] contains the L29P PFE gene, a mutant previously made by site-directed mutagenesis of pJOE2792[29]. The plasmid pJOE2792 contains the wild-type *P. fluorescens* SIK WI inserted as an NdeI/BamHI fragment. Expression of the recombinant protein by pJOE2792 and pL29P PFE are regulated by a rhamnose-inducible promoter. In this paper, the plasmid containing the L29P PFE plasmid (pL29P) was used as the template for saturation mutagenesis at the 29 position. The large size of pL29P (5.1 Kbp) prevents full amplification during PCR. Therefore, 2 sets of primers were made to amplify two halves of pL29P. A second PCR step was done linking the 2 amplified DNA from the first PCR. Mutagenic primers, Table 3.4, were designed so that the amplified products from the first PCR would have a 19-20 mer overlap. The first PCR reaction (50 μL) for saturation mutagenesis, using *Platinum taq* DNA polymerase kit (Invitrogen, Carlsbad, CA), was performed by initially heating the mixture of pL29P (50 ng), dNTPs (0.2 mM) , primers (0.2 pmol) , $MgSO_4$ (1.5 mM), and 1X buffer to 96 °C for 2 min, followed by 29 cycles of 96 °C for 30 s, 55 °C for 30 s, 72 °C for 3 min and then a final extension step for 10 min at 72 °C.

The polymerase chain reaction using two megaprimers as described in the experimental section amplified the pL29P plasmid[1] The forward primer contained a degenerate codon which coded for one of all twenty possible amino acids at position 29 was used to amplify the pL29P plasmid to make a plasmid with different codons at the 29 position. The plasmids were inserted into *E. coli* DH5a-T1 and the resulting transformants were grown overnight on agar plates containing ampicillin. Colonies were picked and the plasmids sequenced to identify all 18 variants. The identified mutants were grown in Luria broth containing 2% rhamnose to induce expression of protein. The bacteria were collected and lysed and the proteins, which contained an N-terminal 6x-His tag, were purified by nickel-affinity chromatography. Seventeen variants were isolated as soluble proteins indicating that position 29 tolerates most substitutions with the exception for arginine. The variant L29R did not express as a soluble protein so its activity could not be measured.

Initial rates for L29I PFE catalyzed hydrolysis were measured using the colorimetric assay *para*-nitrophenol (pNP) in 5 mM BES at pH 7.2. The ionized form of pNP absorbs at 404 nm. (yellow) but turns colorless when protonated. The assay monitors the decrease in pNP concentration which is used to calculate the initial rate for acetate release.

Table 3.4. Sequences of PCR primers for saturation mutagenesis.

	Name	Sequence
set 1	PFE_L29_saturation_F	tgttgttcagccacggttggNNKctggatgccgacatgtggg
	PFE2700R	CCTTATCCGGTAACTATCGTCTTGAGTCCA
set 2	PFE_L29_R	accgtggctgaacaacaccggttaccgc
	PFE2700F	TGGACTCAAGACGATAGTTACCGGATAAGG

The amplified PCR products were separately treated with *Dpn*I (1 U for 1 h at 37 °C, Invitrogen, Carlsbad, CA,), an endonuclease that cleaves template DNA, which is methylated, but not the amplified product DNA. Next, the PCR product was purified to remove enzymes, primers, buffers, and dNTPs using *MinElute* (Stratagene). The purified PCR products were mixed together in a 1:1 ratio for a second round of PCR to join the two DNA strands together. Reaction conditions were similar to the first round of PCR except the template was product 1 and 2 (200 ng for both). The 5.1 Kb product was purified using *MinElute* (Stratagene), then transformed into *E. coli* BL21-DE3 competent cells by the heat-shock method. Transformed cells were plated on LB (Luria broth)-agar containing ampicillin (0.1 mg/mL) and grown for 17 h at 37 °C. Individual colonies were picked and inoculated into sterile 96-well plates containing LB (1.2 mL with 0.1 mg/mL ampicillin) and grown for 17 h at 37 °C with shaking. The overnight culture was inoculated ster-

ile onto LB-agarose containing 0.1 mg/mL ampicillin using sterile 96 pins, grown overnight at 37 °C, then kept at 4 °C for up to 2 weeks. Plasmids were isolated from the 17-h culture using a high-throughput robot (Qiagen, Valencia, CA,). The mutations were confirmed by DNA sequencing using sequencing primers in both the forward (64 bps upstream from the start codon, ATG) and reverse (15 bps downstream from the stop codon, TGA) by the Biomedical Genomics Center (University of Minnesota) using ABI BigDye Terminator version 3.1 chemistry.

3.3.3 Protein expression and purification. Typically, LB media (5 mL containing 0.1 mg/mL ampicillin) was inoculated from a single colony, then grown overnight at 37 °C. The overnight grown culture was diluted (1:100) with fresh LB media (100 mL containing 0.1 mg/mL ampicillin) and grown at 37 °C until an absorbance at 600 nm of 0.6 was reached. Filter-sterilized rhamnose (20% *w/v*) was added to a concentration of 2% (w/v) to induce protein expression and the culture was incubated for an additional 3 h at 37 °C. The induced culture was centrifuged (4,000 x g, 15 min) and the cell paste was resuspended in buffer A (50 mM NaH_2PO_4, 300 mM NaCl, 20 mM imidazole) to a concentration of 20% (*w/v*). The resuspended culture was flash frozen in liquid nitrogen, thawed to room temperature, lysozyme added (final concentration of 1 mg/mL) and incubated on ice for 30 min. The cell lysate was centrifuged (10,000 x g, 60 min) and the supernatant was poured onto a column of Ni-NTA agarose resin (5 mL, Invitrogen) pre-equilibrated with buffer A (25 mL). The column was washed with buffer B (50 mL, 50 mM NaH_2PO_4, 300 mM NaCl, 40 mM imidazole) and the protein was eluted with buffer C (10 mL, 50 mM NaH_2PO_4, 300 mM NaCl, 250 mM imidazole). Typical yield was 10 - 15 mg protein. Protein concentrations were measured by absorbance at 280 nm using the calculated extinction coefficient of PFE (35,410 $M^{-1}cm^{-1}$)[30].

3.3.4 Steady-state kinetic parameters for perhydrolysis of acetic acid. Kinetic parameters for perhydrolysis were determined using the monochlorodimedone (MCD) assay[16], where the amount of enzyme added was adjusted to give a linear dependence of the reaction rate to enzyme concentration. All reactions contained MCD (0.0472 mM) and sodium bromide (149 mM). The concentrations of hydrogen peroxide and acetic acid

were varied to give evenly spaced data points on both sides of apparent K_M. When varying the concentration of hydrogen peroxide, the concentration of acetic acid was 2.00 M; when varying the concentration of acetic acid, the concentration of hydrogen peroxide was 10 mM.

3.3.5 Steady-state kinetic parameters for hydrolysis of peracetic acid. Initial rates were measured using a pHstat to monitor the release of acetate from hydrolysis of peracetic acid at pH 7.2 by titration using 0.01N NaOH. The amount of substrate was varied from 5 to 0.05 mM peracetic acid in a 10 mL solution. A solution of 0.01N NaOH was added to increase the pH to 7.2. The amount of enzyme added was 10 ng to insure that the initial rates for the first few minutes were linear.

3.3.6 Steady-state kinetic parameters for hydrolysis of methyl, ethyl acetate, and e-caprolactone. Initial rates were measured using a pH indicator assay[17] which monitors the decrease in absorption of *p*-nitrophenoxide upon protonation to the phenol (pNP) (ε_{404} = 16.6 x 10^3 M^{-1} cm^{-1}) at pH = 7.2. To stabilize the pH, the assay mixture contained a small amount of buffer (5 mM *N, N*-bis(2-hydroxyethyl)-2-aminoethanesulfonic acid (BES), so the initial rates were adjusted to include the protons that were buffered by BES: $v_{true} = v_{obs.}$*(1 + 5 mM BES)/(0.81 mM pNP). A typical reaction mixture contained 10 to 450 mM of either methyl, ethyl acetate or e-caprolactone with 0.81 mM pNP, 5 mM BES and 0.010 to 1 μg enzyme.

3.3.7 Steady-state kinetic parameters for perhydrolysis of methyl and ethyl acetate. Initial rates for perhydrolysis were determined using the monochlorodimedone (MCD) assay[16], where the amount of enzyme added was adjusted (5 ng/mL to 100 ng/mL) to give a linear dependence of the reaction rate to enzyme concentration. All reactions contained MCD (0.0472 mM) and sodium bromide (149 mM) and 100 mM citrate buffer at pH 6.5. The concentration of either ethyl acetate or methyl acetate were varied to give a minimum of 3 data points above and below the apparent K_m, while hydrogen peroxide concentration was kept constant at 14.7 mM. The kinetic parameters were found by fitting the initial rates to the Michaelis-Menten equation using nonlinear regression with OriginLab v. 8.0 (OriginLab, Massachusetts, USA). The single substrate Michaelis-

Menten model is valid because the second substrate, hydrogen peroxide is completely saturated.

3.3.8 Nucleophile competition between hydrogen peroxide and water. Initial rates for perhydrolysis and hydrolysis were determined by pH-stat at 23 ˚C with 0.01N NaOH as the titrant. The amount of hydrogen peroxide was varied from 14.7 to 147 mM while the concentration of ethyl acetate was held constant at 188 mM. The reaction solution was adjusted with 0.01N NaOH before the addition of enzyme to pH 7.2. The amount of protein added was 1.2 μg/mL for wild-type PFE and L29I PFE. For perhydrolysis, the 166 mM of NaBr is added to react with peracetic acid to form BrOH. At pH 7.2, BrOH ionizes to release a proton. This initial rate accounts for both hydrolysis and perhydrolysis. For hydrolysis in the presence of hydrogen peroxide, the amount of acid released corresponds to the amount of titrant added. Additionally, 166 mM of NaCl is added as a substitute for the absence of NaBr. Subtraction of perhydrolysis + hydrolysis rate from rate of hydrolysis gives the rate for perhydrolysis. The initial rate data was fit using the formula which describes on β_0, a parameter used to describe the selectivity of competing nucleophiles.

3.3.9 Isotope exchange of acetic acid with 18O-water. Initial rates for enzyme catalyzed isotope exchange was measured by observing the relative abundance of acetic acid and O18-acetic acid using gas chromatography/mass spectrometry. In a typical reaction, 45 mol% of 18O-water and 1M acetic acid pH 5.0 are mixed with enzyme (0.08 mg for L29I, 0.16 mg for L29P, 1.0 mg for wild-type PFE) to a final volume of 0.10 mL. At time points of 3, 5, 7, 10, and 13 minutes (for wild-type, the time points are taken from 21 to 60 minutes at 7 minute intervals), 1.0 μL aliquot is withdrawn and flash frozen in liquid nitrogen. Before the sample is analyzed, the 1.0 μL aliquot is diluted with 1.5 mL of 2.5 mM phosphoric acid, mixed and a 1.0 μL aliquot is injected into a gas chromatography (Varian Star 3400 CX) with DB-FFAP column (J&W Scientific). An ion trap mass spectrometer is used to detect the relative abundance of both isotopes by integrating their respective area. We found that the isotope exchange in the absence of a catalyst to be nearly

indistinguishable from the noise level. This observation is consistent with the work of Llewellyn and O'Connor[31].

3.3.10 Crystallization, data collection and structure determination of L29I-PFE. Initial crystallization were screened using the sitting-drop vapor-diffusion method in a 96-well plate. Hampton Crystallization HT (Hampton) was used as the precipitating reagent. After 1 week of growth at 20 °C , several crystals were observed in a well containing 2 M $(NH_4)_2SO_4$ and 0.1 M Bis-Tris. Crystallization conditions were further optimized by: varying the pH from 5.0−8.0, varying the concentration of $(NH_4)_2SO_4$ from 1.5 to 2 M, varying the concentration of Bis-Tris from 0.05 to 0.1 M and contained between 1.9 M $(NH_4)_2SO_4$ and 0.05-0.2 M Bis-Tris and by varying the concentration of protein solution from 10 to 18 mg/mL. The best crystallization conditions were 1.75 M $(NH_4)_2SO_4$, 0.1 M Bis-Tris pH 6.6, (3 µl to 7 µl of protein [15 mg/mL] to precipitant) incubated for 1.5 weeks at 20 °C. Crystals were flash-frozen to 93 K after brief immersion in a cryoprotectant solution consisting of precipitant solution with 25% v/v glycerol. Data for L29I PFE was collected at the Advanced Light Source (ALS) synchrotron. CCP4[32] and Coot[33] were used for all refinement and visualization, Table 5. Wild-type PFE (1VA4)[34] was used as the model for molecular replacement. Initial refinement using CCP4 showed unresolved densities around the oxyanion loop (carbonyl of W28 and αN of I29) in the $2(F_{obs}-F_{calc})$ map. Our initial model showed a type I turn in the oxyanion loop as having too much density around the carbonyl of W28 and not enough density around the αN of I29. Upon flipping the peptide backbone to a type II turn and another round of refinement, the $2(F_{obs}-F_{calc})$ map showed too much density around the αN of I29 and not enough density around the carbonyl of W28. A good density fit was only obtained by lowering the occupancy of the carbonyl W28 and αN of I29 to 50%.

Table 3.5. Data-collection and refinement statistics for L29I and L29I/Ac PFE.

	L29I PFE	L29I PFE/Ac
Data Collection		
Space Group	$P3_2$	$P3_2$

Unit-cell parameters		
$a = b$ (Å)	146.01	146.06
c (Å)	129.76	128.99
α = β (°)	90	90
γ (°)	120	120
No. reflections		
Observed	696418	1285074
Unique	282257	227594
R_{sym} (%)		
Overall	8.4	6.9
Highest Shell (1.86-1.8 Å)	34.8	40.6
Completeness (%)		
Overall	98.4(89.8)	99.9 (99.9)
I/σ (I)		
Overall	5.7 (1.9)	6.3 (2.3)
Refinement		
Resolution range (Å)	63.63-1.80	43.00-1.94
R_{work} (highest shell) (%)	18.8 (36.0)	19.4 (40.6)
R_{free} (highest shell) (%)	22.1 (41.0)	23.0 (44.1)
R.m.s deviations from ideality		
Bond lengths (Å)	0.02	0.04
Bond angles (°)	1.49	2.45
Ramachandran analysis		
Most favored (%)	98.1	98.2
Allowed (%)	1.9	1.8
Disallowed (%)	0	0
Final model		
No. of atoms		
Protein	13042	13046
Solvent	2512	1128
Mean B factor (Å^2)		
Main chain	23.54	23.06
Side chain	24.51	26.44
Solvent	41.01	30.85

3.3.11 Molecular Modeling

The protein structure of L29P PFE/acetate (PDB: 3Hi4) and L29I PFE/acetate were prepared using the Protein Preparation Wizard (Schrodinger) to remove water molecules further than 5 Å from the nearest heteroatom, while glycerol and sulfate were also removed at this point. Five out of the six protein chains in the crystal structure were removed to reduce calculation time. Hydrogen atoms were added to all heteroatoms and minimized using the OPLS_2005 forcefield until an rmsd of < 0.05 Å was reached. The entire protein structure was geometry optimized using the same forcefield until until an rmsd of < 0.3 Å was reached.

The enzyme-T_d1 intermediate was built using Maestro (Schrödinger) by attaching the acetic acid molecule already present in the crystal structure to S94-Oγ. For L29I, the acetic acid closest to the oxyanion hole was used for this purpose. The geometry of the intermediate along with additional acetate or water present in the structure was geometry optimized using the OPLS_2005 forcefield in the program Macromodel v 9.1 (Schrodinger) until an rmsd of < 0.05 Å was reached. The structure of the entire protein and water molecules were minimized using the same forcefield until a rmsd of 0.05 Å was reached.

3.4 Discussion

Perhydrolysis of acetic acid involves two steps: formation of the acetyl enzyme intermediate and cleavage of the acetyl enzyme with hydrogen peroxide. The rate determining step is likely the first step, the formation of the acetyl enzyme intermediate. To increase the rate of perhydrolysis one could either increase the rate of formation of the acetyl enzyme intermediate (first step) or increase the selectivity of hydrogen peroxide over water in the second step. Our initial hypothesis for why L29P PFE is 100-fold more efficient (k_{cat}/K_m) perhydrolase for acetic acid than wild-type PFE was because L29P PFE is more selective for hydrogen peroxide over water in this second step.

Two experiments indicate that this hypothesis is incorrect. First, comparing the hydrolase and perhydrolase abilities of L29P PFE shows it is a 10-fold better hydrolase. Using methyl acetate as the acyl donor, L29P PFE is catalyzes hydrolysis with a k_{cat}/K_m

of 200 $s^{-1} M^{-1}$ versus perhydrolysis with a k_{cat}/K_m of 20 $s^{-1} M^{-1}$. In comparison, wild-type PFE shows a similar catalytic efficiency for both hydrolysis (k_{cat}/K_m = 600 $s^{-1} M^{-1}$) and perhydrolysis (k_{cat}/K_m = 300 $s^{-1} M^{-1}$). Thus, the L29P mutation in PFE has decreased its ability to catalyze perhydrolysis of methyl acetate 15-fold, but decreased its ability to catalyze hydrolysis of methyl acetate only slightly - 3-fold. This observation is not consistent with an increase in selectivity for hydrogen peroxide in L29P PFE. For acetic acid, where hydrolase activity can't be measured, the L29P mutation increased perhydrolysis activity 100-fold and it is this increase that we seek to explain. (Esters with a larger alcohol moiety, such as *p*-nitrophenyl acetate, are poor substrates for L29P PFE because the mutation reduces the size of the alcohol binding pocket[1]. In these cases, neither hydrolysis, nor perhydrolysis occurs.)

Second, the selectivity of L29P PFE for hydrogen peroxide over water is similar to that for wild-type PFE. Measuring this selectivity used the kinetic model developed previously for acyl transfer to alcohols. Perhydrolysis is an acyl transfer to hydrogen peroxide and this kinetic model also fit the experimental data well. This model predicts two selectivities - one a low hydrogen peroxide concentration (β_0) and another a high hydrogen peroxide concentration ($1/\gamma$). The selectivity at low hydrogen peroxide concentrations, β_0, is approximately two fold lower that for wild type: 170 versus 330, while at high hydrogen peroxide concentrations, $1/\gamma$, the selectivity is about 50% higher than for wild type: 15 versus 11. In both cases, the small changes in selectivity cannot account for the 100-fold increase in the perhydrolysis activity of L29P PFE over wild type.

Saturation mutagenesis at position 29 of PFE revealed six variants with at least 4-fold higher perhydrolase activity for acetic acid over wild-type. In particular, the L29I PFE variant showed 100-fold higher specific activity for acetic acid perhydrolysis than the wild-type. Similar to L29P PFE, the L29I variant was less selective for hydrogen peroxide over water than wild-type PFE (β_0 = 160 versus 330 for wild-type). This is a second example of a PFE variant with increased activity for perhydrolysis of acetic acid, but without an increase in the selectivity of hydrogen peroxide over water.

The second possibility for why L29P PFE and L29I are better perhydrolases is that the formation of the acyl enzyme is faster for L29P PFE than for wild type. Consistent with this hypothesis, we found that L29P and L29I catalyze the isotope exchange between acetic acid and $H_2{}^{18}O$ faster (26 and 58 fold faster) than the wild-type. By comparison L29P and L29I catalyzed perhydrolysis of acetic acid is also faster (43 and 83 fold change in k_{cat}) than wild-type PFE by a similar amount to the rate of isotope exchange. Thus, the mutations that alter the activity for acetic acid perhydrolysis increase the formation of acyl enzyme intermediate.

X-ray structures suggest a molecular basis for these kinetic results. First, why is the first hypothesis incorrect? Previous x-ray structures and modeling of L29P PFE identified a potential hydrogen bond between hydrogen peroxide and the enzyme, but not between water and the enzyme[22]. This extra hydrogen bond accounts for the high selectivity of L29P PFE for hydrogen peroxide over water (β_0 = 160) and its high affinity hydrogen peroxide tightly (Km = 1.8 mM). However, this extra hydrogen bond does not lead to an improvement over wild type because wild-type PFE also contains an extra hydrogen bond, but in a different location. This extra hydrogen bond in wild-type PFE leads to a similar selectivity for hydrogen peroxide over water (β_0 = 330) and high affinity hydrogen peroxide (Km = 3.3 mM). Both enzymes form an extra hydrogen bond with hydrogen peroxide, but not with water. Both are selective for hydrogen peroxide, but both are similarly selective and this similar selectivity cannot account for the different perhydrolysis abilities.

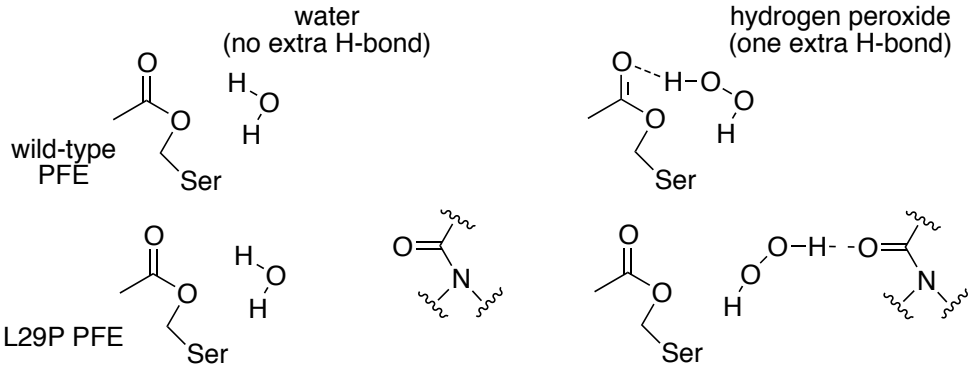

Figure 3.10. Proposed extra hydrogen bonds formed in the active sites of wild-type PFE (top row) and L29P PFE (bottom row) between water (first column) and hydrogen peroxide (second column). Water does not form any extra hydrogen bonds in the active site. Hydrogen peroxide is proposed to form one extra hydrogen bond to both wild-type PFE and L29P PFE, but the extra hydrogen bond differs in location for the two cases. In wild-type PFE, the hydrogen bond acceptor is the acetyl enzyme carbonyl carbon. This hydrogen bond is similar the intramolecular hydrogen bond in peracetic acid. In L29P PFE, the hydrogen bond acceptor is a main chain carbonyl oxygen. For clarity, the hydrogen bond between the nucleophile, either hydrogen peroxide or water, and the catalytic histidine, His251, is not shown, but is expected to be present in all four cases.

The extra hydrogen bond differs in the two cases. In wild-type PFE, the hydrogen bond acceptor is the carbonyl oxygen of the acetyl enzyme intermediate. This proposed hydrogen bond is similar to the internal hydrogen bond in peracetic acid [28]. A water molecule is smaller and therefore cannot simultaneously make this hydrogen bond and be productively positioned to attack the carbonyl carbon of the acetyl enzyme intermediate. In L29P PFE, the L29P substitution changes the Trp28-Pro29 peptide bond from *trans* to *cis*, which moves the main-chain carbonyl oxygen of Trp28 1.1 Å closer to the active site Ser94Oγ. The carbonyl oxygen of Trp28 can accept a hydrogen bond from hydrogen peroxide while simultaneously positioning it to attack the carbonyl carbon of the acetyl enzyme. As before, water is too small to simultaneously make the hydrogen bond to Trp28 and be positioned for attack of the acetyl enzyme. For hydrogen peroxide to make the hydrogen bond to Trp28, it must break the hydrogen bond to the carbonyl oxygen of the acetyl enzyme. Thus, only one extra hydrogen bond forms in wild type PFE and in L29P PFE. Because there is no difference in the number of extra hydrogen bonds, their selectivities for hydrogen peroxide are similar.

The higher perhydrolysis activities of L29P PFE and L29I PFE stems from a faster formation of the acetyl enzyme intermediate from acetic acid. The x-ray crystal structure of L29P soaked with acetic acid at pH 5.0 suggest a structural basis for this increase, Figure 2 from Yin *et* al.[1]. The structure shows acetic acid in a catalytically productive orientation. The carbonyl oxygen accepts hydrogen bonds from both N-H of the oxyanion hole and the carbonyl carbon lies 2.8 Å from Ser94-Oγ. The structure also

shows a water molecule at hydrogen bond distanced between the acetic acid and Trp28 carbonyl oxygen. This water molecule promotes a productive orientation of acetic acid for nucleophilic attack. Wild-type PFE cannot have a similar water molecule because The Trp28 carbonyl oxygen is 1.1 Å further away. Promoting the productive orientation in L29P PFE can increase the rate of formation of the acetyl enzyme intermediate. This increased rate increases the rate of perhydrolysis and isotope exchange between $H_2{}^{18}O$ and acetic acid.

X-ray crystal structure of L29I PFE shows that the carbonyl oxygen of Trp28 cannot be a hydrogen bond acceptor from hydrogen peroxide. The loop containing Trp28 is a mixture of type I and II turn conformations. In the type I turn, the Trp28 carbonyl points away from the active site, so it cannot accept a hydrogen bond from hydrogen peroxide. Instead, hydrogen peroxide presumably makes an extra hydrogen bond to the carbonyl oxygen of the acetyl enzyme intermediate as it does in wild-type PFE.

The crystal structure of L29I soaked in acetic acid pH 5.0 also shows acetic acid close to the oxyanion hole, and in a productive orientation, Figure 9. The distance between oxygen of acetic acid and two amides of the oxyanion hole are 3.7 Å (W28) and 3.5 Å (M95). The S94-Oγ is in close proximity (2.9 Å) to the carbonyl acetate for a nucleophilic attack.

The structure shows a second acetate/acetic acid molecule interacts with the productively bound acetic acid. However, the position of the second acetate/acetic acid is ambiguous in the crystal structure; distance between the methyl group and main-chain carbonyl of W28 is 2.5 Å, too close for a carbon oxygen distance. Therefore, we modeled the first tetrahedral intermediate (T_d1) in order to test if the second acetate/acetic acid molecule can form a hydrogen bond network. Molecular modeling of T_d1 with the type I turn shows that the second acetate forms a hydrogen bond network while acetic acid or a type II turn disrupts important hydrogen bonds, Figure 3.9a. We also modeled L29P in a similar manner and show that a water molecule can form a hydrogen bond network in a similar manner as the second acetate for L29I, Figure 3.9b. Thus, molecular modeling and

kinetic analysis shows that some hydrolases show faster perhydrolysis of acetic acid because they form the acetyl enzyme more faster.

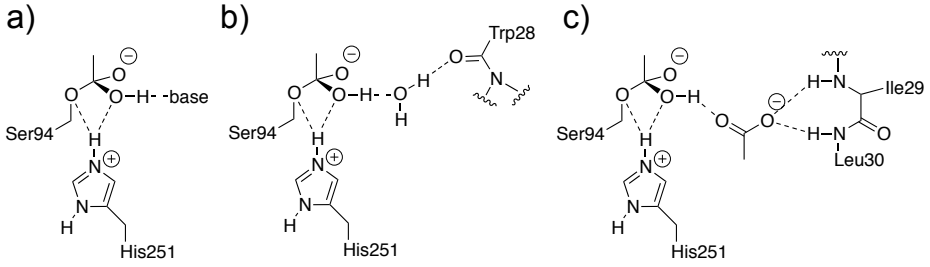

Figure 3.11. Molecular mechanisms to promote acetyl enzyme formation. a) Proton transfer from the catalytic histidine to serine Oγ of the tetrahedral intermediate reforms starting acid, while proton transfer to the OH group leads to the acetyl enzyme intermediate. A base hydrogen bonded to the OH group will favor proton transfer to the OH and increase the fraction of this tetrahedral intermediate that can form acetyl enzyme. b) In the classic carboxylic acid perhydrolase with a proline in the oxyanion loop, a water molecule can serve as the base. The carbonyl oxygen of Trp28 holds the water molecule with a hydrogen bond. c) In the new carboxylic acid perhydrolase with at type I β turn in the oxyanion loop, an acetate can serve as the base. The N–H's of I29 and L30 holds the acetate in place with a hydrogen bond.

This new hypothesis also explains why other L29X variants show improved perhydrolysis activity. The improved perhydrolysis towards acetic acid can either bind to a second acetic acid molecule or form a hydrogen bond network with water and acetic acid. The variants L29V, L29A, L29G, and L29M are likely to create more room by causing the oxyanion loop to switch from a type II to I turn that would allow a second acetate at the active site. The variants L29S, L29E, and L29T may act as proton acceptors in place of a water molecule to stabilize the acetic acid substrate for nucleophilic attack. We also analyzed the absolute ratio of peracetic acid over acetate generated by select L29X variants (supplemental information). Among the 14 variants analyzed, the wild-type PFE showed the highest selectivity (2.1 peracetic acid/acetate). By contrast L29I (0.044) and L29P PFE (0.38) showed the worst selectivity. These results show that accumulation of peracetic acid is further complicated by hydrolysis of the product.

Thus, we have identified the kinetic basis of improved perhydrolysis activity of hydrolases toward acetic acid. Other hydrolases such as (-) γ-lactamase and dihydro-courmarine hydrolases likely use the same mechanism as L29P PFE for perhydrolysis of acetic acid since both all of these catalysts contain a proline at the oxyanion loop. Conclusion on how to make a good acid perhydrolase. To engineer an acid perhydrolase, researchers should focus on making mutations at the oxyanion loop of an α/β hydrolase scaffold. The mutation can be a substitution with proline to create a *cis* isomer to bridge a water molecule with the carboxylic acid. Alternatively, the mutation(s) on the loop should be performed to allow an additional substrate to bind to the active site or a side-chain residue that substitutes the water molecule.

Another group of perhydrolases are those that catalyze perhydrolysis of esters. These perhydrolases are important when high concentrations of peracetic acid are needed. Perhydrolysis of carboxylic acids is thermodynamically controlled (Keq ~ 3) and under conditions used in the monochlorodimedone assay (500 mM acetate pH 5.5, 10 mM H_2O_2), only 0.045 mM peracetic acid will form.

Acid perhydrolases are not good for perhydrolysis of esters. Acid perhydrolases are known to catalyze the reverse reaction, hydrolysis of peracetic acid, in some cases near the diffusion limit. Perhydrolysis of esters using acid perhydrolases may form peracetic acid, but the product would be quickly hydrolyzed to form acetate. Thus, the accumulation of peracetic acid would be considerably low by using acid perhydrolases as the catalyst.

In some applications, researchers require higher amounts of peracetic acid than is practical from an acetic acid source[[9], [10]]. Acetic acid concentrations greater than 2 M become a denaturant for proteins while even higher acid concentrations become a hazard to handle. In this case, ester perhydrolysis would be favorable since the reaction is kinetically controlled.

3.5 Supplemental Information

3.5.1 Screening of L29X variants

Using colorimetric assays, the L29X variants were screened for their ability to catalyze hydrolysis of p-nitrophenyl acetate and for their ability to catalyze the perhydrolysis of acetic acid, Table S1. All L29X variants catalyzed hydrolysis of p-nitrophenyl acetate at least two fold slower than wild type *Pseudomonas fluorescens* esterase (PFE). The best hydrolase was L29I which catalyzed hydrolysis two fold slower than wild-type. The worst hydrolase was L29D, which catalyzed hydrolysis 14-fold slower than wild-type. In contrast to the decrease hydrolysis activity, several L29X variants showed improved per-hydrolase activity towards acetic acid. The best perhydrolase was L29I, which catalyzed perhydrolysis 100-fold faster than the wild-type and 1.5-fold faster than L29P PFE. Other variants which showed 4-fold higher activity over the wild-type were L29S, L29V, L29A, and L29E, highlighted in bold in Table 3.6.

Table 3.6. Initial rate of hydrolysis of *p*-nitrophenyl acetate and perhydrolysis of acetic acid catalyzed by L29X variants of PFE. [a]

Enzyme	**Hydrolysis[a] (U/mg)**	**Perhydrolysis[b] (U/mg)**
L29I	5.1	**14**
L29P	0.10	**9.9**
L29S	3.3	**1.1**
L29V	1.9	**0.96**
L29A	2.1	**0.91**
L29E	2.3	**0.65**
L29G	2.1	0.53
L29M	1.9	0.33
L29T	1.9	0.31
wild-type	14	0.15
L29Q	0.6	0.12
L29K	1.3	0.03
L29H	0.30	0.018
L29Y	3.3	0.015
L29F	6.9	0.014

L29C	2.1	0.014
L29N	2.5	0.0072
L29W	4.3	<0.001
L29D	0.098	<0.001

[a] Bold font marks the specific activities that are at least 4-fold higher than wild-type PFE. Purified PFE variants were used in each assay. 1 U = 1 μmol product formed/min. [b]Hydrolysis of 0.33 mM *p*-nitrophenyl acetate in 8 vol% acetonitrile at pH 7.2 releases p-nitrophenol, of which half is ionized at pH 7.2. The release of p-nitrophenol was measured spectrophotometrically ($\varepsilon_{404\ nm}$ = 16,600 M^{-1} cm^{-1}). [c]Perhydrolysis of 1.0 M acetate pH 5.5 with 10 mM H_2O_2 was assayed using the monochlorodimeodone assay[16] where peracetic acid reacts with bromide to form hypobromous acid, which reacts with monochlorodimedone ($\varepsilon_{290\ nm}$ = 19,900 M^{-1} cm^{-1}) to form bromochlorodimedone.

3.5.2 Perhydrolysis to hydrolysis ratio of selected L29X variants. The relative initial amounts of perhydrolysis to hydrolysis of ethyl acetate were measured for the twelve fastest perhydrolases among the L29X variants, including wild type, Table S2. During the 20 min reaction time, the amount of peracetic acid formed varied approximately three fold (11.3-29.6 mM) for the different variants, while the amount of acetic acid formed varied approximately six fold (8.6 - 53.6 mM). Wild type PFE and L29N gave the highest ratio of peracetic acid to acetic acid (2.1; entries 1 and 8). Variants L29F and L29M generated approximately equal amounts of peracetic acid and acetic acid (entries 4 and 7). Variant L29I gave the lowest ratio of peracetic to acetic acid and generated approximately 23-fold more acetic acid than peracetic acid. In spite of this low ratio, some variants (e.g., L29I) formed a comparable amount of peracetic acid because these variants catalyzed both hydrolysis and perhydrolysis faster than wild type.

Table 3.7. Amounts of peracetic acid and acetic acid formed by selected L29X variants from ethyl acetate.[a]

Entry	Enzyme (PFE)	Peracetic acid [mM]	Acetic acid [mM]	Ratio of PAA/AA[b]
1	WT	18.1	8.6	2.1
2	L29A	20.4	33.3	0.61
3	L29C	17.2	26.7	0.64
4	L29F	18.6	17.4	1.1

5	L29G	23.5	29.4	0.86
6	L29I	11.3	262	0.044
7	L29M	22.1	22.2	1.0
8	L29N	19.9	9.6	2.1
9	L29T	25.4	43.6	0.58
10[c]	L29P	14.0	53.6	0.38
11	L29S	29.6	45.2	0.65
12	L29V	20.9	29.6	0.71

[a]Reaction conditions: 0.1 mg/mL enzyme; 100 mM citrate buffer, pH 6.5; 250 mM H_2O_2; 600 mM ethyl acetate; 37 ºC; 20 min reaction time; quenched by 50 mM H_3PO_4 (final concentration). [b] PAA = Peracetic acid; AA = Acetic acid. [c] L29P reacts very slowly with ethyl acetate, so methyl acetate was used in this case.

The perhydrolysis to hydrolysis ratio of ethyl acetate was determined by measuring the concentration of peracetic and acetic acids using HPLC. To generate peracetic acid, 0.1 mg/mL of L29X enzyme (final concentration) was mixed with 250 mM H_2O_2, 600 mM ethyl acetate, and 100 mM citrate at pH 6.5. The reaction mixture was allowed to react under 37 °C for 20 minutes with the shaking speed of 700 rpm before being quenched by diluting one part of the reacting mixture in nine parts of 50 mM phosphoric acid. The concentration of peracetic acid was measured using the Karst assay[35], adapted as in Yin *et* al.[10] The assay involves oxidation of thioanisole with peracetic acid and quantifying the resulting sulfoxide by HPLC. To measure acetic acid, the quenched solution was analyzed by HPLC using ACE 5 C18 column (250 × 4.6 mm) eluted with 0.1% H_3PO_4 with 20 mM H_2SO_4 with a flow rate of 0.5 mL/min and detected at 210 nm.The retention times for hydrogen peroxide and acetic acid was 5.3 min and 10.5 min respectively. A standard curve was measured using the peak area of acetic acid versus concentration, Figure 3.12.

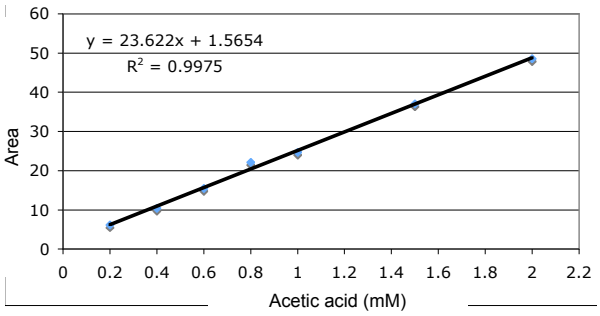

Figure 3.12. Calibration curve for measurement of acetic acid by HPLC.

3.5.3 Analysis of steric interactions of L29I structures. The mutation from Leu to Ile is equivalent to moving a δ-methyl group to the β-methylene carbon. This change in the location of the methyl group creates a steric clash with neighboring side-chains which limit the number of possible rotamers. In the L29I apo structure, the side chain contains internal steric clash between δ- and γ-methyl groups (2.7 Å and 2.8 Å), Figure 3.13A and B. Steric clash between the γ-methyl group of L29I and main-chain amide (2.7 Å) is also present along with the methylene group being too near to the main-chain carbonyl (2.8 Å). Further, the main-chain carbonyl shows a gauche conformation with respect to the methylene carbon of I29 (17.7˚ and 1.9˚). Neither type I or II turn relieve steric interactions, therefore neither turns are favored. The L29I structure complexed with acetate shows a different rotamer of I29 than the apo L29I structure. This new rotamer relieves the internal steric clash caused by the apo structure but adds different steric strains such as a syn-pentane interaction as seen in Figure 3.13C and D.

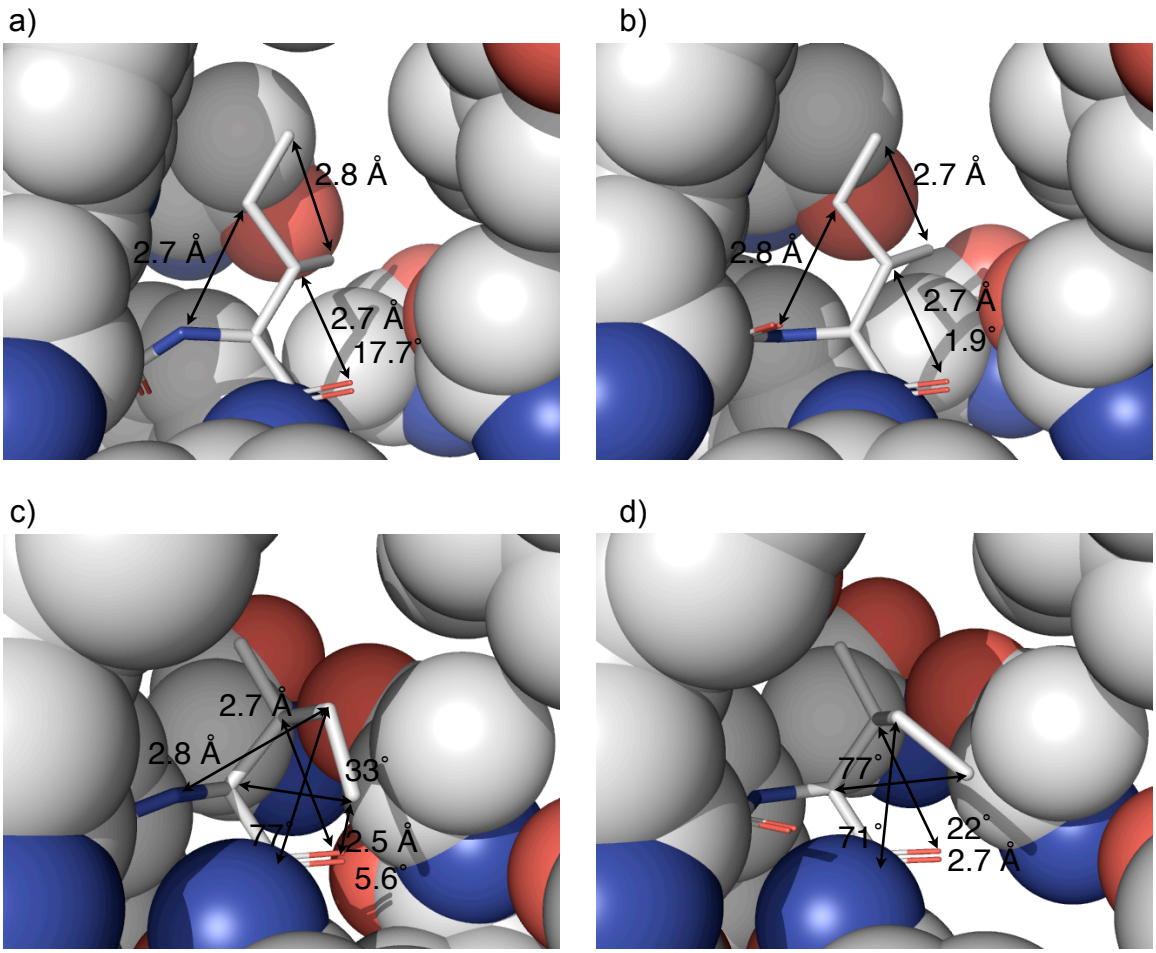

Figure 3.13. Steric interactions of the L29I residue in the L29I PFE apo and acetate x-ray crystal structures. A) Chain c of L29I without acetate favors a type I turn. The conformation shows several steric clashes between the side chain and main chain amide and carbonyl. The dihedral angel between the L30 amide and beta methylene of I29 shows a gauche conformation. B) Chain e of L29I without acetate favors type II turn. The dihedral angel between L30 and beta methylene shows a gauche conformation. C) The addition of acetate at pH 5.0 causes a rotamer switch which relieves the internal steric clash of L29I side chain as seen in the apo structure. Chain c favors the type I turn but the new rotomer of I29 causes new steric clash and also a shows an unfavorable syn-pentane interaction between the L30 carbonyl and the delta methyl group of I29 side-chain. D) Chain d favors the type II turn and also shows the *syn*-pentane interaction but without the steric clash between the amide backbone and methylene carbon of I29.

3.5.4 Molecular modeling of L29I-T_d1 intermediate with either acetic acid or acetate. Like the crystal structure of the apo enzyme, the crystal structure of L29I/acetate shows a mixture of type I and II turns in the oxyanion loop. The crystal structure of L29I/

acetate contain two acetate molecules – The first acetate, ACT1 is in a productive orientation for attack by the S94-Oγ while the second acetate, ACT2 is positioned near the oxyanion loop and forms a hydrogen bond (2.5 Å) with ACT1, Figure 3.8. The catalytic role of ACT2 is unclear because the distance between methyl group of ACT2 and main chain carbonyl are likely much further in solution due to nonpolar-polar repulsion. Here we modeled the enzyme-Td1 intermediate of L29I using either type I or II orientation and with either acetate or acetic acid. The Td1 intermediate represents a structure similar to the first transition state where the catalytic serine performs nucleophilic attack upon acetic acid. A successful model must contain all four key catalytic hydrogen bonds. These hydrogen bonds are from the oxyanion to the two amides (M95 and W28) and the His-NεH to Ser-Oγ and Td1-OH. The L29I-Td1 intermediate with acetate forms all of the key hydrogen bonds necessary for catalytic activity and an extra hydrogen bond network using the second acetate as a bridge. Other Td1 intermediate models using type II turn with acetate or acetic acid and type I turn with acetic acid were not successful, key hydrogen bonds necessary for catalysis were missing.

The type I turn of L29I-Td1 intermediate with acetate (Figure 3.14a) shows the acetate stabilizes the Td1 intermediate using a hydrogen bond network. The Td1 intermediate retains all of the catalytically important hydrogen bonds; the His-NεH hydrogen bond with Ser-Oγ and Td1-OH, while the oxyanion forms hydrogen bonds to the two amides (M95 and W28). In addition, the acetate forms a H-bond with the Td1-OH and is held in place by two amides (I29 and L30). This structure represents the molecular basis of how L29I increases perhydrolysis.

The type I turn of L29I-Td1 intermediate with acetic acid (Figure 3.14b) shows the acetic acid destabilizes Td1. The oxyanion does not form a hydrogen bond with the amide of M95 (3.9 Å), instead the OH of acetic acid forms a substitute. The Td1-OH also forms a hydrogen bond with a water molecule. This water molecule comes from the original crystal structure. Removing the water molecule would likely result in a structure similar to Figure 3.14d. This structure predicts that acetic acid is not the correct substrate because of the missing catalytic hydrogen bond.

The type II turn of L29I-Td1 intermediate with acetate (Figure 3.14c) shows the acetate forming a hydrogen bond with OH of Td1. The Td1 intermediate retains all the catalytically important hydrogen bonds. The acetate itself is not held by any side-chains, water molecules, or van der Waal interactions. Therefore, the stability of the hydrogen bond between the acetate and OH of Td1 may not be as stable as in the type I turn of L29I-Td1 intermediate with acetate.

The type II turn of L29I-Td1 intermediate with acetic acid (Figure 3.14d) shows the acetic acid destabilizes the Td1 intermediate. The Td1 does not contain all the catalytically important hydrogen bonds; the histidine does not form a hydrogen bond with Ser-Oγ, but only to OH, while the oxyanion does not form a hydrogen bond to the amide of M95. The OH of acetic acid forms a hydrogen bond with the oxyanion and with the OH of Td1. The missing hydrogen bonds of Td1 would make this structure unlikely to be a way to stabilize the Td1 intermediate to form the acetyl-enzyme.

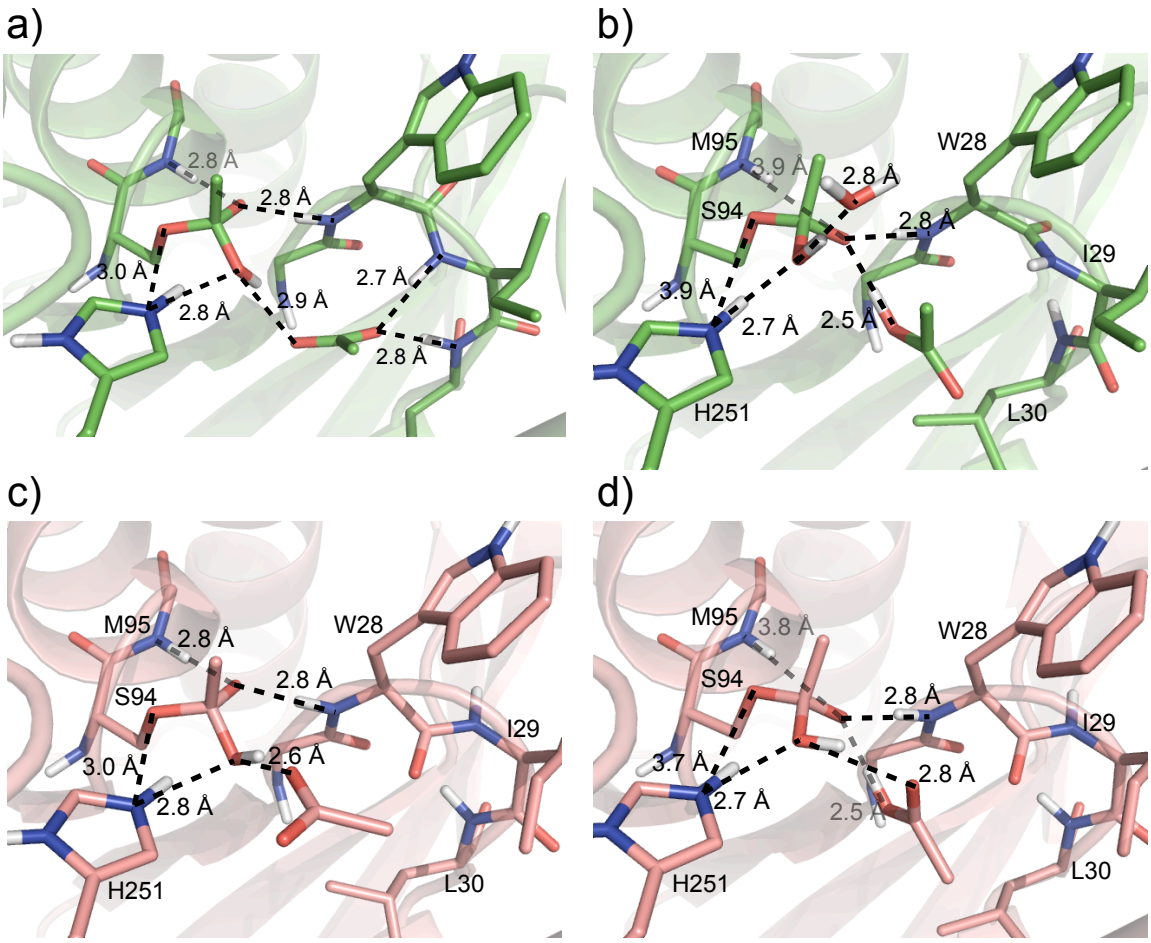

Figure 3.14. Molecular modeling of L29I-Td1 with extra acetate or acetic acid. Starting from the crystal structure L29I/acetate, the acetic acid nearest to the oxyanion hole was covalently linked to the active size serine to form a tetrahedral intermediate. The top row represents the L29I with a type I using either acetate a) or acetic acid b). The bottom row represents L29I with a type II turn in the oxyanion loop using either acetate c) or acetic acid d). MacroModel version 8.x using the OPLS_2005 forcefield was used optimize the geometry until an R.M.S.D < 0.05 Å was reached.

3.5.4 Nucleophile selectivity measurement for L29I PFE. L29I PFE nucleophile selectivity was measured by varying the concentration of hydrogen peroxide, Figure 3.15. The method to measure the initial rates of perhydrolysis and hydrolysis is identical to Figure 3.4. Selectivity parameters (β_0, $1/\gamma$) were solved using the formula in insert of Figure 3.5. This figure is not included in the main manuscript in order to emphasize the importance of nucleophile selectivity without introducing a new variant.

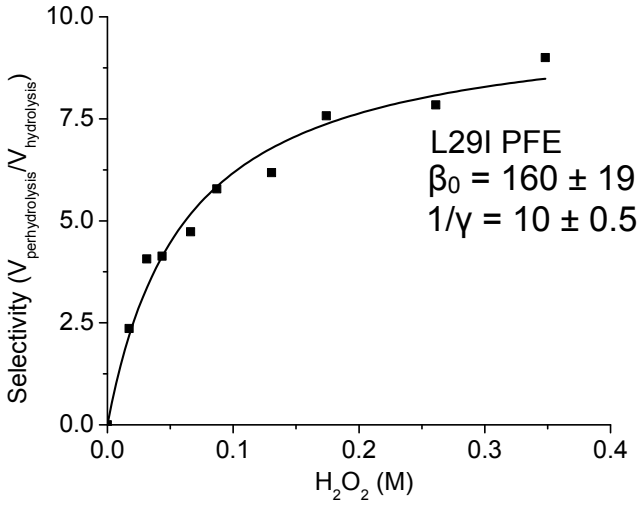

Figure 3.15. Nucleophile selectivity using L29I PFE.

Chapter 4

Chapters 2 and 3 focus on carboxylic acid perhydrolases, which favor formation of the acetyl-enzyme intermediate from carboxylic acids. In this chapter, we use carboxylic acid perhydrolase, esterase, and a lipase to measure the kinetic requirements for a good ester perhydrolase. Unlike carboxylic acid perhydrolase, ester perhydrolases must minimize hydrolysis of peracetic acid in order to maximize product accumulation.

Kinetic requirements for ester perhydrolases for generation of high concentrations of peracetic acid

Enzyme-catalyzed perhydrolysis of esters yields peroxycarboxylic acids in a kinetically controlled reaction. To make high concentrations of peroxycarboxylic acid using an ester perhydrolase, the perhydrolase should favor, first, esters over peroxycarboxylic acid as the acyl donor and second, hydrogen peroxide over water as the nucleophile. The perhydrolysis of ethyl acetate catalyzed by esterase from Pseudomonas fluorescens (PFE) fits a kinetic model developed for aminolysis of esters[1]. Using this model reveals that PFE favors hydrogen peroxide over water (β_0 = 260 M^{-1}, $1/\gamma$ = 39). However, wild-type PFE shows high selectivity for peracetic acid over ethyl acetate hydrolysis (α = 100); thus, the competing hydrolysis of peracetic acid limits the amount of peracetic acid that forms to a maximum of 70 mM. Site-saturation mutagenesis focused at the active site (eleven positions total) combined with screening for higher amounts of peracetic acid identified an improved variant – F162L PFE – that accumulates nearly twice as much peracetic acid. The selectivity of F162L PFE for hydrogen peroxide over water increased marginally at low concentrations of hydrogen peroxide (β_0 = 300 M^{-1}), but decreased 7-fold relative to wild type PFE at high concentrations ($1/\gamma$ = 5.3). The selectivity of F162L PFE for peracetic acid over ethyl acetate hydrolysis (α = 1.6) decreased 63-fold and accounts for the higher accumulation of peracetic acid.

4.2 Introduction

Peroxycarboxylic acids, especially peracetic acid, are effective oxidants for chemical synthesis and industrial applications. In organic synthesis, peracetic acid converts ketones to esters (Baeyer-Villiger oxidation), olefins to epoxides, silyl ether enolates to hydroxyketones (Rubottom oxidation), sulfides to sulfoxides and sulfones[2]. Peroxycarboxylic acids also bleach laundry[3] and wood pulp[4], disinfection of viruses and microbes[5], and remove lignin from lignocellulosic materials for biofuels applications[6,7,8].

Although the starting materials, acetic acid and hydrogen peroxide, are inexpensive, concentrated solutions of peracetic acid may explode, which makes storing and transporting peracetic acid expensive and inconvenient. On site generation of only the needed amounts of peracetic acid eliminates this hazard and would allow more widespread use of this useful reagent. Chemical methods to convert hydrogen peroxide to peracetic acid are inconvenient because they use acetyl chloride or acetic anhydride under strongly acidic conditions which can't be done by the end user (consumers). Enzymatic methods are a promising alternative because they work under mild conditions and can be done in situ with the application.

In situ enzymatic generation of peracetic acid is a promising alternative route to this useful reagent. Perhydrolases are serine esterases that catalyze the formation of peroxycarboxylic acids from hydrogen peroxide and either a carboxylic acid or a carboxylic acid ester, Figure 4.1. This formation of peroxycarboxylic acids is unlikely the natural function of perhydrolases since peroxycarboxylic acids are highly reactive and toxic. Perhydrolysis is most likely a side reaction of another function such as hydrolysis of lactones[9] or detoxification of peracids formed by other reactions. This ability of some enzymes to catalyze additional reactions beyond their natural function is called catalytic promiscuity.

Perhydrolysis of carboxylic acids like acetic acid is reversible and thus thermodynamically controlled, Figure 4.1a. The amount of peracetic acid formed depends on the equilibrium constant (K_{eq} ~3)[10] and the concentrations of the starting materials. Under typical conditions (500 mM acetate, pH 5.5, 10 mM H_2O_2), the equilibrium amount of

peracetic acid is only 0.045 mM. This amount is too low for most oxidation applications. One approach is to lower the concentration of water by adding organic solvent and thereby increase the equilibrium amount of peracetic acid, but the use of organic solvent brings health, safety, and environmental concerns.

Another way to increase the amount of peracetic acid is to replace the carboxylic acid with a carboxylic acid ester. Perhydrolysis of esters like ethyl acetate is effectively irreversible and thus kinetically controlled, Figure 1b. The amount of peracetic acid formed is determined by the relative rates of three reactions: perhydrolysis of ethyl acetate, hydrolysis of ethyl acetate and hydrolysis of peracetic acid.

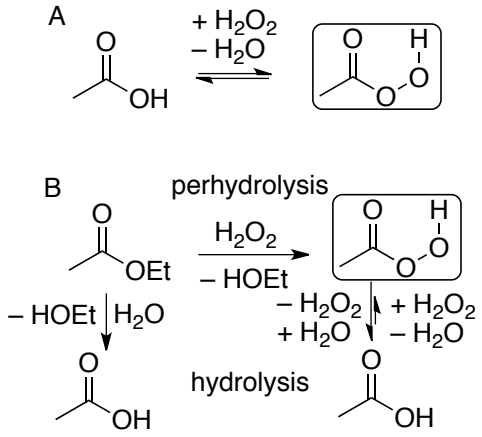

Figure 4.1. Perhydrolysis of A) acetic acid is a thermodynamically controlled reaction, with an equilibrium constant of ~3, while perhydrolysis of B) ethyl acetate is a kinetically controlled reaction. Perhydrolysis of ethyl acetate is effectively irreversible because reactions mixtures typically contain little ethyl alcohol. Two hydrolysis reactions compete with perhydrolysis of ethyl acetate: hydrolysis of ethyl acetate and hydrolysis of peracetic acid.

Wild-type PFE catalyze perhydrolysis using a similar mechanism as acyl-transfer catalyzed by penicillin acylase[11]. The free enzyme binds and reacts with ethyl acetate to release ethanol and form the acetyl-enzyme intermediate, Figure 4.2. Hydrogen peroxide and water both compete for the acetyl-enzyme intermediate. The acetyl-enzyme can react with water to form acetate or with hydrogen peroxide to for peracetic acid. However, at the acetyl-enzyme-H_2O_2 complex, water can compete with hydrogen peroxide and form

acetate. Thus, the ratio between perhydrolysis and hydrolysis dependence on hydrogen peroxide concentration is nonlinear.

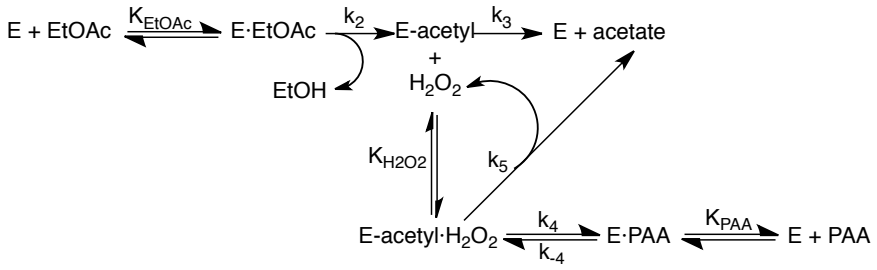

Figure 4.2. Kinetic schemes for enzyme catalyzed perhydrolysis of esters. More complex mechanism where acyl-enzyme•hydrogen peroxide complex may also undergo hydrolysis. This mechanism predicts that ratio of peracid to acid will reach a plateau upon increasing hydrogen peroxide concentration because once the acyl-enzyme•hydrogen peroxide complex is saturated with hydrogen peroxide, increasing its concentration will not increase the amount of perhydrolysis. This scheme was adapted from Youshko *et* al.[1]

Fink and Bender[12] first proposed a mechanism similar to Figure 4.2 to account for the nonlinear relationship of the relative amount of acyl transfer to nucleophile concentration using papain to catalyzed acyl-transfer and hydrolysis reactions. Water can outcompete the acyl-enzyme• H_2O_2 complex to form acetate.

Youshko and coworkers[1] used a similar model for acyl transfer of penicillin acylase. Their kinetic model contains three selectivity parameters that can be adapted for perhydrolysis studies. Parameter $\alpha = (k_{-4}/K_{PAA})/(k_2/K_{EtOAc})$ (unitless) is the ratio of hydrolysis of peracetic acid to the hydrolysis of ethyl acetate. A higher values of α indicate preferential hydrolysis of PAA over ethyl acetate. A low value for α favors accumulation of high concentrations of peracetic acid since less product isdestroyed. Parameter $\beta_0 = k_4/k_3K_{H2O2}$ (units of M^{-1}) is the ratio between synthesis and hydrolysis of PAA at low hydrogen peroxide concentrations. An enzyme with a higher β_0 is more selective for synthesis of PAA over hydrolysis of the ester. Parameter $1/\gamma = k_4/k_5$, is the ratio of hydrolysis and formation of PAA through the acyl-enzyme•H_2O_2 complex. An enzyme with a higher $1/\gamma$ is more selective for H_2O_2 over water at the acyl-enzyme• H_2O_2 complex and would accumulate more peracetic acid. Measuring the specificity constants (k_{cat}/K_m) for hy-

drolysis of peracetic acid and ethyl acetate yields the parameter α. Measuring the ratio of perhydrolysis over hydrolysis as a function of hydrogen peroxide and fitting the data to equation 1 reveals parameters β_0 and $1/\gamma$.

$$\left(\frac{V_{perhydrolysis}}{V_{hydrolysis}}\right)_{initial} = \left(\frac{[H_2O_2]*\beta_0}{1+\beta_0*\gamma*[H_2O_2]}\right) \qquad \text{equation (1)}$$

This paper establishes the following kinetic criteria for an efficient ester perhydrolase: 1) esters must be good substrates for the enzyme, 2) perhydrolysis of the ester must be favored over hydrolysis of the ester (high β_0 and $1/\gamma$), and 3) subsequent hydrolysis of peracid must be minimized (low α). We use these parameters to predict the maximum accumulation of peracetic acid.

First, we determine the maximum accumulation of peracetic acid using wild-type PFE and L29P PFE, a carboxylic acid perhydrolase. Despite high substrate concentrations (>500 mM), we obtained only 14% yield. ^{1}H-NMR measurements show that the enzyme is not deactivated, rather hydrolysis of peracetic acid likely contributes to this low yield.

We engineered PFE to improve higher accumulation of peracetic acid. and to serve as a side-by-side comparison with wild-type PFE to determine which kinetic criteria affect maximum accumulation of peracetic acid. We determine kinetic criteria 1) by measuring the steady-state kinetic constants for perhydrolysis and hydrolysis of ethyl acetate using CalB, wild-type and variants of PFE. Steady-state kinetic constants show that the F162L PFE (11,000 s^{-1} M^{-1}) improves hydrolysis of ethyl acetate by 74-fold over the wild-type PFE (300 s^{-1} M^{-1}).

We determine the kinetic criteria for 2) and 3) by measuring H_2O/H_2O_2 competition and peracetic acid/ethyl acetate hydrolysis competition using wild-type and F162L PFE as a model. Our hypothesis is that maximum accumulation of peracetic acid for PFE is hydrolysis – increasing the kinetic constant for ethyl acetate hydrolysis increases peracetic acid accumulation. The model is useful in determining the limit of peracetic acid accumulation and to determine its maximum formation.

4.2 Results

4.2.1 Steady-state accumulation of peracetic acid and acetate. Accumulation of peracetic acid by wild-type PFE and variants reach a steady-state concentration, Figure 4.3a. In the presence of 500 mM ethyl acetate and 500 mM hydrogen peroxide, wild-type PFE forms a maximum of 70 mM peracetic acid. L29P PFE is a carboxylic acid perhydrolase – this variant accumulates less than 10 mM of peracetic acid because hydrolysis of the product is near diffusion control[13]. The other variant, F162L PFE accumulates nearly twice as much peracetic acid as wild-type PFE. Despite the presence of high substrate concentrations, conversion of ethyl acetate to peracetic acid is low, 14% for wild-type PFE and 26% for F162L PFE. Since perhydrolysis of esters is a kinetically controlled reaction, either the catalyst is being deactivated by peracetic acid or hydrolysis is occurring.

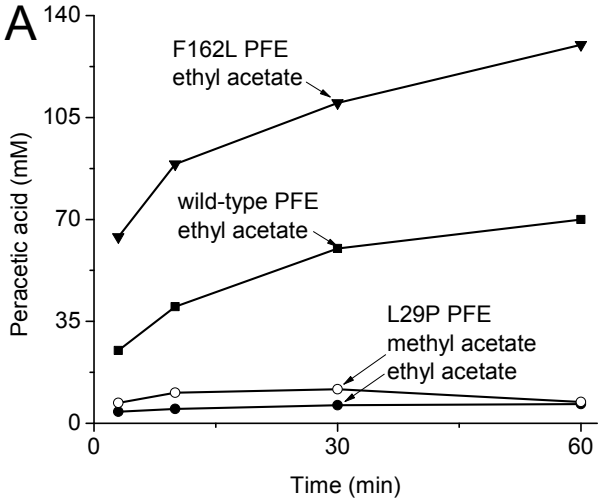

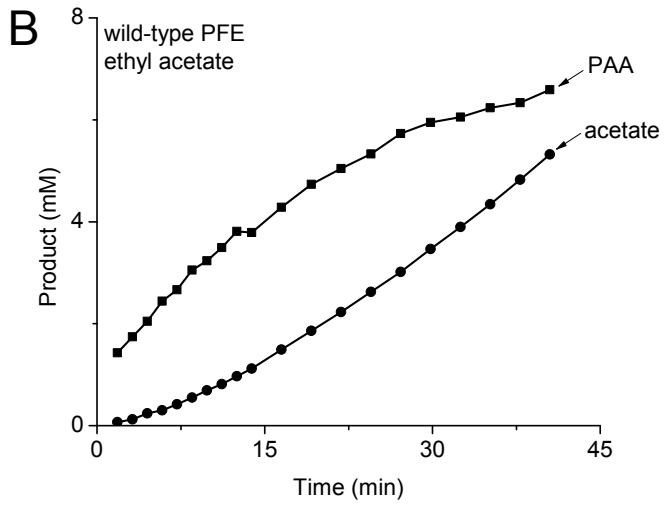

Figure 4.3. Formation of peracetic acid during perhydrolysis of ethyl acetate catalyzed by wild-type PFE and variants. A) Variant F162L PFE accumulates 130 mM peracetic acid in 60 min, while wild type PFE accumulates 70 mM. Variant L29P PFE is a poor perhydrolase for both ethyl and methyl acetate since it accumulates <10 mM peracetic acid. Reaction conditions: 600 mM ethyl acetate or 1 M methyl acetate, 500 mM H_2O_2, sodium phosphate buffer (100 mM, pH 7.2), 0.5 mg/mL enzyme, 23 °C. Values are corrected for the small amount of spontaneously generated peracetic acid (<3 mM in 60 min). B) Monitoring perhydrolysis of ethyl acetate by ^{1}H-NMR shows that although accumulation of peracetic acid stops, accumulation of acetic acid continues. These reaction conditions are more dilute compared with those in panel A and therefore a lower steady state amount of peracetic acid accumulates. Reaction conditions: 200 mM ethyl acetate, 87 mM H_2O_2, sodium phosphate buffer (100 mM, pH 7.2), 0.035 mg/mL enzyme, 23 °C. Supplementary information contains example ^{1}H-NMR spectra from which this data was derived. The lines connecting the measured values are for visual clarity only.

We use wild-type PFE to show that the catalyst is not deactivated by peracetic acid when steady-state is reached, rather a switch to hydrolysis activity occurs based on H^1-NMR (600 MHz) at 23 ˚C, Figure 4.3b. To measure both peracetic acid and acetate as a function of ethyl acetate, 84 mM of hydrogen peroxide and 200 mM of ethyl acetate was used in the ^{1}H-NMR assay. The reaction, with 15% D_2O is initiated by addition of 0.58 μM wild-type PFE.

Progress curves from wild-type PFE shows that peracetic acid formation is hyperbolic, as confirmed in Figure 4.3b but the formation of acetate is non-linear nor hyper-

bolic. In the early stage of catalysis, formation of acetate versus peracetic acid is negligible, but over time the former product is generated faster than the later. At the early stage, acetate is generated mainly from ethyl acetate since the concentration of peracetic acid is much less. At late stage, hydrolysis of peracetic acid also contributes to the accumulation of acetate since the catalyst has a low K_m. Thus, formation of acetate is comprised from both the rate of hydrolysis of both ethyl acetate and peracetic acid. To test whether maximum accumulation of peracetic acid is limited by hydrolysis, we engineer an improved variant of PFE using site-saturation mutagenesis at the active site.

4.2.2 Site saturation mutagenesis reveals a 2-fold improved perhydrolase. To find a perhydrolase that could accumulate higher concentrations of peracetic acid, we created and screened a small saturation mutagenesis library focused on residues in the active site of PFE that directly interact with the substrate, intermediates, and products, Figure 4.4a. The residues chosen for mutagenesis are within 6 Å of the catalytic serine 94 and point toward the active site. These residues which lie closest to the active site have a better potential of finding improved perhydrolase activity since they can interact with either the substrate or enzyme-intermediates. Since we are looking for an improvement in new catalytic activity, closer mutations are more likely to be better than further mutants[14]. We chose to analyze and pick mutants in a step-wise manner; meaning that if a better mutant was found for position x, then the following positions that had not been screened will also have the same mutation at x.

For the first round of site-saturation mutagenesis, we use the wild-type PFE and target the following positions: 29, 28, 93, 125, 198, 95, 162. We found two improved variants, F162L accumulated twice as much peracetic acid as wild-type PFE. In the next round, we started with the F162L PFE variant and focused on the remaining positions: 225, 224, 121, 194, 93, 95, and 125. We realize that not all beneficial mutants may be additive and this strategy could miss single mutants with improved properties. Our purpose is to find a mutant with an improved perhydrolase activity so that we can analyze the rate determining step for accumulating peracetic acid.

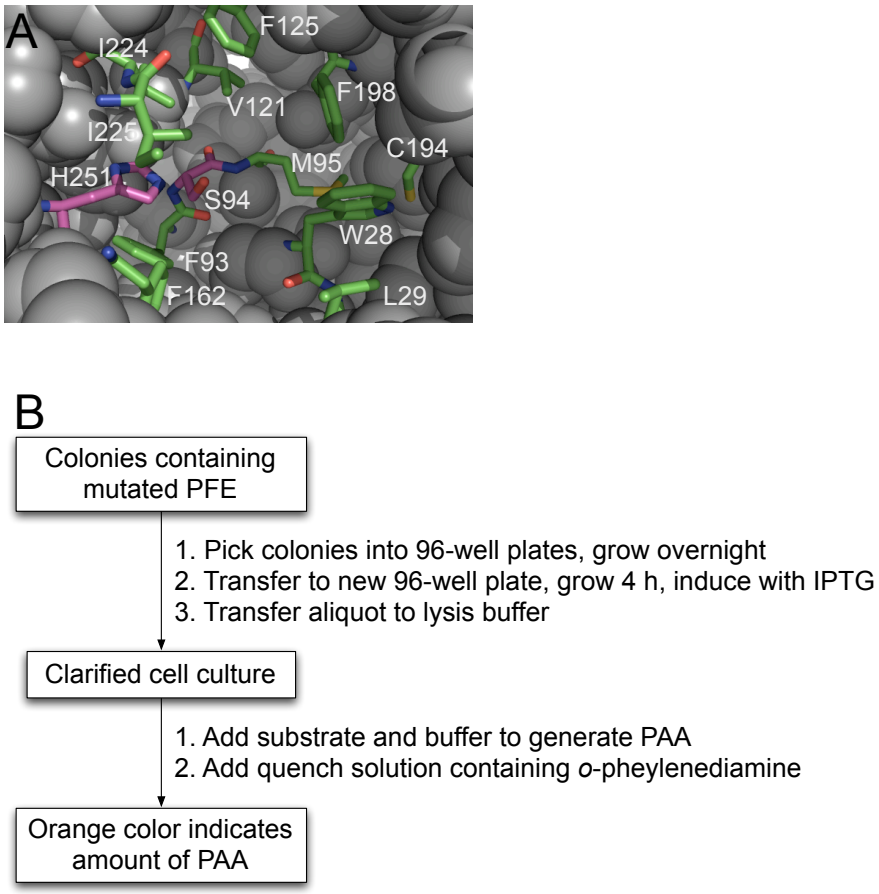

Figure 4.4. Location of amino acid substitutions for directed evolution and screening strategy. A) Target residues for site-saturation mutagenesis in PFE. Twelve amino acids residues lie within 10 Å of the catalytic S94 (magenta). Single amino acid substitutions were first tested at seven positions: 28, 29, 93, 125, 198, 95, and 162, which yielded only one variant that accumulated twice as much peracetic acid as wild-type PFE: F162L. The F162L variant was used as a template to test for an additional substitution at the remaining four positions (121, 194, 224, 225), but no large increases were found. B) Screening PFE variants for increased peracetic acid accumulation. Individual colonies were picked into 96-well plates containing LB media with ampicillin and grown overnight. An aliquot of this culture is transferred to fresh 96-well plates and grown for ~ 4 h to maintain similar cell density. Next, protein expression was induced with IPTG. An aliquot of each culture was transferred to 96-well plates containing cell lysis buffer and incubated for 1 h at 37 °C. To generate peracetic acid, substrates (600 mM EtOAc, 500 mM H_2O_2) and buffer (50 mM phosphate, pH 7.2) are added and incubated for 10 min at 25 °C. To measure the amount of accumulated peracetic acid, a quench buffer (500 mM phosphoric acid, pH 2.0) containing *o*-phenylenediamine (100 mM) was added. After 20 min, the orange color is measured at 458 nm.

We use a simple colorimetric screening method to look for improvements in individual variants, Figure 4.4b. A PCR-based method is used to make saturation mutagenesis library of independent positions. The resulting linear DNA was transformed into *E.coli* TOP10 and grown on LB plates containing ampicillin. Transformants typically produced thousands of individual colonies. The individual colonies (>1000) were picked into 96-well plates, induced for protein expression, then lysed to release the expressed engineered protein.

To screen for improved variants in the library, we added substrates (500 mM ethyl acetate, 500 mM H_2O_2) and incubated for 10 min to generate PAA. The amount of accumulated PAA was determined by adding *o*-phenylenediamine (100 mM, OPD), which reacts with peracetic acid to produce an orange colored 2,3-diaminophenazine (λ_{max} = 458 nm). Several wells containing wild-type PFE served as controls. Researchers previously used OPD to assay peroxidases[15], but here we adapted it to measure amount of peracetic acid.

Screening results for single and double mutants, Figure 4.5. Most of the variants containing a single amino acid substitution showed normalized activities less than or equal to the wild type indicating that the they accumulated less or similar amounts of peracetic acid, Figure 5A. The 93 and 225 positions showed only four and ten catalytically active variants, indicating a low tolerance for mutations at this site. The nine mutants that generated twice as much peracetic acid were further investigated. These nine mutants were all identified as PFE F162L. This variant was used as a template to screen the remaining six positions as double mutants, Figure 4.5b. The double mutants at 121, 194, and 125 position showed improved activity over the single mutant F162L PFE. However, upon purification and more stringent assay conditions, the double mutants did not show significant improvement over the single mutant F162L PFE. We separately assayed positions 28 and 29 separately from the site-saturation libraries in Figure 4.5. The 28 and 29 mutants showed no significant improvements for peracetic acid accumulation. These positions were created for a separate research project where the details will be mentioned elsewhere.

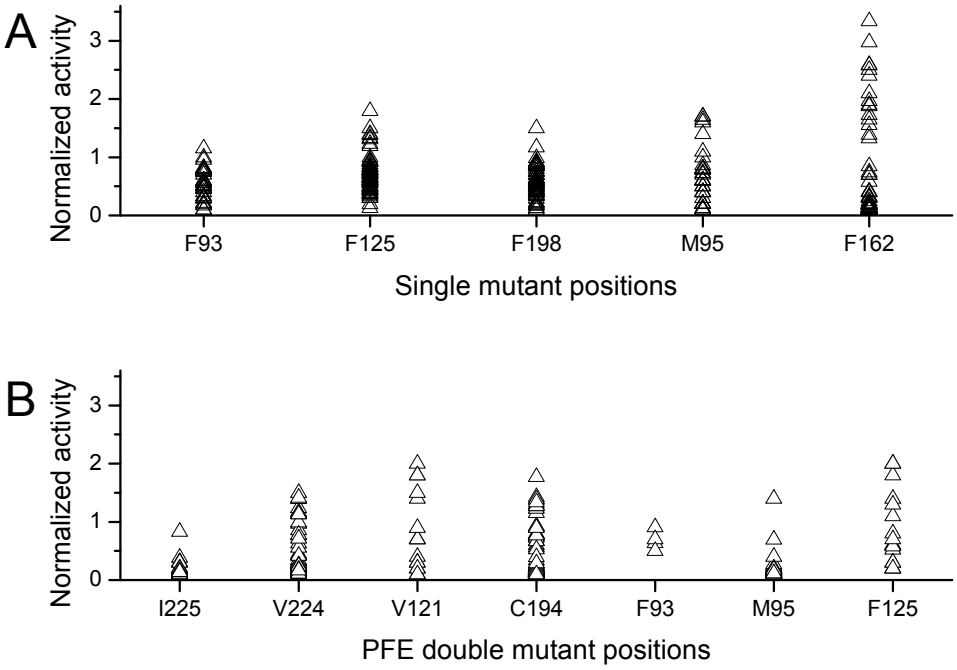

Figure 4.5. Normalized amount of accumulated peracetic acid by variants from site-saturation libraries. A) First round of mutagenesis at five positions normalized against wild-type PFE. Nine variants at F162 accumulated more peracetic acid than the wild type PFE. Sequencing identified all these variants as F162L. B) Second round of mutagenesis to introduce a second mutation in F162L PFE targeted seven other positions. Some variants at the 121, 194, and 125 positions showed improvements. A total of 188 colonies were screened for each position. Inactive variants (normalized amount of accumulated peracetic acid <0.1) are not included in these plots.

Next, we determine the stead-state kinetics for perhydrolysis using wild-type and variants of PFE as well as CalB.

4.2.3 Steady-state measurement of perhydrolysis using wild-type and variants of PFE and CalB. The first kinetic criteria for a good perhydrolase for esters is that the ester must be a good substrate. We determine whether ethyl acetate is a good substrate for CalB or wild-type and variants of PFE by measuring the steady state kinetics for perhydrolysis. Perhydrolysis is measured using the colorimetric monochlorodimedone assay[16]. This assay determines the initial rate of perhydrolysis by reacting peracetic acid with sodium bromide to form hypobromous acid. Hypobromous acid bromonates monochloro-

dimedone, which absorbs at 290 nm (ε = 19,900 $cm^{-1}M^{-1}$) to form bromochlorodimedone. We measure perhydrolysis using F162L PFE and compare the kinetic constants to wild-type PFE (an esterase), L29P PFE (a carboxylic acid perhydrolase) and CalB (a lipase), Table 4.1.

The first order rate constant for F162L PFE (32 s^{-1}) is 2.6-fold better than wild-type PFE (12 s^{-1}), at least 64-fold better than L29P PFE (<0.5 s^{-1}), and 32-fold better than CalB (1 s^{-1}). The F162L PFE's (K_m = 8.8 mM) affinity towards ethyl acetate improved by 1.7-fold over the wild-type (K_m = 15 mM). The overall catalytic efficiency for F162L PFE (4000 $s^{-1}M^{-1}$) improved by 5-fold over the wild-type PFE (800 $s^{-1}M^{-1}$).

L29P PFE (5.1 s^{-1}) is a carboxylic acid perhydrolase because the first ordered rate constant is 43-fold faster than wild-type PFE (0.12 s^{-1}) for perhydrolysis of acetic acid. However, the L29P (<0.5 s^{-1}) variant is at least 24-fold slower than wild-type PFE (12 s^{-1}) for perhydrolysis of ethyl acetate. A switch from ethyl to methyl acetate improves the first ordered rate constant from <0.5 s^{-1} to 8.7 s^{-1}.

Not surprising, CalB is not a perhydrolase, the first ordered rate constant is 12-fold lower than wild-type PFE, an esterase. CalB's affinity towards ethyl acetate is 6-fold higher than wild-type PFE – using long chain esters would likely improve the K_m for CalB.

Table 4.1. Perhydrolysis of ethyl acetate and acetic acid catalyzed by CalB, PFE and its variants.[a]

Enzyme	k_{cat} [s^{-1}]	V_{max} [U/mg]	K_m [mM]	k_{cat}/K_m [s^{-1} M^{-1}]
Ethyl acetate				
Wild-type PFE	12 ± 0.50	24 ± 1.0	15 ± 2.1	800
L29P PFE[b]	<0.5	<1	>600 mM	0.9
F162L PFE[c]	32 ± 0.75	64 ± 1.5	8.8 ± 0.8	4000
CalB[d]	1 ± 0.30	2 ± 0.50	87 ± 0.59	10
Acetic acid				
Wild-type PFE[e]	0.12 ± 0.020	0.24 ± 0.040	500 ± 100	0.2
L29P PFE[d]	5.1 ± 0.40	10 ± 0.80	210 ± 60	20

[a]Perhydrolysis of acetic acid (pH 5.5, 0.1-1 M acetate buffer) and acetate esters (pH 6.5, 100 mM citrate buffer) were measured using the monochlorodimedone assay[16] at 23 °C with 10 mM H_2O_2 for PFE and 1.0 M for CalB. [b]Perhydrolysis was very slow and showed no evidence of saturation with ethyl acetate up to its solubility limit so the individual values of k_{cat} and K_m could not be measured. The specificty constant (k_{cat}/K_m) was determined from plot of activity versus substrate concentration, Figure 4.10 in the supporting information). [c]The K_m for hydrogen peroxide was found to be 5.2 mM ± 1.2. [d]The K_m for hydrogen peroxide was found to be 100 mM ± 18. [e]Data from Yin *et* al.[13].

4.2.4 Hydrolysis of ethyl acetate and peracetic acid. Another way to determine whether ethyl acetate is a good substrate is to measure hydrolysis. We measure the steady-state kinetic constants for hydrolysis of ethyl acetate using CalB, wild-type and variants of PFE. Hydrolysis of ethyl acetate is determined by using the colorimetric para-nitrophenol assay at pH 7.2[17]. Hydrolysis of peracetic acid is determined by using a pHstat.

For hydrolysis, F162L PFE is 5-fold faster than wild-type PFE and 64-fold faster than L29P PFE in terms of k_{cat}. F162L PFE's K_m for ethyl acetate decreased by 9-fold versus wild-type and is 43-fold lower than L29P PFE. Thus, the lower k_{cat} and K_m contribute to the improved catalytic efficiency k_{cat}/K_m of F162L PFE, which is 37-fold better than wild-type PFE and 2,800-fold better than L29P PFE. CalB is similar to wild-type PFE in terms of k_{cat} and K_m. CalB is 3.7-fold better than wild-type PFE in terms of k_{cat}/K_m. For hydrolysis of peracetic acid, CalB is similar to PFE enzymes in terms of k_{cat}, but

the K_m is 1,000-fold higher. Peracetic acid may be too polar for this enzyme, therefore the affinity is much higher than the PFE variants.

Hydrolysis of peracetic acid for wild-type PFE and L29P PFE have been previously measured[13], but not for F162L PFE or CalB. F162L PFE has a slightly lower k_{cat} and higher K_m for peracetic acid hydrolysis compared to wild-type PFE. CalB on the other hand has a K_m for peracetic acid that's 1,000-fold higher than wild-type PFE but similar k_{cat}. The high k_{cat} shows that peracetic acid is a good acylating agent, but formation of the Michaelis complex can be hindered if the enzyme active site is nonpolar.

Table 4.2. Hydrolysis of ethyl acetate and peracetic acid catalyzed by PFE and its variants.

Enzyme	**k_{cat}^{app} [s^{-1}]**	**V_{max} [U/mg]**	**K_m^{app} [mM]**	**k_{cat}/K_m^{app} [s^{-1} M^{-1}]**
Ethyl acetate				
Wild-type PFE	9.0 ± 1.0	18 ± 2.0	33 ± 1.0	300
L29P PFE[a]	0.67 ± 0.05	1.3 ± 0.010	160 ± 30	4
F162L PFE	43 ± 1.2	87 ± 2.3	3.8 ± 0.27	11,000
CalB	31 ± 4.0	57 ± 7.4	40 ± 14	800
Peracetic acid				
Wild-type PFE[a]	100 ± 3	200 ± 6.0	0.041 ± 0.005	2 x 10^6
L29P PFE[a]	139 ± 2	280 ± 4.0	<0.003	>5 x 10^7
F162L PFE	75 ± 2.4	150 ± 4.8	0.051 ± 0.0084	1 x 10^6
CalB	54 ± 0.82	100 ± 1.5	75 ± 0.59	700

Hydrolysis of ethyl acetate was measured using the pH indicator *p*-nitrophenol at 23 °C, pH 7.2[17]. Hydrolysis of peracetic acid was measured at pH 7.2 using a pH-stat, which controlled the addition of 0.010 N NaOH to keep the pH constant. [a]Data from Yin *et al.*[13] where the rate of hydrolysis was measured at pH 7.2.

Next, competing reactions for perhydrolysis and hydrolysis of peracetic acid and ethyl acetate are measured together. The data is used to fit key parameters which determine whether wild-type PFE and F162L PFE meet the kinetic criteria for 2) and 3). These key parameters are also used to predict the maximum accumulation of peracetic acid.

4.2.5 Measuring competition between hydrogen peroxide and water. We test whether CalB, wild-type and F162L PFE meet the second criteria for a good perhydrolase, higher selectivity towards hydrogen peroxide over water. Perhydrolysis and hydrolysis were measured in a hydrogen peroxide solution using a pH-state at pH 7.2 as in Yin *et* al.[11], Figure 4.6. Hydrolysis was determined by titrating the amount of protons released using 0.01 N NaOH. Perhydrolysis was measured by adding sodium bromide to the hydrogen peroxide solution. Sodium bromide reacts with peracetic acid to form hypobromous acid. Hypobromous acid reacts with hydrogen peroxide to from hydrogen bromide. The amount of hydrogen bromide formed is titrated with 0.01N NaOH using the pH-stat.

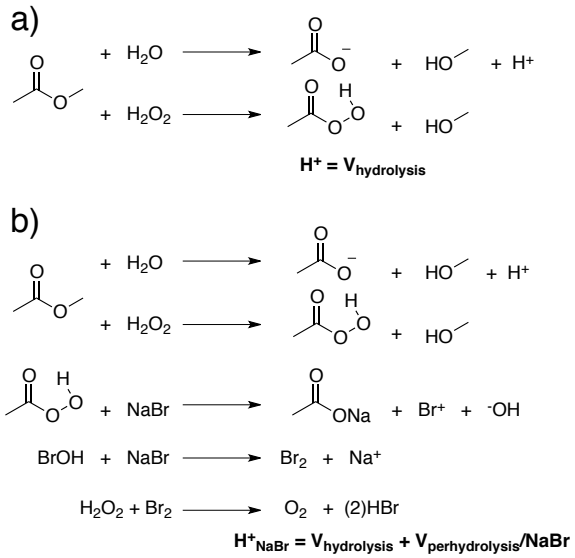

Figure 4.6. Measuring the relative amounts of perhydrolysis and hydrolysis of ethyl acetate using a pHstat. a) Hydrolysis of ethyl acetate at pH 7.2 releases a proton, but the accompanying perhydrolysis of ethyl acetate does not release significant amounts of proton because peracetic acid (pK_a = 8.2) remain mainly protonated. b) In the presence of sodium bromide, peracetic acid reacts with bromide to also generate a proton after several steps.

Measuring the rate of proton release without NaBr reveals the rates of hydrolysis, while measuring the rate of proton release with NaBr reveals the sum of hydrolysis and perhydrolyis. The rate of perhydrolysis is the difference between the two rates, equation 2. A plot of the rate

$$V_{perhydrolysis} = V_{H^+(NaBr)} - V_{H^+} \qquad \text{equation (2)}$$

of perhydrolysis relative to hydrolysis (the selectivity for perhydrolysis) as a function of hydrogen peroxide concentration shows a hyperbolic saturation curve, Figure 4.7. The relative amount of perhydrolysis increases with increasing hydrogen peroxide concentration and then reaches a plateau. The data was fit to the formula derived by Youshko and coworkers[1] shown in Figure 4.7 (insert) using nonlinear regression with Originlab v. 8.0 (Northampton, MA).

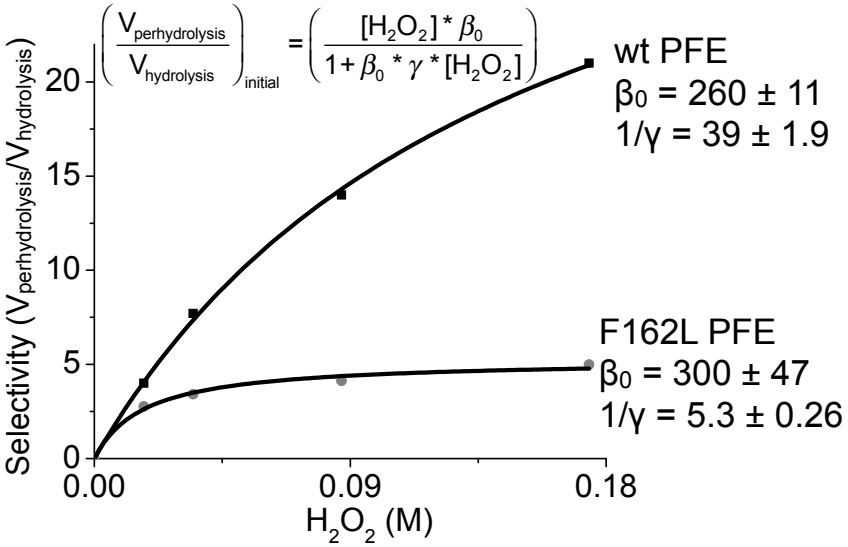

Figure 4.7. Perhydrolysis to hydrolysis ratio ($V_{perhydrolysis}/V_{hydrolysis}$) as a function of [$H_2O_2$]. The initial rate of perhydrolysis and hydrolysis were determined by pH-stat at 23 ˚C. The amount of protein added was 1.2 μg/mL for wild-type PFE and 0.15 μg/mL for F162L PFE. The curve was fit using the formula which describes the dependence of P/H on β_0 and γ. The F162L PFE variant shows faster saturation than wild-type PFE.

We attempted to measure the nucleophile selectivity parameters for CalB, but we were unable to observe a saturation effect with hydrogen peroxide. Two possible reasons why we observe a non-saturating effect as a function of hydrogen peroxide concentration. The K_m of CalB for hydrogen peroxide is 100 mM, under the experimental conditions, hydrogen peroxide is not yet saturated; this means that at 180 mM hydrogen peroxide concentration, CalB is only 64% saturated. Alternatively, CalB uses a different mechanism than PFE and variants.

4.2.6 Measuring competition between ethyl acetate and peracetic acid hydrolysis. We measure $\alpha = (k_{-4}/K_{PAA})/(k_2/K_{EtOAc})$ to determine whether wild-type and F162L PFE meet the third kinetic criteria for a good perhydrolase. The parameter α can be determiend from the second order rate constants for hydrolysis of peracetic acid and ethyl acetate, but for PFE, this method does not correctly predict the maximum amount of peracetic acid. Therefore, we determine alpha by directly measuring the the rate of hydrolysis of peracetic acid and ethyl acetate in the presence of both substrates.

Hydrolysis of peracetic acid and ethyl acetate were measured by determining the concentration of peracetic acid and ethanol by HPLC and GC, respectively. The hydrolysis reaction consists of 400 mM ethyl acetate, 27 mM peracetic acid, 0.2 mg/mL of catalase (*aspergillus niger*), and 100 mM phophate buffer at pH 7.2. Hydrolysis is initiated by mixing 16 ng of either wild-type or F162L PFE to the hydrolysis reaction. The concentration of peracetic acid and ethyl acetate are determined at five separate time intervals (0, 3, 5, 7, and 9 mins) and performed in triplicate with and without catalyst. The initial rate for hydrolysis is determined by fitting the data using linear regression. The ratio of hydrolysis of peracetic acid over ethyl acetate is multiplied by the relative concentration of ethyl acetate over peracetic acid to obtain α. Selectivity parameters for wild-type and F162L PFE are summarized in Table 4.3.

Table 4.3. Selectivity parameters for perhydrolysis of ethyl acetate catalyzed by PFE variants.

Enzyme	α	$\beta_0(M^{-1})$	1/γ
wtPFE	100 (350)[a]	260 ± 11	39 ± 1.9
F162L PFE	1.6 (47)	300 ± 47	5.3 ± 0.26
Penicillin acylase [b]	9.0	378	50

The initial rate of perhydrolysis and hydrolysis were determined by pH-stat. Selectivity parameters were determined by fitting the ratio of perhydrolysis to hydrolysis as a function of nucleophile concentration using the formula in Youshko *et* al.[1] The parameter α is the hydrolysis of product over acyl donor, while, β_0 is the synthesis over hydrolysis ratio

under low nucleophile concentrations and γ is the hydrolysis of product over synthesis ratio at the acyl-enzyme-nucleophile complex.
[a]The parameter α in parenthesis contain adjustments from the uncatalyzed rate for ethyl acetate hydrolysis. See the footnote for additional details.
[b] From Youshko *et* al.[1] for the acyl-transfer of D-phenyl glycine amide using 7-aminodesacetoxycephalosporanic acid to form cephalexin.

Wild-type PFE has high nucleophile selectivity (β_0 = 260 M^{-1}, $1/\gamma$ = 39) at high and low nucleophile concentrations. Both parameters are similar to those for penicillin acylase. However α for wild-type PFE (α = 100[1]) is 12-fold higher than Penicillin acylase (α = 9). A higher α for wild-type PFE means that hydrolysis of the product, peracetic acid is preferred over the hydrolysis of ethyl acetate.

The F162L PFE, a variant that accumulates two-fold more PAA than wild-type PFE, is equally selective for hydrogen peroxide as wild-type PFE, but is less selective at the acyl-enzyme•hydrogen peroxide complex. The most dramatic improvement is α, where the F162L PFE decreases the selectivity for product hydrolysis by 74-fold. The decrease in α is due to the 10-fold lower K_m (0.0038 M) and 5-fold higher k_{cat} (43 s^{-1}) towards ethyl acetate hydrolysis compared to wild-type PFE (K_m = 0.033 M, k_{cat} = 9 s^{-1}). Increasing hydrolysis of the acyl donor at the cost lower selectivity at the acyl-enzyme•H_2O_2 complex results in an increase in the PAA accumulation for this variant.

4.2.7 Predicting maximum PAA concentration. The selectivity parameters α, β_0 and γ are combined into equation 2[1] to predict maximum formation of peracetic acid and acetate.

$$\frac{d[PAA]}{d[AcO^-]} = \frac{\beta_0 * [H_2O_2] * [EtOAc] - \alpha * [PAA] * (1 + \beta_0 * \gamma * [H_2O_2])}{(1 + \beta_0 * \gamma * [H_2O_2]) * ([EtOAc] + \alpha * [PAA])} \qquad \text{equation (2)}$$

[1] A significant amount of uncatalyzed hydrolysis of ethyl acetate was detected, which led to a large correction for the enzyme catalyzed hydrolysis rate. This large correction is due to the low rate of enzyme catalyzed hydrolysis of ethyl acetate. Excess hydrogen peroxide in the solution may contribute to the apparent uncatalyzed hydrolysis rate. Additional experiments are required to determine which α is correct.

The experimentally determined concentration of peracetic acid is 70 mM. The selectivity parameters correctly predict a maximum accumulation of 70 mM peracetic acid for wild-type PFE, Figure 4.8a. However, using the adjusted α parameter (in Table 3, parenthesis), the predicted maximum amount of peracetic acid is than 22 mM. For the F162L PFE variant, the model predicts maximum peracetic acid formation at 210 mM. However, we experimentally determine the maximum accumulation of peracetic acid to be 130 mM. One reason that can explain for this discrepancy is that the F162L PFE is less stable than the wild-type, and becomes deactivated before the catalyst is able to reach the predicted maximum. Qualitatively, we observe significant precipitation while generating 130 mM peracetic acid at 30 minutes. The wild-type PFE does not show significant precipitation even at 60 minutes. Alternatively, the model adapted from acyl-transfer using penicillin acylase cannot be used for perhydrolysis using PFE.

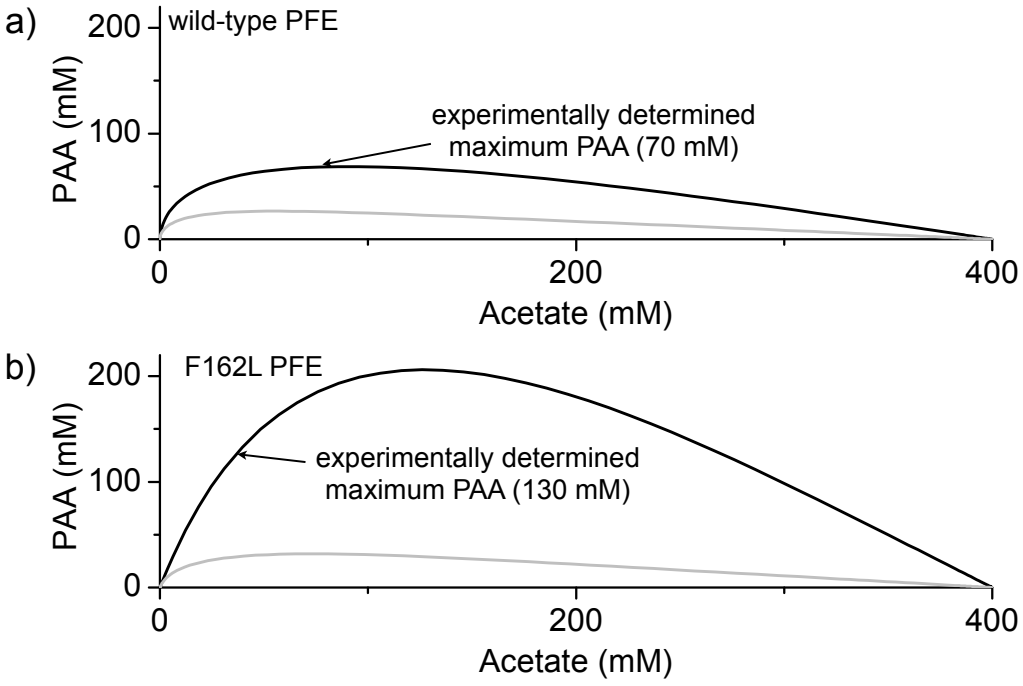

Figure 4.8. Maximum predicted formation of PAA as a function of acetate. a) Predicted maximum product formation for wild-type PFE using using $\beta_0 = 260\ M^{-1}$, $1/\gamma = 39$ and either $\alpha = 100$ (black lines) or $\alpha = 350$, (grey lines). b) Predicted maximum product formation for F162L PFE using using $\beta_0 = 300\ M^{-1}$, $1/\gamma = 5.3$ and either $\alpha = 1.6$ (black

lines) or α = 47, (grey lines). The starting concentrations are as follows: 400 mM ethyl acetate, 500 mM H_2O_2. Equation 2 was used to fit both parameters.

Additional experiments measuring the maximum product formation as a function of either ethyl acetate or hydrogen peroxide are required. The amount of acetate must also measured as a means to critically validate the selectivity parameters.

4.3 Materials and Methods

4.3.1 General. All chemicals were purchased from Sigma Aldrich of the highest purity possible. Expression and purification of wild-type, L29P, F162L and variants from the 28 and 29 library was as described in Yin *et* al.[8]. Enzyme purity was judged to be at least 90% by SDS-PAGE. The mutants from 29 and 28 library were confirmed by DNA sequencing using sequencing primers in both the forward (64 bp upstream from the start codon, ATG) and reverse (15 bp downstream from the stop codon, TGA) direction by the Biomedical Genomics Center (University of Minnesota) using ABI BigDye Terminator version 3.1 chemistry. For all other libraries, mixed templates were sequenced using sequencing primers from Yin *et* al.[8]. The sequence yields a mixture of nucleotides at the mutation site. The ratio of nucleotides was consistent with that expected for an NNK codon.

4.3.2 Purification of soluble *Candida antarctica* lipase B. *Candida antarctica* lipase B (CalB) from Novozymes, (Denmark) contained catalase as well as other contaminating proteins. To purify CalB, 20 mL of 9 mg/mL stock protein (180 mg) was dialyzed against 1 L of 50 mM phosphate buffer at pH 7.2 three times. The dialyzed CalB solution was then passed through 5 mL of pre-equillibrated anion-exchange resin DE52 (Whatman, UK). CalB did not bind to the resin but catalase and most of the contaminating protein did. The purified enzyme was dialyzed against 5 mM BES and 50 mM NaCl until the phosphate concentration was calculated to be 0.005 mM. A total of 100 mg of purified CalB was obtained after the final dialysis.

4.3.3 Steady-state kinetics for the perhydrolysis of esters. The monochlorodimedone (MCD) assay[16] was used to measure the initial rates for the formation of peracetic acid

from either ethyl or methyl acetate at 23 °C. Peracetic acid reacts with bromide to form hypobromous acid which then brominate MCD. The absorbance decrease in MCD (19,900 $M^{-1}cm^{-1}$) concentration is monitored spectrophotometrically at 290 nm, thus peracetic acid is detected indirectly. This assay contains hydrogen peroxide (10 mM) citrate buffer (100 mM, pH 6.5), monochlorodimedone (0.047 mM) and sodium bromide (149 mM). For CalB, the hydrogen peroxide concentration is 1.0 M since the K_m is 100 mM. The acetate ester concentration varied from 0.27 mM to 600 mM to yield data above and below the K_m value. Solubility of ethyl acetate limited its concentration to a maximum of 600 mM while the stability of the enzyme limited the concentration of hydrogen peroxide to a maximum of 1.0 M. The enzyme concentration (0.001 mg/mL to 0.01 mg/mL) was adjusted so that increases in enzyme concentration gave a linear increase in reaction rate. In parallel, a reaction without enzyme was measured to give the initial rate for the chemical reaction. This spontaneous reaction rate was subtracted from the rate measured in enzyme-containing sample to give the true enzyme-dependent rate. The kinetic parameters V_{max} and K_m, were determined from a best fit a plot of initial rate as a function of substrate concentration to the Henri-Michaelis-Menten equation. Fitting was done by nonlinear regression (Origin 8.5, Originlab, Northampton, MA) with the formula $v = (V_{max}*x)/(K_m + x)$, where v is the initial rate and x is the substrate concentration.

4.3.4 Steady-state kinetics for the hydrolysis of ethyl acetate. Initial rates were measured using a pH indicator assay – formation of acetic acid causes a decreases in absorption of *p*-nitrophenoxide[17] upon protonation to the phenol (ε_{404} = 16.6 x $10^3 M^{-1}cm^{-1}$) at pH 7.2 at 23 °C. A typical reaction mixture contained ethyl acetate (0.2-200 mM), *p*-nitrophenoxide (0.81mM), *N,N*-bis(2-hydroxyethyl)-2-aminoethanesulfonic acid)BES, 5 mM) buffer, and enzyme (0.01 - 5 μg). The BES buffer stabilizes the pH of the solution. The calculation of rated accounts for the protons that were buffered by BES: $v_{true} = v_{obsd}(1 + 5 \text{ mM BES})/(0.81 \text{ mM pNP})$.

4.3.5 Selectivity parameters β_0 and γ. Initial rates for perhydrolysis and hydrolysis were determined by pH-stat at 23 ˚C with 0.010 N NaOH as the titrant. The amount of hydrogen peroxide was varied from 14.7 to 147 mM while the concentration of ethyl acetate

was held constant at 188 mM. The reaction solution was adjusted with 0.010 N NaOH before the addition of enzyme to pH 7.2. The amount of protein added was 1.2 μg/mL for wild-type PFE and 0.15 μg/mL for F162L PFE. For perhydrolysis, the 166 mM of NaBr is added to react with peracetic acid to form BrOH. At pH 7.2, BrOH ionizes to release a proton. This initial rate accounts for both hydrolysis and perhydrolysis. For hydrolysis in the presence of hydrogen peroxide, the amount of acid released corresponds to the amount of titrant added. Additionally, 166 mM of NaCl is added as a substitute for the absence of NaBr. Subtraction of perhydrolysis + hydrolysis rate from rate of hydrolysis gives the rate for perhydrolysis. The initial rate data was fit using the formula which describes on β_0, a parameter used to describe the selectivity of competing nucleophiles.

4.3.6 Selectivity parameter α. The hydrolysis reaction consists of a 10 mL solution of 400 mM ethyl acetate, 27 mM peracetic acid, and 100 mM phophate buffer at pH 7.2. Addition of peracetic acid causes the pH to drop (acetic acid), therefore 0.3 mL of 1N NaOH was added to neutralize the pH. A final concentration of 0.2 mg/mL of catalase (*aspergillus niger*) is added with stirring for 5 min to remove hydrogen peroxide. Hydrolysis is initiated by mixing 16 ng of either wild-type or F162L PFE to the hydrolysis solution. The concentration of peracetic acid and ethyl acetate are determined at five separate time intervals (0, 3, 5, 7, and 9 mins) and performed in triplicate with and without catalyst.

To analyze ethanol concentration, a 0.5 mL aliquote is taken from the hydrolysis solution and quenched with 0.005 mL of 88% phosphoric acid to deactivate esterase activity. A 0.4 mL aliquote of the quenched solution is mixed with 0.4 mL of 250 mM phosphoric acid and 500 mM dithiothreitol (DTT) to react with peracetic acid for 10 min. After the incubation, 0.001 mL of the solution is injected into the gas chromatographer with a flame ionization detector and a DB-FFAP column (J&W Scientific). To determine the peracetic acid concentration, a modified Karst assay[18] was used as in Yin *et* al.[8]. From the quenched solution, 0.05 mL is added to 0.350 mL of 50 mM methyl tolyl-sulfide and incubated for 20 min. Peracetic acid reacts with methyl tolyl-sulfide to form methyl tolyl-sulfoxide. To remove remaining hydrogen peroxide, a 0.5 mL solution of 50

mM triphenyl phosphine is added to the solution and incubated for 30 min. The products are analyzed by HPLC using a C8 (XDB8) column.The initial rate for hydrolysis is determined by fitting the data using linear regression. The α parameter is calculated by multiplying the ratio of hydrolysis of peracetic acid over ethyl acetate with relative concentration of ethyl acetate over peracetic acid.

4.3.7 Determining an accumulated amount of peracetic acid. The determination relies on the reaction of peracetic acid with excess methyl-tolyl sulfide (MTS) to form methyl-tolyl sulfoxide (MTSO). The excess of MTS prevents further oxidation of MTSO to the sulfone. In a second step, addition of triphenyl phosphine (TPP) quenches any hydrogen peroxide by forming triphenyl phosphine oxide (TPPO)[18]. Typically, a 0.05 mL aliquot of 70-200 mM PAA solution is quenched in 0.95 mL of 50 mM phosphoric acid (pH ~2) to inactivate the catalyst. An aliquot (0.1 mL containing 3.5-10 mM peracetic acid) of the quenched solution is added to an MTS solution (0.3 mL, 6.7 mM in 1:3 acetonitrile/ water). The reaction is manually shaken for 3-4 sec and incubated for 20 min at 23 °C in a light free box. A solution of TPP (0.5 mL of 20 mM in acetonitrile) is added, manually shaken for 3-4 sec and then incubated for a further 30 min at 23 °C. A 10 µL aliquot of the solution is injected onto a C8 XDB8 (Agilent, Santa Clara, CA) eluted with a gradient of aqueous (ddi H_2O/10%methanol) and acetonitrile at 1 mL/min. The time dependent ratio of aqueous to acetonitrile composition of the mobile phase is: 0 min: 60:40, 3 min: 40:60, 3.5 min: 20:80, 4.5 min: 20:80, 5.5 min: 40:60, 6.5 min: 60:40, 10 min: 60:40. The concentration of peracetic acid is determined by comparing the integrated area of the MTSO peak (2.53 min) to the standard curve while taking any dilution factors into account. The amount of peracetic acid generated by an enzyme was corrected for any spontaneously generated peracetic acid measured in a “blank” reaction.

4.3.8 ^{1}H-NMR measurement of peracetic acid and acetate. NMR measurements were performed in Wilmad 542 thin-walled NMR tubes using a 600 MHz NMR spectrophotometer (Varian, Santa Clara, CA) in sodium phosphate buffer (100 mM, pH 7.2) containing 15 vol% D_2O. The longest relaxation time (T_1 = 4.4 s) was for acetate and the 90° pulse width was 6 µs. The water signal was suppressed using presaturation and the pulse

sequence used for subsequent experiments are: preaquisition delay = 20 s, satdly = 1.5 s, power = 6, gain = 30, number of transients = 1.

The perhydrolysis reaction was initiated by adding either wild-type PFE (17.5 μg) or F162L (2.5 μg) to 0.8 mL (final volume) solution of ethyl acetate (13-209 mM), hydrogen peroxide (174 mM) in sodium phosphate buffer (100 mM, pH 7.2) containing 15 vol% D_2O. In a second set of experiments, the ethyl acetate was fixed at 209 mM while hydrogen peroxide varied from 43.5 to 174 mM. Spectra were collected every 80 s to measure the peracetic acid, acetate, and ethyl acetate. Progress curves for the reactions are show in Figure 4.3b.

4.3.9 Site-saturation mutagenesis libraries. Site-saturation mutagenesis libraries were made using polymerase chain reaction (PCR) with non-overlapping primers, Table 4.5. The plasmid, pJOE2792[19] contains the wild-type PFE gene from *P. fluorescens* SIK WI, which was used as a template for PCR amplification. The forward primer contains a degenerate codon (NNK) at the target site and is flanked by 20 nt sequence at both the 5' and 3' end. The reverse primer contains 40 nts upstream from the degenerate codon.

Table 4.4. Nucleotide sequence of primers used to make site-saturation mutagenesis libraries

Primer name	Forward sequence 5'-3'	Reverse sequence 5'-3'
F93NNK	CCTCAAGGAGGT-GACCCTGGTGGGC**NNK**TCCAT-GGGCGGCGGCGA	GCCCACCAGGGTCACCTCCTT-GAGGTCCAGGTGTTCGATCAACTG
M95NNK	GGAGGT-GACCCTGGTGGGCTTCTCC**NNK**G GCGGCGGCGATGTGGC	GGAGAAGCCCACCAGGGT-CACCTCCTTGAGGTCCAGGT-GTTCGAT
V121NNK	GTGGCCGGCCTGGTGCTGCTGGG CGCC**NNK**ACCCCGCTGTTCGG	GGCGCCCAGCAGCAC-CAGGCCGGCCACCCGTGCGCTG-CCGTGGC
F125NNK	GTGCTGCTGGGCGCCGTCACCCC GCTG**NNK**GGCCAGAAGCCCGA	CAGCGGGGTGACGGCGCCCAG-CAGCACCAGGCCGGCCACCCGTG
F162NNK	TCAGCGATTTCAACG-CACCG**NNK**TATGGCATCAA-CAAGGGCCAGG	CGGTGCGTTGAAATCGCTGAT-GAACTGCGCGCGATCCTTCAGCAG
C194NNK	CTGGCCTCGCTCAAGGCCACGGT GGAT**NNK**GTCACCGCGTTCGC	ATCCACCGTGGCCTTGAG-CGAGGCCAGCAGGGCGATTTG-CAGGG

Primer name	Forward sequence 5'-3'	Reverse sequence 5'-3'
F198NNK	AAGGCCACGGTGGATTGCGTCAC CGCG**NNK**GCCGAAACCGACTT	CGCGGTGACGCAATC-CACCGTGGCCTTGAGCGAGGC-CAGCAGGG
I224NNK	CTGGTGATC-CATGGCGATGGCGAC-CAG**NNK**GTGCCGTTCGAGAC	CTGGTCGCCATCGCCATGGAT-CACCAGGGTGGGTACGTCGATCT
V225NNK	GTGATCCATGGCGATGGCGACCA-GATC**NNK**CCGTTCGAGACCAC	GATCTGGTCGCCATCGCCATGGAT-CACCAGGGTGGGTACGTCGA

The P*fx* polymerase (Invitrogen) was used to amplify the template DNA with the forward and reverse primers. The following is a typical PCR (50 μL) cycle parameter: 95 °C for 15 s, 55 °C for 6.5 min, 68 °C for 30 s for 30 cycles. The template DNA was degraded by addition of D*pn*I, a DNA endonuclease which cleaves methylated DNA, for 1 h at 37 °C. Next, a 1 μL aliquot of the amplified product was used to transform *E. coli* TOP10 chemically competent cells using heat-shock[20]. The transformants were plated onto Luria-Bertani (LB) agar plates containing ampicillin (0.1 mg/mL); then grown overnight at 37 °C. Typically, the number of colonies ranged from 500 to 1,000. Several colonies were picked and verified by DNA sequencing.

4.3.10 Screening libraries using the *o*-phenylenediamine assay. Individual colonies were picked into deep well (1.5 mL) 96-well plates containing growth media (Luria Bertani broth, 0.20 mL containing ampicillin (0.1 mg/mL)) using a robot picker (Genetix) at the University of Minnesota High throughput facility. A total of 186 colonies were picked and screened for each library, which gives an 99.7% probability that all nineteen amino acid substitutions were tested at least once[21]. The plates were incubated at 37 °C for 20 h without shaking, then aliquots (10 μL) were transferred to new 96-well plates containing fresh growth media (Luria Bertani broth, 0.20 mL containing ampicillin (0.1 mg/mL) and rhamnose (2 w/v%)) and the plates incubated (700 rpm, 37 °C, 18 h) express proteins. An aliquot (10 μL) of the cultures was transferred to transparent 96-well plates containing cell lysis solution (Cellytic Express (Sigma Aldrich) 90 μL, 50 mg/mL in 50 mM sodium phosphate, pH 7.2). The mixture was shaken (30 s) using a Spectramax 384 spectrophotometer, then incubated at 37 °C for 1 h. The lysed cells were allowed to cool to 23 °C for

30 min, after which perhydrolysis substrates solution (100 μL, 0.5 M ethyl acetate, 0.5 M H_2O_2, in sodium phosphate buffer, 50 mM, pH 7.2) was added, mixed, and incubated at 23 °C for 10 min. The reaction mixture was quenched with acidic *o*-phenylenediamine (250 mM, 50 μL 500 mM phosphoric acid pH 2) and incubated at 23 °C for 10 min with shaking in a Spectramax 384 spectrophotometer. The product, 2,3-diaminophenazine, absorbtion at 458 nm was recorded by a Spectramax 384 spectrophotometer. Tarche et *al*. (1987) used a similar method to assay horseradish peroxidase. Horseradish peroxidase catalyzed the oxidation of OPD to 2,3-diaminophenazine with hydrogen peroxide. In our assay PAA oxidizes OPD without the aid of a catalyst.

4.4 Discussion

Ester perhydrolysis is a preferred reaction because the equilibrium constant for perhydrolysis of acetic acid is small. However, the competing reactions, ester and product hydrolysis can also occur and limit the final amount of peracetic acid produced. We therefore propose a definition for ester perhydrolases that can be useful to compare different enzymes that catalyze perhydrolysis. A good perhydrolase for esters must accept the desired ester substrate, have good nucleophile selectivity for hydrogen peroxide over water, and have a high specific activity for perhydrolysis.

Acyl-transferase from *M. smegmatis* (MsAcT)[22] is a perhydrolase because it favors esters as a substrate, has high perhydrolase activity (700 U/mg) towards propylene glycol diacetate and the perhydrolysis to hydrolysis ratio was 4 for triacetin. Site-saturation mutagenesis found the S54V mutant[23] showed a higher ratio of 10.5 (maximum accumulation of peracetic acid not reported). Another good perhydrolase is the enzyme isolated from *Thermatogae maritima* (*T. maritima*) which favors perhydrolysis of triacetin (61 U/mg)[24] and has a perhydrolysis to hydrolysis ratio of 6.5. Site-saturation mutagenesis revealed a mutant, C277S which increased the specific activity to 777 U/mg and the selectivity to 16. The lipase, CAL-B is an example that does not fit into the criteria of a good perhydrolase because it generates a small amount of peracetic acid (5 mM).

The specific activity for perhydrolysis of ethyl acetate is 2 U/mg and the selectivity for hydrogen peroxide over water is poor.

We measure the steady-state kinetic constants for perhydrolysis and hydrolysis using wild-type, F162L PFE, and Cal-B. Both wild-type and F162L PFE are good catalysts for perhydrolysis, k_{cat} = 12 s^{-1} and 32 s^{-1} respectively. In contrast, Cal-B is a poor catalyst for perhydrolysis, the first ordered rate constant is 1 s^{-1}. In addition, Cal-B's affinity toward hydrogen peroxide is poor (100 mM). Thus, Cal-B is a poor perhydrolase. The rate constants are good indicators as to whether a catalyst is a good perhydrolase. To predict how much peracetic acid will be accumulated, direct measurement of competing reactions (Perhydrolysis versus hydrolysis) must be measured.

We use wild-type PFE and an improved variant F162L to measure selectivity parameters for perhydrolysis. Wild-type PFE is highly selective for hydrogen peroxide at low and high concentrations (β_0 = 260 M^{-1}, $1/\gamma$ = 39). The F162L PFE variant also has similar hydrogen peroxide selectivity at low concentrations (β_0 = 300 M^{-1}), but at high concentrations the selectivity ($1/\gamma$ = 5.3) is lower than wild-type PFE by 7-fold. We also measure α, the selectivity for hydrolysis of peracetic acid over ethyl acetate. Wild-type PFE prefers to hydrolyze peracetic acid over ethyl acetate (α = 100). By contrast, the F162L (α = 1.6) is only slightly more selective for peracetic acid hydrolysis over ethyl acetate. The minor single substitution from Leu to Phe decreased the selectivity for peracetic acid hydrolysis by 74-fold over the wild-type. We also note that wild-type PFE catalyzed hydrolysis of ethyl acetate is slow (0.13 mM/min) and involves are large correction for the uncatalyzed rate (0.083 mM/min). It's not clear whether the uncatalyzed rate is due to experimental error. Thus, using α =100 correctly predicts maximum peracetic acid formation, while using the corrected α value predicts a lower peracetic acid maximum than experimentally observed. To clarify this discrepancy, another method to measure hydrolysis will be used to determine the rate of both catalyzed and uncatalyzed hydrolysis of ethyl acetate in the presence of peracetic acid.

To generate 70 mM of peracetic acid using wild-type PFE as a catalyst, 400 mM of ethyl acetate and 500 mM H_2O_2 are required. This low conversion is primarily due to

the high selectivity towards hydrolysis of peracetic acid. Alternatively, peracetic acid could deactivate wild-type PFE by introducing oxygens and causing the protein to denature. We monitor the formation of peracetic acid and acetate by ^{1}H-NMR to show that while peracetic acid reaches a plateau, acetate continues to form. Thus, maximum formation of peracetic acid is controlled by the enzyme's selectivity parameters.

We engineer a better perhydrolase through directed evolution targeting mutants at the active site. Eleven residues in the active site (W28, F93, M95, F162, C194, F143, F198, F125, V121, V225, I224) were substituted for 19 other common amino acids to evaluate the improvement in perhydrolysis activity. The single mutant, F162L initially showed a 2-fold higher perhydrolase activity from the screening assay. This mutant can accumulate up to 115 mM of peracetic acid within 10 minutes, versus 60 mM for wild-type PFE. To further improve the accumulation of peracetic acid, a double mutation library using the F162L PFE as a template was made. The positions 121, 194 and 125 showed improvements over the F162L PFE. These variants were isolated and individually purified. Disappointingly, the double mutations failed to show improvements over the F162L PFE variant under more stringent assay conditions. One explanation for the false positive is that the protein variants expressed more protein than the F162L single mutant which would have contributed to a higher activity. Several other improvements could be made to this assay, such as introducing multiple mutations simultaneously. Despite some shortcomings, we were able to identify a variant with improved perhydrolysis properties which can be used to compare with the wild-type PFE.

To generate higher amounts of peracetic acid using PFE, the selectivity for peracetic acid hydrolysis must be lowered even further. One way to do this is to create more mutations to identify a variant that's less selective for hydrolysis. Another way is to use a less polar substrate than ethyl acetate, such as triacetin. The larger triacetin molecule allows additional van der Waal contact with side-chain residues of PFE, which can be modified.

Although we now know that the molecular basis of carboxylic acid perhydrolases increase the formation of the acetyl-enzyme intermediate, the analogous ester perhydro-

lases is more difficult to determine. One reason for this difficulty is that ester perhydrolases have different folds – MsAcT is a SGNH fold[22], PFE[25] and perhydrolase from *T. maritima*[26] are classical α/β hydrolase folds. Thus, it's possible that ester perhydrolases can use different molecular basis. The kinetic requirements for ester perhydrolases also make determining the molecular basis difficult. An ester perhydrolase must have both high selectivity towards hydrogen peroxide while maintaining low selectivity towards hydrolysis of peracetic acid. The variant F162L PFE has identical high selectivity for hydrogen peroxide at low concentrations as wild-type PFE but reduced selectivity at high concentrations. However, the selectivity towards peracetic acid hydrolysis is lowered by 74-fold compared to the wild-type.

The position of this F162L PFE variant lies near the alcohol binding pocket and away from the substrate channel, Figure 4.9a. Analysis of the wild-type PFE crystal structure (PDB: 1VA4) shows that the F162L residue, along with F93 and L30 form a "gate" which prevents glycerol from entering the active site, Figure 4.9b.

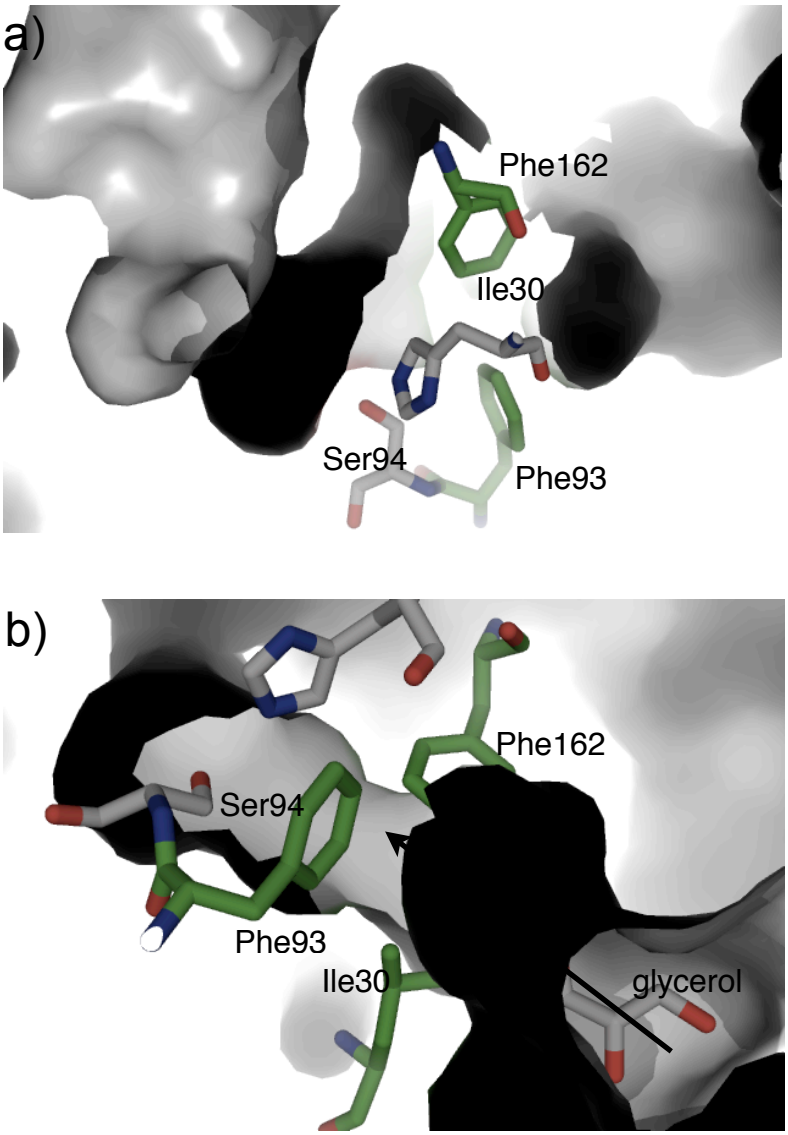

Figure 4.9. Substrate channels of wild-type PFE. a) Substrate channel leading directly to the Ser94 can be used for both acyl-donor and nucleophile. By contrast, the substrate channel in b) can only accommodate water, hydrogen peroxide and other nucleophiles.

This "gate" could be a second substrate channel for either water or hydrogen peroxide. The mutation Phe to Leu could make the second substrate channel less selective for hydrogen peroxide. Meanwhile, this substitution makes more room in the alcohol pocket which allows the enzyme to bind and react with ethyl acetate more efficiently.

To test whether the second substrate channel selects for hydrogen peroxide, the remaining two residues (F93, and I30) can be substituted for alanine. These substitutions

will decrease nucleophile selectivity without affecting selectivity towards ethyl acetate or peracetic acid hydrolysis.

4.5 Supplemental Information

L29P catalyzed perhydrolysis of ethyl acetate. We measure the activity of L29P catalyzed perhydrolysis as a function of ethyl acetate concentration up to the saturation point (600 mM), Figure 4.10. At the substrate saturation point, the progress curve continued to be linear, indicating that K_m is greater than 600 mM. Therefore, we cannot accurately determine K_m and V_{max}, but only the second ordered rate constant, which can be found by fitting the slope of activity versus substrate concentration.

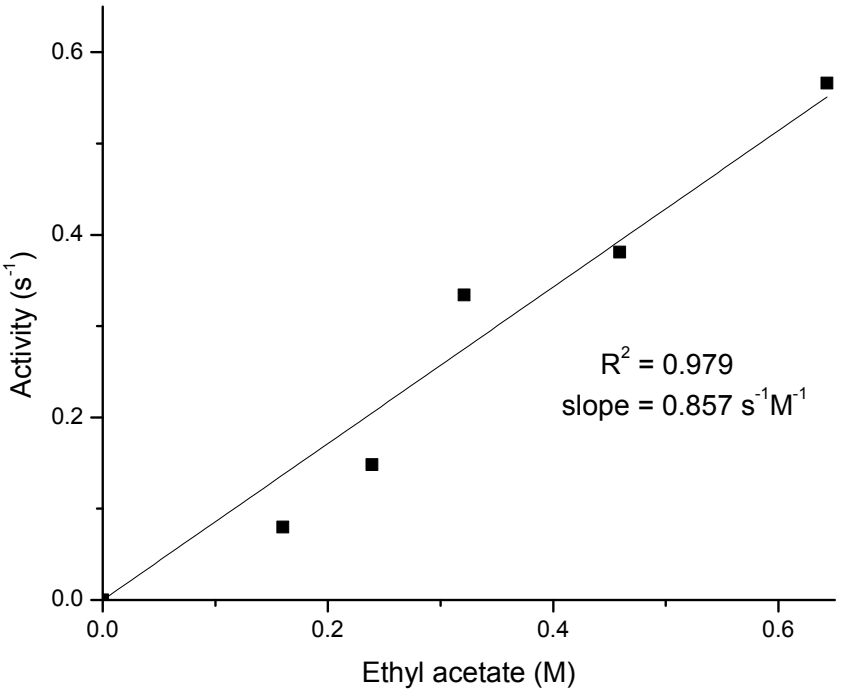

Figure 4.10. Progress curve for L29P catalyzed perhydrolysis. The monochlorodimedone assay was used to measure perhydrolysis activity at 23 ˚C. The ethyl acetate concentration was varied while keeping the hydrogen peroxide concentration at 10 mM.

Chapter 5

In chapter 4, the F162L PFE variant was engineered to accumulate higher amounts of peracetic acid (130 mM). In this chapter, the F162L PFE variant is used to improve the efficiency of lignocellulose pretreatment.* Enzymatically generated peracetic acid reacts converts lignin into smaller and more soluble lignin pieces. The chemoenzymatic process is further improved by forming peracetic acid in a biphasic layer which allows the reuse of enzyme. The pretreatment reaction conditions were also optimized by increasing the temperature to 60 ˚C and reducing the reaction time to 6 hours.

*This chapter is a copy of a published article and is reproduced with permission from Bioresour. Technol., Vol. 102, Yin, D.L.T.; Jing, Q.; AlDajani, W.W.; Tschirner, U.; Schilling, J.; Kazlauskas, R.J., “Improved pretreatment of lignocellulosic biomass using enzymatically-generated peracetic acid”, 5183-5192, Copyright 2011, Elsevier, License number: 2766510355217 (See Appendix for reprint).

Improved pretreatment of lignocellulosic biomass using enzymatically-generated peracetic acid

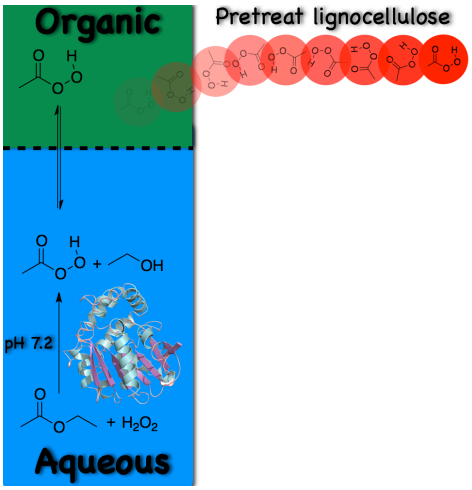

Release of sugars from lignocellulosic biomass is inefficient because lignin, an aromatic polymer, blocks access of enzymes to the sugar polymers. Pretreatments remove lignin and disrupt its structure, thereby enhancing sugar release. In previous work, enzymatically generated peracetic acid was used to pretreat aspen wood. This pretreatment removed 45% lignin and the subsequent saccharification released 97% of the sugars remaining after pretreatment. In this paper, the amount of enzyme needed is reduced ten fold using first, an improved enzyme variant that makes twice as much peracetic acid and second, a two-phase reaction to generate the peracetic acid, which allows enzyme reuse. In addition, the eight pretreatment cycles are reduced to only one by increasing the volume of peracetic acid solution and increasing the temperature to 60 ˚C and the reaction time to 6 h. For the pretreatment step, the weight ratio of peracetic acid to wood determines the amount of lignin removed.

5.1. Introduction

Lignocellulosic biomass, such as bioenergy crops and trees (e.g., switchgrass, aspen wood) or agricultural and forestry wastes (e.g., wood residues, corn stover, straw), are potential low cost sources of fermentable sugars. However, the conversion of lignocellulosic biomass into sugars is currently inefficient and expensive. This lignocellulose recalcitrance is one of the primary economic barriers to biofuel and bioproduct synthesis. The sugar polymers are embedded in plant cell walls, which naturally resist chemical, physical and enzymatic degradation. In particular, lignin, an aromatic polymer that is a major component of lignocellulosic biomass, blocks access of enzymes to sugar polymers.

Partial removal of lignin from biomass significantly improves subsequent enzymatic hydrolysis of cellulose and hemicelluloses to fermentable sugars[1,2]. However, natural enzymatic reactions that degrade lignin are slow and require days, weeks or even months. One reason for the slow reaction is that natural enzymatic reactions must use reaction intermediates that are compatible with living microorganisms. Industrial use of lignocellulosics as feedstocks will require faster pretreatment methods.

Most pretreatment methods disrupt cell walls to expose the sugar polymers. For example, dilute acid at high temperatures, ammonia fiber explosion (AFEX), steam explosion or wet oxidation break up the material[3, 4, 5], but do not remove much lignin. These pretreatments have limited effectiveness, and can generate side products that inhibit later fermentations[6, 7].

Chemical pretreatments that remove lignin are more effective. Pretreatment with ozone[8, 9], hydrogen peroxide[10], organic solvents[11] or strong caustic[12] all remove lignin, but only the oxidative reagents are selective for lignin. The other reagents also remove some of the sugars and are therefore undesirable.

A promising lignin-selective reagent is peracetic acid[13]. Peracetic acid converts lignin to soluble fragments by two different mechanisms. First, peracetic acid reduces the molecular weight of lignin polymers by cleaving β-aryl ether bonds and both carbon-carbon and carbon-oxygen bonds linked to the aromatic rings[14]. Second, peracetic acid

causes other reactions that increase the water solubility of lignin: dealkylation of *O*-methyl groups, introduction of hydroxyl groups to aromatic rings and cleavage of the aromatic rings into muconic acids[14]. These reactions increase the polarity of lignin and create water-soluble lignin fragments that wash away from the lignocellulosic biomass. Peracetic acid-treated biomass can be efficiently fermented to make ethanol[15]. However, peracetic acid is expensive and can be explosive in concentrated form. This safety hazard increases the cost of storage and transport of peracetic acid.

In-situ generation of peracetic acid eliminates transportation and storage by generating this oxidant as needed. Enzymes are potential catalysts for the synthesis of peracetic acid from hydrogen peroxide and acetate esters such as ethyl acetate, Figure 2.1. Although natural enzymes can catalyze this synthesis it is unlikely that their natural role is synthesis of peracetic acid[16]. Peracetic acid is a highly reactive oxidant that reacts with and inactivates biomolecules. The ability to make peracetic acid is an extra, unexpected reaction of many hydrolases.

Perhydrolysis is the cleavage of an ester by hydrogen peroxide, Figure 5.1, and is mechanistically similar to hydrolysis. Many esterases catalyze perhydrolysis, but perhydrolases are a subgroup of esterases that are especially efficient at perhydrolysis. The active site of both esterases and perhydrolases contains a Ser-His-Asp catalytic triad. For example, *Pseudomonas fluorescens* esterase (PFE) is an esterase that catalyzed hydrolysis of a broad range of esters such as ethyl acetate (k_{cat} = 9 s^{-1}). It also catalyzed slow perhydrolysis of acetic acid (k_{cat} = 0.12 s^{-1}) and perhydrolysis of ethyl acetate (k_{cat} = 12 s^{-1}). PFE-catalyzed perhydrolysis of ethyl acetate forms up to 70 mM peracetic acid within 30 minutes[1].

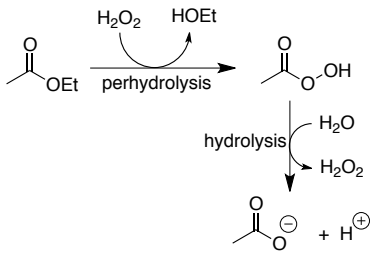

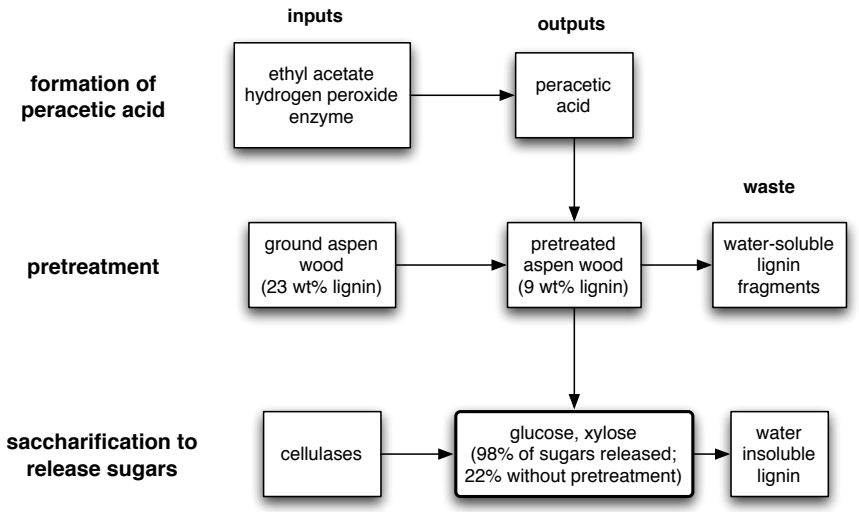

Figure 5.1. Enzyme-catalyzed formation of peracetic acid and its use to pretreat aspen wood. Top: Perhydrolysis of ethyl acetate yields peracetic acid. A subsequent undesirable hydrolysis of this peracetic acid yields acetic acid and the starting hydrogen peroxide. Esterase from *Pseudomonas fluorescens* (PFE) catalyzes both reactions. Bottom: Conversion of aspen wood biomass to fermentable sugars involves three steps: formation of peracetic acid, pretreatment of aspen wood with peracetic acid, and saccharification of the pretreated aspen wood. The pretreatment of aspen wood with peracetic acid removed about half of the lignin and made the saccharification more efficient. Without pretreatment, cellulases released only 22% of the available glucose, but released 98% after pretreatment. The lignin fractions also include some sugars due to inefficiencies.

Duncan *et* al.[1] used this perhydrolysis to make peracetic acid and use to pretreat aspen wood, Figure 5.1. Without pretreatment, the cellulases released only 22% of the available glucose, but with peracetic acid pretreatment, they released 98% of the available glucose. Although this improvement is dramatic, the procedure was complex and required up to 40 g of enzyme per kilogram of aspen wood. In this paper the complexity and amount of enzyme are reduced. Improving the saccharification step was not a goal of this research; that step uses a modified NREL procedure only to measure the effectiveness of the pretreatment.

5.2. Results

5.2.1 F162L PFE for generation of peracetic acid. Duncan *et* al.[1] used wild-type PFE to catalyze the perhydrolysis of ethyl acetate. Recently, using directed evolution, Yin *et*

al., (in preparation) discovered a variant Phe162Leu PFE that generated about twice as much peracetic acid. This paper uses this improved variant to generate peracetic acid. In a typical procedure, a solution of F162L PFE (0.5 mg/mL) in aqueous hydrogen peroxide (1.7 M, 100 mM sodium phosphate buffer, pH 7.2) containing dissolved ethyl acetate (500 mM) and generated 115 mM peracetic acid in 10 minutes.

5.2.2 Reuse of enzyme. The amount of peracetic acid generated increases for 10-30 min and then stays constant. Initially, this behavior was attributed to inactivation of the enzyme by peracetic acid, but further experimentation showed that the enzyme remains active. The constant amount of peracetic acid is a steady state concentration from a balance between enzyme-catalyzed formation of peracetic acid and enzyme-catalyzed hydrolysis to acetic acid and hydrogen peroxide, Figure 1 (Yin et al., in preparation). This important observation meant that the enzyme could be reused to make more peracetic acid.

A biphasic reaction mixture enabled the separation of the product peracetic acid and the enzyme for reuse. The two-phase reaction contained equal parts of aqueous solution (0.5 mg F162L PFE, 1.7 M H_2O_2, 250 mM sodium phosphate pH 7.2) and a second phase of ethyl acetate. The enzyme remained in the aqueous phase, while the product peracetic acid partitioned approximately equally between the aqueous and ethyl acetate phases. Removal of the ethyl acetate phase containing peracetic acid and replacement with fresh ethyl acetate allowed peracetic acid accumulation to start again. The process could be repeated up to 18 times without adding new enzyme, H_2O_2, or buffer, Figure 5.2. In this approach, a total of 42.5 mg of PAA could be generated using only 0.5 mg of enzyme. Compared to aqueous conditions where only 8.74 mg of PAA could be generated with the same amount of enzyme, this represents a five-fold improvement. The amount of peracetic acid generated decreases with each reuse due to an ~14% loss of enzyme activity in each cycle and to a decrease in the amount of hydrogen peroxide available. The concentration of hydrogen peroxide after 18 cycles was half of the starting concentration due its removal as peracetic acid. The ethyl acetate phase also extracted a small amount of hydrogen peroxide (1.0-1.4%). Walton and Lewis[17] reported that ethyl acetate ex-

tracted 40% of the hydrogen peroxide from an aqueous solution, but under our conditions (200 mM phosphate, pH 7.2), we found a much smaller amount.

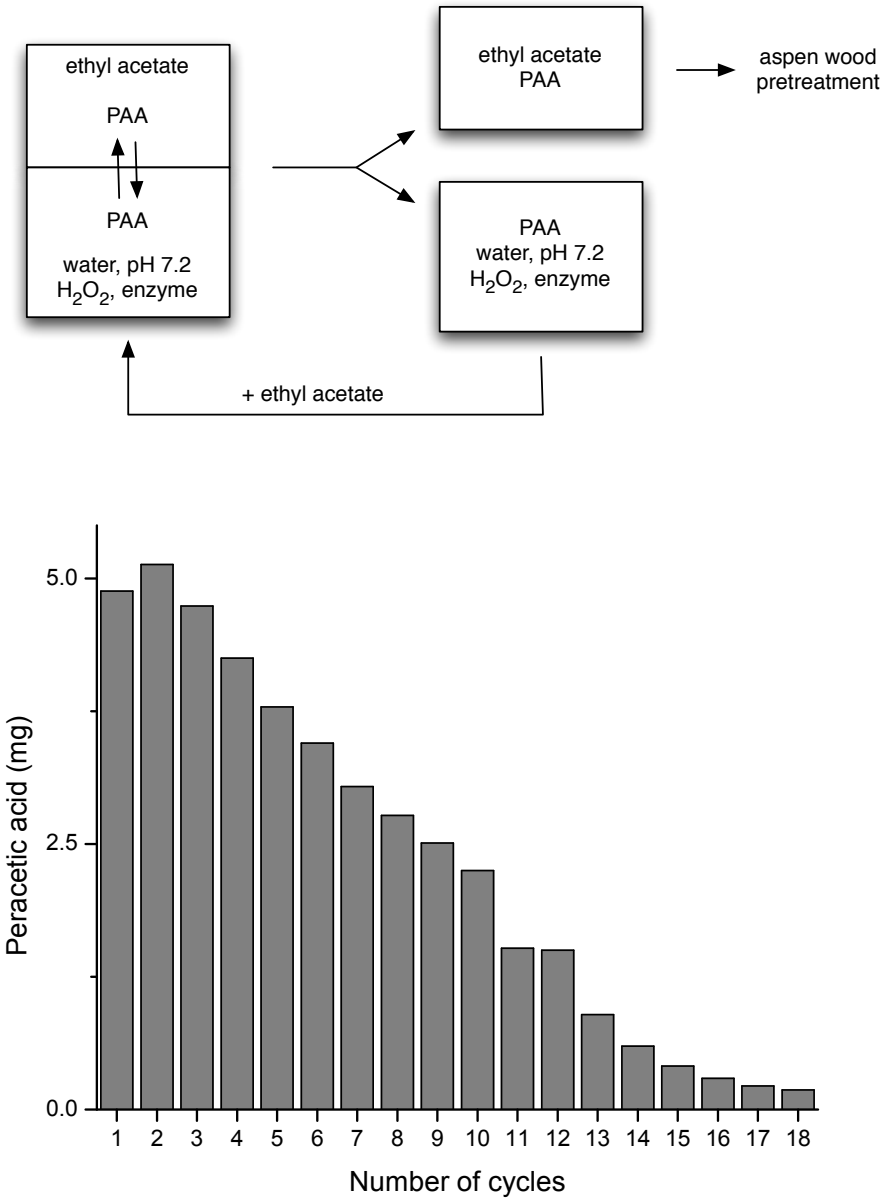

Figure 5.2. Multiple reuse of enzyme by decanting the ethyl acetate phase. Top: An aqueous phase containing enzyme, buffer and hydrogen peroxide was stirred with ethyl acetate for 10 min, then the ethyl acetate phase was decanted and fresh ethyl acetate was added for the next cycle. Bottom: The amount of PAA generated decreases in subsequent cycles due to enzyme deactivation. The enzyme activity was measured after cycles 1, 2, 3, 4, 6, and 12, which showed an average 14% decrease in activity per cycle. Reaction conditions: F162L PFE (0.5 mg), 0.5 mL ethyl acetate and 0.5 mL of 250 mM Na phos-

phate pH 7.2 with 1.7 M H_2O_2. After 18 cycles, the pH of the aqueous solution was at 7. Chemical perhydrolysis of ethyl acetate contributes <10% of enzyme generated peracetic acid.

An alternative to the two-phase reaction is immobilization of the enzyme, which would also allow removal and reuse of the enzyme or construction of a flow type reactor to make peracetic acid.

5.2.3. More hydrophobic peracids. Since the reuse of the enzyme relies on the extraction of the peracid from an aqueous into an organic solution, more hydrophobic peracids could increase the proportion of peracid extracted. Peracetic acid partitions approximately equally between water (56%) and ethyl acetate (44%). The peracetic acid remaining in the aqueous phase lowers the yield and slowly deactivates the enzyme.

Other ethyl esters were tested using the same two-phase procedure, but the reaction time was increased from 10 min to 30 min to ensure that the peracid reached a steady state concentration. Ethyl propionate, butyrate, and valerate, formed the corresponding peracid at about half of the rate as ethyl acetate and after 30 min yielded 219, 160, and 70 mM of peracid, respectively. A larger fraction of these peracids partitioned into the organic layer: 63%, 78%, 80% respectively. The larger esters - heptanoate, caproate, and decanoate - were not substrates for F162L PFE.

Hydrophobic peracids such as perbutyric acid could be more efficient at removal of lignin from lignocellulose because more hydrophobic peracids might react faster or more selectively with the hydrophobic lignin substrate. However, perbutyric and peracetic acid removed similar amounts of lignin. Pretreating aspen with 10 mL of 116 mM perbutyric acid lowered the lignin content to 16.3% and released 35.6% of glucose from cellulose. For comparison, pretreating aspen wood with 10 mL of 115 mM peracetic acid lowered the lignin content to 17% and released 35% of glucose from cellulose. Although perbutyric acid showed ~50% more favorable partitioning into the organic phase than ethyl acetate, the latter was chosen as the substrate because of its lower cost and because the very unpleasant smell of butyric acid also limits its application.

5.2.4. Optimizing the pretreatment conditions. Previous pretreatment used 70 mM peracetic acid at a ratio with wood of 0.043 g PAA/g dry weight aspen wood powder, re-

peated for 8 separate cycles (total 0.343 g PAA/g dry weight wood, reacted at 37 °C for 4 h)[1]. The improved perhydrolase PFE F162L produced 115 mM PAA, approximately doubling the concentration of PAA used previously. This increase in concentration meant that fewer cycles were needed to remove the same amount of lignin. To further increase the amount of lignin removed using PFE F162L-generated peracetic acid, the temperature and time for the pretreatment of aspen wood was optimized, Figure 5.3. Longer times and higher temperatures were better up to the point where high temperatures start to degrade the peracetic acid. A temperature of 60 °C for 6 h removed the most lignin for a given amount of peracetic acid.

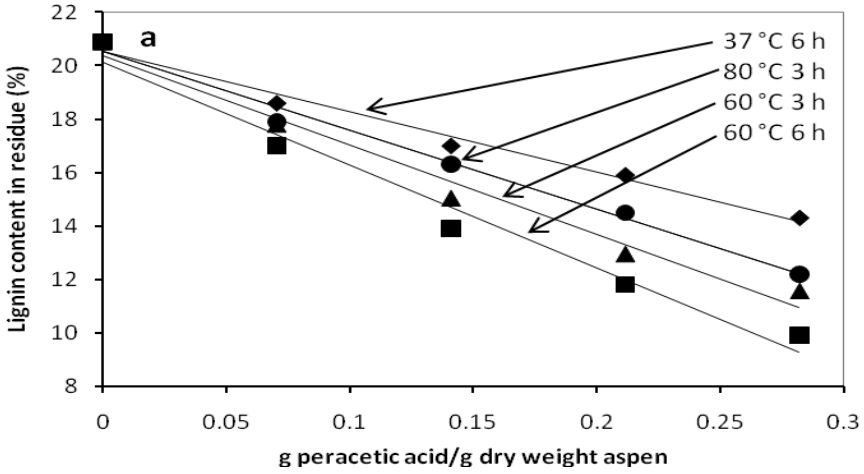
a
37 °C 6 h
80 °C 3 h
60 °C 3 h
60 °C 6 h
Lignin content in residue (%)
g peracetic acid/g dry weight aspen

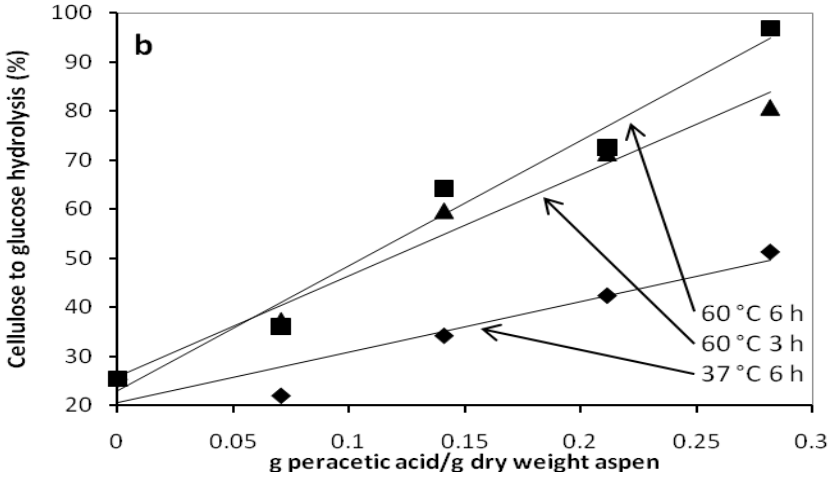
b
60 °C 6 h
60 °C 3 h
37 °C 6 h
Cellulose to glucose hydrolysis (%)
g peracetic acid/g dry weight aspen

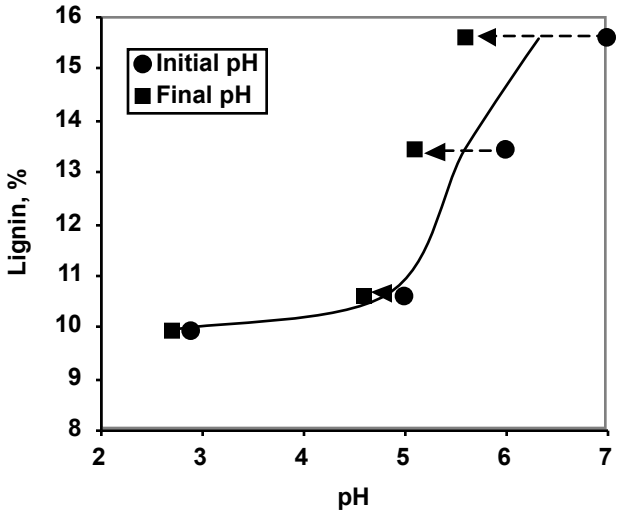
Initial pH
Final pH
Lignin, %
pH

Figure 5.3. Changes in lignin content and glucose release with differing amounts of peracetic acid per gram of wood at different temperatures and pH. **a)** For a given reaction condition, the total lignin content decreased linearly with the amount of peracetic acid added (R^2 for all lines ≥0.97). For given amount of peracetic acid, pretreatment at 60 °C for 6 h removed the most lignin, while 37 °C for 6 h removed the least lignin. At the highest loading of peracetic acid (0.282 g/g dry weight aspen wood), the lignin content dropped to 11.6% after 3 h reaction and to 9.9% after 6 h reaction. **b)** Percent glucose release from glucan in aspen wood powder rose with increasing amounts of peracetic acid (2 x greater glucose release after pretreatment with the highest peracetic acid loading (0.282 g /g dry weight aspen wood)) (R^2 for all lines ≥0.89). At the highest peracetic acid loading (0.282 g /g dry weight aspen wood) raising the temperature from 37 °C to 60 °C reduced lignin content by 4.4% while glucose release increased 41.6%. Increasing the length of the reaction from 3 h to 6 h reduced lignin content by 8.3% and glucose release increased by 16.2%. **c)** Lignin removal from aspen wood meal with aqueous PAA was most effective below pH 5. A suspension of wood (1.30 g aspen) and PAA (115 mM) in buffer (100 mM $NaHPO_4$, 40 mL total volume) was adjusted to the initial pH (*circles*) with 50% NaOH. After 6 h at 60 °C, the pH had decreased to the final pH (*squares*). The curve passes through average of these two pH values.

Increasing the temperature from 37 to 60 °C removed about 50% more lignin, Figure 5.3a. Four pretreatment cycles at 37 °C for 6 h reduced the lignin content from 20.9% to 14.3% using a total peracetic acid loading of 0.282 g PAA/g dry weight aspen wood powder. The lignin content is further reduced to 9.9% by increasing the temperature to 60 °C for 6 h. However, further temperature increase to 80 °C removed less, not more, lignin (20.9% to 12.2%). The higher temperature may promote decomposition of peracetic acid. Danielewicz and Surma-Ślusarska (18) reported fast decomposition of peracetic acid during kraft pulp treatment at 70 and 80 °C but not at 50 °C which are consistent with the observation that 80 °C was less effective than 60 °C.

Increasing the pretreatment time from 3 h to 6 h also increased the amount of lignin removed. After 3 h the lignin content had reduced to 11.6% compared with 9.9% after 6 h exposure at the same concentration of PAA.

When more lignin was removed, more glucose was released from cellulose in the subsequent enzymatic saccharification of the wood powder, Figure 5.3b. Duncan *et* al.[1] and others[19, 20, 21] previously reported this correlation. In earlier work, the highest glucose release was 98% after 8 cycles at 37 °C and 4 h using 70 mM PAA (total 0.343 g

PAA/g dry weight aspen wood powder). By increasing the temperature to 60 °C, the pretreatment time to 6 h, and the PAA concentration to 115 mM, only 4 cycles were needed for a similar glucose release (97%). The total amount of PAA used was 17.8% lower: 0.282 g PAA/g dry aspen powder.

The PAA pretreatment was most effective below pH 5, Figure 5.3c. The initial pH of each solution of peracetic acid was adjusted to 2.7, 5.0, 6.0 or 7.0 with 50% w/w NaOH, then the wood suspension was stirred at 60 °C for 6 h. The final pH's of the solutions were 2.9, 4.6, 5.1 and 5.6, respectively. The pH decreases as PAA (pK_a = 8.5) is converted to acetic acid (pK_a = 4.8) and as the oxidation of lignin generates other organic acids. Above pH 5, the same amount of peracetic acid removed less lignin, likely because peracetic acid spontaneously decomposes faster at higher pH[22]. This result is similar to the reported optimum pH for a similar reaction - pulp bleaching - using peracetic acid. Peracetic acid bleached pulp most effectively between 49 and 71 °C and pH 4 and 6 Devenyns *et* al.[23]. For bleaching, pH below 4 was undesirable because it reduced pulp viscosity[24], but for biofuel applications this does not matter.

5.2.5. Eliminating multiple cycles by increasing the volume of solution. Because F162L PFE generates a maximum of 115 mM peracetic acid, the ratio of PAA-to-wood was increased by increasing the PAA solution volume without increasing the amount of wood added. Higher liquid-to-wood ratios could eliminate multiple pretreatment cycles, Figure 5.4. The liquid: wood varied from 10:1 up to 40:1 (v/w) and is plotted according to the total amount of peracetic acid. For example, 4 cycles of a 10:1 liquid: wood reaction gave similar lignin loss and saccharification yields as 2 cycles at 20:1 and as 1 cycle at 40:1. At the 40:1 ratio, this single cycle reduced lignin more than half the original content and resulted in a glucose yield of 99.7%. Lignin content could be reduced further using 3 cycles at 20:1 yielding 4% residual lignin. There is no advantage to remove this much lignin since saccharification already released nearly 100% of the glucose when the wood contained 10% lignin. Thus, the multiple cycles can be replaced by one cycle at 40:1 ratio (40 L PAA solution to 1 kg dry aspen). This simplification would reduce the number of cycles from 4 to 1 and the treatment time from 24 h to 6 h.

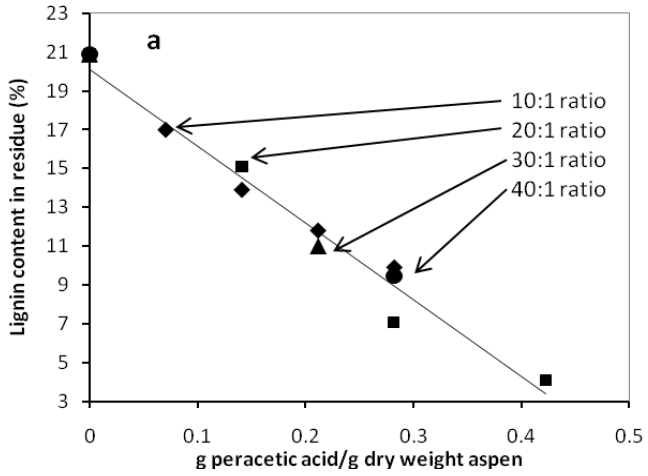
a
Lignin content in residue (%)
g peracetic acid/g dry weight aspen
10:1 ratio
20:1 ratio
30:1 ratio
40:1 ratio

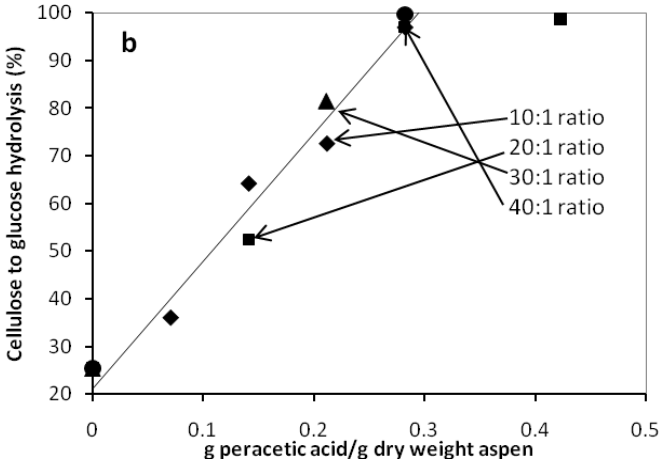
b
Cellulose to glucose hydrolysis (%)
g peracetic acid/g dry weight aspen
10:1 ratio
20:1 ratio
30:1 ratio
40:1 ratio

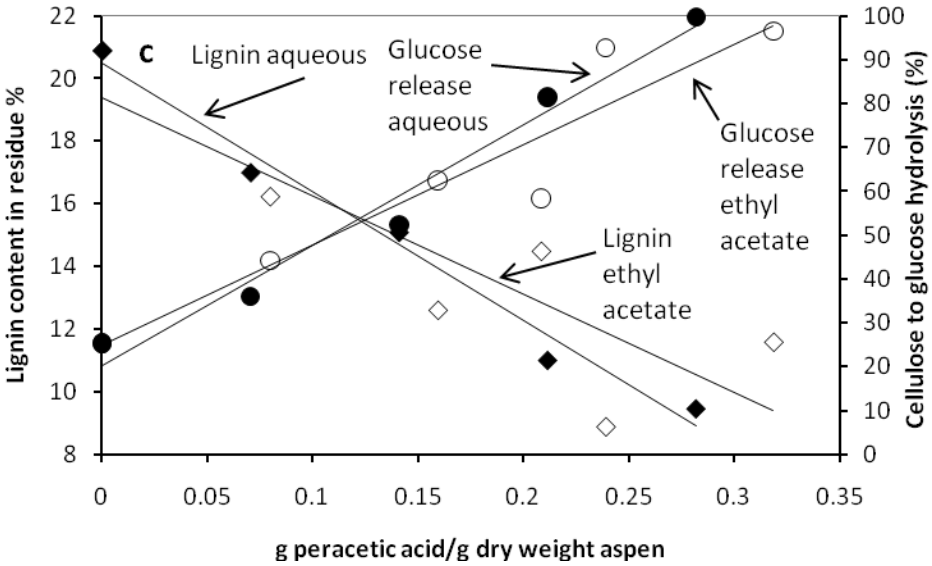
c
Lignin aqueous
Glucose release aqueous
Glucose release ethyl acetate
Lignin ethyl acetate
Lignin content in residue %
Cellulose to glucose hydrolysis (%)
g peracetic acid/g dry weight aspen

Figure 5.4. The effectiveness of the pretreatment depends on the ratio of peracetic acid to aspen wood. The amount of peracetic acid was increased either by repeated treatments (diamonds and squares) or by increasing the ratio of liquid-to-wood (10:1 diamonds, 20:1 squares, 30:1 triangles, 40:1 circles). **a)** Lignin content in the aspen wood powder decreased when ratio of total amount of PAA: aspen wood powder was increased (R^2 for line 0.9669). Lignin removal was greatest after 3 cycles of a 20:1 ratio (0.422 g PAA/g dry weight aspen wood powder). **b)** Glucose release from cellulose in the aspen wood powder increased when the ratio of PAA: aspen wood powder was increased (R^2 for line 0.95). Glucose release was greatest by either using 2 cycles of a 20:1 ratio (0.282 g PAA/ g dry weight aspen wood powder) or 1 cycle of a 40:1 ratio 0.282 g PAA/g dry weight aspen wood powder). **c)** Both aqueous solutions of peracetic acid and ethyl acetate solutions of peracetic acid were similarly effective in pretreating aspen wood. Lignin content (diamonds; use left y-axis) in pretreated aspen wood decreased with increasing ratios of PAA solution-to-wood. The amount of glucose released (circles; use right y-axis) upon subsequent enzymatic saccharification increased with increasing ratios of PAA-to-aspen. Closed symbols are PAA in phosphate buffer and open symbols are PAA in ethyl acetate.

5.2.6. Peracetic acid in ethyl acetate. This method of reusing the enzyme generates peracetic acid in ethyl acetate instead of in aqueous solution. This switch in solvent did not affect the efficiency of lignin removal and glucose release, Figure 5.4c. Increasing amounts of PAA increased the amount of lignin removed thus increase the amount of glucose released from the remaining cellulose. Using 0.282 grams of PAA to pretreat 1 gram of aspen wood, 300 grams of aspen wood could be pretreated with 1 gram of F162L PFE. Under aqueous conditions using wild-type PFE, only 30 grams of aspen wood could be pretreated per gram of enzyme. Therefore, 10-fold less enzyme is needed to treat the same amount of wood.

5.2.7. Material balance. Material balance flow diagrams track the amount of materials used, the outputs and waste as well as the changes in feedstock composition, Figure 5.5. The best case aqueous (boxes) and ethyl acetate (rounded, dotted-line boxes) peracetic acid experiments run at 12.4-g dry weight scale were extrapolated to 1 kg dry weight. Each experiment used 0.282 g of peracetic acid per gram of aspen meal, a 40:1 ratio of solution to aspen meal and 60 °C for 6 hrs for the pretreatment. The subsequent hydrolysis used a scaled down standard NREL LAP-009 procedure for saccharification[25]. The biphasic PAA generation was better because it removed more lignin and less carbohy-

drates during pretreatment, which lead to increased glucose yield from the enzyme hydrolysis.

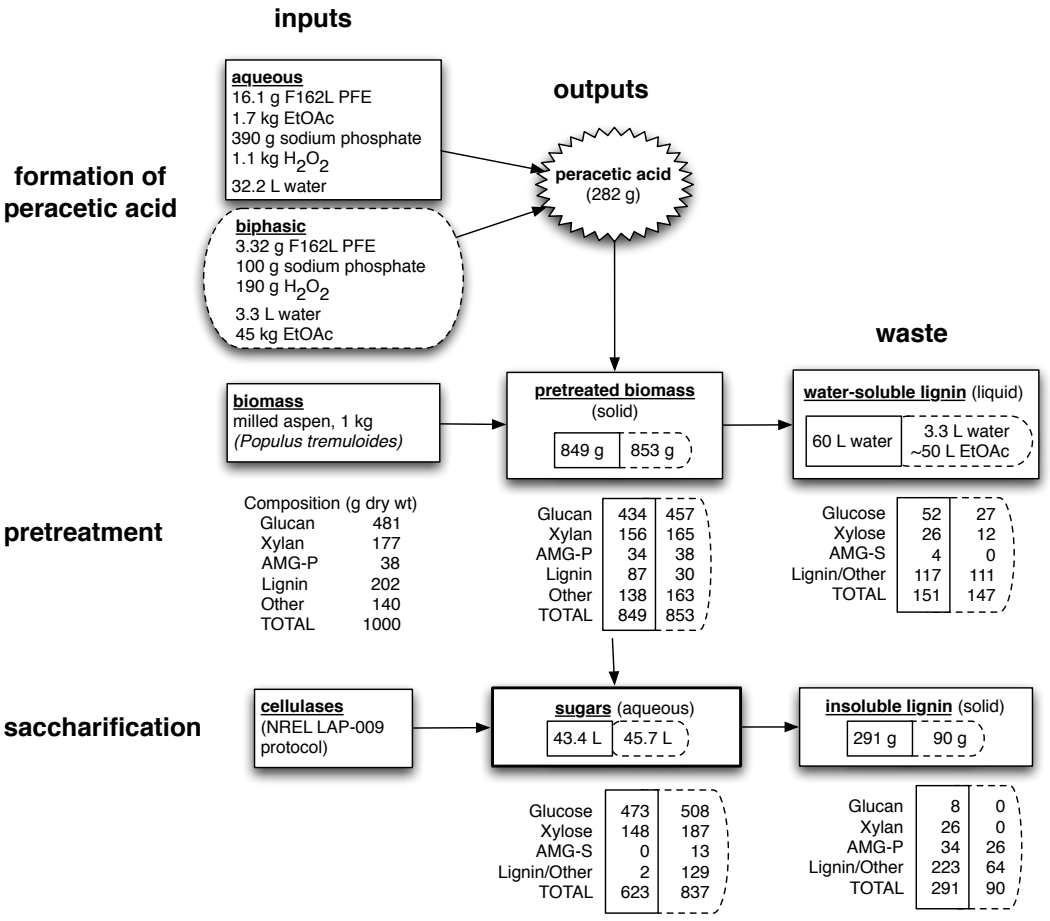

Figure 5.5. Material balances for 1 kg of milled aspen wood extrapolated from the results of 12.4-g dry weight scale experiments. Solid line boxes indicate experiments with aqueous peracetic acid, while boxes in dotted lines indicate peracetic acid in ethyl acetate formed in a biphasic reaction. Pretreatment conditions were 60 °C for 6 hrs and the saccharification used a scaled down standard NREL LAP-009 procedure. Pretreatment with aqueous PAA followed by saccharification yielded 473 g (88.5%) of glucose from the aspen wood powder into the liquid for further processing, with the loss of 151 g biomass (115 g of lignin). Pretreatment with organic PAA (scheme in dotted lines) followed by saccharification yielded 508 g (95.0%) glucose from the aspen wood into the liquid for further processing with the loss of 147 g biomass (172 g lignin). Polysaccharides in the solid are given as glucan or xylan, while the sugars in liquids are given as glucose or xylose. AMG-S: total of arabinose, mannose and galactose sugars. AMG-P: total of arabinan, mannan, and galactan polymers. A given mass of glucan will yield upon hydrolysis a slightly larger mass of glucose due to the gain of the mass of the water.

The pretreatment with aqueous PAA (rectangular solid-line boxes) removed 151 g of biomass. The majority (115 g) was lignin (57% of total lignin available), but 10% of the cellulose and 13% of the xylose fraction of the hemicellulose were also removed. After saccharification, 473 g of glucose was released, yielding 88.5% cellulose-to-glucose conversion after including glucose lost during pretreatment, 148 g of xylose, yielding 73.2% xylan to xylose after including xylose lost during pretreatment. The fermentable sugar release was 621 g. The polysaccharides in solid biomass gain the weight of a water molecule upon hydrolysis to form sugars. Conversion of glucan to glucose and xylan to xylose increased the mass by a factor of 1.11 and 1.14, respectively. For example, complete hydrolysis of 100 g of cellulose yields 111 g of glucose.

The pretreatment with organic PAA (rounded dotted line boxes), removed a similar amount of biomass, 147 g. The majority (172 g) was lignin (85% of total lignin available), but 5% of the cellulose and 6% of the xylose fraction of the hemicellulose were also removed. After saccharification, 508 g of glucose was released, yielding 95.1% cellulose-to-glucose conversion after including glucose lost during pretreatment, 187 g of xylose, yielding 92.5% xylan to xylose after including xylose lost during pretreatment. The fermentable sugar release was 767 g.

During the pretreatment, aqueous generated PAA removed a similar amount of biomass as the organic generated PAA but the composition of the lost biomass was different. Aqueous generated PAA removed less lignin and more carbohydrates compared with the organic generated PAA. Both pretreatment methods reduced the lignin content below the 11% target. The increased amount of carbohydrate in the organic generated PAA treated aspen wood powder meant that more cellulose was available for hydrolysis to glucose by the commercial enzymes than the aqueous generated PAA treated aspen wood. After pretreatment with organic generated PAA and saccharification 767 g fermentable sugars had been released compared with 621 g from aqueous generated PAA pretreatment and saccharification.

Efficient lignin removal depended mostly on the pretreatment time and temperature and on the amount of peracetic acid relative to biomass. The temperature and reac-

tion time increase from 37 °C to 60 °C and from 4 h to 6 h yielded the greatest improvement, nearly doubling saccharification yields to nearly 100% for a given amount of peracetic acid. For a pretreatment of 6 h at 60 °C, aspen wood requires 0.285 g peracetic acid per g of wood. This realization allowed the replacement of a multi-step treatment with a single step treatment by increasing the reaction volume. Either procedure uses the same amount of peracetic acid, but the single step procedure is simpler.

The new procedure reduces enzyme use, chemical use, reaction time, and waste production, Table 5.1. The amount of enzyme required to make enough PAA to pretreat 1 kg of aspen wood dropped from 32.2 g to 16.1 g when using the improved enzyme without recycling. The amount of enzyme dropped another five-fold using the biphasic (ethyl acetate) method to 3.32 g. Optimizing the pretreatment conditions by increasing the amount of liquid to aspen powder reduced the number of cycles from 8 to 1. This reduction of cycles reduced the amount of liquid waste produced (680 L to 60 L), the amount of chemicals (buffer and hydrogen peroxide) used (2874 g to 291.5 g) and the reaction time (32 h to 6 h). The only negative of the optimized procedure is an increase in pretreatment temperature from 37 °C to 60 °C. Although the biphasic method uses more ethyl acetate, after reaction with the wood, most of the ethyl acetate may be recycled.

Table 5.1. Comparison of inputs, waste and pretreatment conditions for generation of peracetic and pretreating 1 kg of aspen wood powder.

	Duncan et al. (1) aqueous buffer	This work aqueous buffer	This work Biphasic (ethyl acetate) [1]
inputs			
enzyme	32.2 g	16.1 g	3.32 g[a]
sodium phosphate	774 g	387 g	99.5 g
hydrogen peroxide	2,100 g	1,050 g	192 g
ethyl acetate	3.78 L	1.89 L	50 L (recycled[b])
PAA generated	343 g	282 g	282 g

Pretreatment conditions	8 cycles, 37 °C, 32 h total	1 cycle, 60 °C, 6 h total	1 cycle, 60 °C, 6 h total
output			
Liquid	680 L aqueous	60 L aqueous	3.3 L aqueous ~49 L ethyl acetate (recycle[b])
Solid	80 g	291 g	90 g
Fermentable sugar	581 g	588 g	763 g

[a]based reuse of the enzymes as in Figure 5. [b]most of the ethyl acetate can be recycled, but this recycling has not been tested.

5.3 Materials and Methods

5.3.1 General. Wild-type and F162L PFE were prepared as in Yin *et* al.[16]. The proteins were purified by nickel affinity chromatography using Ni-NTA resin (Qiagen) and imidazole (80 mM) in the wash buffer to elute a contaminating catalase. The eluted protein was dialyzed and concentrated using Amicon centrifuge filters (Millipore) with a molecular weight cut-off of 10,000 Daltons.

5.3.2. Quantitation of peracetic acid. The amount of peracetic acid was measured using the Karst assay[26] where peracetic acid reacts with excess methyltolylsulfide (MTS) to form methyltolylsulfoxide (MTSO). The amount of MTSO was measured by HPLC using a C8 column XDB8 (Agilent) eluted with a gradient of water with 10% methanol and acetonitrile at a flow rate of 1 mL/min, Table 5.2. MTSO eluted at 2.5 min and the amount was measured by the area of the peak measured at 225 nm and a calibration curve.

Table 5.2. Changes in the HPLC mobile phase composition as function of time to measure methyltolylsulfoxide (MTSO) and thus the amount of peracetic acid.

Time	Mobile phase composition[a]
(min)	water/10%methanol: acetonitrile
0	60:40
3	40: 60
3.5	20: 80
4.5	20: 80
5.5	40: 60
6.5	60: 40
10	60: 40

[a]The first number indicates the volume percentage of water containing 10 vol% methanol and the second number indicates the percentage of acetonitrile.

5.3.3 Formation of peracetic acid in aqueous solution. A solution (40 mL) containing buffer (sodium phosphate, pH 7.2, 100 mM) ethyl acetate (500 mM), hydrogen peroxide (1.0 M), and PFE F162L (0.5 mg/mL) in a 50-mL centrifuge tube was incubated for 10 min at 23 °C. HPLC analysis indicated 115 mM of PAA. This solution was used pretreat aspen wood without further purification.

5.3.4. Formation of peracetic acid in two-phase reaction. An aqueous solution (200 mL, 1.7 M H_2O_2, 200 mM sodium phosphate pH 7.2, 0.5 mg/mL of F162L PFE) and ethyl acetate (400 mL) was mixed at 23 ˚C for 30 minutes at 150 rpm in a 1-L round bottom flask. The ethyl acetate layer containing 130 mM peracetic acid was decanted and used to directly pretreat 13 grams of aspen wood.

5.3.5 Reuse of enzyme in two-phase reaction. Ethyl acetate (0.5 mL) was added to a aqueous solution (0.5 mL) containing sodium phosphate buffer (250 mM, pH 7.2), hydrogen peroxide (1.7 M), and PFE F162L (0.5 mg/mL) in a 1.5-mL centrifuge tube and the mixture was shaken (900 rpm) at room temperature. After 10 min, the reaction tube was centrifuged (30 s at 1000 rpm), the ethyl acetate phase containing peracetic acid was removed with a pipette and replenished with fresh ethyl acetate. The combined ethyl ace-

tate phases were used to pretreat aspen wood. Both wild type (data not shown) and F162L PFE lose ~14% of their activity in each cycle. A control reaction without enzyme formed <10% of the amount of peracetic acid that formed with enzyme. (Data are in Figure 2.) The conditions used to test other ethyl esters (propionate, butyrate, caproate, heptanoate, decanoate) are identical except the reaction time was extended to 30 min.

5.3.6. Pretreatment of aspen wood. Bark-free chips of aspen (*Populus tremuloides* Michx.) wood from a Minnesota paper mill were air-dried and milled to 40-mesh in a Wiley mill. The milled aspen wood before pretreatment contained 4.5 wt% water. Milled aspen wood (1.3 g) was stirred at 300 rpm with a magnetic stir bar in peracetic acid solution (40 mL, 115 mM) in either aqueous buffer (sodium phosphate, 100 mM, pH 7.2) or ethyl acetate in a sealed 100-mL glass bottle for 6 h at 60 ˚C. The suspension was filtered and the aspen wood was washed with distilled water (40 mL).

As described by Duncan *et* al.[1], dry weights were determined by oven drying a sample of the feedstock for 48 h and 100 °C according to NREL protocol for determination of total solids in biomass, LAP-001[27]. The composition of the aspen was determined before and after each pretreatment. After acid hydrolysis of the feedstock with sulfuric acid, insoluble lignin was determined with the TAPPI method[28]. Acid-insoluble lignin removed from the solution by filtering and determined by oven-dry weight of residual lignin on filter paper.

5.3.7. Saccharification of aspen. Aspen meal was saccharified by treatment with Celluclast 1.5L (Sigma, St Louis, MO, USA, 60 FPU/g cellulose) and Novozyme 188 (Sigma, 64 pNPGU/g cellulose) for 7 days according to NREL method for the enzymatic saccharification of lignocellulosic biomass, LAP-009[25]. Celluclast 1.5L contains, besides cellulase activity, an approximately equal amount of xylanase activity[29]. The procedure was modified to use 25 mg of cellulose instead of 100 mg previously described by Duncan *et* al.[1]. The liquids obtained after the saccharification, were analyzed with HPLC with a BIO-RAD Carbo-C Refill Cartridges, 30 × 4.6 mm (guard column) in line with BIO-RAD Aminex HPX-87P, 300 × 7.8 mm (analytical column) eluted at 85 °C with HPLC grade water flowing at 0.6 mL/min or with a BIO-RAD De-Ashing Refill Car-

tridges, 30 × 4.6 mm (guard column) in line with VARIAN MetaCarb 87P, 300 × 7.8 mm (analytical column) eluted at 80 °C at 0.3 mL/min.

5.4. Discussion

Decreasing the lignin content from 22 to 11 wt% in aspen wood allows nearly complete saccharification of the sugars, Figure 5.6. A comparison of the residual lignin content with glucose release for all samples during this research project shows that as lignin content drops, glucose release increases. This enhancement reaches its maximum at around 11% lignin content, giving us a target for lignin removal. Thus, only ~ 50% of total lignin content needs to be removed to reach maximum gains. Reaction medium selection (phosphate buffer or ethyl acetate) also has no measureable effect, so these variables can be changed to decrease cost and increase convenience without compromising the yield of sugars.

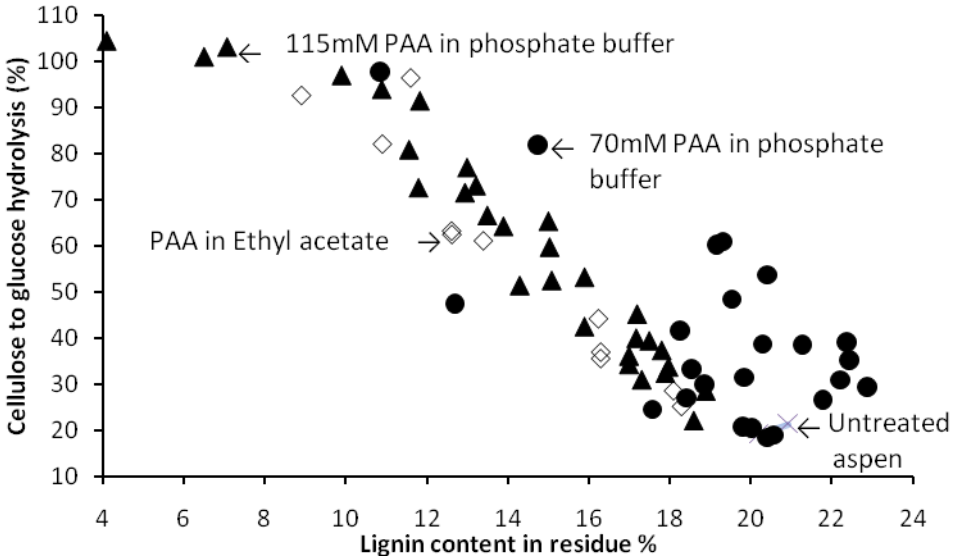

Figure 5.6. Cellulose to glucose release (y-axis) reaches 100% once about half of the lignin in aspen wood is removed. Removing more than half gives no additional advantage. All pretreatment conditions tested behave similarly.

The amount of enzyme needed is still too high for a practical application. Assuming a large-scale enzyme cost of US $100/kg enzyme[30], 3 g enzyme/kg aspen wood cor-

responds to $0.30/kg of wood. Since 1 kg of aspen wood yields 0.1 gal of ethanol (100 gallons of ethanol from 1 ton of hardwood sawdust[31], this cost corresponds to $3 enzyme/gallon of ethanol, which is approximately 100-fold still too high. (The 3 g of esterase/kg aspen wood is similar to the amount of β-glucosidase used in the saccharification step, also 3 g enzyme/kg aspen wood. Optimization of the saccharification step was not a goal of this research; the NREL procedure uses a large amount of enzyme to ensure that the saccharification is not a limiting step to sugar release.) Immobilization technologies as well as improvements in the catalytic properties of the enzyme have made much larger improvements in other processes (e.g., a >40,000-fold improvement in the catalytic efficiency of a transaminase by directed evolution[32], so it is reasonable to expect that the cost of the enzyme can be decreased.

Another way to reduce the amount of enzyme needed is to improve the efficiency of the reaction of peracetic acid with lignin. Using 0.285 g of peracetic acid per gram of aspen wood removed approximately half of the lignin or 10 wt%, which corresponds to 0.10 g. In mole terms, 0.285 g of peracetic acid is 3.75 mmol, while 0.10 g of lignin corresponds to 0.50 mmol of lignin monomer, assuming an average monomer molecular weight of 200 g/mol. Thus, breaking lignin polymer into soluble fragments required approximately 7.5 mol of peracetic acid for each mole of lignin monomer solubilized. It may be possible to cleave the lignin with less peracetic acid.

The ethyl acetate required also increases the cost of the current method. Most of the ethyl acetate can likely be recycled, but this recycling has not yet been investigated. One way to reduce the amount of ethyl acetate required would be to use acetate esters within the lignocellulose to replace the ethyl acetate. Aspen wood contains 3.5 wt% acetyl groups, which could generate about one quarter of the peracetic acid (0.062 g PAA/g aspen wood) currently needed for pretreatment.

A preliminary comparison of this approach with the dilute acid pretreatment - the most cost-effective pretreatment option for corn stover by Kazi et al.[33] and generally well-accepted as a more viable pretreatment alternative - shows two potential cost savings. Assuming fixed upstream feedstock and handling costs and unaffected downstream

bioconversion steps like fermentation, the peracid pretreatment 1) eliminates neutralization and conditioning steps, and 2) allows reuse of solvents and peracid-generating enzymes. The neutralization/conditioning steps contributed to 4.27% of a modeled project investment totaling $220.1M[34]. Removing this step saves $9.4 M. Uncertainties remain about whether milled wood could be replaced by wood chips. A high (87%) recovery of perhydrolase enzyme would lower its cost per run to 13% of total and lower its cost per ethanol gallon from nearly $3 to $0.39. Recovery of ethyl acetate also appears feasible, but was not investigated in this work.

Other potential advantages are higher yields and process integration potential. Nearly 95.1% yield of the original holocellulose fraction was recovered as glucose, which results in a theoretical ethanol yield of 121 gal per dry ton, versus the 89.8 modeled for Aden and Foust[34]. The process is also biologically-based, offering potential for integration with downstream steps, that is, the yeast fermentation might make enzyme and ethyl acetate to further reduce costs.

Enzyme-generated peracetic acid is an effective pretreatment for aspen wood that enables release of all of the sugars. The efficiency of the enzyme-generation and pretreatment has been dramatically improved in this work, but further improvements are needed before. Further improvements should focus on reducing the amount of enzyme and ester needed.

Chapter 6

Computer modeling was used to rationalize higher perhydrolysis activity. The molecular modeling generated static structures which allows mechanisms to be ruled out. In this chapter, molecular dynamics is used to explain how lipase from Candida rugosa prefers the (*S*)-enantiomer over the (*R*)-enantiomer.* Molecular modeling is not enough to examine all of the possible orientations that each enantiomer adopts. Thus, molecular dynamics is used to sample many conformations, including higher energy ones that are missed by molecular dynamics.

*This chapter is a copy of a published article and is reproduced with permission from Adv. Synth. Catal., Vol. 353, Colton, I.J.; Yin, D.L.T.; Grochulski, P.; Kazlauskas, R.J., "Molecular basis of chiral acid recognition by Candida rugosa lipase. X-Ray structure of transition state analog and modeling of the hydrolysis of methyl 2-methoxy-2-phenylacetate.", 2529-2544, Copyright 2011, John Wiley & Sons, License number: 2760430940157 (See Appendix for reprint).

Molecular basis of chiral acid recognition by *Candida rugosa* lipase. X-Ray structure of transition state analog and modeling of the hydrolysis of methyl 2-methoxy-2-phenylacetate.

Lipase from *Candida rugosa* shows high enantioselectivity toward α-substituted chiral acids such as 2-arylpropionic acids. To understand how *Candida rugosa* lipase (CRL) distinguishes between enantiomers of chiral acids, we determined the X-ray crystal structure of a transition-state analog covalently linked to CRL. CRL shows moderate enantioselectivity (E = 23) toward methyl 2-methoxy-2-phenylacetate, **1**-methyl ester, favoring the (*S*)-enantiomer. We synthesized phosphonate (R_C,$R_P$$S_P$)-**3**, which, upon reaction with CRL, mimics the transition state for hydrolysis of (*S*)-**1**-methyl ester, the fast-reacting enantiomer. An X-ray crystal structure of this complex shows a catalytically productive orientation with the phenyl ring in the hydrophobic tunnel of the lipase. Phe345 crowds the region near the substrate stereocenter. Computer modeling of the slow-reacting enantiomer identified four possible conformations for the corresponding slow reacting enantiomer: three conformations where two substituents at the stereocenter have been exchanged relative to the fast-reacting enantiomer and one conformation with an umbrella-like inversion orientation. Each of these orientations disrupts the orientation of the catalytic histidine, but the molecular basis for disruption differs in each case showing that multiple mechanisms are required for high enantioselectivity.

6.1 Introduction

Lipases often accept unnatural esters substrates and show high enantioselectivity and are therefore useful in organic synthesis. One of the best studied lipases for its enantioselectivity toward chiral acids is lipase from *Candida rugosa* (CRL). This lipase shows high enantioselectivity toward many carboxylic acids with a stereocenter at the α-position. Examples include 2-arylpropionic acids such as naproxen (aryl = 2-(6-methoxy)naphthyl), which are non-steroidal anti-inflammatory drugs and 2-aryloxypropionic acids, such as dichlorprop (aryloxy = 2,4-dichlorophenoxy), which are herbicides, and can also reduce blood cholesterol levels[1,2].

An empirical rule predicts the favored enantiomer of chiral carboxylic acids for *Candida rugosa* catalyzed reactions,[3] Figure 6.1. The rule applies to carboxylic acids with stereocenter at the α-position and relies on the sizes of the substituents at the stereocenter. This rule suggests that CRL distinguishes enantiomers based on the size of the substituents.

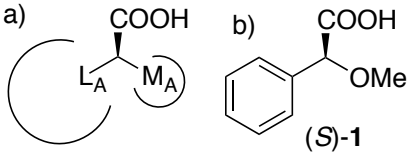

Figure 6.1. An empirical rule based on substituent size predicts the faster-reacting enantiomer in hydrolyses of esters catalyzed by purified *Candida rugosa* lipase. a) Generic structure of the acid predicted to form faster from the corresponding ester. L_A represents a large substituent, while M_A represents a medium substituent. b) An example of a carboxylic acid that fits this rule. Hydrolysis of racemic methyl 2-methoxy-2-phenylacetate favors the (*S*)-enantiomer shown by a factor of 23 over the the (*R*)-enantiomer[4].

The molecular details of this enantioselectivity are still unclear. One cannot accurately predict the degree of enantioselectivity, nor can one predict which amino acid substitutions will increase enantioselectivity. An understanding of these details is essential for rational design of enantioselective enzyme-catalyzed reactions. This understanding could also help organic chemists design chemical catalysts with high enantioselectivity.

The compound 2-methoxy-2-phenylacetic acid (*O*-methylmandelic acid, **1**) is the focus of this work. Enantiomerically pure 2-methoxy-2-phenylacetic acid is a useful rea-

gent for the NMR analysis of absolute stereochemistry of amines and alcohols[5]. Lipase from *Aspergillus niger* resolved the corresponding vinyl ester of **1** by transesterification with methanol in isopropyl ether with an enantioselectivity of 25,[6] but this lipase is not considered in this paper. This chiral acid is similar in structure to 2-arylpropionic acids mentioned above and is general example for the CRL catalyzed hydrolysis of esters of chiral acids.

The genome of the yeast *Candida rugosa* contains at least seven lipase isozymes named lip1-7. The isoenzymes differ in amino acid sequence (≥80% amino acid sequence identity among lip1-5, ≥65% among 1-7), isoelectric point and degree of glycosylation[7]. Commercial samples of *Candida rugosa* lipase are non-recombinant enzymes and contain multiple isozymes. Gel electrophoresis (SDS-PAGE) of commercial samples of CRL shows a major band and minor band. The major band corresponds to lip1, while the minor band is a mixture of isozymes lip2-5. In addition, commercial samples of CRL contain a small amount of contaminating protease[8]. The x-ray crystal structures of three isozymes have been solved: lip1,[9,10] lip2[11] and lip3[12].

The isozymes differ in their enantioselectivity toward acids and secondary alcohols, but show the same enantiopreference[13, 14]. Isoenzyme lip1, the focus of this paper, shows the highest enantioselectivity toward ibuprofen (2-(4-(2-methylpropyl)phenyl)propanoic acid), which, among the compounds tested, is closest in structure to compound **1**. Besides isoenzyme composition, the purification procedure can also change the enantioselectivity, but not the enantiopreference, of CRL[14, 15, 16]. The working hypothesis is that purification steps such as treatment with organic solvents can change the conformation of the lipase, possibly from the closed to the open conformation.

Commercial samples of CRL show low enantioselectivity (E = 8) toward methyl 2-methoxy-2-phenylacetate, **1**-methyl ester, favoring the (*S*)-enantiomer[4]. Purified CRL (A-form, which likely corresponds to lip1) shows higher enantioselectivity: E = 23 (*S*)[4]. This paper focuses on the molecular basis for this enantioselectivity.

CRL-catalyzed hydrolysis of esters occurs in two steps: acylation of the active site serine followed by deacylation, Figure 6.2. The acylation step involves the first tetrahe-

dral intermediate, T_d1, while the deacylation step involves the second tetrahedral intermediate, T_d2. The first irreversible step in hydrolysis is the acylation step. (Although in principle, this step is reversible, in practice the concentration of leaving group alcohol is low so it is effectively irreversible.) This acylation step is also likely the rate-determining step because substrates with a better leaving group react faster. Kinetic studies of another lipase showed that acylation was the rate determining step[17].

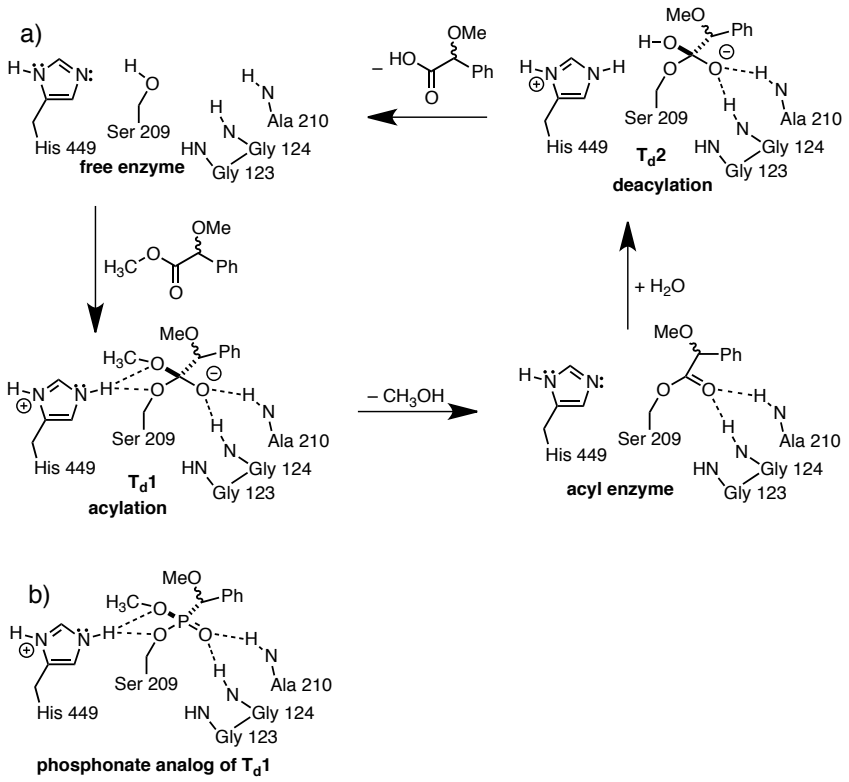

Figure 6.2. a) Mechanism of CRL-catalyzed hydrolysis of racemic methyl 2-methoxyl-2-phenylacetate ((±)-**1**-methyl ester) involves two tetrahedral intermediates and an acyl enzyme intermediate. The rate-determining step is the formation of the acyl enzyme intermediate, which involves formation and collapse of the first tetrahedral intermediate. The transition state for the reaction therefore resembles the first tetrahedral intermediate. For clarity, this scheme omits the third member of the catalytic triad, Glu341. b) A stable phosphonate mimics the first tetrahedral intermediate and also the transitions state for hydrolysis of (±)-**1**-methyl ester.

A tetrahedral intermediate exists for only a short time, but a stable phosphonate mimics this intermediate. We synthesized phosphonate inactivators that could react with the active site serine in CRL and make a stable phosphonate. We solved the x-ray crystal

structure of the CRL-phosphonate complex corresponding to the tetrahedral intermediate for the fast-reacting enantiomer of **1**-methyl ester. We also synthesized the phosphonate corresponding to the slow-reacting enantiomer, but it did not form a complex with CRL. We investigated the orientations of the slow reacting enantiomer using molecular modeling and identified the multiple molecular interactions required to prevent its reaction. This understanding an essential first step to rational design of higher enantioselectivity, but also shows the complexity and difficulty of the task.

6.2 Results

6.2.1 Synthesis of transition state analogs

Racemic inactivators. Two racemic inactivators - the chloro and *p*-nitrophenyl (PNP) derivatives, (±)-**3** and (±)-**4**, were prepared as diastereomeric mixtures, Figure 6.3. Benzaldehyde and dimethylphosphite condensed over solid KF to form dimethyl(1-hydroxyphenylmethyl)phosphonate, (±)-**2**, according to a literature procedure[19] in 88% yield. Methylation of (±)-**2** using methyl iodide and Ag_2O afforded dimethyl[1-(methoxy)phenylmethyllphosphonate in 66% isolated yield. This methylation was the most difficult reaction to optimize in this synthesis. Initial trials using basic conditions (Mel/K_2CO_3 in EtOAc or Mel/KOH in DMSO) yielded an uncharacterized decomposition product, likely due to reversion of (±)-**2** back to starting materials under basic conditions[18] and subsequent decomposition. Using the neutral silver oxide to increase the electrophilicity of methyl iodide avoided these problems. A stoichiometric amount of methyl iodide gave inconsistent yields for this methylation step, likely due to evaporation of methyl iodide, but using methyl iodide as the solvent eliminated this problem and was the optimum way to carry out this step. Hydrolysis of dimethyl[1-(methoxy)phenylmethyllphosphonate using aqueous base afforded the monoacid in 85% yield. Monochlorination, using 1.5 eq oxalyl chloride in refluxing dichloromethane, yielded a 4:1 diastereomeric mixture of monochlorophosphonates, (±)-**3**. Reaction of the monochlorophosphonates with *p*-nitrophenol and triethylamine resulted in a 1:1 mixture of diastereomers, (±)-**4** in 20% overall yield.

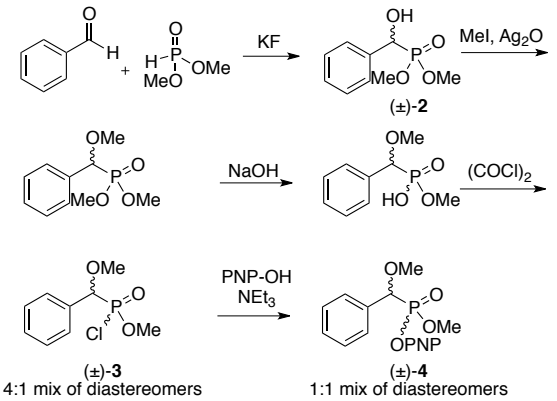

Figure 6.3. Synthesis of racemic inactivators chloro derivative (±)-**3** and *p*-nitrophenyl derivative (±)-**4**. Only the chloro derivative (±)-**3** inactivated lipase from *Candida rugosa*. PNP = *p*-nitrophenyl

Inactivator (±)-**3** inactivated lipase from *Candida rugosa*, but inactivator (±)-**4** did not. Incubation of 10^3-fold excess of (±)-**3** dissolved in dichloromethane with an aqueous solution of lipase from *Candida rugosa* eliminated >99% of the hydrolytic activity within 8 min. In contrast, overnight incubation of a 10^4-fold excess of (±)-**4** with CRL, eliminated <5% of the hydrolytic activity. Since the chlorophosphonate (±)-**3** was a good inactivator, we prepared compound **3** with a single configuration at the carbon center.

Inactivator 3 having a single configuration at the carbon center. The chloro derivative **3** with a single configuration at the carbon center was prepared similarly, but with the addition of a lipase-catalyzed kinetic resolution, Figure 6.4. Secondary alcohol (±)-**2** was converted to to the acetate, (±)-**5**, which was resolved using lipase from *Rhizopus oryzae* (Amano FAP 15) yielding (*S*)-**2** (78% recovery, 68% ee) and recovered starting acetate (*R*)-**5** (65% recovery, 88% ee *R*). These enantiomeric purities correspond to an *E* of 32, significantly lower than the reported *E* of >100 for this resolution by Li & Hammerschmidt[23]. To increase the enantiomeric purity, the acetate was resolved two more times with the same enzyme. Reincubation of the acetate (68% ee *R*) with lipase for an additional 26.8% conversion, then separation and reincubation for an additional 10.3% conversion yielded the remaining acetate in >98% ee *R*, 0.4 g, 14% overall yield; 50% yield is the maximum in a resolution. This acetate was cleaved with triethylamine-methanol to yield (*R*)-**2** for the next step in the synthesis. To prepare enantiomerically

pure (*S*)-**2**, we reacetylated enantiomerically enriched (*S*)-**2** to the acetate (*S*)-**5** and carried out a second hydrolysis catalyzed by the lipase until 46% conversion, which yielded the yielded (*S*)-**2** in >98% ee, 0.11 g (4.4% overall yield).

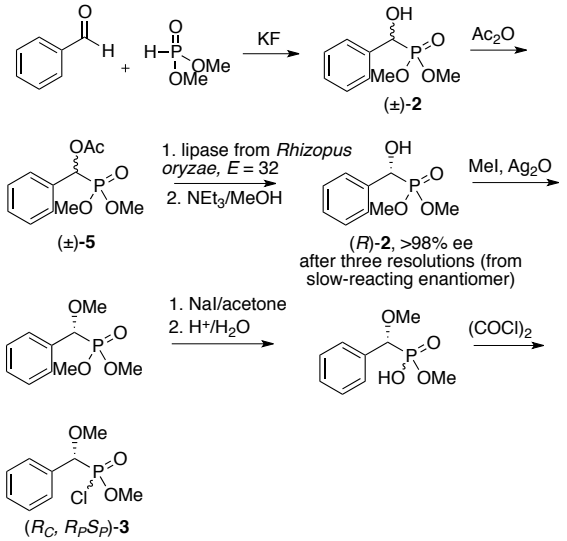

Figure 6.4. Synthesis of inactivator (R_C,R_PS_P)-**3**, which, upon reaction with lipase from *Candida rugosa*, mimics the transition state for the CRL-catalyzed hydrolysis of (*S*)-**1** methyl ester (fast-reacting enantiomer). A key step in the synthesis of inactivator (R_C,R_PS_P)-**3** was a lipase-catalyzed resolution of acetate (±)-**5** by lipase from *Rhizopus oryzae* catalyzed hydrolysis. An analogous route (not shown) formed phosphonate (S_C,R_PS_P)-**3**, which mimics hydrolysis of the slow-reacting (*R*)-enantiomer of **1**-methyl ester.

Methylation of (*R*)-**2** used silver oxide and excess methyl iodide as developed for the racemic alcohol, (±)-**2**. The overall yield for the hydrolysis of the acetate and methylation was 50%. Hydrolysis of (*R*)-dimethyl[1-(methoxy)phenylmethyllphosphonate to the monoacid used 1.5 eq NaI in refluxing acetone, followed by acidification to afford (*R*)-monoacid (83% yield). These milder conditions for the hydrolysis, as compared to the NaOH used to hydrolyze the racemate in Figure 6.3, minimized the possibility for racemization at the resolved stereocenter. The enantiomeric purity of **2** was measured after reacetylation with acetic anhydride to the acetate **5**, by ^{1}H-NMR in the presence of a chiral shift reagent, Eu(hfc)$_3$, but the enantiomeric purity of the subsequent compounds could not be measured. Finally, chlorination of the monoacid using 100 eq of oxalyl chloride yielded a 4:1 mixture of the two phosphonochloridates, (R_C,R_PS_P)-**3** as observed by

^{1}H- and ^{31}P-NMR. Reaction of the monoacid with less oxalyl chloride yielded substantial amount of pyrophosphonate side product, which did not inactivate CRL.

An analogous route (not shown) formed phosphonate (S_C,R_PS_P)-**3**, which mimics hydrolysis of the slow-reacting (*R*)-enantiomer of **1**-methyl ester.

6.2.2 X-ray crystal structure. Covalent enzyme-inhibitor complex was prepared by adding excess (R_C,R_PS_P)-3 diastereomeric mixture dissolved in 2-methyl-2,4-pentanediol to the purified CRL solution. The inhibited protein crystallized under conditions similar to those for the open form CRL[9]. The crystal structure was solved by isomorphous replacement with the open form CRL structure. As expected from the synthesis, the configuration at the carbon stereocenter was *R*, Figure 6.5. The configuration at phosphorus was also a single configuration (S_P) although the inhibitor was a mixture of both configurations at phosphorus. Presumably, the inhibitor with one phosphorus configuration reacted much faster that the other leading to only the fast-reacting phosphorus configuration bound to the lipase.

The overall structure is identical to the open form of *Candida rugosa* lipase[9]. The lipase adopts the α/β hydrolase fold. The protein scaffold is formed by a central 11-stranded mixed β-sheet and an N-terminal 3-stranded β-sheet. The flap is in its open conformation is stabilized by Glu 66 which is preceded by a proline at one hinge and by the Pro92 cis-trans isomerization at the other hinge. The x-ray structure of the closed form of CRL[10a] was solve previously using different crystallization conditions and without a phosphonate inhibitor. The transition state analog in the current structure is well defined in the electron density. There are 3 sugar molecules and 175 water molecules identified in the electron density. The overall geometry of the molecule is very good (Table 6.1) with the final R/R_{free}=17/21%, average B-factor of 22.6 Å^2 and good stereochemistry.

The crystal structure of the transition state analog confirms that the stereocenter matches the fast reacting enantiomer because of the good fit of this stereoisomer with the measured electron density, Figure 6.5. The electron density obtained by running a simulated annealing refinement with the analog and nearby protein atoms (within 3.5 Å) omitted. The calculated unbiased difference map confirms the selected enantiomer.

The carbon stereocenter of the inhibitor lies at the mouth of a tunnel with the phenyl ring pointing inside the hydrophobic tunnel, Figure 6.5. This tunnel accomodates the fatty acyl chains of other inhibitors. The methoxyl substituent at the carbon stereocenter points toward Phe296, while the hydrogen at the carbon stereocenter points toward Phe344.

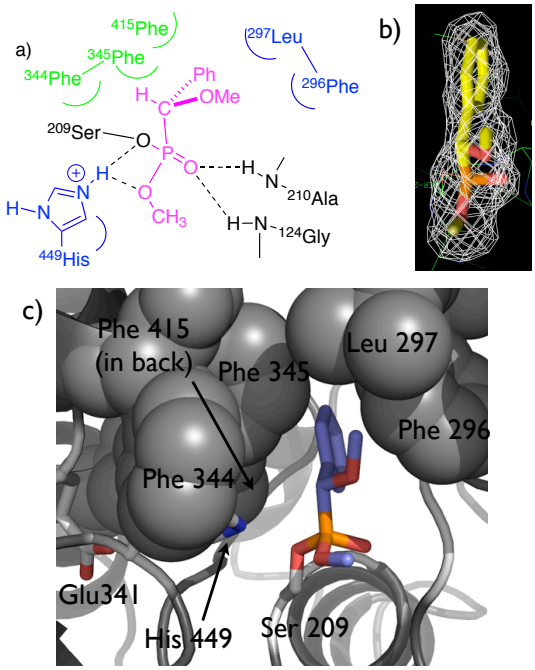

Figure 6.5. Phosphonate transition state analog for hydrolysis of (*S*)-**2** in the active site of CRL. a) Schematic diagram b) The model of the phosphonate fits well in the observed electron density. The mesh represents the difference simulated annealing omit map at the 3 sigma level. The inhibitor and all protein atoms within a 3.5 Å sphere from the inhibitor were excluded from calculations. c) X-ray crystal structure. The analog mimics a catalytically productive orientation because the phosphorus links covalently to the catalytic serine (Ser209) and the analog makes good hydrogen bonds (O–N distances <3.2 Å) to the catalytic histidine (His449; shown as sticks for clarity) and the oxyanion hole (Ala210, Gly124). The carbon stereocenter lies at the entrance to a tunnel with the phenyl group pointing inside the tunnel. Residues Phe344, Phe345, and Phe415 (mostly hidden by Phe344 and Phe345) block the left side of the tunnel entrance. A hydrogen substituent can fit here, but not an –OMe substituent. Residues Leu297 and Phe296 form the right side of the tunnel entrance. Site-directed mutagenesis experiments previously identified Phe344 and Phe345 as important to enantioselectivity of CRL toward 2-aryl propionic acids.

Similar crystals formed using the phosphonate mimicking the slow reacting enantiomer showed no inhibitor in the active site. Presumably the slow reacting enantiomer fits so poorly that this inhibitor did not react with the lipase.

6.2.3 Modeling to find possible orientations of the slow-reacting enantiomer. To identify the orientation of the slow enantiomer, we used molecular modeling. There are four ways that the slow enantiomer can bind in the same place in CRL as the fast enantiomer. Three of these possibilities involve an exchange of two substituents at the stereocenter and one possibility involves an umbrella-like inversion orientation,[18] Figure 6.6. An analogy to these different possibilities is the two different ways that you can overlay your right and left hand, Figure 6.6b. In one way the two palm face in the same direction, but the finger do not align, which is similar to one of the exchange of substituents possibilities. In the second way, the palms face in opposite directions, but fingers line up correctly, which is similar to the umbrella-like inversion. High enantioselectivity requires the lipase to prevent reaction of the slow enantiomer in any of these four orientations.

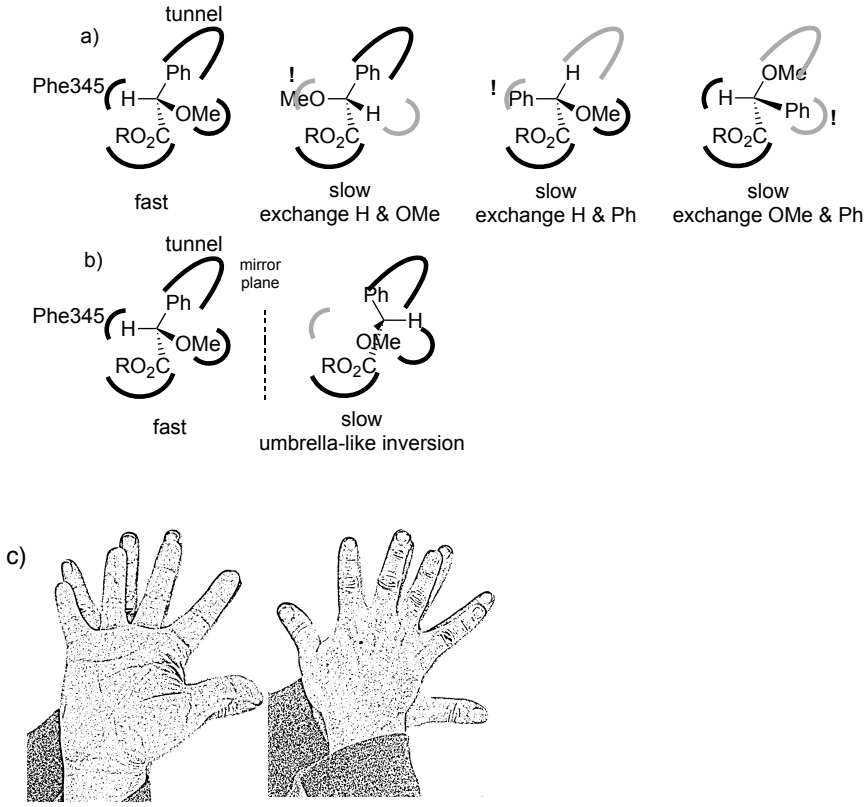

Figure 6.6. Possible orientations of the slow enantiomer of **1** in the active site of *Candida rugosa* lipase. a) Schematic of the fast-reacting enantiomer of methyl 2-methoxy-2-phenylacetate ((*S*)-**1**, left) and three possible exchange-of-substituents orientations for the slow enantiomer ((*R*)-**1**, right three structures). The curves lines represent the active site; gray curves indicate the two positions that have mismatched substituents for the slow enantiomer. The exclamation points mark points where steric interactions disfavor the three orientations for the slow enantiomer. b) Schematic of the fast-reacting enantiomer (*S*, left) and an umbrella-like inversion orientation of the slow enantiomer (*R*, right) in the same site. The mirror plane shown relates the two substrate molecules. This reflection places the hydrogen substituent of the slow enantiomer in a new location leaving the original site empty (gray curve). C) An analogy to these different possible orientations is the two ways to overlay your right hand on top of your left hand. On the left panel, the fingers match with each other, but the palms face in opposite directions: bottom hand palm faces down, while top hand palm faces up. On the right panel, the fingers do not overlay correctly, but both palms face down.

To identify how CRL prevents hydrolysis of (*R*)-**1** in all four possible orientations, we modeled tetrahedral intermediates corresponding to these four possibilities. These tetrahedral intermediates were built using the crystal structure of the phosphonate analog for hydrolysis of (*S*)-**1** as the model. The modeling used the OPLS 2005 force field[24] for the lipase and tetrahedral intermediate and a TIP3P model[25] for the water solvent. A molecular dynamics simulation generated multiple conformations of each possible orientation to mimic the multiple conformations possible during the reaction.

The tetrahedral intermediate must form four catalytically important hydrogen bonds with the lipase: from the two N–H's of the oxyanion hole (Ala124, Gly210) to the oxyanion oxygen of the tetrahedral intermediate and from N_{ε}–H of the catalytic histidine to the alcohol oxygen of the tetrahedral intermediate and to O_{γ} of active site serine, see Figure 6.3 above. Conformations containing all five catalytically essential hydrogen bond were considered catalytically productive, while those missing one or more hydrogen bonds were considered nonproductive. The fraction of catalytically productive conformations among all the conformations generated by molecular dynamics in each case indicate the likelihood that the reaction can occur. Since the enantioselectivity of CRL lip1 toward **1** is 23, we expect the fraction of catalytically productive conformations to be 23-fold lower for (*R*)-**1** as compared to (*S*)-**1**.

This modeling approach is similar to the near-attack-complex modeling developed by Bruice and coworkers[19]. A near attack complex is not an intermediate, but a fleeting structure where the distances and angles are close to those needed for the reaction. Our approach differs by not modeling a near attack complex, but the tetrahedral intermediate. Lipase catalyzes hydrolysis of an ester involves the formation and collapse of a tetrahedral intermediate. The structures of the transition states for formation and collapse of the tetrahedral intermediate are similar to the tetrahedral intermediate, so this modeling approach models the reactivity of each case.

Modeling correctly predicts that the tetrahedral intermediate for hydrolysis of (*S*)-**1**-methyl ester adopts a catalytically productive orientation, Table 6.1. The geometry of the 250 structures generated by the molecular dynamic simulation were measured to identify hydrogen bonds between the lipase and the tetrahedral intermediate. Hydrogen bonds were defined as a n O–N distance of <3.55 Å and an O–H–N angle >120° (180° is ideal). These criteria are permissive to include the entire range of hydrogen bond distances observed in proteins[20]. The (*S*)-enantiomer formed all four catalytically essential hydrogen bonds to the protein in 51% of the structures, which is consistent with the experimental result that (*S*)-**1**-methyl ester is a good substrate. The structures of the modeled tetrahedral intermediate were similar to the phosphonate x-ray crystal structure; Figure 6.7 shows a typical structure.

Table 6.1. Percentage of conformations that contain a hydrogen bond between the partners indicated.[a]

	Oxyanion oxygen of tetrahedral intermediate		**His449-N_ε–H**			
Conformation	**Ala124-N–H, %**	**Gly210-N–H, %**	**Ser209 -Oγ, %**	**Me-O, %**	**All four productive H-**	**Glu208-O (nonproductive), %[b]**
(*S*)	82 (100)	100 (100)	93 (89)	78 (88)	**51**	7.5 (59)

(*R*)-exchange H/	100 (100)	12 (100)	0.79 (0)	87 (0)	**0**	100 (100)
(*R*)-exchange	100 (100)	100 (100)	60 (1.6)	0.40 (2.8)	**0**	99 (98)
(*R*)-exchange H/	100 (100)	100 (100)	100 (99)	0.39 (99)	**0.39**	25 (0.40)
(*R*)-umbrella	98 (100)	100	0.39 (0)	65 (0)	**0**	100 (100)

[a]Percentage of the structures where the N–O distance is <3.55 Å. The numbers in parentheses indicate the percentage of the structures where the N–H–O angle is >120°. The data is in Figures S-1, S-2, and S-3 in the supporting information. [b]In some nonproductive structures a catalytically nonproductive hydrogen bond formed between the catalytic histidine and the side chain of Glu208.

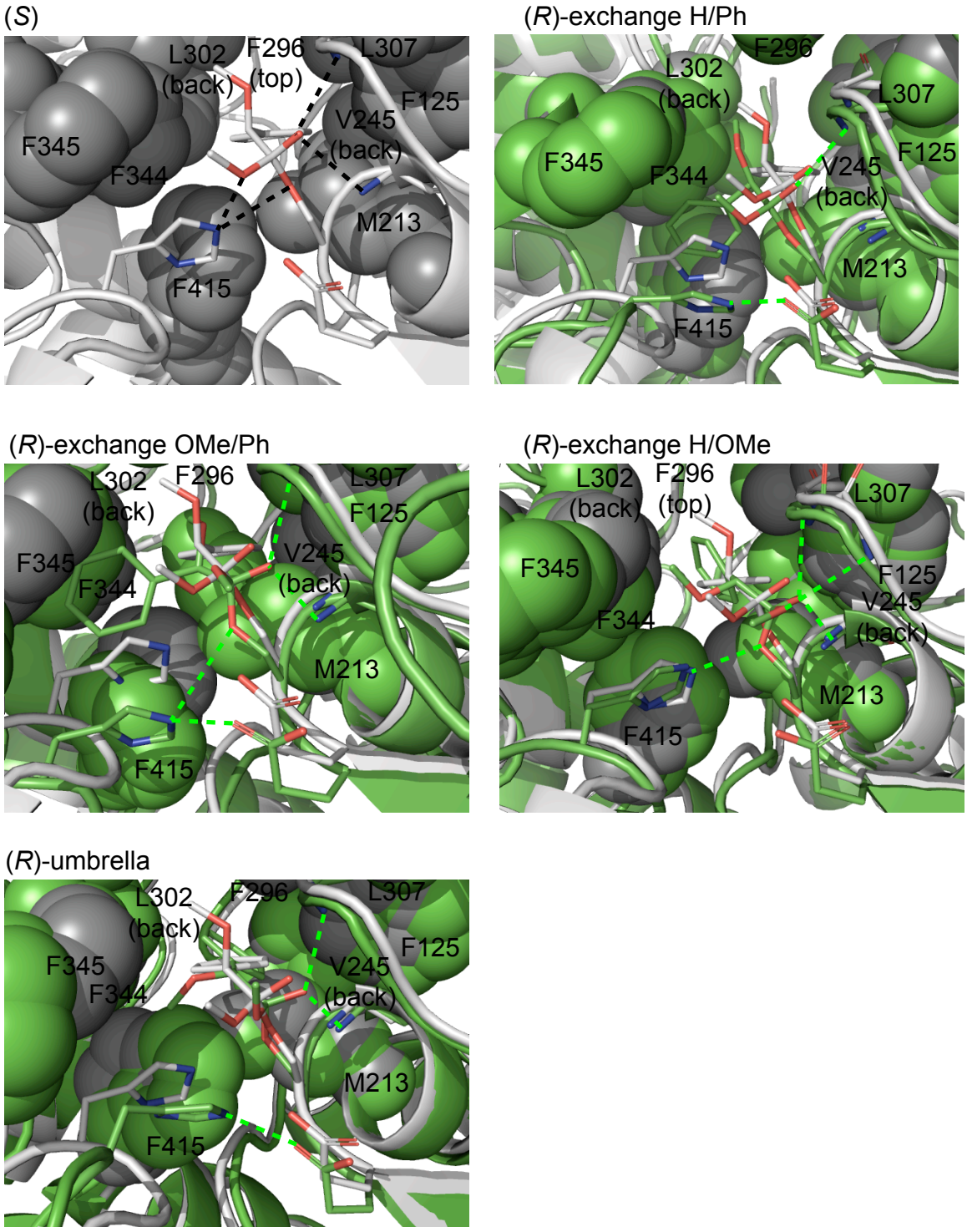

Figure 6.7. Representative structures from molecular dynamics modeling of tetrahedral intermediates for hydrolysis of (*S*)- and (*R*)-**1**. For (*S*)-**1** (gray), all four catalytically important hydrogen bonds are present (dotted lines). In all four orientations of (*R*)-**1** (green overlaid on the gray structure of (*S*)-**1**), one or both of the hydrogen bonds from the catalytic histidine to either the catalytic serine O_γ or the substrate's ester oxygen are missing.

Modeling also correctly predicts that the slow enantiomer react very slowly because it only rarely adopts a catalytically productive orientation, Table 6.1. Almost all orientations disrupt at least one of the two hydrogen bonds to the catalytic histidine. The exception is the (*R*)-exchange H/OMe orientation where one of the 250 modeled conformations (0.4%) showed intact catalytic hydrogen bonds. The rarity of this catalytically productive conformation indicates that reaction of the (*R*)-enantiomer is much slower than for the (*S*)-enantiomer.

The (*R*)-exchange H/Ph orientation disrupts three key hydrogen bonds in most conformations: two from the catalytic histidine to the catalytic serine O_γ and to the substrate's ester oxygen and one from Ala124 N–H to the oxyanion oxygen. The side chains of Phe415 and Phe345 restrict the space available for the phenyl group, so it bumps into the catalytic histidine and moves the imidazole ring, Figure 6.7. The hydrogen bond donor atom, N_ε moves by 3.3 Å as compared to the (*S*) enantiomer and thus breaks the two hydrogen bonds between His-N_ε the tetrahedral intermediate. The overall tetrahedral intermediate moves by 1.0 Å towards the reader's left, which disrupts a key hydrogen bond between the oxyanion and main-chain amide of Ala210. None of the conformations identified by molecular dynamics contain all four essential hydrogen bonds; thus, none were catalytically productive.

The (*R*)-exchange OMe/Ph orientation disrupts the two key hydrogen bonds between the catalytic histidine and the catalytic serine O_γ and the substrate's ester oxygen. The initial model for this orientation places the phenyl group point upward where it clashes with Phe296. During geometry optimization, the substrates phenyl group moves, bumps into the catalytic histidine and moves the imidazole ring, Figure 6.7. The hydrogen bond donor atom, N_ε moves by 3.6 Å as compared to the (*S*) enantiomer and thus breaks the two hydrogen bonds between His-N_ε the tetrahedral intermediate.

The (*R*)-exchange H/OMe orientation disrupts only one hydrogen bond – between the catalytic histidine and the substrate's ester oxygen. The methoxy group at the stereocenter bumps into Phe344 causing the entire tetrahedral intermediate to shift 0.7 Å to the

reader's right. The shift breaks a key hydrogen bond between His449 and the ester oxygen. In one conformation out of 250 (0.40%) all catalytically essential hydrogen bond are present.

The (*R*)-umbrella orientation disrupts only one hydrogen bond – between the catalytic histidine and the catalytic serine O_γ. As the phenyl group moves to a position similar to the (*S*)-enantiomer, the methoxy group at the stereocenter bumps into the catalytic histidine and moves the imidazole ring, Figure 6.5. The hydrogen bond donor atom, N_ε moves by 3.0 Å as compared to the (*S*) enantiomer and thus breaks the hydrogen bonds between His-N_ε and the catalytic serine O_γ.

In place of the disrupted hydrogen bond between the catalytic histidine and either the catalytic serine or substrate ester OMe, a new hydrogen bond forms between His-Nε and Glu-O, Table 1. This hydrogen bond is not catalytically productive because it does not stabilize the tetrahedral intermediate. The fast reacting enantiomer (*S*)-**1**-methyl ester form this hydrogen bond only rarely, 7.5% of the time. In contrast, the slow reacting enantiomer orientations usually make this non-productive hydrogen bond. Three orientations – exchange H/Ph, exchange OMe/Ph, and umbrella - make it nearly all the time. The (*R*)-exchange H/OMe orientation make this hydrogen bond only 25% of the time, but it also forms another nonproductive hydrogen bond between the ester oxygen and the main-chain amide of Gly123 – this hydrogen bond forms 31% of the time. This hydrogen bond is non productive because the N–H cannot donate a proton to leaving group OMe because the pK_a of an amide N–H (~17) is higher than the pK_a of methanol[15].

The slow enantiomer most likely reacts via either the (*R*)-exchange H/OMe orientation or the (*R*)-umbrella orientation. These orientation are closest to a catalytically productive orientation because they lack only one hydrogen bond as compared to three for (*R*)-exchange H/Ph and two for (*R*)-exchange OMe/Ph. The other three orientations also make a nonproductive hydrogen bond with the catalytic histidine all the time, but this exchange H/OMe orientation makes nonproductive hydrogen bonds only 56% of the time. This non productive hydrogen bond occupies the histidine and prevents reaction. We hypothesize that protein engineering efforts to increase enantioselectivity should focus on

further destabilizing the (*R*)-exchange H/OMe orientation and the (*R*)-umbrella orientation.

The modeling does not quantitatively match the experimental results. We identified only one out of 1000 modeled conformations (0.1%) for the slow reacting enantiomer that were catalytically productive. Since 51% of the conformations were catalytically productive for the fast-reacting enantiomer and the slow reacting enantiomer reacts 23-fold slower, quantitative agreement requires ~2% of the conformation for the slow reacting enantiomer to be catalytically productive. The reason for the lack of agreement is unknown and could be due to imperfect modeling or due to an underestimate of the enantioselectivity; for example, if the enzyme contained a contaminating less enantioselective isozyme.

6.3 Materials and methods

6.3.1 General. Chemicals and lipase from *Candida rugosa* (L-1754) was purchased from Sigma Aldrich. FAP 15 lipase (*Rhizopus oryzae*) was purchased from Amano International Enzyme Co. (Troy, VA). ^{1}H-NMR spectra were recorded in $CHCl_3$ at 200 MHz with $CHCl_3$ as an internal standard (δ 7.26). ^{13}C-NMR spectra were recorded in $CHCl_3$ at 50 MHz with $CHCl_3$ as an internal standard (δ 66.5) and were proton decoupled. ^{31}P-NMR spectra were recorded in $CHCl_3$ at 121 MHz with 85% phosphoric acid (0 ppm) as an external standard.

6.3.2 (±)-Dimethyl(1-hydroxyphenylmethyl)phosphonate (±)-2. Following a literature procedure[21], benzaldehyde (0.53 g, 0.51 mL, 5 mmol) and dimethyl phosphite (0.55 g, 0.46 mL, 5 mmol) were consecutively added to anhydrous potassium fluoride (25.8 mmol, 1.50 g). The reaction mixture was manually stirred until it thickened and then solidified within 5 min. Twenty-five mL of CH_2Cl_2 were added and the solid was extracted for 5 min. The suspension was filtered and the filtrate evaporated in vacuo to afford a white solid, (±)-**2** (0.95 g, 4.39 mmol, 88% yield).^{1}H-NMR δ 7.51-7.27 (m, 5H), 5.05 (d , J_{H-P} = 11. 1 Hz), 4.68 (br s, 1H), 3.68 (d, 3H, $^{3}J_{H-P}$ = 10.5 Hz), 3.66 (d, 3H, $^{3}J_{H-P}$ = 10.3 Hz). [lit.[22]: ^{1}H-NMR ($CDCl_3$, 400 MHz) δ 7.50-7.29 (m, 5H, C_6H_5), 5.05 (d, 1H, J =

10.8 Hz, PhC*H*), 4.11 (br s, 1H, OH), 3.70, 3.67 (2 x d, 2 x 3H, J = 10.3 Hz, $P(OMe)_2$).] ^{13}C-NMR δ 136.5, 128.3 (d, J = 2.0 Hz), 128.1 (d, J = 3.1 Hz), 127.0 (d, J = 6.0 Hz), 70.5 (d, $^1J_{C-P}$ = 160 Hz), 53.9 (d, $^2J_{C-P}$ = 7.1 Hz), 53.6 (d, $^2J_{C-P}$ 7.3 Hz). ^{31}P-NMR δ 24.3 (s).

6.3.3 (±)-Dimethyl[1-(methoxy)phenylmethyl]phosphonate. (±)-**2** (1 g, 4.6 mmol), silver(I) oxide (2.14 g, 9.2 mmol), acetic acid (0.53 mL, 0.55 g, 9.2 mmol) and methyl iodide (15 mL, 241 mmol) were combined and stirred in the dark for 22 h. The reaction mixture was diluted with CH_2Cl_2, filtered, and washed with 50 mL water. The CH_2Cl_2 layer was separated, dried and filtered. Purification by flash chromatography using 5:1 CH_2Cl_2/EtOAc (R_f = 0.32) yielded 0.70 g, 3.0 mmol, 66% yield). ^{1}H-NMR δ 7.46-7.36 (m, 5H), 4.56 (d, 1H, $^2J_{H-P}$ = 15.8 Hz), 3.72 (d, 3H, $^3J_{H-P}$ = 9.0 Hz), 3.67 (d, 3H, $^3J_{H-P}$ = 8.8 Hz), 3.40 (s, 3H). ^{13}C-NMR δ 133.9, 128.4-128.2 (m), 127.7 (d, J = 6.0 Hz), 80.0 (d, $^1J_{C-P}$ = 168.9 Hz), 58.4 (d, $^3J_{C-P}$ = 14.8 Hz), 53.5 (d, $^2J_{C-P}$ = 7.0 Hz), 53.3 (d, $^2J_{C-P}$ = 6.9 Hz). ^{31}P-NMR δ 21.9 (s). MS (CI/NH_3) *m/z* (rel intensity) 231 (27, M + H^+), 121 (100).

6.3.4 (±)-Methyl[1-(methoxy)phenylmethyllphosphonic acid. (±)-Dimethyl[1-(methoxy)phenylmethyl]phosphonate (0.60 g, 2.6 mmol) was hydrolyzed to the mono acid by refluxing in aqueous sodium hydroxide (2.7 M) for 5 h. The solution was acidified to pH 1 with 1 N HCI and then extracted with CH_2Cl_2 (2 x 50 mL) and ether (2 x 50 mL). Further extractions with CH_2Cl_2 (2 x 50 mL) and EtOAc (1 x 50 mL) did not remove the majority of the product, so the water was evaporated off under reduced pressure and the residue was extracted with CH_2Cl_2 (3 x 50 mL). The combined organic extracts were dried with magnesium sulphate, filtered and evaporated under reduced pressure yielding the mono acid (0.46 g, 2.2 mmol, 85% yield.) ^{1}H-NMR δ 9.91 (br s, 1H), 7.40-7.31 (m, 5H), 4.42 (d, 1H, $^2J_{H-P}$ = 15.8 Hz), 3.60 (d, 3H, $^3J_{H-P}$ 10.6 Hz), 3.38 (s, 3H). ^{13}C-NMR δ 134.0, 128.2, 127.9 (d, J = 5.2 Hz), 79.8 (d, $^1J_{C-P}$ 171.0 Hz), 58.6 (d, $^3J_{C-P}$ = 14.2 Hz), 53.1 (d, $^2J_{C-P}$ = 6.7 Hz). ^{31}P-NMR δ 23.3 (s). MS (CI/NH_3) *m/z* (rel intensity) 217 (16, M + H^+), 121 (100).

6.3.5 (±)-Methyl[1-(methoxy)phenylmethyl]phosphonochloridate (±)-3. Oxalyl chloride (0.80 g, 0.55 mL, 6.3 mmol) was added to a solution of (±)-methyl[1-(methoxy)phenylmethyllphosphonic acid (0.0136 g, 0.063 mmol) in dichloromethane (13

mL) and the mixture was refluxed for 18.5 h under N_2. Evaporation of the solvent under reduced pressure yielded (±)-**3** as a mixture of diastereomers of the phosphonochloridate (70%) and pyrophosphonate derivatives (30%, ^{31}P-NMR δ 13.3 (app t)) as determined by ^{31}P-NMR. ^{1}H-NMR δ 7.51-7.39 (in, 5H), 4.74 (d, 1H, $^{2}J_{H-P}$ = 11.4 Hz), 3.87 (d, 3H, $^{3}J_{H-P}$ = 12.8 Hz), 3.86 (d, 3H, $^{3}J_{H-P}$ = 12.8 Hz), 3.49 (s, 3H). ^{31}P-NMR δ 36.7 (s), 36.6 (s).

6.3.6 (±)-Methyl, *p*-nitrophenyl[1-(methoxy)phenylmethyllphosphonate (±)-4. Oxalyl chloride (78 μL, 0.113 g, 0.89 mmol) was added to a solution of (±)-methyl[1-(methoxy)phenylmethyllphosphonic acid (0.128 g, 0.59 mmol) in dichloromethane (7 mL) and the mixture was refluxed for 14 h under N_2. The solvent and excess oxalyl chloride were removed under reduced pressure and the chlorophosphonate was redissolved in dichloromethane (7 mL). *p*-Nitrophenol (0.092 g, 0.65 mmol) was added followed by triethylamine (91 μL, 0.066 g, 0.65 mmol) and the mixture was stirred overnight under N_2. The mixture was purified by column chromatography using 20:1 CH_2Cl_2/EtOAc (R_f = 0.17) to yield a 1:1 mixture of diastereomers, (±)-**4** (0.040 g., 1.2 mmol, 20% overall yield). ^{1}H-NMR δ 8.17 (d, 2H, ^{3}J = 9.2 Hz), 7.52-7.34 (m, 5H), 7.24 (d, 2H, ^{3}J = 9.4 Hz), 4.74 (d, IH, $^{2}J_{H-P}$ = 15.4 Hz), 4.72 (d, 1H, $^{2}J_{H-P}$ = 15.0 Hz), 3.84 (d, 3H, $^{3}J_{H-P}$ = 11.0 Hz), 3.77 (d, 3H, $^{3}J_{H-P}$ = 11.0 Hz), 3.43 (s, 3H) . ^{31}P-NMR δ 17.8 (s). MS (CI/NH_3) *m/z* (rel intensity) 338 (4.6, M + H^+), 121 (100).

6.3.7 (±)- Dimethyl[1-(acetyloxy)phenylmethyl]phosphonate, (±)-5. (±)-**2** (0.200 g, 0.92 mmol), K_2CO_3 (0.26 g, 1.9 mmol), *N*,*N*-dimethyl aminopyridine (6 mg, 0.05 mmol) and acetic anhydride (0.130 mL, 1.4 mmol) were added to ethyl acetate (20 mL) and the mixture was stirred at room temperature overnight. The mixture was filtered to remove K_2CO_3, and the filtrate was washed with water (1 x 20 mL). The water layer was extracted with EtOAc (2 x 25 mL), and the combined organic extracts were dried with magnesium sulphate. Evaporation of the solvent in vacuo afforded a clear oil (0. 19 g, 0.75 mmol, 81% yield). ^{1}H-NMR δ 7.51-7.33 (m, 5 H), 6.17 (d, 1H, $^{2}J_{H-P}$ = 13.5 Hz), 3.73 (d, 3H, $^{3}J_{H-P}$ = 10.7 Hz), 3.65 (d, 3H, $^{3}J_{H-P}$ = 10.6 Hz), 2.19 (s, 3H). [lit.[23]: ^{1}H-NMR ($CDCl_3$, 400 MHz) δ 7.50-7.32 (m, 5H, C_6H_5), 6.17 (d, 1H, J = 13.3 Hz, PhC*H*), 3.72, 3.65 (2 x d, 2 x 3H, J = 10.3 Hz, $P(OMe)_2$), 2.18 (3H, s, MeCO).]

6.3.8 Kinetic resolution of (±)-dimethyl[1-(acetyloxy)phenylmethyl]phosphonate, (±)-5. (±)-**5** (2.8 g, 10.8 mmol) was added to an Erlenmeyer flask (500 mL) followed by 3/1 hexanes/tert-butyl methyl ether (20 mL) and phosphate buffer (10 mM, pH 7.00, 100 mL). Lipase F-AP 15 (509 mg), dissolved in phosphate buffer (50 mM, pH 7.00, 60 mL) and adjusted to pH 7.00, was added to the phosphonate mixture. The pH was maintained at 7.00 with 0.50 N NaOH by automatic titration using a pH stat. The reaction was stopped at 43.8% conversion by acidifying the reaction mixture to pH 4 with 1 N HCl. The mixture was extracted with CH_2Cl_2 (1 x 100 mL), EtOAc (1 x 50 mL) and again with CH_2Cl_2 (1 x 100 mL). The combined organic extracts were filtered through a pad of diatomaceous earth. The aqueous layer was also filtered through a pad of diatomaceous earth and the filtrate was further extracted with CH_2Cl_2 (1 x 100 mL). The organic extracts were combined, dried with $MgSO_4$, filtered and the solvent evaporated under reduced pressure. The remaining starting material acetate and product alcohol were separated by flash chromatography using 5:1 CH_2Cl_2/EtOAc to elute the acetate (*R*)-**5** (1.22 g, 4.7 mmol, 78% recovery, 68% ee $Eu(hfc)_3$ chiral shift reagent) and then 100% EtOAc to elute the product alcohol (*S*)-**2** (0.66 g, 3.1 mmol, 65% recovery, 88% ee by $Eu(hfc)_3$ chiral shift reagent following reacetylation).

To increase the enantiomeric purity of the product alcohol, (*S*)-**2,** a sample was resolved a second time. (*S*)-**2** (0.504 g, 2.3 mmol, 88% ee) was reacetylated with acetic anhydride (0.357g, 0.330 mL, 3.5 mmol) and K_2CO_3 (0.650 g, 4.7 mmol) using *N*,*N*-4-dimethylaminopyridine (0.0156 g) as catalyst in EtOAc (20 mL). The reaction mixture was filtered, washed with dd H_2O (50 mL), dried with $MgSO_4$ and the solvent evaporated under reduced pressure to yield (*S*)-**5**. (0.54 g, 2.1 mmol, 90% yield). A sample of (*S*)-**5** (0.49 g, 1.9 mmol, 88% ee) was dissolved with 3/1 hexanes/*tert*-butyl methyl ether (10 mL) added to phosphate buffer (50 mM, pH 7.0, 100 mL). Lipase FAP-15 (220 mg dissolved in phosphate buffer (50 mM, pH 7.00, 50 mL) was added and the pH was maintained at 7.00 with 0.50 N NaOH by automatic titration using a pH stat. The reaction was stopped at 46% conversion by acidifying the reaction mixture to pH 3.9 with 1 N HCl. The reaction mixture was filtered through a pad of diatomaceous earth. The filtrate was

extracted with CH_2Cl_2 (3 x 100 mL). A small portion of emulsion which remained throughout the extractions was separately filtered through a small pad of diatomaceous earth and washed with CH_2Cl_2. The filtrate of this filtered emulsion was combined with the original CH_2Cl_2 extracts. The starting material was separated from the product alcohol by column chromatography using 5:1 CH_2Cl_2/EtOAc in order to elute the remaining substrate, (*S*)-**5** (0.233 g, 0.90 mmol, 88% recovery), then 100% EtOAc to elute the product alcohol, (*S*)-**2** (0.112 g, 0.52 mmol, 59% recovery, > 98% ee by $Eu(hfc)_3$ chiral shift reagent following reacetylation).

To increase the enantiomeric purity of the acetate, (*R*)-**5**, a sample (1.00 g, 3.9 mmol, 68% ee) was resolved a second time. The sample was mixed with 3/1 hexanes/ *tert*-butyl mediyl ether (20 mL) and phosphate buffer (50 mM, pH 7.00, 130 mL). Lipase FAP 15 (505 mg dissolved in phosphate buffer, 50 mM, pH 7.00, 50 mL) and adjusted to pH 7.00, was added and the pH was maintained at 7.00 with 0.50 N NaOH by automatic titration using a pH stat. The reaction was stopped after 16.5% conversion by adjusting the reaction mixture to pH 4 using 1 N HCl. The top organic layer was separated. The aqueous layer was filtered through a pad of diatomaceous earth and extracted with CH_2Cl_2 (3 x 100 mL). The original organic layer from the enzyme reaction and the combined CH_2Cl_2 extracts were filtered through a fresh pad of diatomaceous earth and dried with $MgSO_4$. The acetate was purified by flash chromatography using 5:1 CH_2Cl_2/EtOAc to afford enantiomerically enriched (*R*)-**5** (0.75 g, 2.9 mmol, 90% recovery based on the pH stat percent conversion, 92.7% ee by $Eu(hfc)_3$ chiral shift reagent). A sample of this material (0.5 g, 1.9 mmol) was hydrolyzed for an additional 10.3% conversion in the same manner to afford (*R*)-**5** (0.40 g, 1.6 mmol, >98% ee by $Eu(hfc)_3$ chiral shift reagent).

6.3.9 (*R*)-Dimethyl[1-(methoxy)phenylmethyl)phosphonate. (*R*)-**5** (0.34 g, 1.33 mmol) was reacted with dry MeOH (15 mL) and freshly distilled triethylamine (2 mL) for 18.5 h at room temperature. The solvent and amine were removed under reduced pressure and finally under high vacuum. To this crude product was added Ag_2O (0.62 g, 2.7 mmol), Mel (15 mL) and acetic acid (0. 160 g, 0. 152 mL, 2.7 mmol) and the mixture was stirred

in the dark overnight. The methyl iodide was then evaporated off with a stream of air. The product was redissolved in CH_2Cl_2, filtered, concentrated under reduced pressure, and purified by flash chromatography using 5:1 CH_2Cl_2/EtOAc to afford (*R*)-**2** (0.157 g, 0.68 mmol, 50% yield overall). The ^{1}H-NMR spectrum was identical to the racemic standard.

6.3.10 (*R*)-Methyl[1-(methoxy)phenylmethyl)phosphonic acid. (*R*)-Dimethyl[1-(methoxy)phenylmethyl)phosphonate (0.047 g, 0.21 mmol) was refluxed in freshly distilled acetone with NaI (0.046 g, 0.31 mmol) for 22 h. The fine product salt was filtered and rinsed with absolute ethyl ether. The salt was dissolved in water, acidified to pH 1 and the water was evaporated off under reduced pressure. The residue was extracted with dichloromethane (25 mL), dried with $MgSO_4$, filtered and the solvent removed under reduced pressure to yield the mono acid (0.036 g, 0.17 mmol, 81.3% yield). The ^{1}H-NMR spectrum was identical to the racemic standard.

6.3.11 (R_C,$R_P$$S_P$)-Methyl[1-(methoxy)phenylmethyl]phosphonochloridate, (R_C,$R_P$$S_P$)-3. Oxalyl chloride (1.59 g, 1.09 mL, 12.5 mmol) was added to a solution of (*R*)-Methyl[1-(methoxy)phenylmethyl)phosphonic acid (0.027 g, 0.125 mmol) in dichloromethane (15 mL) and the mixture was refluxed for 18.5 h under N_2. Evaporation of the solvent under reduced pressure yielded (R_C,$R_P$$S_P$)-**3** as a mixture of diastereomers according to ^{31}P-NMR. The ^{1}H-NMR spectrum was identical to the racemic standard.

6.3.12 (*S*)-Dimethyl[l-(methoxy)phenylmethyl]phosphonate. To (*S*)-**2** (0.108 g, 0.50 mmol, >98% ee) was added Ag_2O (0.232 g, 1.0 mmol), MeI (10 mL) and acetic acid (0.060 g, 0.057 mL, 1.0 mmol). The mixture was stirred in the dark for 24 h. The MeI was then evaporated off with a stream of air. The product was redissolved in CH_2Cl_2, filtered and concentrated under reduced pressure. The product was purified by flash chromatography using 5/1 CH_2Cl_2/EtOAc to afford (*S*)-dimethyl[l-(methoxy)phenylmethyl]phosphonate (0.058 g, 0.25 mmol, 50% yield). This compound had an identical ^{1}H-NMR spectrum to the racemic standard.

6.3.13 Inactivation of purified CRL using (±)-3. An aqueous solution of purified CRL (0.55 mg, 0.0092 μmol in MES buffer, 10 mM, pH 6, 1 mL) was added to a dichloromethane solution of freshly synthesized chlorophosphonate, (±)-**3** (9.2 μmol in 1 mL) and

vigorously stirred for eight minutes. The aqueous phase was removed, centrifuged for 1 min and tested for activity using the enzyme assay described below.

6.3.14 Enzyme assay. An aliquot (5 μL) of enzyme solution followed by an aliquot of *p*-nitrophenyl acetate (5 μL of a 50 mM solution in acetonitrile) were added to phosphate buffer (1.0 mL, pH 7.5, 10 mM) at 25 °C. The initial rate of formation of *p*-nitrophenolate was monitored at 404 nm for 30 s. An extinction coefficient of 11600 $M^{-1}cm^{-1}$, which accounts for the incomplete ionization of *p*-nitrophenolate at pH 7.5 was used to calculate activity. Crude CRL showed 30 U/g solid (1 U/mg protein) with this assay. U = 1 μmol of ester hydrolyzed per minute.

6.3.15 X-ray crystal structure. Covalent enzyme-inhibitor complex was prepared by adding the inhibitor dissolved in 2-methyl-2,4-pentanediol (MPD) to the protein solution. The inhibited protein was crystallized under conditions similar to those used for native protein[9]. The crystals are isomorphous with the native crystals of CRL in the open form, Table 6.2. Diffraction data were collected on R-AXIS II image plate area detector and all refinements were done with CNS[24] and all modeling was done using O[25] and COOT[26]. Coordinates were deposited with the Protein Data Bank (www.pdb.org) and have the code 3RAR.

Table 6.2. Data collection and refinement statistics for x-ray structure of the complex of inactivator (R_C, R_PS_P)-**2** with *Candida rugosa* lipase, which mimics reaction of the fast-reacting enantiomer (*S*)-**1**.

Crystal parameters and diffraction data	
X-ray source	CuK_α
Space group	$C222_1$
Unit cell dimensions (Å)	a = 65.0 b = 97.5 c = 176.1
Data collection statistics	
Total number of accepted reflections	51,648
Total number of unique reflections[a]	23,670 (2,716)

Resolution range (Å)	54.1 - 2.2
Highest shell (Å)[a]	2.3 - 2.2
R_{merge} (%)[b]	9.2 (23.0)
Mean I/σI	10.5 (3.1)
Completeness (%)	81.0 (62.5)
Refinement statistics	
Protein molecules in asymmetric units	1
Number of water molecules	175
Number of sugar molecules	3
Number of Ca^{2+}	2
Final R/R_{free} factors[c]	17/21
Average B-factor ($Å^2$)	22.6
r.m.s deviations Bond lengths (Å)	0.006
r.m.s deviations Bond angles (°)	1.3
Ramachandran statistics: favored (%), allowed (%), outlier (%)	93.4, 5.1, 1.5

[a]Data for the highest resolution shell are given in parentheses.
[b]$R_{merge} = |\Sigma_{hkl} \Sigma_i|I_i(hkl) - \langle I(hkl)\rangle|/\Sigma_{hkl} \Sigma_i|I_i (hkl)$, where I(hkl) is the observed intensity and $\langle I(hkl)\rangle$ is the average intensity obtained from multiple observations of symmetry-related reflections after rejection.
[c]$R=\Sigma||Fo| - |Fc||/\Sigma|Fo|$, where Fo and Fc are the observed and calculated structure factors, respectively. R_{free} is calculated using 9.9% of the reflections randomly excluded from refinement.

6.3.16 Molecular modeling. Hydrogen atoms were added to the CRL-phosphonate x-ray crystal structure using the software Maestro (Schrödinger, Portland OR; www.schrodinger.com) to correspond to a pH of 7.0, except for the catalytic histidine, which was protonated. Water molecules far from heteroatoms (>5 Å) were removed. The geometry was optimized using the program Macromodel v. 9.0 (Schrödinger) using the OPLS_2005 force field[27] until an rmsd (root mean square deviation) of <0.3 Å was reached. To model the tetrahedral intermediate for hydrolysis of (*S*)-**1**, the phosphorus atom was replaced by carbon atom, the oxygen corresponding to the oxyanion was assigned a formal negative charge, and the geometry of the structure was optimized to an rmsd of <0.05 Å. To model the four different conformations of the tetrahedral intermedi-

ate for hydrolysis of (*R*)-**1**, the substituents at the stereocenter were exchanged as indicated in Figure 6.1 and the umbrella structure was generated by moving the hydrogen atom to form (*R*) enantiomer without moving the other functional groups. Each conformation was modeled independently and was geometry optimized to an rmsd of <0.05 Å. Molecular dynamics simulations used the software Desmond (D.E. Shaw Research, New York, NY). The protein surrounded by 33885 water molecules (TIP3P model[28]) to create a box sized 109 Å x 109 Å x 95 Å. Seventeen sodium ions were added to neutralize the negative charge of the protein. Sixty-two additional sodium and chloride ions were added to correspond to an ionic strength of 0.10 M. The system was equilibrated to 300 K and 1 atm pressure by using Berendsen thermostat and barstat method[29]. The molecular dynamics simulation was for 1.2 ns with a step time of 1 fs and recorded every 4.8 ps yielding 250 structures. The Coulomb interaction was cut off at 15 Å and the long-range electrostatic interaction was calculated with particle mesh Ewald method. The four catalytically essential hydrogen bonds, His449 to SerOγ and ester oxygen, the two hydrogen bonds to the oxyanion, and the catalytically nonproductive hydrogen bond His449 to Glu208 were deemed present if the N–O distance was <3.5 Å and the N–H–O angle was >120°. A catalytically productive conformation was one that contained all four catalytically essential hydrogen bonds and did not contain the nonproductive hydrogen bond. Table x lists the fraction of catalytically productive conformation out of the 250 total conformations.

6.4 Discussion

6.4.1 Orientation of the fast-reacting enantiomer. Previous computer modeling and extrapolation from x-ray crystal structures indicated that chiral acids with an α-stereocenter bind to CRL with the stereocenter positioned at the mouth of the tunnel and the large substituent extending into the tunnel. The x-ray structure reported in this paper confirms this hypothesis. The phenyl group lies inside the tunnel, while the medium substituent (methoxy) points upward near Phe 296 and Leu297 residues, while the hydrogen points toward Phe 344, Phe 345 and Phe 415. The binding site for chiral secondary alco-

hols overlaps with this region. The hydrophobic region consisting of Phe 296, 344, 345 and Leu297 also corresponds to the 'large pocket' for secondary alcohols.

6.4.2 Orientation of the slow-reacting enantiomer. Previous modeling and experiments with chiral acids proposed differing orientations of the slow-reacting enantiomer, likely because the researchers studied different chiral acids. Both the proposed orientations are exchange-of-substituents conformations, while our proposed umbrella-like inversion orientation is a new proposal.

Molecular modeling of the CRL-catalyzed resolution 2-arylpropionic acids suggested that the slow enantiomer reacts via a hydrogen/medium (methyl) exchange-of-substituents orientation[30, 31, 32]. Modeling naproxen (aryl = 6-methoxy-2-naphthyl) in the active site of CRL placed the aryl group in tunnel. For the fast-reacting enantiomer, the methyl group at the stereocenter pointed toward Phe296, as does the methoxy group in the phosphonate structure in this paper. For the slow reacting enantiomer, the hydrogen and methyl group at the stereocenter exchange positions, Figure 6.8. This is the same conclusion that we came to for **1**-methyl ester, whose structure is closest to the 2-arylpropionic acids. Modeling of 2-(4-substituted phenoxy)propionic acid also suggested that the methyl and hydrogen exchange locations when the slow enantiomer reacts[33].

The enantioselectivity of CRL toward naproxen *increases* at higher temperatures indicating that entropic effects favor the fast reacting enantiomer[34]. The fast enantiomer may be more flexible in the active site, while the slow enantiomer can only react via a rarely reached conformation.

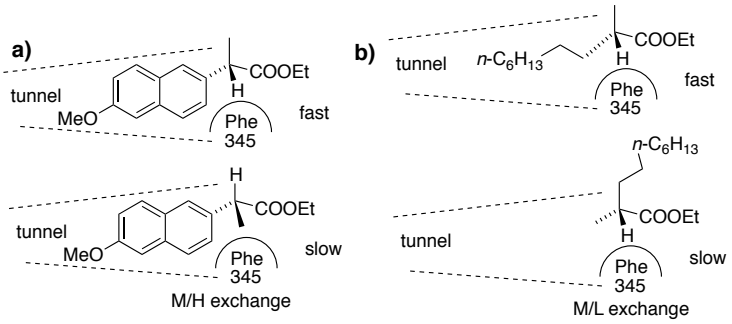

Figure 6.8. Different proposed orientations of the slow enantiomer in CRL-catalyzed resolutions of chiral acids. a) For 2-arylpropionic acids, the slow enantiomer likely reacts via a medium (methyl)/hydrogen exchange. b) For 2-methylalkanoic acids, where the

large group (*n*-alkyl) is more flexible, the slow enantiomer likely reacts via a medium (methyl)/large (*n*-alkyl) exchange.

In contrast, the slow enantiomer of 2-methylalkanoic acids, where the large group is *n*-alkyl, likely reacts in reacts via a medium (methyl)/large (*n*-alkyl) exchange-of-substituents orientation[35]. The experimental evidence is that adding long chain alcohols decreases the enantioselectivity of the CRL-catalyzed esterification of 2-methyldecanoic acid from E = 83 (90 mM n-heptanol) to E = 37 (900 mM *n*-heptanol). The decreased enantioselectivity stems from slower reaction of fast enantiomer, but no change in the reaction rate of the slow enantiomer. To fit the slow-reacting enantiomer, Holmquist and coworkers first exchanged the locations of the hydrogen and methyl group, but found that this orientation displaced the catalytic histidine and was therefore not catalytically productive. Next, they exchanged the methyl and *n*-alkyl groups. The methyl group pointed into the tunnel, while the alkyl group was near Phe296 and extended toward the solvent. Enantioselective inhibition by the long chain alcohols occurs when the alcohol binds in the tunnel. This binding does not affect the binding of the slow-reacting enantiomer, but it blocks the fast-reacting enantiomer, resulting in lower enantioselectivity.

Further support for this exchange of medium and large group locations came from a reversal of enantioselectivity for substrates that do not fit into the tunnel[37]. The CRL-catalyzed hydrolysis of ethyl 2-methyl-6-(2-thienyl)hexanoate favored the (*R*)-enantiomer, in contrast to (*S*)-2-methyldecanoate. The 2-thienyl group made the alkyl chain to large to fit in the tunnel, so it binds near Phe 296 and extends toward the solvent. This reversal supports the notion that the methyl/*n*-alkyl exchange is a catalytically productive orientation and can account for the reaction of the slow enantiomer of 2-methyldecanoic acid.

Increasing the enantioselectivity of CRL toward chiral acids is difficult for two reasons. First, different orientations of the slow enantiomer are possible. High enantioselectivity requires preventing reaction via all of them, which is complex since changes that hinder one orientation may help another orientation. Second, exchanging amino acids near the substrate is a gigantic change on a molecular scale. Changing one amino acid,

e.g. Phe to Leu, removes several atoms; assuming no addition rearrangements, the side chain is now at least 2 Å further from the substrate. This is a large distance on a molecular scale. Contrast this change to the ability to increase the cylinder size in an engine by a millimeter, which is a much more subtle change. The alternative in protein engineering is to change not the amino acids directly in contact with the substrate, but the next sphere so that the large changes in structure are more distributed and effect on the substrate binding site is more subtle.

Site directed mutagenesis experiments and a comparison of isoenzymes identified Phe345 and Phe296, but not Phe344, as important to the high enantioselectivity of CRL (lip1) toward 2-arylpropionic acids, but did not identify substitutions to increase the enantioselectvity of CRL (lip1), Table 6.3. Site directed mutagenesis indicates that Phe345 is essential for high enantioselectivity toward naproxen, a 2-arylpropionic acid, but that Phe344 is not essential. Substitution of Phe345 with valine decreased the enantioselectivity of CRL (lip1 isozyme, same as the one in this paper) from 32 to 2.6[30]. Substitution of Phe344 with valine had no significant effect on enantioselectivity. The enantioselectivity changes with ketoprofen, another 2-arylpropionic acid, were similar[30]. Comparison of the enantioselectivity of CRL isoenzymes[7] also indicates that Phe344 is not essential for enantioselectivity and further identifies Phe296 as essential for high enantioselectivity toward ibuprofen, also a 2-arylpropionic acid. Three lipase isoenzymes (lip1-3) have 80% of the amino acids are identical, but two amino acids differ in the tunnel entrance region where the α-steroecenter of a carboxylic acid binds, Table 6.3. Isoenzymes lip1 and lip3 showed high enantioselectivity toward ibuprofen[14]. Since these isoenzymes differ at position 344 (Phe in lip1 versus Ile in lip3), the similar enantioselectivity indicates that this position is not essential for enantioselectivity. In contrast, lip2, which has a valine at 296 instead of phenylalanine in lip1 and lip3, has lower enantioselectivity toward ibuprofen (E = 15). Isoenzyme lip2 also has a leucine at 344, but this is unlikely to affect enantioselectivity because valine or isoleucine at this position did not affect enantioselectivity.

Table 6.3. Amino acid substitutions near the mouth of the tunnel decrease enantioselectivity of CRL toward 2-arylpropionic acids.

isozyme	296	344	345	E	reference
lip1	Phe	Phe	Phe	>50; ibuprofen 32; naproxen	[14, 30]
lip1 - Phe344Val	Phe	Val	Phe	29; naproxen	[30]
lip1 - Phe345Val	Phe	Phe	**Val**	2.6; naproxen	[30]
lip1 - Phe344,345Val	Phe	Val	**Val**	7.6; naproxen	[30]
lip2	**Val**	Leu	Phe	15; ibuprofen	[14]
lip3	Phe	Ile	Phe	>50; ibuprofen	[14]

Mutations in the lid region, which is far from the substrate binding site, had minor effects on enantioselectivity, most likely by altering the proportion of open and closed forms[38]. Researchers replaced the lid region (residues 66-93) in lip1 with the corresponding sequence in lip3 to create lip1lid3. This replacement introduced six changes in the amino acids sequence at positions 69, 74, 76, 88, 91, and 93. The changed amino acids do not contact the substrate and the closest one lies >15 Å from the phosphonate. Under some conditions, the enantioselectivity of lip1lid3 was slightly lower than the enantioselectivity of lip1 toward the 2-chloroethyl ester of 2-hydroxycaproic acid. The reaction was a transesterification with methanol in isooctane. The enantioselectivities were similar (E = 10 for lip1, 8 for lip1lid3) with a water activity of 0.06, but differed slightly (E = 20 for lip1, 13 for lip1lid3) at a water activity of 0.53. The authors suggested that catalysis occurs in the closed form of the lipase with low enantioselectivity and in the open form of the lipase with higher enantioselectivity. The substitutions on the lid alter the proportion

of open and closed forms. These experiments do not help much in identifying key residues.

Mutations within the tunnel of a related lipase, lipase from *Geotrichum candidum*, which also contains a tunnel, could increase the enantioselectivity toward 2-methylalkanoic acids from E = 32 to 54, a moderate increase[39]. These amino acids were far from the stereocenter and the molecular basis for this change is unknown.

In spite of these extensive and detailed studies of the enantioselectivity of CRL toward chiral α-substituted carboxylic acids, researchers still cannot predict which amino acid substitutions will increase enantioselectivity. The problems is difficult because all possible orientations of the slow enantiomer must be considered. In particular, the umbrella-like inversion orientation has not been previously considered, but the computer modeling in this paper suggests that the slow enantiomer can react via this orientation. The molecular dynamics approach in this paper could compare the four possible orientations of the slow enantiomer and identify the ones most likely to react thereby lowering the enantioselectivity. Extending this approach to test possible amino acid substitutions may enable rational design of more enantioselective lipases.

6.5 Supporting information

6.5.1 MD trajectories of catalytically essential hydrogen bonds for (*S*)-1 and the four (*R*)-1 orientations

Molecular dynamics simulates the multiple conformations possible for each orientation of the transition state analog. Here we measure which of these conformations contains all four catalytically essential hydrogen bonds between the transition state analog and the enzyme. The reasoning is that orientations that allow formation of the catalytically essential hydrogen bonds are reactive conformations, while orientations that lack these hydrogen bonds do not react.

The first two catalytically essential hydrogen bonds are between the oxyanion oxygen of the transition state analog and two main chain N–H from the enzyme (Ala124, Gly210), Figure 6.9. The (*S*)-**1** orientation and three of the four (*R*)-orientations contain these two hydrogen bonds most of the time. The (*R*)-exchange H/Ph is missing one of the hydrogen bond (to Ala124) most of the time since the O–N distance is >3.55 Å most of the time. Hydrogen bond angles (N-H-O) are >120° (180° is ideal) all the time. (Data not shown.)

The next two hydrogen bonds are between His449-Nε and Ser209-Oγ and methyl ester oxygen, Figure 6.10. For (*S*)-**1**, the distance for both pairs of atoms are less than 3.55 Å most of the time. However, for all four (*R*)-**1** orientations, one or both hydrogen bond distances are >3.55 Å and are therefore missing. The bond angles (N-H-O) for these hydrogen bonds correspond to an angle that's <120˚ when the distances are >3.55 Å. However, bond angles >120˚ do not always correspond to bond distances <3.55 Å, therefore both angle and distance had to be measured in tandem state a conclusion, Figure 6.11.

The results of Figure 6.9, 6.10, and 6.11 are summarized in Table 6.1 of the main text.

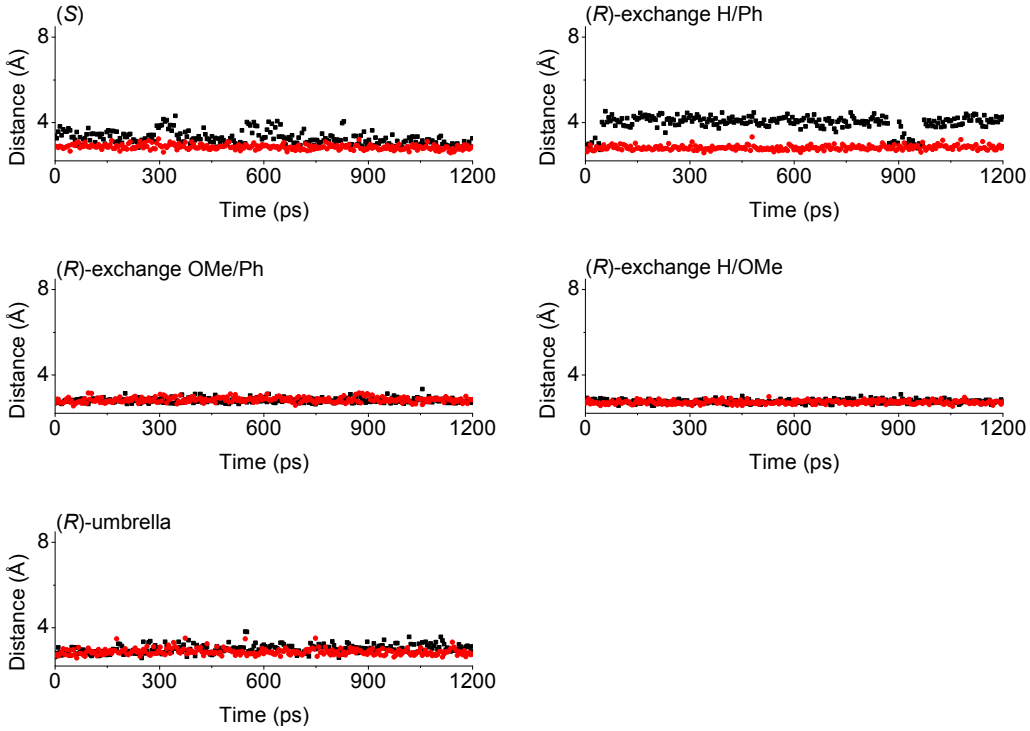

Figure 6.9. Distances between the oxyanion oxygen and Ala124-N–H (black squares) and between the oxyanion oxygen and Gly210 N–H (red circles) over the course of the molecular dynamics simulation (250 structures). Distances <3.55 Å indicate a hydrogen bond.

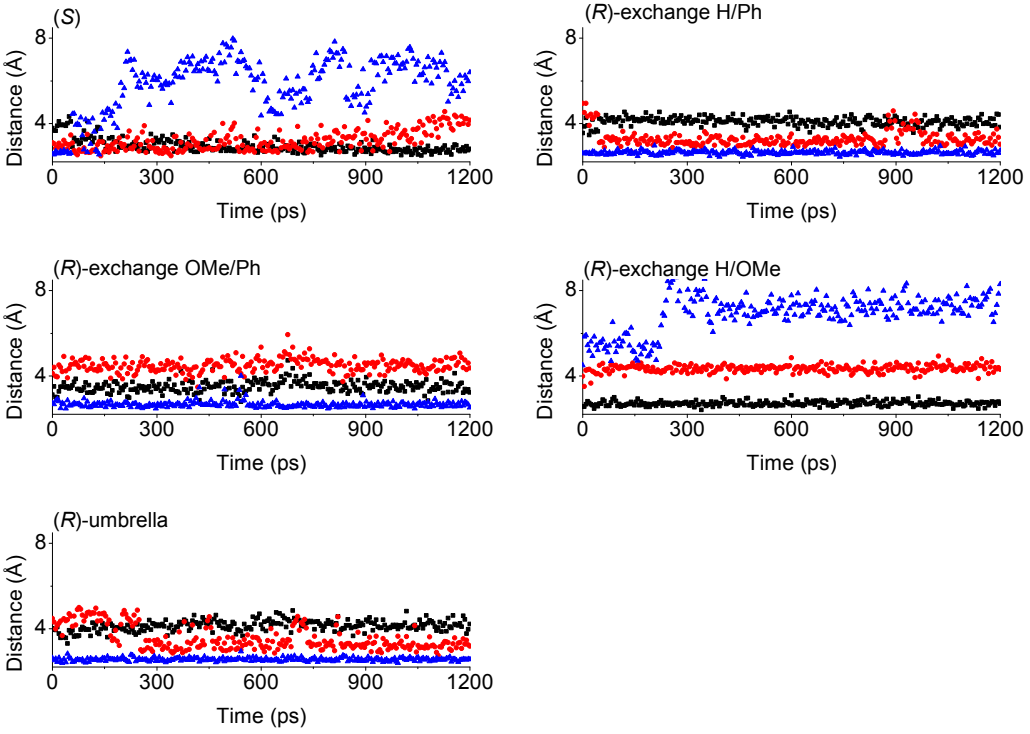

Figure 6.10. Hydrogen bonds formed by His449 Nε–H during the molecular dynamics simulation (250 structures). The distance to Ser209-Oγ (black squares) and the substrate's methyl ester oxygen (red circles) identify catalytically essential hydrogen bonds, while the distance to Glu208-Oε (blue triangles) identifies a catalytically nonproductive hydrogen bond. Distances <3.55 Å indicate a hydrogen bond. The fast reacting enantiomer (*S*)-**1** forms the two catalytically productive hydrogen bonds, but not the catalytically nonproductive hydrogen bond. In contrast, the different orientations of (R)-1 break at least one of the catalytically productive hydrogen bonds and usually replace it with the catalytically nonproductive hydrogen bond.

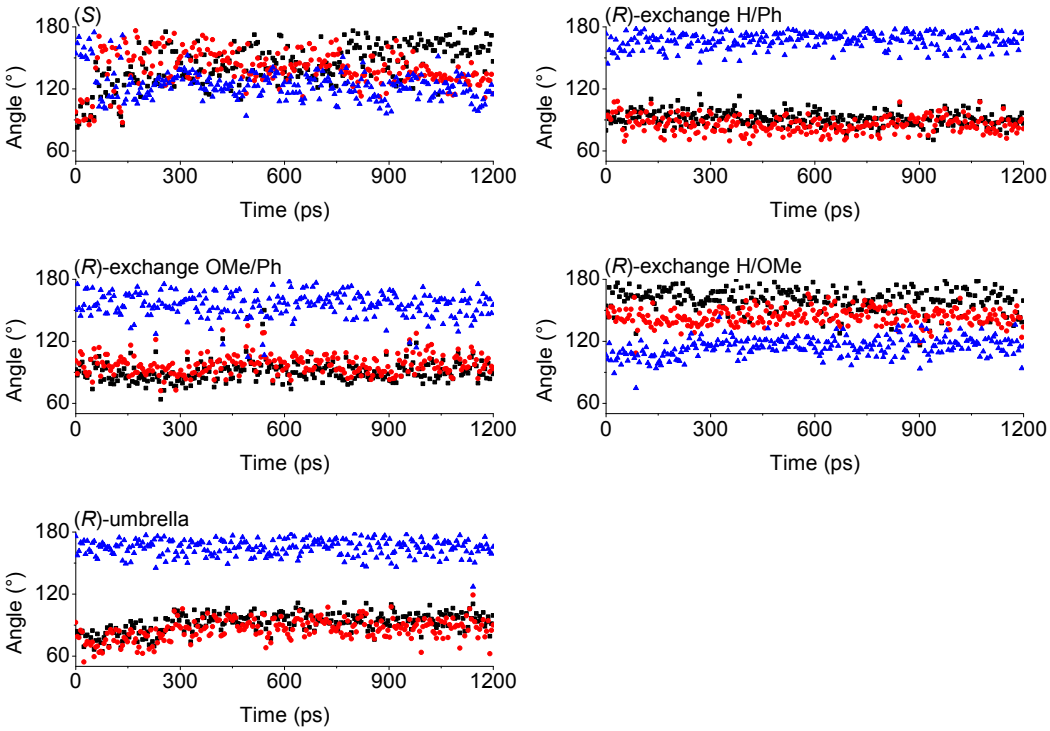

Figure 6.11. Hydrogen bond angles (N–H–O) involving His449 Nε–H during the molecular dynamics simulation (250 structures). The angle to Ser209-Oγ (red circles) and the substrate's ester oxygen (black squares) identify catalytically essential hydrogen bonds, while the angle to Glu208 Oε (blue triangles) identifies a catalytically nonproductive hydrogen bond. Angles >120° (180° is ideal) indicate a hydrogen bond. The fast reacting enantiomer (*S*)-**1** forms the two catalytically productive hydrogen bonds, but not the catalytically nonproductive hydrogen bond. Although the angles for the catalytically nonproductive hydrogen bond are often in the acceptable range, Figure S2 above shows that the distances are too long to be a hydrogen bond. In contrast, the different orientations of (*R*)-**1** break at least one of the catalytically productive hydrogen bonds and usually replace it with the catalytically nonproductive hydrogen bond. The (R)-exchange H/OMe orientation has suitable bond angles to make hydrogen bonds, but Figure S2 above

shows that distance for one of them (to the substrate's ester oxygen) is too long to form a hydrogen bond.

6.5.2 MD trajectories of new, nonproductive hydrogen bonds for the (*R*)-exchange H/OMe orientation

In some orientations, new, catalytically nonproductive hydrogen bonds formed. The most common nonproductive hydrogen bond was between His449-Nε and MeO at the stereocenter found in 5.2% of the structures and between methyl ester oxygen to the main-chain amide of Gly123 found in 31% of the structures. The results of Figure 6.12 are summarized in the results section of the main manuscript.

With the exception of (R)-exchange H/Ph, the His449-Nε makes a new hydrogen bond with Glu208-Oε instead of the methyl ester oxygen.

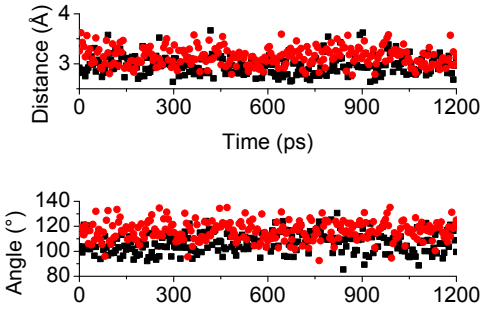

Figure 6.12. Catalytically nonproductive hydrogen bond distances and angles during the molecular dynamics simulation (250 structures) of the (*R*)-exchange H/OMe conformation. The distance from His449 Nε to MeO (square) and the hydrogen bond angle from N-H-O (square) occur 5.2% of the time to form a catalytically nonproductive hydrogen bond. The distance from Gly123 main-chain amide to the methyl ester oxygen (circle) and the hydrogen bond angle from N-H-O (circle) occur 31% of the time to form a catalytically nonproductive hydrogen bond.

Summary, conclusions, and future work

Enzyme catalyzed perhydrolysis is an important reaction to study because the product, peracid is applicable for organic synthesis and to consumer goods. Using enzymes, to generate peracid is a way to bypass storage hazards and also the use of harsh chemicals, such as acids and or organic solvents. Naturally occurring enzymes known as perhydrolases catalyze the reversible perhydrolysis of carboxylic acids. Their mechanism and molecular basis up until recently is not understood.

In chapter 2, the steady-state kinetic constants of perhydrolysis and hydrolysis using L29P PFE (a model carboxylic acid perhydrolase) and wild-type PFE is measured to better understand the mechanism of perhydrolases. The L29P PFE variant uses an esterase-like mechanism based on mass spectrometry evidence. It's also shown that L29P PFE catalyzes the hydrolysis of peracetic acid near diffusion control, which suggests its natural role is to degrade peracetic acid. The crystal structure of L29P PFE confirms a *cis*-Pro amide bond near the active site which confers the main-chain carbonyl to move closer to the active site serine.

We hypothesize that carboxylic acid perhydrolases such as L29P PFE increase the rate of perhydrolysis of acetic acid by selecting hydrogen peroxide over water. Molecular modeling of a tetrahedral intermediate with hydrogen peroxide forms an extra hydrogen bond with a main-chain carbonyl of the oxyanion loop for L29P PFE, but not possible for wild-type. Alternatively, carboxylic acid perhydrolases lower the activation barrier for the formation of the acetyl-enzyme intermediate, which is the rate-limiting step for perhydrolysis of acids. We test the first hypothesis by measuring the selectivity of hydrogen peroxide and show that L29P is less selective than wild-type. L29P PFE increase the rate of acetyl enzyme based on evidence of isotope exchange of acetic acid using 18O-water . Thus, carboxylic acid perhydrolases increase the acetyl-enzyme formation, and does not necessarily select for hydrogen peroxide.

Sequence and structural alignment of carboxylic acid perhydrolases show that the proline at the oxyanion loop is conserved among perhydrolases. We test whether proline

is necessary for perhydrolysis by site-saturation mutagenesis at the 29 position. We identify the L29I variant which has 2-fold higher perhydrolysis activity than L29P PFE, a model carboxylic acid perhydrolase. Thus, proline is not essential for carboxylic acid perhydrolysis, contrary to previously published results. Crystal structure of the L29I variant soaked with acetic acid at pH5.0 reveals two acetic acid/acetate molecules. A molecular model of the first tetrahedral intermediate shows the second acetate forming a stable hydrogen bond network with the intermediate. The first tetrahedral intermediate of L29P/acetate was also modeled and shows a water molecule forming a hydrogen bond network with the intermediate and the main-chain carbonyl. Based on the kinetics, and crystal structure of both L29P/acetate and L29I/acetate structures, we revise the molecular basis of carboxylic acid perhydrolases; to increase perhydrolysis, an enzyme must have a general base to form a hydrogen bond to stabilize the first tetrahedral intermediate.

We test how much peracetic acid can be accumulated using L29P and wild-type PFE. Wild-type PFE accumulates 70 mM of peracetic acid while L29P PFE accumulates less than 10 mM. We attribute the low accumulation amount for L29P to the fast hydrolysis of peracetic acid. ^{1}H-NMR measurement of peracetic acid and acetate accumulation progress with wild-type PFE shows that the enzyme is not deactivated, rather hydrolysis of peracetic acid occurs. To test whether hydrolysis of peracetic acid limits maximum product accumulation, we engineer a better ester perhydrolase by constructing a focused site-saturation library at the active site (11 positions). We identify the variant F162L PFE which accumulates nearly twice as much peracetic acid as wild-type. Stead-state kinetics reveal that hydrolysis of ethyl acetate is 74-fold faster than wild-type.

We also measure the nucleophile competition and find that the F162L variant has equal selectivity for hydrogen peroxide at low nucleophile concentrations, but 7-fold lower selectivity at high nucleophile concentrations. We also measure competing hydrolysis reaction between peracetic acid and ethyl acetate. The F162L variant shows 63-fold higher selectivity for ethyl acetate over peracetic acid hydrolysis compared to the wild-type. Thus, to increase the accumulation of peracetic acid for PFE, the hydrolysis of peracetic acid must be minimized. We made several attempts to predict the maximum ac-

cumulation of peracetic acid using the empirically determined selectivity parameters. Some of the results are encouraging, but further controls for the uncatalyzed hydrolysis reactions are necessary to insure that the results are accurate. While we were unable to predict the maximum peracetic acid accumulation for wild-type and F162L PFE, we were able to understand the kinetic limitation to peracetic acid accumulation. It would be insightful to see whether hydrolysis of peracetic acid is the limiting factor for other ester perhydrolases.

The molecular basis of enzyme catalyzed ester perhydrolysis is still not understood. Kinetic measurements for PFE and variants show that product accumulation can be increased at the cost of lowering nucleophile selectivity. The F162L PFE may be responsible for selecting hydrogen peroxide in concert with other residues to form a "gate" in a second substrate channel. This second substrate channel could be responsible for selecting different nucleophiles. Additional experiments using variants around the "gate" is needed to test this hypothesis.

Pretreatment of 1 gram of aspen wood to release 100% of the sugars requires up to 470 mM of peracetic acid. In chapter 5, we use the F162L PFE variant to generate peracetic acid for lignocellulose pretreatment. We combine the F162L variant with a biphasic system to continuously generate peracetic acid without additional enzyme. Several other process are optimized such as reaction time and pretreatment temperature. These optimizations lead to a 10-fold improvement over a previously published results for aspen wood pretreatment using enzyme generated peracetic acid. Despite this success, the process is still not economical, the amount of peracetic acid required to pretreat lignoceullose must be lowered. The reaction conditions for lignocellulose pretreatment using peracetic acid must be further optimized by using less oxidizer. Also, the source of peracetic acid must come from a renewable source such as acetyl groups already attached to lignocellulose.

Chapter 6 uses a different enzyme (*Candida rugosa* lipase) and studies a different reaction (enantioselectivity of a chiral ester) than the previous chapters. The aim is to understand the molecular basis of CRL selectivity towards the (*S*) enationmer. A crystal structure of a phosphonate inhibitor mimicking the (*S*)-enantiomer exists, but not for the

(*R*); the (*R*)-phosphonate inhibitor was difficult to synthesize and could not be crystalized with CRL. We modeled all four orientation of the (*R*)-enantiomer in CRL and performed molecular dynamics to sample additional conformations. The MD simulations show that the (*R*)-enantiomer causes disruptions of catalytic hydrogen bonds while forming unproductive hydrogen bonds to other residues. Thus, the MD simulations provide an explanation of how CRL selects for the (*S*)-enantiomer.

Bibliography

Chapter 1

1 Radzicka, A.; Wolfenden, R., A proficient enzyme. *Science* **1995,** *267* (5194), 90-93.

2. Nieves, R. A. E., C.I.; Elander, R.T.; Himmel, M.E., Survey and analysis of commercial cellulase preparatoins suitable for biomass conversion to ethanol. *World J. Microbiol. Biotechnol.* **1998,** *14* (2), 301-304.

3. Stephanopoulos, G., Challenges in engineering microbes for biofuels production. *Science* **2007,** *315* (5813), 801-804.

4. DiCosimo, R.; Panova, A.; Mersingera, L. I.; Liu, Q.; Foo, T.; Roe, D. C.; Spillan, W. L.; Sigmund, A. E.; Ben-Bassat, A.; Wagner, L. W.; O'Keefe, D. P.; Wu, S.; Petrillo, K. L.; Payne, M. S.; Breske, S. T.; Gallagher, F. G., Chemoenzymatic synthesis of glycolic acid. *Adv Synth Catal* **2007,** *349* (8-9), 1462-1474.

5. Nakamura, T.; Nagasawa, T.; Yu, F.; Watanabe, I.; Yamada, H., A new catalytic function of halohydrin hydrogen halide lyase, synthesis of beta-hydroxynitriles from Epoxides and Cyanide. *Biochem Bioph Res Co* **1991,** *180* (1), 124-130.

6. Huisman, G. W.; Fox, R. J.; Davis, S. C.; Mundorff, E. C.; Newman, L. M.; Gavrilovic, V.; Ma, S. K.; Chung, L. M.; Ching, C.; Tam, S.; Muley, S.; Grate, J.; Gruber, J.; Whitman, J. C.; Sheldon, R. A., Improving catalytic function by ProSAR-driven enzyme evolution. *Nat Biotechnol* **2007,** *25* (3), 338-344.

7. Savile, C. K.; Janey, J. M.; Mundorff, E. C.; Moore, J. C.; Tam, S.; Jarvis, W. R.; Colbeck, J. C.; Krebber, A.; Fleitz, F. J.; Brands, J.; Devine, P. N.; Huisman, G. W.; Hughes, G. J., Biocatalytic asymmetric synthesis of chiral amines from ketones applied to sitagliptin manufacture. *Science* **2010,** *329* (5989), 305-309.

8. Harakeh, M. S., Inactivation of enteroviruses, rotaviruses and bacteriophages by peracetic-acid in a municipal sewage effluent. *FEMS Microbiol Lett* **1984,** *23* (1), 27-30.

9. Koivunen, J.; Heinonen-Tanski, H., Peracetic acid (PAA) disinfection of primary, secondary and tertiary treated municipal wastewaters. *Water Res* **2005,** *39* (18), 4445-4453.

10. Kurschner, L. M., Diken, G.M. Use of peracetic acid to sanitize processed fowl. 1997.

11. Jankovic, M.; Sinadinovic-Fiser, S., Prediction of the chemical equilibrium constant for peracetic acid formation by hydrogen peroxide. *J Am Oil Chem Soc* **2005,** *82* (4), 301-303.

12. Greenspan, F. P., The convenient preparation of per-acids. *J. Am. Chem. Soc.* **1946,** *68* (5), 907-907.

13. Phillips, B.; Frostick, F. C.; Starcher, P. S., A new synthesis of peracetic acid. *J. Am. Chem. Soc.* **1957,** *79* (22), 5982-5986.

14. Scheer, M.; Grote, A.; Chang, A.; Schomburg, I.; Munaretto, C.; Rother, M.; Söhngen, C.; Stelzer, M.; Thiele, J.; Schomburg, D., BRENDA, the enzyme information system in 2011. *Nucleic Acids Res.* **2010**.
15. Carr, P. D.; Ollis, D. L., Alpha/beta hydrolase fold: an update. *Protein Pept Lett* **2009,** *16* (10), 1137-48.
16. Cheeseman, J. D.; Tocilj, A.; Morley, K.; Park, S.; Schrag, J. D.; Kazlauskas, R. J., X-ray crystal structure of pseudomonas fluorescens aryl esterase reveals possible structural explanations for substrate preference and enantioselectivity. *Abstr Pap Am Chem S* **2004,** *228*, U189-U190.
17. Holmquist, M., Alpha/Beta-Hydrolase fold enzymes: structures, functions and mechanisms. *Curr Protein Pept Sc* **2000,** *1* (2), 209-235.
18. Gruber, K.; Gugganig, M.; Wagner, U. G.; Kratky, C., Atomic resolution crystal structure of hydroxynitrile lyase from *Hevea brasiliensis*. *Biol. Chem.* **1999,** *380* (7-8), 993-1000.
19. Breuer, M.; Ditrich, K.; Habicher, T.; Hauer, B.; Keßeler, M.; Stürmer, R.; Zelinski, T., Industrial methods for the production of optically active intermediates. *Angew. Chem. Int. Ed.* **2004,** *43* (7), 788-824.
20. Houde, A.; Kademi, A.; Leblanc, D., Lipases and their industrial applications. *Appl Biochem Biotech* **2004,** *118* (1), 155-170.
21. van Pee, K. H.; Sury, G.; Lingens, F., Purification and properties of a nonheme bromoperoxidase from Streptomyces aureofaciens. *Biol. Chem.* **1987,** *368* (9), 1225-32.
22. Haag, T.; Lingens, F.; van Pée, K.-H., A Metal-Ion- and cofactor-independent enzymatic redox reaction: halogenation by bacterial nonheme haloperoxidases. *Angew. Chem. Int. Ed.* **1991,** *30* (11), 1487-1488.
23. Hecht, H. J.; Sobek, H.; Haag, T.; Pfeifer, O.; van Pee, K. H., The metal-ion-free oxidoreductase from Streptomyces aureofaciens has an [alpha]/[beta] hydrolase fold. *Nat. Struct. Mol. Biol.* **1994,** *1* (8), 532-537.
24. Picard, M.; Gross, J.; Lubbert, E.; Tolzer, S.; Krauss, S.; vanPee, K. H.; Berkessel, A., Metal-free bacterial haloperoxidases as unusual hydrolases: Activation of H2O2 by the formation of peracetic acid. *Angew. Chem. Int. Ed.* **1997,** *36* (11), 1196-1199.
25. Morris, D. R.; Hager, L. P., Chloroperoxidase. *J. Biol. Chem.* **1966,** *241* (8), 1763-1768.
26. Hofmann, B.; Tolzer, S.; Pelletier, I.; Altenbuchner, J.; van Pee, K. H.; Hecht, H. J., Structural investigation of the cofactor-free chloroperoxidases. *J. Mol. Biol.* **1998,** *279* (4), 889-900.
27. Kirk, O.; Conrad, L. S., Metal-free haloperoxidases: Fact or artifact? *Angew. Chem. Int. Ed.* **1999,** *38* (7), 977-979.
28. Choi, K. D.; Jeohn, G. H.; Rhee, J. S.; Yoo, O. J., Cloning and nucleotide-sequence of an esterase gene from *Pseudomonas fluorescens* and expression of the gene in *Escherichia coli*. *Agr. Biol. Chem. Tokyo* **1990,** *54* (8), 2039-2045.

29. Krebsfanger, N.; Zocher, F.; Altenbuchner, J.; Bornscheuer, U. T., Characterization and enantioselectivity of a recombinant esterase from *Pseudomonas fluorescens*. *Enzyme Microb. Tech.* **1998,** *22* (7), 641-646.
30. Liu, A. M. F.; Somers, N. A.; Kazlauskas, R. J.; Brush, T. S.; Zocher, F.; Enzelberger, M. M.; Bornscheuer, U. T.; Horsman, G. P.; Mezzetti, A.; Schmidt-Dannert, C.; Schmid, R. D., Mapping the substrate selectivity of new hydrolases using colorimetric screening: lipases from Bacillus thermocatenulatus and Ophiostoma piliferum, esterases from Pseudomonas fluorescens and Streptomyces diastatochromogenes. *Tetrahedron: Asymmetry* **2001,** *12* (4), 545-556.
31. Bernhardt, P.; Hult, K.; Kazlauskas, R. J., Molecular basis of perhydrolase activity in serine hydrolases. *Angew Chem Int Ed Engl* **2005,** *44* (18), 2742-6.
32. Lorenz, P.; Eck, J., Metagenomics and industrial applications. *Nature reviews. Microbiology* **2005,** *3* (6), 510-6.
33. Kazlauskas, R. J.; Bornscheuer, U. T., Finding better protein engineering strategies. *Nat Chem Biol* **2009,** *5* (8), 526-9.
34. Leung, D. W.; Chen, E.; Goeddel, D. V., A method for random mutagenesis of a defined DNA segment using a modified polymerase chain reaction. *Technique* **1989,** *1*, 11-15.
35. Kim, M.-S.; Lei, X., Enhancing thermostability of *Escherichia coli* phytase AppA2 by error-prone PCR. *Appl. Microbiol. Biotechnol.* **2008,** *79* (1), 69-75.
36. Stemmer, W. P., DNA shuffling by random fragmentation and reassembly: in vitro recombination for molecular evolution. *Proc. Natl. Acad. Sci. U.S.A.* **1994,** *91* (22), 10747-10751.
37. Stemmer, W. P. C., Rapid evolution of a protein in vitro by DNA shuffling. *Nature* **1994,** *370* (6488), 389-391.
38. Case, D. A.; Wang, J. M.; Wolf, R. M.; Caldwell, J. W.; Kollman, P. A., Development and testing of a general amber force field. *J Comput Chem* **2004,** *25* (9), 1157-1174.
39. Morse, P. M., Diatomic Molecules According to the Wave Mechanics. II. Vibrational Levels. *Physical Review* **1929,** *34* (1), 57.
40. Allinger, N. L., Conformational analysis. 130. MM2. A hydrocarbon force field utilizing V1 and V2 torsional terms. *J. Am. Chem. Soc.* **1977,** *99* (25), 8127-8134.
41. Leach, A. R., *Molecular modelling principles and applications*. Pearson Education Limited: Harlow, 2001.
42. Padhi, S. K.; Fujii, R.; Legatt, G. A.; Fossum, S. L.; Berchtold, R.; Kazlauskas, R. J., Switching from an Esterase to a Hydroxynitrile Lyase Mechanism Requires Only Two Amino Acid Substitutions. *Chemistry & Biology* **2010,** *17* (8), 863-871.
43. Pauling, L., Nature of forces between large molecules of biological interest. *Nature* **1948,** *161*, 707-709.
44. Segel, I. H., *Enzyme kinetics Behavior and Analysis of rapid equilbrium and steady-state enzyme systems.* John Wiley and Sons: New York, 1975.

45. King, E. L.; Altman, C., A Schematic Method of Deriving the Rate Laws for Enzyme-Catalyzed Reactions. *The J. Phys. Chem.* **1956,** *60* (10), 1375-1378.
46. Cleland, W. W., Determining the Chemical Mechanisms of Enzyme-Catalyzed Reactions by Kinetic Studies. In *Advances in Enzymology and Related Areas of Molecular Biology*, John Wiley & Sons, Inc.: 2006; pp 273-387.
47. Bender, M. L.; Zerner, B., The Kinetic Consequences of the Acyl-Enzyme Mechanism for Reactions of Specific Substrates with Chymotrypsin. *J. Am. Chem. Soc.* **1964,** *86* (18), 3669-3674.
48. Fink, A. L.; Bender, M. L., Binding sites for substrate leaving groups and added nucleophiles in papain-catalyzed hydrolyses. *Biochemistry* **1969,** *8* (12), 5109-18.
49. Youshko, M. I.; Chilov, G. G.; Shcherbakova, T. A.; Svedas, V. K., Quantitative characterization of the nucleophile reactivity in penicillin acylase-catalyzed acyl transfer reactions. *Biochim. Biophys. Acta.* **2002,** *1599* (1-2), 134-140.

Chapter 2

1. Björkling, F., Frykman, H., Godtfredsen, S. E., and Kirk, O. (1992) Lipase-catalyzed synthesis of peroxycarboxylic acids and lipase-mediated oxidations, *Tetrahedron 48*, 4587–4592.
2. Picard, M., Gross, J., Lübbert, E., Tölzer, S., Krauss, S., van Pée, K.-H., and Berkessel, A. (1997) Metal-free bacterial haloperoxidases as unusual hydrolases: activation of H_2O_2 by the formation of peracetic acid, *Angew. Chem. Int. Ed. Engl. 36*, 1196–1199.
3. Warwel, S., and Klaas, M. R. (1995) Chemoenzymic epoxidation of unsaturated carboxylic acids, *J. Mol. Catal. B: Enzym. 1*, 29–35, Klaas, M. R., and Warwel, S. (1997) Lipase-catalyzed preparation of peroxy acids and their use for epoxidation, *J. Mol. Catal. A: Chem. 117*, 311–319, de Zoete, M. C., van Rantwijk, F., Maat, L., and Sheldon, R. A. (1993) Selective oxidation of penicillin G with hydrogen peroxide and with enzymatically generated peroxyoctanoic acid, *Recl. Trav. Chim. Pays-Bas 112*, 462–463.
4. Hegarty, A.F., *Comprehensive Organic Chemistry*, Pearson Higher Education: New York, **1995**, pp. 1105–1118.
5. Selected references: a) ten Brink, G. J., Arends, I. W. C. E., and Sheldon, R. A. (2004) The Baeyer-Villiger reaction: new developments toward greener procedures, *Chem. Rev. 104*, 4105–4123, b) Harrison, C. R., and Hodge, P. (1976) Oxidation of some penicillins and other sulphides by use of a polymer-supported peroxy-acid, *J. Chem. Soc. Perkin. Trans. 1 21*, 2252–2254, c) Drago, R. S., Mateus, A. L. M. L., and Patton, D. (1996) Stoichiometric and catalytic oxidation of organic substrates with *in-situ*-generated peracids, *J. Org. Chem*. *61*, 5693–5696, d) Doumaux, A. R, McKeon, A. R. J. E, Trecker, D. J.(1969) Metal ion-catalyzed peroxide oxidation of organic substrates. Selective synthesis of imides, *J. Am. Chem. Soc*. *91*, 3992–3993, e) Sugimoto, H., and Sawyer, D.T. (1985) Iron(II)-induced activation of hydroper-

oxides for the dehydrogenation and monooxygenation of organic substrates in acetonitrile, *J. Am. Chem. Soc. 107*, 5712–5716.

6. Ollis, D. L., Cheah, E., Cygler, M., Dijkstra, B., Frolow, F., Franken, S. M., Harel, M, Remington, S. J., Silman, I., Schrag, J., Sussman, J. L., Verschueren, K. H. G., and Goldman, A. (1992) The α/β hydrolase fold, *Protein Eng. 5*, 197–211.
7. Pelletier, I., and Altenbuchner, J. (1995) A bacterial esterase is homologous with non-heme haloperoxidases and displays brominating activity, *Microbiology 141*, 459–468.
8. Hecht, H. J., Sobek, H., Haag, T., Pfeifer, O., and van Pée, K.-H. (1994) The metal-ion-free oxidoreductase from *Streptomyces aureofaciens* has an α/β hydrolase fold, *Nat. Struct. Biol. 1*, 532–537.
9. Hofmann, B., Tölzer, S., Pelletier, I., Altenbuchner, J., van Pée, K.-H., and Hecht, H. J. (1998) Structural investigation of the cofactor-free chloroperoxidases, *J. Mol. Biol. 279*, 889–900.
10. Kirk, O., and Conrad, L. S. (1999) Metal-free haloperoxidases: fact or artifact? *Angew. Chem. Int. Ed. Engl. 38*, 977–979.
11. Bugg, T. D. H. (2004) Diverse catalytic activities in the α/β-hydrolase family of enzymes: activation of H_2O, HCN, H_2O_2, and O_2, *Bioorg. Chem. 32*, 367-375.
12. Gruber, K., Gartler, G., Krammer, B., Schwab, H., Kratky, C. (2004) Reaction mechanism of hydroxynitrile lyases of the α/β-hydrolase superfamily: The three-dimensional structure of the transient enzyme-substrate complex certifies the crucial role of LYS236, *J. Biol. Chem. 279,* 20501-20510.
13. Bernhardt, P., Hult, K., and Kazlauskas, R. J. (2005) Molecular basis of perhydrolase activity in serine hydrolases, *Angew Chem. Int. Ed. 18*, 2742–2746.
14. Kirner, S., Krauss, S., Sury, G., Lam, S. T., Ligon, J. M., and van Pée, K.-H. (1996) The nonheme chloroperoxidase from *Pseudomonas fluorescens* and its relationship to pyrrolnitrin biosynthesis, *Microbiology 142*, 2129–2135.
15. Gasteiger, E., Hoogland, C., Gattiker, A., Duvaud, S., Wilkins, M. R., Appel, R. D., Bairoch, A. (2005) *Protein Identification and Analysis Tools on the ExPASy Server*, (In) John M. Walker (ed): *The Proteomics Protocols Handbook*. Humana Press: New Jersey, p. 571-607
16. Morris, D. R., and Hager, L. P. (1966) Chloroperoxidase I. Isolation and properties of the crystalline glycoprotein. *J. Biol. Chem. 241*, 1763–1768.
17. Fersht, A. (1999) *Structure and Mechanism in Protein Science*, Freeman: New York, p 172.
18. Janes, L. E., Löwendahl, A. C., and Kazlauskas, R. J. (1998) Quantitative screening of hydrolase libraries using pH indicators: identifying active and enantioselective hydrolases, *Chem. Eur. J. 4*, 2324–2331.
19. Cheeseman, J. D., Tocilj, A., Park, S., Schrag, J. D., and Kazlauskas, R. J. (2004) X-Ray crystal structure of an aryl esterase from *Pseudomonas fluorescens, Acta Crystallogr. D 60*, 1237–1243.

20. Pflugrath, J. W. (1999) The finer things in X-ray diffraction data collection, *Acta Crystallogr., D: Biol. Crystallogr. D55*, 1718-1725.
21. Jones, T. A., Zou, J.-Y., Cowan, S. W., and Kjeldgaard, M. (1991) Improved methods for building protein models in electron density maps and the location of errors in these models, *Acta Crystallogr., Sect. A: Found. Crystallogr. A47*, 110-119.
22. Murshudov, G. N., Vagin, A. A., and Dodson, E. J. (1997) Refinement of macromolecular structures by the maximum-likelihood method, *Acta Crystallogr., Sect. D: Biol. Crystallogr. D53*, 240-255.
23. Perrakis, A., Morris, R., and Lamzin, V. S. (1999) Automated protein model building combined with iterative structure refinement, *Nat. Struct. Biol. 6*, 458-463.
24. Read, R. J. (1986) Improved Fourier coefficients for maps using phases from partial structures with errors, *Acta Crystallogr., Sect. A: Found. Crystallogr. A42*, 140-149.
25. Laskowski, R. A. (1993) PROCHECK: a program to check the stereochemical quality of protein structures, *J. Appl. Crystallogr. 26*, 283-291.
26. Pettersen, E. F., Goddard, T. D., Huang, C. C., Couch, G. S., Greenblatt, D.M., Meng, E. C., and Ferrin, T. E. (2004) UCSF Chimera - A visualization system for exploratory research and analysis, *J. Comput. Chem. 25*, 1605-1612.
27. DeLano, W. L. (2008) The PyMOL Molecular Graphics System, DeLano Scientific, Palo Alto, California, USA. http://www.pymol.org
28. Vagin, A. A., and Teplyakov, A. *J.* (1997) MOLREP: an automated program for molecular replacement, *Appl. Crystalogr. 30,* 1022-1025.
29. Emsley, P., and Cowtan, K. (2004) Coot: model-building tools for molecular graphics, *Acta Crystallogr., D: Biol. Crystallogr.* D60, 2126-2132.
30. Lovell, S. C., Davis, I. W., Arendall, W. B., III, de Bakker, P. I. W., Word, J. M., Prisant, M. G., Richardson, J. S., and Richardson, D. C. (2003) Structure validation by Cαα geometry: φ, ψ and Cβ deviation, *Prot. Struct. Func. Genet. 50*, 437-450.
31. Jorgensen, W. L., Maxwell, D. S., and Tirado-Rives, J. (1996), Development and testing of the OPLS All-Atom Force Field on conformational energetics and properties of organic liquids, *J. Am. Chem. Soc. 118*, 11225-11236.
32. Wilmouth, R. C., Clifton, I. J., Robinson, C. V., Roach, P. L., Aplin, R. T., Westwood, N. J., Hajdu, J., and Schofield, C. J. (1997) Structure of a specific acyl enzyme complex formed between β-casomorphin-7 and porcine pancreatic elastase, *Nature Struct. Biol. 4*, 456–462.
33. Wilmouth, R. C., Li, Y.-H., Wright, P. A., Claridge, T. D. W., Aplin, R. T., and Schofield, C. J. (2000) Reaction of clavams with elastase reveals a general method for inhibiting `serine' enzymes, *Tetrahedron 56*, 5729–5733
34. Everett, A. J., and Minkoff, G. J. (1953) The dissociation constants of some alkyl and acyl hydroperoxides, *Trans. Faraday Soc. 49*, 410-414.
35. Fersht, A. (1999) *Structure and Mechanism in Protein Science*, W. H. Freeman and Company: New York, p. 117–118.

36. Blacklow, S. C., Raines, R. T., Lim, W. A., Zamore, P. D., and Knowles, J. R. (1988) Triosephosphate isomerase catalysis is diffusion controlled, *Biochemistry 27*, 1158–1165.
37. van Pée, K.-H., Hecht, H.-H., Berkessel, A., Schrapek, T., Laatsch, H. (1996) Enzymatic, active oxygen-releasing mixture and peracid production. 07/03/96 WOI96066909
38. Krebsfänger, N., Zocher, F., Altenbuchner, J., and Bornscheuer, U. T. (1998) Characterization and enantioselectivity of a recombinant esterase from *Pseudomonas fluorescens, Enzyme Microb. Technol.* 22, 641–646.
39. Kataoka, M., Honda, K., and Shimizu, S. (2000) 3,4-Dihydrocoumarin hydrolase with haloperoxidase activity from *Acinetobacter calcoaceticus* F46, *Eur. J. Biochem. 267*, 3-10.
40. Line, K., Isupov, M. N., and Littlechild, J. A. (2004) The crystal structure of a (–) γ-lactamase from *Aureobacterium* species reveals a tetrahedral intermediate in the active site, *J. Mol. Biol. 338*, 519-532.
41. Friesner, R. A., Banks, J. L., Murphy, R. B., Halgren, T. A., Klicic, J. J., Mainz, D. T., Repasky, M. P., Knoll, E. H., Shaw, D. E., Shelley, M., Perry, J. K., Francis, P., and Shenkin, P. S. (2004) Glide: A new approach for rapid, accurate docking and scoring. 1. Method and assessment of docking accuracy, *J. Med. Chem*. *47*, 1739–1749
42. Li, Z., Sau, A. K., Furdui, C. M., and Anderson, K.S. (2005) Probing the role of tightly bound phosphoenolpyruvate in *Escherichia coli* 3-deoxyD-manno-octulosonate 8-phosphoate synthase catalysis using quantitative time-resolved electrospray ionization mass spectrometry in the millisecond time range, *Anal. Biochem. 343,* 25-47.
43. Lee, W., Vojcic, L., Despotovic, D., Prodanovic, R., Maurer, K.-H., Schwaneberg, U., and Zacharias, M. (2009), Rationalizing perhydrolase activity of aryl-esterase and subtilisin Carlsberg mutants by molecular dynamics simulations of the second tetrahedral intermediate state, *Theor. Chem. Acc.* online doi: 10.1007/s00214-009-0611-3.
44. Li, C., Hassler, M., and Bugg, T. D. H. (2008) Catalytic promiscuity in the α/β-hydrolase superfamily: hydroxamic acid formation, C–C bond formation, ester and thioester hydrolysis in the C–C hydrolase family, *ChemBioChem 9*, 71–76.
45. Caldini, G., Cenci, G., Manenti, R., and Morozzi, G. (1998) The ability of an environmental isolate of *Pseudomonas fluorescens* to utilize chrysene and other four-ring polynuclear aromatic hydrocarbons, *Appl. Microbiol. Biotechnol. 44*, 225-229.
46. Honda, K., Kataoka, M., Sakuradani, E., and Shimizu, S. (2003) Role of *Acinetobacter calcoaceticus* 3,4-dihydrocoumarin hydrolase in oxidative stress defence against peroxoacids, *Eur. J. Biochem. 270*, 486-494.
47. Janković, M., and Sinadinović-Fišer, S. (2005) Prediction of the chemical equilibrium constant for peracetic acid formation by hydrogen peroxide, *J. Amer. Oil Chem. Soc. 82*, 301-303, Zhao, X., Zhang, T., Zhou, Y., and Liu, D. (2007) Prepara-

tion of peracetic acid from hydrogen peroxide: Part I: Kinetics for peracetic acid synthesis and hydrolysis, *J. Mol. Catal. A Chem. 271*, 246-252.

48. Chipman, D., Barak, Z., and Schloss, J. (1998) Biosynthesis of 2-aceto-2-hydroxy acids: acetolactate synthases and acetohydroxyacid synthases, *Biochim. Biophys. Acta 2*, 401-419.

Chapter 3

1. Yin de, L.T., et al., *Switching catalysis from hydrolysis to perhydrolysis in Pseudomonas fluorescens esterase.* Biochemistry, 2010. **49**(9): p. 1931-42.
2. Harrison, C.R. and P. Hodge, *Oxidation of some penicillins and other sulphides by use of a polymer-supported peroxy-acid.* Journal of the Chemical Society, Perkin Transactions 1, 1976(21): p. 2252-2254.
3. ten Brink, G.J., I.W.C.E. Arends, and R.A. Sheldon, *The Baeyer,àiVilliger Reaction:,Äâ New Developments toward Greener Procedures.* Chemical Reviews, 2004. **104**(9): p. 4105-4124.
4. Doumaux, A.R., J.E. McKeon, and D.J. Trecker, *Metal ion-catalyzed peroxide oxidation of organic substrates. Selective synthesis of imides.* Journal of the American Chemical Society, 1969. **91**(14): p. 3992-3993.
5. Sugimoto, H. and D.T. Sawyer, *Iron(II)-induced activation of hydroperoxides for the dehydrogenation and monooxygenation of organic substrates in acetonitrile.* Journal of the American Chemical Society, 1985. **107**(20): p. 5712-5716.
6. Harakeh, M.S., *Inactivation of Enteroviruses, Rotaviruses and Bacteriophages by Peracetic-Acid in a Municipal Sewage Effluent.* Fems Microbiology Letters, 1984. **23**(1): p. 27-30.
7. Koivunen, J. and H. Heinonen-Tanski, *Peracetic acid (PAA) disinfection of primary, secondary and tertiary treated municipal wastewaters.* Water Research, 2005. **39**(18): p. 4445-4453.
8. Saake, B., et al., *Bleaching of Formacell Pulp from Aspen Wood with Ozone and Peracetic Acid in Organic Solvents.* Holzforschung, 1998. **52**(6): p. 643-650.
9. Duncan, S., et al., *Increased Saccharification Yields from Aspen Biomass Upon Treatment with Enzymatically Generated Peracetic Acid.* Applied Biochemistry and Biotechnology, 2010. **160**(6): p. 1637-1652.
10. Yin, D.L., et al., *Improved pretreatment of lignocellulosic biomass using enzymatically-generated peracetic acid.* Bioresource Technology, 2011. **102**(8): p. 5183-5192.
11. Phillips, B., Starcher, P.S., and Ash, B.D., *Preparation of Aliphatic Peroxyacids.* Journal of Organic Chemistry, 1959. **23**(12): p. 1823-1826.
12. Picard, M., et al., *Metal-free bacterial haloperoxidases as unusual hydrolases: Activation of H2O2 by the formation of peracetic acid.* Angewandte Chemie-International Edition in English, 1997. **36**(11): p. 1196-1199.
13. Hofmann, B., et al., *Structural investigation of the cofactor-free chloroperoxidases.* J Mol Biol, 1998. **279**(4): p. 889-900.

14. Line, K., M.N. Isupov, and J.A. Littlechild, *The crystal structure of a (-) gamma-lactamase from an Aureobacterium species reveals a tetrahedral intermediate in the active site.* J Mol Biol, 2004. **338**(3): p. 519-32.
15. Honda, K., et al., *Role of Acinetobacter calcoaceticus 3,4-dihydrocoumarin hydrolase in oxidative stress defence against peroxoacids.* Eur J Biochem, 2003. **270**(3): p. 486-94.
16. Shaw, P.D., Hager, L.P., *Biological chlorination. III. b-Ketoadipate chlorinase: a soluble enzyme system.* Journal of Biological Chemistry, 1959. **234**: p. 2565-2569.
17. Janes, L.E., A.C. Lowendahl, and R.J. Kazlauskas, *Quantitative screening of hydrolase libraries using pH indicators: Identifying active and enantioselective hydrolases.* Chemistry-a European Journal, 1998. **4**(11): p. 2324-2331.
18. Bray, W.C., Livingston, R.S., *The Catalytic Decomposition of Hydrogen Peroxide in a Brominebromide Solution, and a Study of the steady state.* Journal of American Chemical Society, 1923. **45**(5): p. 1251-1271.
19. Zerner, B., Bender, M.L., *The Kinetic Consequences of the Acyl-Enzyme Mechanism for Reactions of Specific Substrates with Chymotrypsin.* Journal of American Chemistry Society, 1964. **86**(18): p. 3669-3674.
20. Fink, A.L. and M.L. Bender, *Binding sites for substrate leaving groups and added nucleophiles in papain-catalyzed hydrolyses.* Biochemistry, 1969. **8**(12): p. 5109-18.
21. Youshko, M.I., et al., *Penicillin acylase-catalyzed synthesis of beta-lactam antibiotics in highly condensed aqueous systems: Beneficial impact of kinetic substrate supersaturation.* Biotechnology and Bioengineering, 2004. **85**(3): p. 323-329.
22. Bernhardt, P., K. Hult, and R.J. Kazlauskas, *Molecular basis of perhydrolase activity in serine hydrolases.* Angew Chem Int Ed Engl, 2005. **44**(18): p. 2742-6.
23. Weng, M., et al., *Purification, characterization and comparison of two non-haem bromoperoxidases from Streptomyces aureofaciens ATCC 10762.* Journal of General Microbiology, 1991. **137**(11): p. 2539-2546.
24. Bantleon, R., J. Altenbuchner, and K.H. van Pee, *Chloroperoxidase from Streptomyces lividans: isolation and characterization of the enzyme and the corresponding gene.* J Bacteriol, 1994. **176**(8): p. 2339-47.
25. Carr, P.D. and D.L. Ollis, *Alpha/beta hydrolase fold: an update.* Protein Pept Lett, 2009. **16**(10): p. 1137-48.
26. Rose, G.D., L.M. Gierasch, and J.A. Smith, *Turns in Peptides and Proteins.* Advances in Protein Chemistry, 1985. **37**: p. 1-109.
27. Wilmot, C.M. and J.M. Thornton, *Analysis and Prediction of the Different Types of Beta-Turn in Proteins.* Journal of Molecular Biology, 1988. **203**(1): p. 221-232.
28. Hjelmeland, L.M. and G.H. Loew, *Molecular orbital studies of the conformation of peroxyacetic acid.* Chemical Physics Letters, 1975. **32**(2): p. 309-314.
29. Bornscheuer, U.T., et al., *Characterization and enantioselectivity of a recombinant esterase from Pseudomonas fluorescens.* Enzyme and Microbial Technology, 1998. **22**(7): p. 641-646.

30. Gasteiger, E., Hoogland, C., Gattiker, A., Duvaud, S., Wilkins, M.R., Appel, R.D., Bairoc, A., *Protein Identification and Analysis Tools on the ExPASy Server*, in *The Proteomics Protocols Handbook*, J.M. Walker, Editor 2005, Humana Press. p. 571-607.
31. Llewellyn, D.R. and C. O'Connor, *110. Tracer studies of carboxylic acids. Part I. Acetic and pivalic acid.* Journal of the Chemical Society (Resumed), 1964: p. 545-549.
32. Bailey, S., *The Ccp4 Suite - Programs for Protein Crystallography.* Acta Crystallographica Section D-Biological Crystallography, 1994. **50**: p. 760-763.
33. Emsley, P. and K. Cowtan, *Coot: model-building tools for molecular graphics.* Acta Crystallographica Section D-Biological Crystallography, 2004. **60**: p. 2126-2132.
34. Cheeseman, J.D., et al., *X-ray crystal structure of pseudomonas fluorescens aryl esterase reveals possible structural explanations for substrate preference and enantioselectivity.* Abstracts of Papers of the American Chemical Society, 2004. **228**: p. U189-U190.
35. Pinkernell, U., S. Effkemann, and U. Karst, *Simultaneous HPLC Determination of Peroxyacetic Acid and Hydrogen Peroxide.* Analytical Chemistry, 1997. **69**(17): p. 3623-3627.

Chapter 4

1. Youshko, M. I.; Chilov, G. G.; Shcherbakova, T. A.; Svedas, V. K., Quantitative characterization of the nucleophile reactivity in penicillin acylase-catalyzed acyl transfer reactions. *Biochimica et Biophysica Acta (BBA) - Proteins & Proteomics* **2002,** *1599* (1-2), 134-140.
2. Hegarty, A. F., *Comprehensive Organic Chemistry*. Pearson Higher Education: New York, 1995.
3. Hickman, W. S., Peracetic acid and its use in fibre bleaching. *Review of Progress in Coloration and Related Topics* **2002,** *32* (1), 13-27.
4. Saake, B.; Lehnen, R.; Schmekal, E.; Neubauer, A.; Nimz, H. H., Bleaching of Formacell Pulp from Aspen Wood with Ozone and Peracetic Acid in Organic Solvents. *Holzforschung* **1998,** *52* (6), 643-650.
5. Harakeh, M. S., Inactivation of Enteroviruses, Rotaviruses and Bacteriophages by Peracetic-Acid in a Municipal Sewage Effluent. *Fems Microbiol Lett* **1984,** *23* (1), 27-30.
6. Poljak, A., Holzaufschluβ mit peressigsäure. *Angewandte Chemie* **1948,** *60*, 45-46.
7. Duncan, S.; Jing, Q.; AlDajani, W. W.; Katona, A.; Schilling, J.; Tschirner, U.; Kazlauskas, R. J., Increased Saccharification Yields from Aspen Biomass Upon Treatment with Enzymatically Generated Peracetic Acid. *Appl Biochem Biotech* **2010,** *160* (6), 1637-1652.

8. Yin, D. L.; Jing, Q.; AlDajani, W. W.; Duncan, S.; Tschirner, U.; Schilling, J.; Kazlauskas, R. J., Improved pretreatment of lignocellulosic biomass using enzymatically-generated peracetic acid. *Bioresource Technol* **2011,** *102* (8), 5183-5192.
9. Kirk, O.; Conrad, L. S., Metal-free haloperoxidases: Fact or artifact? *Angewandte Chemie-International Edition* **1999,** *38* (7), 977-979.
10. Jankovic, M.; Sinadinovic-Fiser, S., Prediction of the chemical equilibrium constant for peracetic acid formation by hydrogen peroxide. *J Am Oil Chem Soc* **2005,** *82* (4), 301-303.
11. Yin, D. L. T.; Purpero, V.; Jing, Q.; Fujii, R.; Kazlauskas, R. J., Revised molecular basis for enzyme catalyzed carboxylic acid perhydrolysis. University of Minnesota: Saint Paul, 2011.
12. Fink, A. L.; Bender, M. L., Binding sites for substrate leaving groups and added nucleophiles in papain-catalyzed hydrolyses. *Biochemistry* **1969,** *8* (12), 5109-18.
13. Yin de, L. T.; Bernhardt, P.; Morley, K. L.; Jiang, Y.; Cheeseman, J. D.; Purpero, V.; Schrag, J. D.; Kazlauskas, R. J., Switching catalysis from hydrolysis to perhydrolysis in Pseudomonas fluorescens esterase. *Biochemistry* **2010,** *49* (9), 1931-42.
14. Morley, K. L.; Kazlauskas, R. J., Improving enzyme properties: when are closer mutations better? *Trends Biotechnol* **2005,** *23* (5), 231-7.
15. Tarcha, P. J.; Chu, V. P.; Whittern, D., 2,3-diaminophenazine is the product from the horseradish peroxidase-catalyzed oxidation of o-phenylenediamine. *Analytical Biochemistry* **1987,** *165* (1), 230-233.
16. Morris, D. R.; Hager, L. P., Chloroperoxidase. *Journal of Biological Chemistry* **1966,** *241* (8), 1763-1768.
17. Janes, L. E.; Lowendahl, A. C.; Kazlauskas, R. J., Quantitative screening of hydrolase libraries using pH indicators: Identifying active and enantioselective hydrolases. *Chem-Eur J* **1998,** *4* (11), 2324-2331.
18. Pinkernell, U.; Effkemann, S.; Karst, U., Simultaneous HPLC Determination of Peroxyacetic Acid and Hydrogen Peroxide. *Analytical Chemistry* **1997,** *69* (17), 3623-3627.
19. Krebsfanger, N.; Zocher, F.; Altenbuchner, J.; Bornscheuer, U. T., Characterization and enantioselectivity of a recombinant esterase from Pseudomonas fluorescens. *Enzyme Microb Tech* **1998,** *22* (7), 641-646.
20. Sambrook, J.; Russell, D., *Molecular cloning: A laboratory manual*. Cold Spring Harbor Press: New York, 2001; Vol. 1.
21. Pelletier, J. N.; Denault, M., Protein library design and screening. In *Protein engineering protocols*, Arndt, K. M.; Müller, K. M., Eds. Humana press: Totowa, 2007; pp 127-154.
22. Mathews, I.; Soltis, M.; Saldajeno, M.; Ganshaw, G.; Sala, R.; Weyler, W.; Cervin, M. A.; Whited, G.; Bott, R., Structure of a novel enzyme that catalyzes acyl transfer to alcohols in aqueous conditions. *Biochemistry* **2007,** *46* (31), 8969-79.

23. Amin, N. S.; Boston, M. G.; Bott, R. R.; Cervin, M. A.; Concar, E. M.; Gustwiller, M. E.; Jones, B. E.; Liebeton, K.; Miracle, G. S.; Oh, H.; Poulose, A. J.; Ramer, S. W.; Scheibel, J. J.; Weyler, W.; Whited, G. M. Perhydrolase. 2008.
24. Dicosimo, R.; Payne, M. S.; Yin, T. Perhydrolase for enzymatic peracid generation. 2010.
25. Cheeseman, J. D.; Tocilj, A.; Morley, K.; Park, S.; Schrag, J. D.; Kazlauskas, R. J., X-ray crystal structure of pseudomonas fluorescens aryl esterase reveals possible structural explanations for substrate preference and enantioselectivity. *Abstr Pap Am Chem S* **2004,** *228*, U189-U190.
26. Genomics, J. C. f. S., Crystal structure of Acetyl xylan esterase (TM0077) from Thermotoga maritima at 2.10 A resolution 2004.

Chapter 5

1. Duncan, S., Jing, Q., Katona, A., Kazlauskas, R.J., Schilling, J., Tschirner, U., Wafa AlDajani, W., 2010. Increased saccharification yields from aspen biomass upon treatment with enzymatically generated peracetic acid. Appl. Biochem. Biotechnol. 160, 1637–1652.
2. Nakagame, S., Chandra, R.P., Saddler, J.N., 2010. The effect of isolated lignins, obtained from a range of pretreated lignocellulosic substrates, on enzymatic hydrolysis. Biotechnol. Bioeng. 105, 871–879.
3. Lee, J.M., Jameel, H., Venditti, R.A., 2010 A comparison of the autohydrolysis and ammonia fiber explosion (AFEX) pretreatments on the subsequent enzymatic hydrolysis of coastal Bermuda grass. Bioresource Technol. 101, 5549–5558.
4. Zheng, Y., Pan, Z., Zhang, R., 2009. Overview of biomass pretreatment for cellulosic ethanol production. Int. J. Agric. Biol. Eng. 2, 51–68.
5. Yan, W., Acharjee, T.C., Coronella, C.J., Vasquez, V.R., 2009. Thermal pretreatment of lignocellulosic biomass. Environ. Prog. Sustainable Energ. 28, 435–440.
6. Luo, C.D., Brink, D.L., Blanch, H.W., 2002 Identification of potential fermentation inhibitors in conversion of hybrid poplar hydrolyzate to ethanol. Biomass Bioenerg. 22, 125–138.
7. Lau, M.W., Dale, B.E., 2010. Effect of primary degradation-reaction products from Ammonia Fiber Expansion (AFEX)-treated corn stover on the growth and fermentation of *Escherichia coli* KO11. Bioresource Technol. 101, 7849–7855.
8. Neely, W.C., 1984. Factors affecting the pretreatment of biomass with gaseous ozone. Biotechnol. Bioeng. 26, 59–65.
9. Vidal, P.F.; Molinier, J., 1988. Ozonolysis of lignin. Improvement of in vitro digestibility of poplar sawdust. Biomass 16, 1–17.
10. Azzam, M., 1989. Pretreatment of cane bagasse with alkaline hydrogen peroxide for enzymatic hydrolysis of cellulose and ethanol fermentation. J. Environ. Sci. Health B, 24, 421–433.

11. Chum, H.L., Johnson, D.K., Black, S., 1988. Organosolv pretreatment for enzymatic hydrolysis of poplars: 1. Enzyme hydrolysis of cellulosic residues. Biotechnol. Bioeng. 31, 643–649.
12. McMillan, J.D., 1994. Pretreatment of lignocellulosic biomass. In: Himmel, M.E., Baker, J.O., Overend, R.P. (Eds.), Enzymatic Conversion of Biomass for Fuels Production. American Chemical Society, Washington, DC, pp. 292–324.
13. Sun, R.C., Tomkinson, J., Zhu, W., Wang, S.Q., 2000. Delignification of maize stems by peroxymonosulfuric acid, peroxyformic acid, peracetic acid, and hydrogen peroxide. 1. Physicochemical and structural characterization of the solubilized lignins. J. Agric. Food Chem. 48, 1253–1262.
14. Lawrence, W., McKelvey, R.D., Johnson, D.C., 1980. The peroxyacetic acid oxidation of a lignin-related β-aryl ether. Svensk Papperstidn. 83, 11–18.
15. Teixeira, L.C., Linden, J.C., Schroeder, H.A. 2000. Simultaneous saccharification and cofermentation of peracetic acid-pretreated biomass, Appl. Biochem. Biotechnol. 84, 111–127.
16. Yin, D.T., Bernhardt, P., Morley, K.L., Jiang, Y., Cheeseman, J.D., Purpero, V., Schrag, J.D., Kazlauskas, R.J., 2010. Switching catalysis from hydrolysis to perhydrolysis in *Pseudomonas fluorescens* esterase. Biochemistry 49, 1931–1942.
17. Walton, J.H., Lewis, H.A., 1916. The partition coefficients of hydrogen peroxide between water and certain organic solvents. J. Am. Chem. Soc. 38, 633-638.
18. Danielewicz, D., Surma-Ślusarska, B., 2006. Oxygen delignification of high-kappa number pine kraft pulp. Fibres and Textiles in Eastern Europe 14, 89–93.
19. Gharpuray, M.M., Lee, Y.-H., Fan, L.T., 1983. Structural modification of lignocellulosics by pretreatments to enhance enzymatic hydrolysis. Biotechnol. Bioeng. 25, 157–172.
20. Sinitsyn, A.P., Gusakov, A.V., Vlasenko, E.Y., 1991. Effect of structural and physicochemical features of cellulosic substrates on the efficiency of enzymatic hydrolysis. Appl. Biochem. Biotechnol. 30, 43–59.
21. Chen, F., Dixon, R.A., 2007. Lignin modification improves fermentable sugar yields for biofuel production. Nat. Biotechnol. 25, 759–761.
22. Yuan, Z., Ni, Y., Van Heiningen, A.R.P., 1997. Kinetics of peracetic acid decomposition: Part I: Spontaneous decomposition at typical pulp bleaching conditions. Can. J. Chem. Eng. 75, 37–41.
23. Devenyns, J., Desprez, F., Troughton, N., 1993. Peracetic acid as a selective prebleaching agent: an effective option for the production of fully bleached TCF Kraft pulps. TAPPI Non-Chlorine Bleaching Conference, Atlanta, GA, Section 8–1, 341.
24. Jääskeläinen, A.-S., Poppius-Levlin, K., 1999. Screening of process parameters affecting the kinetics of pine Kraft pulp delignification with peroxyacetic acid. J. Pulp Pap. Sci. 25, 37–41.
25. Brown, L., Torget, R., 1996. Enzymatic saccharification of lignocellulosic biomass. NREL Laboratory Analytical Procedure LAP #009, National Renewable Energy Laboratory, Golden, CO, USA.

26. Pinkernell, U., Effkemann, S., Karst, U., 1997. Simultaneous HPLC determination of peroxyacetic acid and hydrogen peroxide. Anal. Chem. 69, 3623–3627.
27. Sluiter, A., Hames, B., Hyman, D., Payne, C., Ruiz, R., Scarlata, C., Sluiter, J., Templeton, D., Wolfe, J., 2008. Determination of total solids in biomass and total dissolved solids in liquid process samples. NREL Laboratory Analytical Procedure, National Renewable Energy Laboratory, Golden, CO, USA.
28. TAPPI T 222 om-02, 2002. TAPPI Test Method: Acid-insoluble lignin in wood and pulp.
29. Rodriguez, C., Hiligsmann, S., Ongena, M., Charlier, R., Thonart, P., 2005. Development of an enzymatic assay for the determination of cellulose bioavailability in municipal solid waste. Biodegradation 16, 415–422.
30. Rozzell, J.D., 1999. Commercial scale biocatalysis: myths and realities. Bioorg. Med. Chem. 7, 2253–2261.
31. U.S. Department of Energy, www1.eere.energy.gov/biomass/ethanol_yield _calculator.html (accessed Aug 2010)
32. Savile, C.K., Janey, J.M., Mundorff, E.C., Moore, J.C., Tam, S., Jarvis, W.R., Colbeck, J.C., Krebber, A., Fleitz, F.J., Brands, J., Devine, P.N., Huisman, G.W., Hughes, G.J. 2010. Biocatalytic asymmetric synthesis of chiral amines from ketones applied to sitagliptin manufacture. Science 329, 305–309.
33. Kazi, F.K., Fortman, J.A., Anex, R.P., Hsu, D.D., Aden, A., Dutta, A., Kothandaraman, G., 2010. Techno-economic comparison of process technologies for biochemical ethanol production from corn stover. Fuel 89, S20–S28.
34. Aden, A., Foust , T., 2009. Technoeconomic analysis of the dilute sulfuric acid and enzymatic hydrolysis process for the conversion of corn stover to ethanol. Cellulose 16, 535–545.

Chapter 6

1. D. R. Feller, V. S. Kamanna, H. A. I. Newman, K. J. Romstedt, D. T. Witiak, G. Bettoni, S. H. Bryant, D. Conte-Camerino, F. Loiodice, V. Tortorella, *J. Med. Chem.* **1987**, *30*, 1265-1267.
2. G. Bettoni, F. Loiodice, V. Tortorelia, D. Conte-Camerino, M. Mambri, E. Ferrannini, S. H. Bryant, *J. Med. Chem.* **1987**, *30*, 1267-1270.
3. S. N. Ahmed, R. J. Kazlauskas, A. H. Morinville, P. Grochulski, J. D. Schrag, M. Cygler, *Biocatalysis* **1994**, *9*, 209-225.
4. S.-H. Wu, PhD thesis, University of Wisconsin, Madison (USA), **1987**, p 120.
5. S. K. Latypov, J. M. Seco, E. Quiñoá, R. Riguera, *J. Org. Chem.* **1995**, *60*, 1538–1545; S.K. Latypov, J. M. Seco, E. Quiñoá, R. Riguera, *J. Am. Chem. Soc.* **1998**, *120*, 877–882.
6. T. Miyazawa, S. Kurita, M. Shimaoka, S. Ueji, T. Yamada, *Chirality* **1999**, *11*, 554-560.

7. Review: P. D. de Maria, J. M. Sanchez-Montero, J. V. Sinisterra, A. R. Alcantara, *Biotechnol. Adv.* **2006**, *24*, 178-194.
8. J. J. Lalonde, C. Govardhan, N. Khalaf, A. G. Martinez, K. Visuri, A. L. Margolin, *J. Am. Chem. Soc.* **1995**, *117*, 6845-6852.
9. P. Grochulski, Y. Li, J. D. Schrag, F. Bouthillier, P. Smith, D. Harrison, B. Rubin, M. Cygler, *J. Biol. Chem.* **1993**, *268*, 12843-12847.
10. P. Grochulski, Y. Li, J. D. Schrag, M. Cygler, *Prot. Sci.* **1994**, *3*, 82-91; P. Grochulski, F. Bouthillier, R. J. Kazlauskas, A. N. Serreqi, J. D. Schrag, E. Ziomek, M. Cygler, *Biochemistry* **1994**, *33*, 3494-3500.
11. J. M. Mancheño, M. A. Pernas, M. J. Martínez, B. Ochoa, M. L. Rúa, J. A. Hermoso, *J. Mol. Biol.* **2003**, *332*, 1059-1069.
12. D. Ghosh, Z. Wawrzak, V. Z. Pletnev, N. Li, R. Kaiser, W. Pangborn, H. Jörnvall, M. Erman, W. L. Duax, *Structure* **1995**, *3*, 279-288; V. Pletnev, A. Addlagatta, Z. Wawrzak, W. Duax, *Acta Crystallogr. D Biol. Crystallogr.* **2003**, *59*, 50-56.
13. K. Lundell, T. Raijola, L. T. Kanerva, *Enzym. Microb. Technol.* **1998**, *22*, 86-93.
14. N. López, M. A. Pernas, L. M. Pastrana, A. Sánchez, F. Valero, M. L. Rúa, *Biotechnol. Prog.* **2004**, *20*, 65-73.
15. S. H. Wu, Z. W. Guo, C. J. Sih, *J. Am. Chem. Soc.* **1990**, *112*, 1990-1995.
16. I. J. Colton, S. N. Ahmed, R. J. Kazlauskas, *J. Org. Chem.* **1995**, *60*, 212-217.
17. K. Nishizawa, Y. Ohgami, N. Matsuo, H., Kisida, H. Hirohara, *J. Chem. Soc., Perkin Trans. 2*, **1997**, 1293-1298.
18. A. Mezzetti, J. D. Schrag, C. S. Cheong, R. J. Kazlauskas, *Chem. Biol.* **2005**, *12*, 427-437.
19. S. Hur, T. C. Bruice. *Proc. Natl. Acad. Sci. USA* **2003**, *100*, 12015-12020.
20. D. F. Sticke, L. G. Presta, K. A. Dill, G. D. Rose, *J. Mol. Biol.* **1992**, *226*, 1143-1159.
21. M. S. Kharasch, R. A. Mosher, I. S. Bengelsdorf, *J. Org. Chem.* **1960**, *25*, 1000-1006.
22. F. Texier-Boullet, A. Foucaud, *Synthesis*, **1982**, 165-166.
23. Y.-F. Li, F. Hammerschmidt, *Tetrahedron: Asymmetry*, **1993**, *4*, 109-120.
24. A. T. Brünger, P. D. Adams, G. M. Clore, W. L. DeLano, P. Gros, R. W. Grosse-Kunstleve, J.-S. Jiang, J. Kuszewski, M. Nilges, N. S. Pannu, R. J. Read, L. M. Rice, T. Simonson, G. L. Warren, *Acta Crystallogr. D Biol. Crystallogr*. **1998**, *54*, 905-921.
25. T. A. Jones, J.-Y. Zou, S. W. Cowan, *Acta Crystallogr. A xxxx,* **1991**, *47*, 110-119.
26. P. Emsley, B. Lohkamp, W. G. Scott, K. Cowtan, *Acta Crystallogr. D Biol. Crystallogr.* **2010**, *66*, 486-501.
27. G. A. Kaminski, R. A. Friesner, J. Tirado-Rives, W. L. Jorgensen, *J. Phys. Chem. B*, **2001**, *105*, 6474-6487.
28. W. L. Jorgensen, J. Chandrasekhar, J. D. Madura, R. W. Impey, M. L. Klein, *J. Chem. Phys.* **1983**, *79*, 926-935.

29. H. J. C. Berendsen, J. P. M. Postma, W. F. van Gunsteren, A. Dinola, J. R. Haak, *J. Chem. Phys.* **1984**, *81*, 3684-3690.
30. M. Botta, E. Cernia, F. Corelli, F. Manetti, S. Soro, *Biochim. Biophys. Acta* **1997**, *1337*, 302-310.
31. F. Manetti, D. Mileto, F. Corelli, S. Soro, C. Palocci, E. Cernia, I. D'Acquarica, M. Lotti, L. Alberghina, M. Botta, *Biochim. Biophys. Acta*, **2000**, *1543*, 146-158.
32. S. Mittal, S. Khanna, A. Roy, P. V. Bharatam, H. P. S. Chawla, *Enzyme Microb. Technol.* **2005**, *36*, 232-238.
33. K. Watanabe, T. Uno, T. Koshiba, T. Okamoto, Y. Ebara, S. Ueji, *Bull. Chem. Soc. Jpn.* **2004**, *77*, 543-548.
34. A. C. Sehgal, R. M. Kelly, *J. Am. Chem. Soc.* **2002**, *124*, 8190-8191.
35. M. Holmquist, F. Haeffner, T. Norin, K. Hult, *Prot. Sci.* **1996**, ***5***, 83-88.
36. P. Berglund, M. Holmquist, K. Hult, H. E. Högberg, *Biotechnol. Lett.* **1995**, *17*, 55-60.
37. P. Berglund, M. Holmquist, K. Hult, *J. Mol. Catal. B Enzym.* **1998***, 5*, 283-287.
38. F. Secundo, G. Carrea, C. Tarabiono, P. Gatti-Lafranconi, S. Brocca, M. Lotti, K.-E. Jaeger, M. Puls, T. Eggert, *J. Mol. Catal. B Enzym*. **2006**, *39*, 166-170.
39. M. Holmquist, P. Berglund, *Org. Lett.* **1999**, *1*, 763-765.

Appendix: Reprints of published articles

BIOCHEMISTRY
including biophysical chemistry & molecular biology
Article

Biochemistry **2010,** *49,* 1931–1942 1931
DOI: 10.1021/bi9021268

Switching Catalysis from Hydrolysis to Perhydrolysis in *Pseudomonas fluorescens* Esterase[†,‡]

De Lu (Tyler) Yin,[§] Peter Bernhardt,[§] Krista L. Morley,[∥] Yun Jiang,[§] Jeremy D. Cheeseman,[∥] Vincent Purpero,[§] Joseph D. Schrag,*[,⊥] and Romas J. Kazlauskas*[,§]

[§]*Department of Biochemistry, Molecular Biology, and Biophysics and The Biotechnology Institute, University of Minnesota, 1479 Gortner Avenue, St. Paul, Minnesota 55108,* [∥]*Department of Chemistry, McGill University, 801 Sherbrooke Street West, Montréal, Québec H3A 2K6, Canada, and* [⊥]*Biotechnology Research Institute, National Research Council of Canada, 6100 Royalmount Avenue, Montréal, Québec H4P 2R2, Canada*

Received July 17, 2009; Revised Manuscript Received January 26, 2010

ABSTRACT: Many serine hydrolases catalyze perhydrolysis, the reversible formation of peracids from carboxylic acids and hydrogen peroxide. Recently, we showed that a single amino acid substitution in the alcohol binding pocket, L29P, in *Pseudomonas fluorescens* (SIK WI) aryl esterase (PFE) increased the specificity constant of PFE for peracetic acid formation > 100-fold [Bernhardt et al. (2005) *Angew. Chem., Int. Ed. 44*, 2742]. In this paper, we extend this work to address the three following questions. First, what is the molecular basis of the increase in perhydrolysis activity? We previously proposed that the L29P substitution creates a hydrogen bond between the enzyme and hydrogen peroxide in the transition state. Here we report two X-ray structures of L29P PFE that support this proposal. Both structures show a main chain carbonyl oxygen closer to the active site serine as expected. One structure further shows acetate in the active site in an orientation consistent with reaction by an acyl-enzyme mechanism. We also detected an acyl-enzyme intermediate in the hydrolysis of ε-caprolactone by mass spectrometry. Second, can we further increase perhydrolysis activity? We discovered that the reverse reaction, hydrolysis of peracetic acid to acetic acid and hydrogen peroxide, occurs at nearly the diffusion limited rate. Since the reverse reaction cannot increase further, neither can the forward reaction. Consistent with this prediction, two variants with additional amino acid substitutions showed 2-fold higher k_{cat}, but K_m also increased so the specificity constant, k_{cat}/K_m, remained similar. Third, how does the L29P substitution change the esterase activity? Ester hydrolysis decreased for most esters (75-fold for ethyl acetate) but not for methyl esters. In contrast, L29P PFE catalyzed hydrolysis of ε-caprolactone five times more efficiently than wild-type PFE. Molecular modeling suggests that moving the carbonyl group closer to the active site blocks access for larger alcohol moieties but binds ε-caprolactone more tightly. These results are consistent with the natural function of perhydrolases being either hydrolysis of peroxycarboxylic acids or hydrolysis of lactones.

Many serine hydrolases catalyze perhydrolysis, the reversible formation of peroxycarboxylic acids from carboxylic acids and hydrogen peroxide (*1*−*3*). Enhancing this reactivity could offer new catalysts for organic synthesis and industry. Peracids can introduce oxygen into olefins, cyclic ketones, amines, and organic sulfur compounds, making them essential oxidants for organic synthesis (*4*, *5*). Industry uses peracids for disinfecting, wastewater treatment, destaining of fabrics, pulp bleaching, and removal of lignin from biomass. Unfortunately, concentrated peracids are explosive and corrosive, but the *in situ* generation of dilute peracids minimizes these hazards. Chemical *in situ* generation of peracids often involves two steps or harsh reaction conditions or hazardous catalysts or a combination thereof (*5*). Enzyme-catalyzed reactions are an environmentally friendly alternative that avoid harsh reaction conditions and hazardous catalysts.

Perhydrolases are a subgroup of serine hydrolases that are particularly efficient at catalyzing perhydrolysis. Perhydrolases have an α/β-hydrolase fold (*6*) and use a Ser-His-Asp catalytic triad (*7*−*9*). Perhydrolysis likely takes place with a ping-pong bi-bi mechanism (*9*, *10*) (Figure 1a). The catalytic serine attacks the carbonyl carbon of a carboxylic acid and displaces water to form an acyl-enzyme intermediate. Next, hydrogen peroxide reacts with this acyl enzyme to form the peracid product and to regenerate the catalyst. Hydrogen bonds from two main chain amides, called the oxyanion hole, activate the carbonyl group for attack and stabilize the tetrahedral intermediate.

Some reactions catalyzed by α/β-hydrolases do not involve a covalent acyl-enzyme intermediate (*11*). For example, hydroxynitrile lyases catalyze the direct attack of cyanide on the aldehyde to form a cyanohydrin (*12*). Bugg proposed that perhydrolysis could also occur by direct attack by hydrogen peroxide on acetic acid without the formation of an acetyl-enzyme intermediate (*11*) (Figure 1b). Support for this mechanism was an X-ray crystal structure of propionate bound to the active site of a perhydrolase in the orientation suggested in Figure 1b.

[†]This research was supported by the University of Minnesota, the National Institutes of Health (Training Grant T32 GM008347 to support T.Y., Research Grant GM24689 (John Lipscomb) to support V.P.), and the Natural Sciences and Engineering Research Council of Canada (postgraduate fellowships to K.L.M. and J.D.C.).

[‡]X-ray coordinates have been deposited in the Research Collaboratory for Structural Bioinformatics, Rutgers University, New Brunswick, NJ (accession numbers 3hea and 3hi4).

*To whom correspondence should be addressed. R.J.K.: e-mail, rjk@umn.edu; fax, 612-625-5780; phone, 612-624-5904. J.D.S.: e-mail, joe@bri.nrc.ca; fax, 514-496-5143; phone, 514-496-2557.

Published on Web 01/29/2010

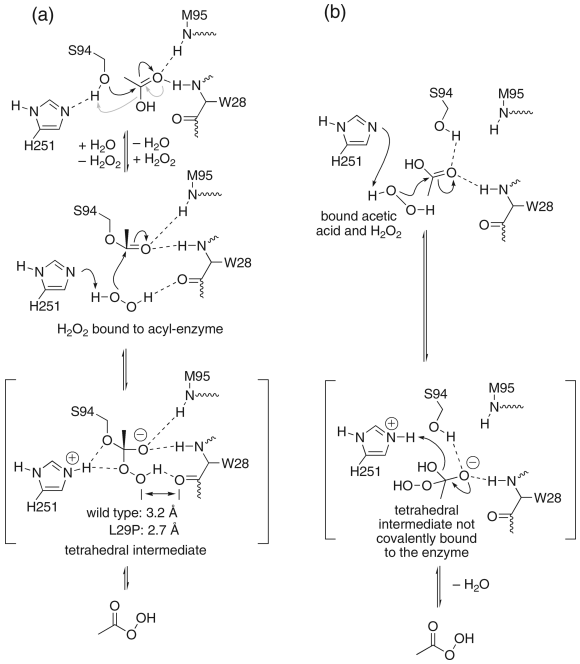

FIGURE 1: Proposed mechanisms for perhydrolysis of acetic acid. The numbering corresponds to the active site of PFE. (a) The ping-pong bi-bi mechanism involves an acetyl-enzyme intermediate. The first diagram shows the enzyme−acetic acid complex. The γ-hydroxyl group of active site serine 94 is a nucleophile that attacks the carbonyl group of acetic acid to form a tetrahedral intermediate (not shown) via the black curved arrows. Next, this tetrahedral intermediate collapses via the release of water (gray curved arrows) to form an acetyl-enzyme intermediate. Finally hydrogen peroxide binds to yield the complex shown in the second diagram. The N−H's of M95 and W28, called the oxyanion hole, donate hydrogen bonds to the carbonyl oxygen. Nucleophilic attack of hydrogen peroxide on the acyl-enzyme forms a second tetrahedral intermediate. In wild-type PFE, the carbonyl oxygen of W28 is too far from the hydrogen peroxide to form a hydrogen bond. The L29P substitution moves this carbonyl 0.5 Å closer to the catalytic serine side chain allowing a hydrogen bond to form and stabilize the tetrahedral intermediate. (b) The ordered bi-bi noncovalent mechanism proposed by Bugg (*11*) does not form an acyl-enzyme intermediate. Both acetic acid and hydrogen peroxide bind the enzyme simultaneously. In this mechanism, acetic acid does not bind to the oxyanion hole, but the γ-hydroxyl group of active site S94 and N−H of W28 donate a hydrogen bond to the carbonyl oxygen of acetic acid. Hydrogen peroxide attacks the bound acetic acid to form a tetrahedral intermediate without covalent links to the enzyme.

Pseudomonas fluorescens esterase (PFE)[1] is a hydrolase, but its amino acid sequence most closely resembles perhydrolases. The amino acid sequence of PFE is 54% identical and 69% similar to that for a perhydrolase from *P. fluorescens* (CPO-F). However, CPO-F is a good perhydrolase (k_{cat} = 1.9 s^{-1}), while PFE is a poor one (k_{cat} = 0.12 s^{-1}). The X-ray structures of the active sites showed subtle differences, but it was unclear which ones were responsible for the different catalytic activities (*9*). Recently, we reported a single amino acid substitution, L29P, in PFE that increased the perhydrolase activity 28-fold to 3.5 s^{-1} (*13*), which is higher than that for CPO-F (*14*). We attributed the increased catalytic efficiency to a new hydrogen bond between a carbonyl oxygen of W28 and the peroxy group of the second tetrahedral intermediate (C═O···O distance 2.7 Å) using molecular modeling (Figure 1a). The wild-type enzyme could not form this hydrogen bond because the carbonyl group was 0.5 Å further away from the active site (C═O···O distance 3.2 Å). In this paper we confirm the structure of the L29P variant by crystallography and the ping-pong bi-bi mechanism for this enzyme by characterization of an enzyme−acetate complex by X-ray crystallography and by detection of an acyl-enzyme intermediate by mass spectrometry. Further kinetic characterization of L29P PFE shows that it is as efficient for perhydrolysis as physically possible because it catalyzes the reverse reaction, hydrolysis of peracetic acid, at a nearly diffusion controlled rate. The L29P substitution also decreases the efficiency of ester hydrolysis but increases the efficiency of lactone hydrolysis.

[1]Abbreviations: BES, *N*,*N*-bis(2-hydroxyethyl)-2-aminoethanesulfonic acid; BPO-A1, perhydrolase from *Streptomyces aureofaciens* ATCC 10762 (previously called a nonheme bromoperoxidase); CPK colors, Corey, Pauling, and Koltun color scheme; CPO-F, perhydrolase from *Pseudomonas fluorescens* (previously called a nonheme chloroperoxidase); CPO-L, perhydrolase from *Streptomyces lividans* TK64 (previously called a nonheme chloroperoxidase); CPO-T, perhydrolase from *Streptomyces aureofaciens* Tü24 (previously called a nonheme chloroperoxidase); LB, Luria−Bertani broth; MCD, monochlorodimedone; Ni-NTA, nickel complexed to nitrilotriacetic acid; OPLS, optimized potential for liquid simulations; PCR, polymerase chain reaction; PDB ID, Protein Data Bank identification code; PFE, *Pseudomonas fluorescens* esterase; pNP, *p*-nitrophenol; rmsd, root-mean-square deviation.

Table 1: Nucleotide Sequences of Primers for Mutagenesis and Sequencing of pL29P[a]

primer name	5′ to 3′ forward sequence	5′ to 3′ reverse sequence
sequencing primers	CGAGAAGGTCGCGAATTC	CTCTCATCCGCCAAAACA
L29P/F93H	AAGGAGGTGACCCTGGTGGGC**CAT**CCATGGGCGGC	GCCGCCCATGGA**ATG**GCCCACCAGGGTCACCTCCTT
L29P/F57H	ACCGCCGCGGC**CAT**GGCCGCTCGG	CCGAGCGGCC**ATG**GCCGCGGCGGT
L29P/F125A	CCGTCACCCCGCTG**GCC**GGCCAGAAGCCCGA	TCGGGCTTCTGGCC**GGC**CAGCGGGGTGACGG

[a]Mutation sites in the primers are marked in bold.

MATERIALS AND METHODS

General. Water was 18 ohm purity using the Milli-Q water system (Millipore, Billerica, MA). All chemicals including acetic acid, hydrogen peroxide, and peracetic acid were bought from Sigma Aldrich. Specific activity measurements were done using Costar 3635 96-well plates (Corning, Lowell, MA) and read using a SpectraMax plus-384 plate reader (Molecular Devices, Sunnyvale, CA). Kinetic constants were determined by measuring the specific activity as a function of change in substrate concentration. Data were fit to the Michaelis−Menten equation, rate = V_{max}[S]/(K_m + [S]), using software from either OriginPro 7.5 (Origin Lab, Northampton, MA) or Kaleidagraph 4 (Synergy Software, Reading, PA). R^2 values were > 0.97 for both mutants and wild-type PFE.

Mutagenesis. Plasmid pJOE2792 (*13*), which is an *Escherichia coli* expression vector, has the PFE gene from *P. fluorescens* SIK WI inserted as an *Nde*I/*Bam*HI fragment. Expression is regulated by a rhamnose-inducible promoter. Previously, the L29P variant of PFE was made using polymerase chain reaction (PCR) based site-directed mutagenesis (*13*). In this paper, the plasmid containing the L29P PFE plasmid (pL29P) was used as the template for the new mutants. Mutagenic primers (Table 1) were designed using PrimerX (http://bioinformatics.org/primerx/) and synthesized by Integrated DNA Technologies (IDT, Coralville, IA). A typical PCR reaction (50 μL) for mutagenesis, using the *Pfu Turbo* polymerase kit (Stratagene, La Jolla, CA), was performed by initially heating the mixture of pL29P, dNTPs, primers, and 1× buffer to 95 °C for 30 s, followed by 16 cycles of 95 °C for 30 s, 55 °C for 1 min, and 68 °C for 5 min 30 s. The amplified PCR product was treated with *Dpn*I (1 unit for 1 h at 37 °C), an endonuclease that cleaves template DNA, which is methylated, but not the amplified product DNA. Next, the PCR product was transformed into *E. coli* DH5α-T1 competent cells (Invitrogen) by the heat-shock method. Transformed cells were plated on LB (Luria−Bertani broth)−agar containing ampicillin (0.1 mg/mL) and grown for 17 h at 37 °C. Individual colonies were picked and inoculated into 15 mL sterile tubes containing LB (5 mL with 0.1 mg/mL ampicillin) and grown for 17 h at 37 °C. Plasmids were isolated from the 17 h culture using a plasmid mini-prep kit (Qiagen, Valencia, CA). The mutations were confirmed by DNA sequencing using sequencing primers in both the forward (64 bp upstream from the start codon, ATG) and reverse (15 bp downstream from the stop codon, TGA) direction by the Biomedical Genomics Center (University of Minnesota) using ABI BigDye Terminator version 3.1 chemistry. The 17 h grown culture of *E. coli* was mixed with glycerol (20% v/v) and then frozen at −80 °C for long-term storage.

Protein Expression and Purification. Typically, LB media (5 mL containing 0.1 mg/mL ampicillin) were inoculated with a single colony and then grown overnight at 37 °C. The overnight grown culture was diluted (1:100) with fresh LB media (100 mL containing 0.1 mg/mL ampicillin) and grown at 37 °C until the absorbance at 600 nm reached 0.6. Filter-sterilized rhamnose (20% w/v) was added to a concentration of 2% (w/v) to induce protein expression, and the culture was incubated for an additional 3 h at 37 °C. The induced culture was centrifuged (4000*g*, 15 min), and the cell paste was resuspended in buffer A (50 mM NaH_2PO_4, 300 mM NaCl, 10 mM imidazole) to a concentration of 20% (w/v). The resuspended culture was flash frozen in liquid nitrogen and thawed to room temperature; lysozyme was added (final concentration of 1 mg/mL) and incubated on ice for 30 min. The cell lysate was centrifuged (10000*g*, 60 min), and the supernatant was poured onto a column of Ni-NTA agarose resin (5 mL, Invitrogen) preequilibrated with buffer A (25 mL). The column was washed with buffer B (50 mL, 50 mM NaH_2PO_4, 300 mM NaCl, 20 mM imidazole), and the protein was eluted with buffer C (10 mL, 50 mM NaH_2PO_4, 300 mM NaCl, 250 mM imidazole). Typical yield was 10−15 mg of protein or 100−150 mg/L of culture broth. Protein concentrations were measured by absorbance at 280 nm using the calculated extinction coefficient of PFE (35410 M^{-1} cm^{-1}) (*15*).

Detection of Acyl-Enzyme Intermediate by ESI Mass Spectrometry. A solution of ε-caprolactone substrate (100 mM in 2 mM citrate buffer, pH 5.5, 10 μL) was mixed with enzyme PFE-L29P (9 mg/mL, 10 μL) at 4 °C. Water−acetonitrile (50:50 with 0.1% formic acid, 20 μL) was added immediately; the sample was loaded in a 50 μL syringe and injected into a 10 μL loop. Addition of formic acid did not significantly alter the pH (pH paper). The reaction likely occurred in the syringe as the solution warmed to room temperature, 23 °C. Electrospray ionization (ESI) mass spectrometry was analyzed using Qstar Pulsar (Applied Biosystems, Foster City, CA) using a Turbo Ionspray as the nebulizer. Bayesian protein reconstruction was used to deconvolute the multiply charged spectra (see Figure S-1 in the Supporting Information) to yield the spectra shown in Figure 3.

Steady-State Kinetic Constants for Perhydrolysis of Acetic Acid. Kinetic constants for perhydrolysis were determined using the monochlorodimedone (MCD) assay (*16*), where the amount of enzyme added was adjusted to give a linear dependence of the reaction rate to enzyme concentration at 23 °C. All reactions contained MCD (0.047 mM) and sodium bromide (149 mM). The concentrations of hydrogen peroxide and acetate were varied to give evenly spaced data points on both sides of apparent K_m, solubility limited acetate concentrations to < 1.5 M, and enzyme stability limited hydrogen peroxide concentrations to < 150 mM. When varying the concentration of hydrogen peroxide, the concentration of acetate was 1.00 M; when varying the concentration of acetate, the concentration of hydrogen peroxide was 9.9 mM. Some of the kinetic constants in this paper differ slightly from those in the preliminary communication (*13*). The current values are believed to be accurate, but we do not clearly understand why they differ.

pH Activity Profiles for Perhydrolysis of Acetic Acid. The initial rate of PFE-catalyzed perhydrolysis was measured

with a near saturating amount of acetate (1.00 M) and hydrogen peroxide (9.9 mM) while varying the pH with either NaOH (1.00 N) or HCl (1.00 N) at 23 °C. Acetic acid served as both a substrate and buffer, which was adjusted to the desired pH immediately before the reaction was initiated with enzyme. The amount of enzyme used varied from 0.050 to 5 μg depending on the mutant being tested and the pH. The data were fit to the equation for a doubly ionizing system using the Solver function of Microsoft Excel. The equation used is rate = $C[H^+]K_1/(K_1K_2 + [H^+]K_1 + [H^+]^2)$, where K_1 is the first acid ionization constant and K_2 is the second acid ionization constant (*17*). C is an arbitrary constant. This equation assumes that only the singly ionized form contributes to catalysis.

Steady-State Kinetic Constants for Hydrolysis of Peracetic Acid. Initial rates of peracetic acid hydrolysis were measured using a pHstat at pH 5.5 at 23 °C. A typical assay (50 mL) contained peracetic acid (0.03−1 mM) and enzyme (typically 3.2 μg for L29P PFE and 11.6 μg for wild-type PFE) constantly mixed with a magnetic stirring bar while monitoring the amount of NaOH (0.01 N) added. The pHstat could not detect hydrolysis below 0.03 mM peracetic acid. To account for the incomplete ionization of acetic acid at pH 5.5, the k_{cat}^{app} value was increased according to the following equation, which was derived from the Hendersen−Hasselbach equation:

$$\text{rate}_{\text{true}} = \text{rate}_{\text{obsd}}/[10^{\text{pH}-\text{p}K_a}/(10^{\text{pH}-\text{p}K_a}+1)] = \text{rate}_{\text{obsd}}/0.834$$

Steady-State Kinetics of L29P PFE-Catalyzed Hydrolysis of ε-Caprolactone. Hydrolysis of ε-caprolactone was monitored colorimetrically by measuring acid release using *p*-nitrophenol as the pH indicator (*18*). Reactions were run at room temperature by mixing ε-caprolactone stock solution (19 μL in acetonitrile), 171 μL of buffer (4.0 mM *N*,*N*-bis(2-hydroxyethyl)-2-aminoethanesulfonic acid (BES), pH 7.2, 0.50 mM *p*-nitrophenol, 0.33 mM Triton X-100), and 10 μL of enzyme (in 4 mM BES buffer, pH 7.2). The hydrolysis rates were determined from the decrease in absorbance at 404 nm as a function of time. The extinction coefficient for *p*-nitrophenoxide is 16600 M^{-1} cm^{-1}. The ratio of [BES]:[*p*-nitrophenol] is 8.47:1 so the protonation of one *p*-nitrophenol molecule indicated the release of 9.47 protons. Each reaction was run in triplicate, and the average values were used for calculations. The formula for the rate calculation is

$$v\ (\text{mmol s}^{-1}) = \frac{1000(\Delta A/\Delta\text{min})}{16600\ \text{M cm}^{-1} \times 0.58\ \text{cm}} \times 9.47 \times 0.0002\ \text{L}$$

Steady-State Kinetic Constants for Hydrolysis of Methyl and Ethyl Acetate. Initial rates were measured using a pH indicator assay which monitors the decrease in absorption of *p*-nitrophenoxide upon protonation to the phenol (pNP) (ε_{404} = 16.6×10^3 M^{-1} cm^{-1}) at pH = 7.2 (*18*) at 23 °C. To stabilize the pH, the assay mixture contained a small amount of buffer (5 mM *N*,*N*-bis(2-hydroxyethyl)-2-aminoethanesulfonic acid (BES), so the initial rates were adjusted to include the protons that were buffered by BES: $v_{true} = v_{obsd}$(1 + 5 mM BES)/(0.81 mM pNP). A typical reaction mixture contained 50−500 mM methyl or ethyl acetate with 0.81 mM pNP, 5 mM BES, and 0.050−5 μg of enzyme.

Crystallization, Data Collection, and Structure Determination of L29P PFE. Initial crystallization screens were performed using the hanging-drop vapor-diffusion method in a 24-well plate. The precipitant solutions ranged in pH from 5.0 to 7.5 and contained between 1 and 2 M $(NH_4)_2SO_4$ and 0−2% polyethylene glycol. Drops contained 3 μL of protein solution (10 mg/mL) and 5 μL of precipitant solution. The best crystallization conditions were 1.7 M $(NH_4)_2SO_4$ and 0.1 M $NaKH_2PO_4$, pH 7.5, which are similar to the best ones for wild-type PFE (*19*). Crystals were flash-frozen to 93 K after brief immersion in a cryoprotectant solution consisting of precipitant solution with glycerol (25% v/v) added. Data for L29P PFE were collected at beamline X29 at the National Synchrotron Light Source, Brookhaven National Laboratory (Upton, NY) using an ADSC (San Diego, CA) Quantum-315 CCD detector. Data were reduced using d*TREK (*20*). Crystals of the L29P PFE were isomorphous with crystals from wild-type PFE (PDB ID 1VA4). Models of the mutant protein were generated from wild-type PFE using the software O (*21*). Refinements were performed using Refmac version 5 of the CCP4 Suite of crystallographic programs (1994) (*22*), summarized in Table 2. Rigid body refinements allowing each of the six polypeptide chains in the asymmetric unit to move independently were followed by restrained maximum likelihood refinement. Medium or loose NCS restraints were used throughout the refinement. Water molecules were placed using ARP/WARP (*23*). Final fitting of the models was done in O using SigmaA weighted $2F_o - F_c$ maps (*24*) The structures were validated using PROCHECK (*25*). The L29P PFE protein crystallized as a dimer of trimers and had no significant deviation from the main-chain conformation of the

Table 2: Data Collection and Refinement Statistics for L29P PFE and L29P PFE with Acetate

	L29P PFE (3hea)	L29P PFE/acetate (3hi4)
data collection		
space group	$P3_2$	$P3_2$
unit cell parameters		
$a = b$ (Å)	145.59	145.49
c (Å)	128.20	129.99
$\alpha = \beta$ (deg)	90	90
γ (deg)	120	120
no. of reflections		
observed	604510	228713
unique	231042	138751
R_{sym} (%)		
overall	5.6	7.9
highest shell	31.3 (1.99−1.9 Å)	26.5 (2.29−2.25 Å)
completeness (%)		
overall	96.5 (93.5)	99.6 (98.8)
$I/\sigma(I)$ overall	10.5 (3.0)	12.3 (2.15)
refinement		
resolution range (Å)	48.11−1.90	39.97−2.25
R_{work} (highest shell) (%)	19.0 (28.9)	16.6 (26.5)
R_{free} (highest shell) (%)	21.2 (30.8)	20.3 (30.7)
rmsd from ideality		
bond lengths (Å)	0.006	0.03
bond angles (deg)	0.930	1.97
Ramachandran analysis		
most favored (%)	91.3	97.03
allowed (%)	8.3	2.57
generously allowed (%)	0.4	0.4
disallowed (%)	0.0	
final model no. of atoms		
protein	12924	12802
solvent (H_2O and glycerol)	1271	1192
mean B factor (Å^2)		
main chain	22.25	27.96
side chain	23.21	29.59
solvent	31.68	35.69

wild-type protein, except at the oxyanion loop close to the active site. Each monomer of the asymmetric unit contained a continuous density from the S94 side chain, which could not be unambiguously identified as glycerol, water, or buffer. Our best guess was a tetrahedral intermediate for hydrolysis of ethyl acetate, which is a poor substrate for L29P PFE. Ethyl acetate was not present in the crystallization buffer, so this assignment is speculative, and this adduct is not shown in Figure 2. The refined structure of L29P PFE was deposited in RCSB Protein Data Bank (www.rcsb.org), PDB ID 3hea. X-ray structures of wild type and L29P and of CPO-F with L29P PFE were superimposed using the software Chimera (*26*) or Pymol (*27*).

Crystallization, Data Collection, and Structure Determination of L29P PFE/Acetate. Crystals of L29P were immersed in mother liquor solution containing glycerol (25% v/v) for 1 min and then transferred to a drop (10 μL) containing mother liquor solution with glycerol (25% v/v) and 250 mM acetate at pH 5.0 ("soak solution") for 30 s. The crystal was then transferred two more times into fresh soak solutions for a total soak time of 90 s; then the soaked crystals were quickly flash-frozen to 77 K. Data for L29P PFE were collected at The Kahlert Structural Biology Laboratory of the University of Minnesota using Rigaku MSC Micromax 007 X-ray generators with R-axis IV++ image plates. Data were collected using Crystal Clear. Crystals of the L29P PFE were isomorphous with crystals from wild-type PFE (PDB ID 1VA4). The structure was solved by molecular replacement using MOLREP (*28*) in the CCP4 Suite of crystallographic programs (1994). Models of the mutant protein were generated from wild-type PFE using the software Coot (*29*). Refinements were performed using Refmac version 5 of the CCP4 Suite of crystallographic programs (1994) (*22*), summarized in Table 2. Rigid body refinements allowing each of the six polypeptide chains in the asymmetric unit to move independently were followed by restrained maximum likelihood refinement. Medium or loose NCS restraints were used throughout the refinement. Water molecules were placed using ARP/WARP (*23*) from CCP4 and Find Waters/Solvate in Coot. Final fitting of the models was done in Coot using SigmaA weighted $2F_o - F_c$ maps. The structures were validated using PROCHECK (*25*) and Molprobity (*30*). The L29P PFE soaked with acetate shows a single acetate molecule in the active site. In addition, the *cis*-Pro 29 bond adopts the same orientation as in L29P PFE. The structure has been deposited in the RSCB Protein Data Bank (www.rcsb.org) as structure 3hi4.

Molecular Modeling. Modeling and visualization of wild-type and L29P PFE were done using Maestro (Schrödinger, Portland, OR) at the Minnesota Supercomputing Institute (University of Minnesota). Macromodel using OPLS-2005 (*31*) force field and the conjugate gradient algorithm were used to optimize the geometry of all structures until the root-mean-square deviation was ≤0.05 Å. First, hydrogens were added to the backbone and side chains of a single subunit of either L29P PFE or wild-type PFE. The ε nitrogen of the catalytic histidine, His251, was protonated for modeling of the first tetrahedral intermediate. The geometry of the hydrogens attached to the subunit were optimized to minimize the energy of the whole structure. Next, the first tetrahedral intermediate for either methyl acetate, ethyl acetate, or ε-caprolactone was built on the catalytic serine 94, and its geometry was optimized. Finally, the geometry of the entire structure and intermediate was optimized.

Docking ε-Caprolactone into PFE Using GLIDE. Structures of PFE wild type and L29P PFE were prepared using Protein Wizard Prep in Maestro, which added missing hydrogen atoms and optimized bond angles and distances. Separately, the structure of ε-caprolactone was prepared and optimized using OPLS-2005. The ε-caprolactone was positioned in the active site such that the carbonyl oxygen of the substrate was within hydrogen bond distance (2.5−3.0 Å) of αN of M95 and W28 while the carbonyl carbon is positioned ~1.5 Å from S94 Oγ. The outer boundary box was set to 20 Å, which covers > 95% of the protein, while the inner boundary box (ε-caprolactone) was set to a maximum of 14 × 14 × 14 Å. A standard precision model was used to generate all poses.

RESULTS

Previously, we used computer modeling to predict the structure of the L29P PFE variant. The predicted structure indicated a change from a trans orientation along the peptide bond for the wild-type protein (L29) to a cis conformation in the variant due to the introduction of proline at position 29. This change in the peptide bond orientation moved the protein main chain and in particular the carbonyl oxygen of W28 closer to the active site. Now we solved an X-ray crystal structure that confirms the predicted structure. In addition, we solved a crystal structure of L29P PFE with substrate acetate bound to the active site to gain further insight into the mechanism.

Crystal Structures of L29P PFE. Two crystal structures of L29P PFE variants both show a similar orientation of the proline at position 29 (Figure 2). L29P PFE (PDB ID 3hea) shows the apoenzyme, while L29P PFE/acetate (PDB ID 3hi4) was soaked in acetate and contains a single acetate in the active site. Both forms of L29P crystallized under similar conditions as wild type and were refined using the $P3_2$ space group with six near-identical monomers comprising the dimer of trimers. Molecular replacement with the wild-type structure solved both structures and allowed the refinement of the model to a final resolution of 1.90 Å for L29P and 2.25 Å for L29P/acetate. Table 2 in the Materials and Methods section summarizes the statistics for both data sets and the final refinement. The L29P structure contained additional electron density in the active site which could not be identified as glycerol, buffer, or water.

The L29P PFE structure superimposed onto the wild-type structure (PDB ID 1VA4 (*19*)) with an $rmsd_{all\text{-}atom}$ of 0.16 Å for the best monomer fit (chain A of L29P PFE and chain A of WT PFE) (Figure 2a). The largest difference with an $rmsd_{backbone}$ of 0.64 Å is in the oxyanion-stabilizing loop containing residues 27−30 between β-strand 1 and α-helix 1. In contrast to the wild-type W28−L29 trans peptide bond, the mutant W28−P29 peptide bond adopts a cis conformation (Figure 2a). This conformational change directs the carbonyl oxygen of the W28 peptide bond toward the catalytic serine residue (W28−C=O···S94−Oγ distances: 6.3 and 5.2 Å for wild-type PFE and L29P PFE, respectively). Another, less significant, change was a shift in the indole ring of the W28 side chain. The 7 position of the indole ring is shifted by 1.3 Å as compared to the wild-type enzyme. The structure of L29P PFE/acetate shows the same cis conformation of the W28−P29 peptide bond, and the protein conformation is otherwise also similar to L29P PFE.

These changes in the active site make L29P PFE similar to a naturally occurring perhydrolase (CPO-F, the perhydrolase from *P. fluorescens*). Superposition of the X-ray crystal structure of L29P PFE/acetate with that of CPO-F/propionate (PDB ID

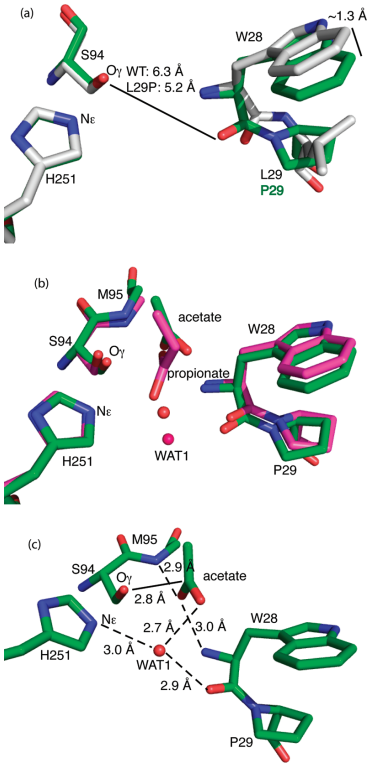

FIGURE 2: Active site X-ray crystal structures of L29P PFE and L29P PFE/acetate. (a) Superposition of L29P PFE (green CPK colors, PDB ID 3hea) and wild-type PFE (white CPK colors, PDB ID 1va4) shows similar conformations of the catalytic triad residues. (Only H251 and S94 are shown.) The leucine 29 to proline substitution changes the W28 to L29 peptide bond conformation from trans to cis, thereby shifting the main chain carbonyl group of W28 closer to the active site serine by 1.1 Å. A second difference is a shift in the indole ring of the W28 residue by ~1.3 Å for the 7 position. (b) Superposition of the structures of L29P PFE/acetate (green CPK colors, PDB ID 3hi4) and perhydrolase CPO-F soaked with propionate (magenta CPK colors, PDB ID 1a8s). Both show similar orientations of the W28 carbonyl group and indole ring, but the acetate, propanoate, and active site water molecules (WAT1, orange for L29P, magenta for CPO-F) have different orientations. (c) L29P PFE/acetate (PDB ID 3hi4) shows the substrate acetate in an orientation consistent with formation of an acetyl-enzyme intermediate. The acetate carbonyl oxygen accepts hydrogen bonds from the two amide N−H's that form the oxyanion hole (M95, W28). The carbonyl carbon of acetate is 2.8 Å from S94−Oγ in this monomer and ranges from 2.8 to 3.1 Å in the six monomers in the asymmetric unit.

1A8S (*9*)) shows a good overall fit of protein ($rmsd_{all\text{-}atom}$ of 0.68 Å when aligning backbone atoms of chain A of L29P PFE with CPO-F) and nearly identical conformations near the active site, including the W28−*cis*-P29 peptide bond and the position of the tryptophan side chain (Figure 2b). One exception to the similarity is that the orientation of the propanoate molecule in CPO-F differs significantly from the orientation of acetate in L29P PFE; see below.

The active site of L29P PFE soaked in acetate (pH 5) contains an acetate and a water molecule in each monomer of the asymmetric unit (Figure 2c). In each monomer, the C═O of acetate accepts hydrogen bonds from the two N−H's in the oxyanion hole. The distances from the oxygen to the αN of M95 and W28 range from 2.8 to 3.1 Å. The methyl group points toward the acyl pocket while the other carboxylic oxygen points toward the alcohol pocket. Since the crystal soak solution was at a pH of 5, the ionization form of acetic acid may be acetate or acetic acid. (The pK_a of 4.8 for acetic acid predicts 61% is in the acetate form and 39% is acetic acid.) The substrate for the reaction is likely acetic acid. The distance between the C═O of acetate and S94−Oγ ranges between 2.8 and 3.1 Å. The single water molecule, "WAT1" observed in the alcohol pocket of PFE makes a hydrogen bond between C═O of W28 (2.9 Å) and C−O (2.7 Å) of acetate. The orientation of the acetate is consistent with the formation of an acetyl-enzyme intermediate. The next mechanistic step could be attack of the active site serine on the acetate carbonyl carbon.

The previous X-ray crystal structure of propanoate bound to CPO-F had a different orientation, which was not consistent with the next step being formation of a propanoyl-enzyme intermediate. These crystals of CPO-F were soaked in propanoate at pH 6.6 (*9*), where propanoate, not propanoic acid, predominates. The pK_a of 4.9 for propanoic acid predicts that 98% is in the propanoate form. The carboxylate anion of propanoate is hydrogen bonded to Nε of H251, which prevents the histidine from acting as a base to deprotonate Oγ of the serine. The catalytically nonproductive orientation of the propanoate is consistent with very low catalytic activity at pH 6.6.

Mass Spectrometry of the Acyl-Enzyme Intermediate. Electrospray ionization mass spectrometry showed an acyl-enzyme during the PFE L29P-catalyzed hydrolysis of ε-caprolactone at pH ~5.5 (Figure 3). The enzyme appeared at the expected mass of 30912 Da, and in the presence of 25 mM ε-caprolactone, an additional peak appeared at 31026 Da. The 114 Da increase in mass is consistent with the formation of an acyl-enzyme intermediate. The observation of the acyl-enzyme intermediate with L29P PFE is consistent with a covalent mechanism and, thus, strongly supports the ping-pong bi-bi mechanism. Further, the X-ray structure of acetate bound to L29P PFE supports the ping-pong bi-bi mechanism. Other serine hydrolases that follow a ping-pong bi-bi mechanism, e.g, porcine pancreatic elastase (*32*, *33*), also show an acyl-enzyme intermediate at low pH.

Attempts to detect the acetyl-enzyme intermediate in L29P PFE in 0.5 M acetate at pH 5.5 were inconclusive. The high concentration of acetate in this solution yielded gave mono-, di-, and trisodium adducts of the enzyme. The disodium adduct (expected at M + 44 Da) and any acetyl-enzyme (expected at M + 42 Da) overlap could not be distinguished. The formation of an ester from an acid is thermodynamically uphill, so the amount of acetyl-enzyme formed from acetate is expected to be small. On the other hand, converting one ester into another can be thermodynamically neutral, so ε-caprolactone should form more acyl-enzyme intermediate. Is it possible to further increase the rate of L29P PFE-catalyzed perhydrolysis? Below we measured the kinetics for the reverse reaction and found that it is near the diffusion limit. Since the reverse reaction cannot be much faster, then the forward rate (k_{cat}/K_m) also cannot be much faster either. The ratio of the forward and reverse reactions is fixed by the equilibrium constant.

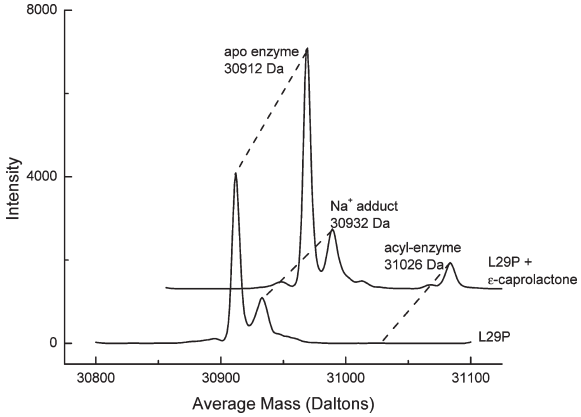

FIGURE 3: Deconvoluted electrospray-ionization spectra show an acyl-enzyme intermediate during the PFE-L29P-catalyzed hydrolysis of ε-caprolactone in citrate/formate buffer, pH ~5.5. Without substrate shows the major peak at 30912 Da, which is consistent with the calculated value of 30911.9 Da using ProtParam (*15*). Addition of 25 mM ε-caprolactone shows an additional peak at 31026 Da, which is 114 Da higher that the free enzyme. This peak is assigned as the covalent acyl-enzyme intermediate. Peaks at lower mass are present in both spectra and are not identified.

Table 3: Steady-State Kinetic Constants for Hydrolysis of Peracetic Acid Catalyzed by Wild-Type PFE and L29P PFE[a]

enzyme	k_{cat} (s^{-1})	K_m (mM)	k_{cat}/K_m (s^{-1} M^{-1})
wild-type PFE	100 ± 3	0.041 ± 0.005	2×10^6
L29P PFE	139 ± 2	< 0.003[b]	$> 5 \times 10^7$

[a]Initial rates were measured at 23 °C by pHstat, which controlled the addition of 0.0100 N NaOH to keep the pH at 5.5. [b]The K_m value for peracetic acid with L29P PFE could not be measured accurately because the pHstat method could not detect hydrolysis of peracetic acid below 0.01 mM. The rate of hydrolysis decreased only when the concentration of peracetic acid was below 0.03 mM. From this value we estimated the K_m to be < 0.003 mM.

Hydrolysis of Peracetic Acid. Perhydrolases catalyze the hydrolysis of peracetic acid to acetic acid and hydrogen peroxide, the reverse of the reaction in Figure 1 above. We monitored the rate of hydrolysis with a pHstat, which controls the addition of base. Peracetic acid (pK_a 8.20 (*34*)) is >99% protonated at pH 5.5, while 85% of the product acetic acid (pK_a 4.75) dissociates to form acetate. Thus, hydrolysis of 1 mol of peracetic acid at pH 5.5 releases 0.85 mol of protons. The observed rates were corrected for the incomplete ionization of acetic acid at pH 5.5 to give the true rates listed in Table 3.

Both wild-type PFE and L29P PFE were excellent catalysts for the hydrolysis of peracetic acid. The k_{cat} values were similar (100 and 139 s^{-1}, respectively), but the K_m for peracetic acid was >14-fold lower for L29P PFE than for the wild-type enzyme (<0.003 versus 0.041 mM). The value of K_m for L29P PFE is only an upper limit because the pHstat method could detect hydrolysis of peracetic acid only above 0.01 mM. The rate of hydrolysis decreased slightly below 0.03 mM peracetic acid, so we estimated that K_m is <0.003 mM. Due to this lower K_m for peracetic acid, the specificity constant is >20-fold higher for L29P PFE than for wild-type PFE. We expect that the true specificity constant is ~100-fold higher for L29P PFE than for wild-type PFE because the specificity constant for the forward reaction is ~100-fold higher for L29P PFE than for wild-type PFE. The Haldane relationship (*35*) requires that the ratio of forward and reverse reactions to equal the equilibrium constant. The lower K_m for peracetic acid for L29P PFE is consistent with the hypothesis that this amino acid substitution stabilizes the peroxy intermediate. Peracetic acid is structurally closer to the peroxy intermediate than either acetic acid or hydrogen peroxide, and its binding to the active site may be favored by the shifted carbonyl group of W28.

This specificity constant for the L29P PFE-catalyzed hydrolysis of ~10^8 s^{-1} M^{-1} approaches the value for bimolecular rate constants of a diffusion-controlled enzyme-catalyzed reaction: 4×10^8 s^{-1} M^{-1} for triose phosphate isomerase (*36*). This high specificity constant indicates that L29P PFE is a highly efficient catalyst for the reaction in Figure 1 and catalyzes hydrolysis of peracetic acid at close to the diffusion limit.

Mutants with Higher k_{cat} for Perhydrolysis. Previously, we compared the amino acid sequences of hydrolases and perhydrolases to identify residues responsible for perhydrolase versus esterase activities in α/β hydrolases. This comparison and subsequent experimentation identified the single amino acid substitution variant L29P PFE (*13*). In this paper, we attempted to further improve L29P PFE by aligning its amino acid sequence with not all perhydrolases, but with the perhydrolases that have the highest specific activity: BPO-A1, a perhydrolase from *Streptomyces aureofaciens* ATCC 10762 (previously called a nonheme bromoperoxidase), CPO-T, a perhydrolase from *S. aureofaciens* Tü24 (previously called a nonheme chloroperoxidase), and CPO-L, a perhydrolase from *Streptomyces lividans* TK64 (previously called a nonheme chloroperoxidase) (*37*). Seventeen residues were conserved in BPO-A1 and CPO-L but not with L29P PFE. We chose H57 and H93 for mutagenesis because they were closest to the active site. We also enlarged the acyl binding pocket of L29P PFE by replacing F125 with Ala. Starting with L29P PFE, additional site-directed mutagenesis yielded the three double mutants: L29P/F93H PFE, L29P/F125A PFE, and L29P/F57H PFE. (See Methods and Materials for details.)

Table 4: Apparent Steady-State Kinetic Constants for Perhydrolysis of Acetic Acid Catalyzed by Wild-Type PFE, L29P PFE, and Double Mutants[a]

enzyme	varied substrate	k_{cat} (s^{-1})	K_m^{app} (mM)	k_{cat}/K_m^{app} (s^{-1} M^{-1})
wild-type PFE	acetic acid[b]	0.12 ± 0.02	500 ± 100	0.2
	hydrogen peroxide	0.094 ± 0.002	3.3 ± 0.2	28
L29P PFE	acetic acid	5.1 ± 0.4	210 ± 60	20
	hydrogen peroxide	4.4 ± 0.2	1.8 ± 0.2	2000
L29P/F93H PFE	acetic acid	11 ± 1	610 ± 120	20
	hydrogen peroxide	9 ± 1	2.7 ± 0.6	3000
L29P/F125A PFE	acetic acid	10 ± 1	340 ± 80	30
	hydrogen peroxide	13 ± 1	4.8 ± 0.7	3000
L29P/F57H PFE	acetic acid	3.3 ± 0.2	380 ± 40	10
	hydrogen peroxide	6.8 ± 0.2	3.3 ± 0.4	1000

[a]Kinetic constants were obtained at 23 °C by varying each substrate independently. The fixed acetic acid concentration was 1.4 M except for L29P PFE where it was 500 mM. The fixed hydrogen peroxide concentration was 9.9 mM, which saturates the active site and therefore yields higher values of k_{cat}. [b]Acetic acid is the likely substrate for the enzyme, so we refer to the substrate as acetic acid even though at pH 5.5 approximately 85 mol % is in the acetate form. The concentrations refer to the sum of both acetic acid and acetate.

Michaelis−Menten kinetic constants for the ping-pong bi-bi reaction were measured by keeping the acetate concentration constant and varying hydrogen peroxide and then by keeping hydrogen peroxide constant and varying acetate. This approach yields apparent kinetic constants for the varied substrate. The Michaelis constants for acetate and hydrogen peroxide are expected to differ, but the k_{cat} values should be the same when the concentration of the constant substrate is high enough to saturate the enzyme.

Initial rates were monitored spectrophotometrically using an indirect assay. Enzyme-generated peracetic acid oxidized bromide ion to bromonium, which reacted with monochlorodimedone to form bromochlorodimedone. The decrease in monochlorodimedone concentration causes a decrease in absorbance at 290 nm (*16*). Reaction rates were measured at five or more different substrate concentrations. The data were fit to the Michaelis−Menten equation using a nonlinear regression and gave a close fit ($R^2 > 0.97$).

The value of k_{cat} improved for L29P PFE ~44-fold for perhydrolysis of acetic acid as compared to wild-type PFE (42-fold higher with acetic acid as the varied substrate, 0.12−5.1 s^{-1}, and 47-fold higher with hydrogen peroxide as the varied substrate, 0.094−4.4 s^{-1}) (Table 4). The value of k_{cat} would be the same in both cases if the enzyme were completely saturated with the constant substrate. The K_m value for acetic acid was high (210 mM) so the acetate concentration of 500 mM did not completely saturate the enzyme. For this reason the value of k_{cat} measured when acetic acid is the constant substrate was slightly lower than when hydrogen peroxide was the constant substrate. The K_m values decreased for L29P PFE as compared to wild-type PFE, but only approximately 2-fold. The K_m for hydrogen peroxide decreased 1.8-fold (3.3−1.8 mM), and the K_m for acetic acid decreased 2.4-fold (500−210 mM). The combined improvements in both k_{cat} and K_m gave a specificity constant (k_{cat}/K_m) improvement 70−100-fold (Table 4).

Two of the double mutants, L29P/F93H PFE and L29P/F125A PFE, showed an additional 2-fold improvement in k_{cat}, but the K_m values increased by a similar amount, so the specificity constants did not change as compared to the single mutant L29P PFE. The k_{cat} values were 11 and 9 s^{-1} for L29P/F93H PFE and 10 and 13 s^{-1} for L29P/F125A PFE, both approximately a 2-fold increase over 5.1 and 4.4 s^{-1} for L29P PFE using acetic acid or hydrogen peroxide as the varied substrate, respectively. The K_m values increased approximately 2-fold. The molecular basis of the improvements in k_{cat} are not clear. Although the F93H substitution is next to the active site serine, molecular modeling of L29P/F93H PFE shows that the Nε of H93 is too far away to hydrogen bond to either H251 (4.4 Å) or S94 (4.9 Å).

Table 5: Steady-State Kinetic Constants for Hydrolysis of Acetate Esters and ε-Caprolactone by Wild-Type PFE and L29P PFE[a]

enzyme	substrate	k_{cat} (s^{-1})	K_m (mM)	k_{cat}/K_m (s^{-1} M^{-1})
wild-type PFE	methyl acetate	25 ± 1	43 ± 3	600
wild-type PFE	ethyl acetate	9 ± 1	33 ± 1	300
wild-type PFE	ε-caprolactone	> 140	> 2000	50[b]
L29P PFE	methyl acetate	7.7 ± 0.2	50 ± 5	200
L29P PFE	ethyl acetate	0.67 ± 0.05	160 ± 30	4
L29P PFE	ε-caprolactone	11 ± 1	39 ± 1	280

[a]Rates of hydrolysis were measured at 23 °C using the pH indicator *p*-nitrophenol at pH 7.2 in 5.0 mM BES buffer. [b]Determined from the initial slope of rate versus substrate concentration, $R^2 = 0.996$.

The third double mutant, L29P/F57H PFE, showed an approximately 1.5-fold decrease in k_{cat} and a similar increase in K_m, so the overall specificity constant decreased approximately 2-fold as compared to L29P PFE: 20 and 2000 s^{-1} M^{-1} as compared to 10 and 1000 s^{-1} M^{-1} for L29P PFE using acetic acid or hydrogen peroxide as the varied substrate, respectively. These results suggest that the histidine at position 57 in perhydrolases does not contribute to catalysis. The pH−rate profiles of these enzymes are in Figure S-2 of the Supporting Information.

Above, we examined the increase in perhydrolysis activity upon making the L29P substitution PFE. This increase is accompanied by a decrease in esterase activity. Below, we we examine the esterase activity of this variant and suggest that steric hindrance created by the L29P substitution causes the decrease. In contrast, the rate of hydrolysis of lactones, which have a different shape from esters, increases in L29P PFE.

Hydrolysis of Esters. Wild-type PFE catalyzes hydrolysis of a wide range of esters (*38*), but L29P PFE catalyzes hydrolysis of only methyl esters efficiently (Table 5). For methyl acetate, both wild-type PFE and L29P PFE show similar kinetic constants. For ethyl acetate, the kinetic constants for wild-type PFE remain similar, but the k_{cat} for L29P PFE decreased 11-fold and the specificity constant decreased 50-fold as compared to methyl acetate. We previously reported similar results for propanoate esters and *p*-nitrophenyl acetate, but without k_{cat} and K_m data (*13*). Both wild-type PFE and L29P PFE catalyze hydrolysis of methyl propanoate at similar rates, but L29P PFE is

5-fold slower that wild-type PFE for propyl propanoate. L29P PFE catalyzes hydrolysis of *p*-nitrophenyl acetate 100-fold slower than wild-type PFE. Poor water solubility of these substrates prevented measurement of the kinetic constants. Thus, esters with an alcohol group larger than methyl appear to be poor substrates for L29P PFE, but the size of the alcohol group has little effect for wild-type PFE.

Molecular Modeling of Ester Hydrolysis. Molecular modeling suggests that as the carbonyl group of W28 moves closer to the catalytic serine in L29P PFE, it creates steric hindrance for alcohol moieties larger than methyl. We modeled the tetrahedral intermediate that forms upon attack of the active site serine on the ester (Figure 4). Key interactions include two hydrogen bonds to the oxyanion oxygen from the backbone amides of M95 and W28 and two hydrogen bonds formed from Nε of H251 to Oγ of S94 and to the alcohol oxygen (Table 6). For wild-type PFE, hydrogen bond distances ranged from 2.7 to 2.9 Å for both methyl acetate and ethyl acetate, which indicate a strong hydrogen bonds. For L29P PFE, all four hydrogen bond distances were 2.8 Å for methyl acetate, but for ethyl acetate the distance between Nε of H251 and the alcohol group was 3.5 Å, which is too far away to make a hydrogen bond. This missing hydrogen bond likely accounts for the 50-fold lower reaction rate.

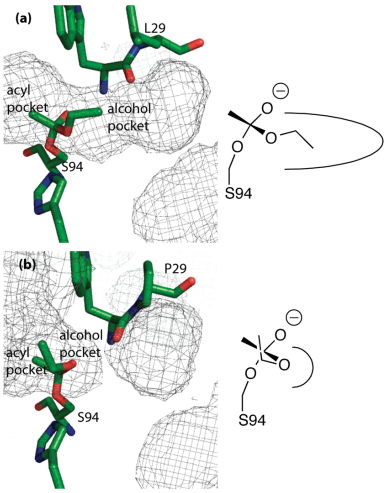

FIGURE 4: Mesh showing water-accessible regions in the active sites of wild-type PFE and L29P with the modeled tetrahedral intermediate for the acetylation of active site serine by ethyl acetate (T_d1). (a) The alcohol pocket accommodates the ethyl group of the tetrahedral intermediate and could also accept a longer alcohol, but not larger acyl groups. The acyl pocket of wild-type PFE is small while the alcohol pocket is larger, as shown on the diagram on the right side. (b) The leucine to proline substitution shifts the main chain W28 carbonyl which pinches off the alcohol pocket. The ethyl group is forced to adopt an unfavorable conformation in the enlarged acyl pocket caused by a shift in the indole ring of W28. A diagram on the right shows that the acyl pocket of L29P is larger than the alcohol pocket. The mesh shows regions accessible to a sphere with a radius of 1.4 Å, which models a water molecule. Water molecules were removed before modeling the mesh regions.

Consistent with these modeling results, the water-accessible regions in the active site show a smaller alcohol-binding region in L29P PFE as compared to wild-type PFE. Wild-type PFE shows a single solvent-accessible region in the active site that fits the tetrahedral intermediate for hydrolysis of ethyl acetate (Figure 4). In contrast, the shift of the W28 C=O moves closer to the active site in L29P PFE and separates the alcohol pocket into two regions. For this smaller pocket to fit a larger alcohol group, the alcohol moiety must twist into a different conformation, thereby breaking a key hydrogen bond. The smaller alcohol-binding region of L29P PFE supports observation of the 50-fold lower specificity constant for ethyl acetate in L29P PFE as compared to wild-type PFE. In addition, L29P causes a shift in the indole ring of W28 that enlarges the acyl pocket.

Hydrolysis of ε-Caprolactone. Several lactonases and lactamases show perhydrolysis activity (*39*, *40*). For this reason, we also measured the ability of PFE and L29P PFE to catalyze the hydrolysis of ε-caprolactone. Steady-state kinetics shows that L29P PFE is an approximately 5-fold better catalyst than wild-type PFE for hydrolysis of ε-caprolactone, due to a higher affinity toward the lactone (Table 5). The kinetic data for L29P PFE fit the Michaelis−Menten equation and yield a K_m of 39 mM and a k_{cat} of 11 s^{-1}, which corresponds to a k_{cat}/K_m of 280 s^{-1} M^{-1}. For wild-type PFE, the rate of hydrolysis increased linearly with increasing ε-caprolactone concentration even at 500 mM (approaching the solubility limit), so we could not fit the data to the Michaelis−Menten equation. The slope of this line was used to estimate the k_{cat}/K_m value of 50 s^{-1} M^{-1}. We estimate that K_m must be >2000 mM (at least four times the highest value tested) and that k_{cat} must be >140 s^{-1} (at least five times the value seen at a substrate concentration of $< k_{cat}/2$). In spite of the higher k_{cat} value for wild-type PFE, L29P PFE would be an approximately 5-fold better catalyst for hydrolysis of ε-caprolactone at the low concentrations expected *in vivo* because it binds ε-caprolactone more tightly. Unlike esters which adopt a trans conformation, lactones adopt a cisoid conformation up to seven-membered rings.

Table 6: Key Hydrogen Bond Distances (Å) in the Modeled First Tetrahedral Intermediate for Hydrolysis of Acetate Esters and ε-Caprolactone by Wild-Type PFE and L29P PFE[a]

enzyme (substrate model)	oxyanion O to M95 Nα	oxyanion O to W28 Nα	His251Nε to S94Oγ	His251Nε to alcohol oxygen
wt PFE (methyl acetate)	2.9	2.7	2.6	2.8
wt PFE (ethyl acetate)	2.9	2.7	2.7	2.7
L29P PFE (methyl acetate)	2.8	2.8	2.8	2.8
L29P PFE (ethyl acetate)	2.7	2.7	2.7	**3.5**

[a]The program suite Maestro was used for visualization and distance measurements. Macromodel using OPLS-2005 force field was used to optimize the geometry of all models using conjugate gradient algorithm to an rmsd of ≤0.05 Å. The distance in bold type is too far to be a hydrogen bond, which indicates a catalytically nonproductive model.

Molecular Modeling of ε-Caprolactone Hydrolysis and Binding. Molecular modeling of the tetrahedral intermediates for hydrolysis of ε-caprolactone yielded hydrogen bond distances of less than 3.0 Å between the Nε of H251 to Oγ of S94 and to the alcohol oxygen for both wild-type PFE and L29P PFE (data not shown). However, the substrate ε-caprolactone bound better to L29P PFE than to wild-type PFE, consistent with the lower K_m of ε-caprolactone with L29P. Docking ε-caprolactone using GLIDE (*41*) found eight different orientations bound to the active site of L29P but only one to wild type. The larger acyl pocket in L29P accommodates the lactone better than does wild-type PFE and can account for the at least 50-fold higher affinity for L29P PFE.

DISCUSSION

Two experiments support the acyl-enzyme mechanism: the detection of the acyl-enzyme intermediate by mass spectrometry and the observation of an acetate complex by X-ray crystallography that is consistent with an enzyme−substrate complex that reacts via an acyl-enzyme. The molecular weight observed for the acyl-enzyme intermediate is also consistent with a noncovalent enzyme-ε-caprolactone complex since the molecular weight is the same as that for the acyl-enzyme intermediate. An example of a noncovalent complex observed by mass spectrometry is phosphoenolpyruvate complexed to 3-deoxy-D-*manno*-octulosonate 8-phosphate (DO8P) synthase (*42*). This enzyme binds phosphoenolpyruvate tightly (K_m = 3.1 μM), which allows the complex to persist during mass spectrometry. In our case, L29P PFE binds ε-caprolactone 10000 times less tightly (K_m = 39 mM), so a noncovalent complex is unlikely. Therefore, the acyl-enzyme intermediate is the most likely assignment. The X-ray crystal structure of the substrate (acetate) complex with PFE favors the acyl-enzyme mechanism because the acetate orientation is consistent with attack of the active site serine at the carbonyl. Importantly, these crystals formed at pH 5.0, near the optimum of 5.5 for perhydrolysis. This structure likely contains the substrate in its reactive form as acetic acid. The pH−activity profiles (see Supporting Information) show that acetic acid not acetate is the reactive form of the substrate. Previous experiments to distinguish the acyl-enzyme mechanism from the noncovalent mechanism for PFE yielded ambiguous results; see discussion in the Supporting Information.

Modeling based on the X-ray structure of L29P PFE and the acyl-enzyme mechanism can explain the observed increase in perhydrolysis (*13*). Molecular modeling of the second tetrahedral intermediate for perhydrolysis using molecular mechanics showed an additional hydrogen bond from hydrogen peroxide to the C═O of W28 of L29P PFE, but the same distance is too far way for wild-type PFE. This hydrogen bond can stabilize the transition state for perhydrolysis and is the molecular basis for the increased perhydrolysis activity. Lee and co-workers (*43*) did additional modeling that agrees with this proposal. They used quantum mechanics to calculate the charges, bond distances, and angles for the second tetrahedral intermediate to create a more accurate model of the second tetrahedral intermediate. Modeling of this tetrahedral intermediate with a molecular mechanics force field showed the same hydrogen bond between hydrogen peroxide and the C═O of W28 of L29P PFE. Further, this hydrogen bond persisted during a molecular dynamics simulation of 5 ns as the conformation of the protein and tetrahedral intermediate changed. The stability of this hydrogen bond supports the notion that it is an important contribution to catalysis. A similar simulation of using wild-type PFE showed no hydrogen bond, even during the molecular dynamic simulation where the C═O of W28 could move closer to the active site. The authors did not model the Michaelis complexes for these reactions, but we hypothesize that this hydrogen bond could also form in the Michaelis complex and account for the increase in k_{cat} by eliminating nonproductive binding of hydrogen peroxide. In wild-type PFE, the hydrogen peroxide binds with a similar affinity but, we hypothesize, in a nonproductive orientation, which hinders catalysis and lowers k_{cat}. Shifting this nonproductive orientation to a productive orientation in L29P PFE increases k_{cat}.

The increase in the specificity constant for reverse reaction, hydrolysis of peracetic acid, is mainly due to decrease in K_m and not an increase in k_{cat} as in perhydrolysis of acetic acid. The substrate is peracetic acid, which is a more complex structure than hydrogen peroxide. It does not bind tightly to wild-type PFE, but adding a hydrogen bond between the carbonyl oxygen of W28 and peracetic acid increases the affinity of the enzyme for this substrate. We hypothesize that nonproductive binding is not significant for this substrate. The new hydrogen bond also accounts for this decrease in K_m.

The high rate of the reverse reaction shows that L29P PFE is a very efficient catalyst near the diffusion limit. For this reason, the specificity constant for the forward reaction cannot be significantly improved. Biocatalysis normally occurs in solutions containing substrate concentrations well above K_m, so k_{cat} is the more important constant. It may be possible to increase k_{cat} at the expense of increasing K_m. Consistent with this expectation, two double mutants, L29P/F125A PFE and L29P/F93H PFE, enhanced the k_{cat} for perhydrolysis of acetic acid 2-fold, but at the cost of increasing K_m as compared to L29P PFE. Bugg and co-workers made a N109H mutation in a C−C hydrolase, which is analogous to the F93H substitution above (*44*). The N109H substitution increased the specific activity of ester aminolysis by hydroxylamine approximately 4-fold. These researchers hypothesized that the substitution may help to orient the hydroxylamine. In our case, the F93H substitution in the L29P PFE increased k_{cat} approximately 2-fold, but the K_m for hydrogen peroxide increased, making it unlikely that this substitution contributes to the binding of hydrogen peroxide. This different explanation for the effects of analogous substitution is consistent with the different proposed mechanism for the two enzymes.

Steric hindrance within the alcohol binding site created by the L29P mutation decreases the esterase activity. The specificity constant for L29P PFE toward hydrolysis of ethyl acetate is 75-fold lower than in the wild-type enzyme. A model of the first tetrahedral intermediate using ethyl acetate shows that the distance between the catalytic H251 and the alcohol group is too far away (3.5 Å) to make a hydrogen bond. In addition, the model reveals a dihedral twist of the alcohol group that resembles the structure of lactones. Consistent with this rationale, the k_{cat}/K_m value for ε-caprolactone increased 5-fold in L29P PFE as compared to wild-type PFE.

One possible biological role for perhydrolases is lactone hydrolysis. L29P PFE, and presumably CPO-F, shows higher lactonase activity than esterases. *P. fluorescens* strains can degrade four-ring polynuclear aromatic hydrocarbons (*45*), which can involve lactone intermediates, so there is a biological role for the lactonase activity. In addition, at least two other lactonases (*39*) and a lactamase (*40*) show perhydrolase activity.

Another biological role of perhydrolases may be to detoxify peracetic acid as suggested previously by Shimizu and co-workers (*46*). Perhydrolases, including L29P PFE, catalyze the hydrolysis of peracetic acid to hydrogen peroxide and acetic acid. Catalase can further detoxify the hydrogen peroxide. The L29P substitution in PFE decreased the K_m for peracetic acid to less than 0.003 mM as compared to wild type of 41 mM. The k_{cat} increased modestly. These kinetic constants would enable the enzyme to detoxify very low concentrations of peracetic acid to protect the cell. Disruption of the perhydrolase gene in a soil bacterium increased its sensitivity to peracetic acid, and conversely, expressing a perhydrolase in *E. coli* increased its resistance to peracetic acid (*46*). The biological role of perhydrolases is unlikely the formation of peracetic acid because the *in vivo* concentrations of acetic acid and hydrogen peroxide are too low to make appreciable amounts of peracid. For example, an *in vivo* concentration of 7 mM acetic acid and 7 mM hydrogen peroxide would yield only ~0.02 μM peracetic acid at pH 7. This value is based on an equilibrium constant of 2 for the perhydrolysis of un-ionized acetic acid and accounts for the predominantly ionized form of acetic acid at pH 7 (*47*). In contrast, Shimizu and co-workers used a 30000-fold higher amount, 600 μM peracetic acid, to inhibit bacterial growth (*46*). A natural source of peracetic acid is the oxidative decarboxylation of pyruvate by thiamin pyrophosphate dependent acetolactate synthases (*48*). This side reaction causes the oxygen sensitivity of some anaerobic organisms, and perhydrolases may reduce this sensitivity. For biocatalysis, however, the synthesis of peracetic acid is a very useful reaction.

These results reported herein also provide insight into mechanisms of divergent evolution of new catalytic activities. The catalytic mechanisms of ester hydrolysis, lactone hydrolysis, and perhydrolysis are similar, so that the wild-type enzyme can catalyze all three of these reactions. The single amino acid substitution L29P dramatically changes the relative efficiency of these reactions by changing the substrate binding. Hydrogen peroxide and lactones bind better; ethyl esters bind worse. Modern divergent enzymes, like the esterase and perhydrolase from *P. fluorescens*, typically differ by tens or even hundreds of amino acid substitutions. Mechanistic analysis suggests that the new catalytic reaction mechanisms require only a few substitutions. The experiments in this paper show how and why a single amino acid substitution dramatically changes catalytic activity.

ACKNOWLEDGMENT

We thank Dr. LeeAnn Higgins and Dr. Bruce Witthuhn at the University of Minnesota Mass Spectrometry Consortium for ESI-MS spectra, Ed Hoeffner at the University of Minnesota Kahlert Structural Biology Laboratory for advice on crystal growth, and the Minnesota Supercomputing Institute for computer modeling facilities and support.

SUPPORTING INFORMATION AVAILABLE

(1) The electrospray ionization mass spectrometry data for detection of the acyl-enzyme intermediate, (2) the pH−rate profile of perhydrolysis catalyzed by mutants and wild-type PFE, and (3) a discussion of previous experiments to distinguish acyl-enzyme versus noncovalent mechanisms for PFE. This material is available free of charge via the Internet at http://pubs.acs.org.

REFERENCES

1. Björkling, F., Frykman, H., Godtfredsen, S. E., and Kirk, O. (1992) Lipase-catalyzed synthesis of peroxycarboxylic acids and lipase-mediated oxidations. *Tetrahedron 48*, 4587–4592.
2. Picard, M., Gross, J., Lübbert, E., Tölzer, S., Krauss, S., van Pée, K.-H., and Berkessel, A. (1997) Metal-free bacterial haloperoxidases as unusual hydrolases: activation of H_2O_2 by the formation of peracetic acid. *Angew. Chem., Int. Ed. Engl. 36*, 1196–1199.
3. Warwel, S., and Klaas, M. R. (1995) Chemoenzymic epoxidation of unsaturated carboxylic acids. *J. Mol. Catal. B: Enzym. 1*, 29–35. Klaas, M. R., and Warwel, S. (1997) Lipase-catalyzed preparation of peroxy acids and their use for epoxidation. *J. Mol. Catal. A: Chem. 117*, 311–319. de Zoete, M. C., van Rantwijk, F., Maat, L., and Sheldon, R. A. (1993) Selective oxidation of penicillin G with hydrogen peroxide and with enzymatically generated peroxyoctanoic acid. *Recl. Trav. Chim. Pays-Bas 112*, 462–463.
4. Hegarty, A. F. (1995) Comprehensive Organic Chemistry, pp 1105−1118, Pearson Higher Education, New York.
5. (a) ten Brink, G. J., Arends, I. W. C. E., and Sheldon, R. A. (2004) The Baeyer-Villiger reaction: new developments toward greener procedures. *Chem. Rev. 104*, 4105–4123. (b) Harrison, C. R., and Hodge, P. (1976) Oxidation of some penicillins and other sulphides by use of a polymer-supported peroxy-acid. *J. Chem. Soc., Perkin Trans. 1 21*, 2252–2254. (c) Drago, R. S., Mateus, A. L. M. L., and Patton, D. (1996) Stoichiometric and catalytic oxidation of organic substrates with *in-situ*-generated peracids. *J. Org. Chem. 61*, 5693–5696. (d) Doumaux, A. R., McKeon, A. R. J. E., and Trecker, D. J. (1969) Metal ion-catalyzed peroxide oxidation of organic substrates. Selective synthesis of imides. *J. Am. Chem. Soc. 91*, 3992–3993. (e) Sugimoto, H., and Sawyer, D. T. (1985) Iron(II)-induced activation of hydroperoxides for the dehydrogenation and monooxygenation of organic substrates in acetonitrile. *J. Am. Chem. Soc. 107*, 5712–5716.
6. Ollis, D. L., Cheah, E., Cygler, M., Dijkstra, B., Frolow, F., Franken, S. M., Harel, M, Remington, S. J., Silman, I., Schrag, J., Sussman, J. L., Verschueren, K. H. G., and Goldman, A. (1992) The α/β hydrolase fold. *Protein Eng. 5*, 197–211.
7. Pelletier, I., and Altenbuchner, J. (1995) A bacterial esterase is homologous with non-heme haloperoxidases and displays brominating activity. *Microbiology 141*, 459–468.
8. Hecht, H. J., Sobek, H., Haag, T., Pfeifer, O., and van Pée, K.-H. (1994) The metal-ion-free oxidoreductase from *Streptomyces aureofaciens* has an α/β hydrolase fold. *Nat. Struct. Biol. 1*, 532–537.
9. Hofmann, B., Tölzer, S., Pelletier, I., Altenbuchner, J., van Pée, K.-H., and Hecht, H. J. (1998) Structural investigation of the cofactor-free chloroperoxidases. *J. Mol. Biol. 279*, 889–900.
10. Kirk, O., and Conrad, L. S. (1999) Metal-free haloperoxidases: fact or artifact? *Angew. Chem., Int. Ed. Engl. 38*, 977–979.
11. Bugg, T. D. H. (2004) Diverse catalytic activities in the α/β-hydrolase family of enzymes: activation of H_2O, HCN, H_2O_2, and O_2. *Bioorg. Chem. 32*, 367–375.
12. Gruber, K., Gartler, G., Krammer, B., Schwab, H., and Kratky, C. (2004) Reaction mechanism of hydroxynitrile lyases of the α/β-hydrolase superfamily: the three-dimensional structure of the transient enzyme-substrate complex certifies the crucial role of LYS236. *J. Biol. Chem. 279*, 20501–20510.
13. Bernhardt, P., Hult, K., and Kazlauskas, R. J. (2005) Molecular basis of perhydrolase activity in serine hydrolases. *Angew. Chem., Int. Ed. 18*, 2742–2746.
14. Kirner, S., Krauss, S., Sury, G., Lam, S. T., Ligon, J. M., and van Pée, K.-H. (1996) The nonheme chloroperoxidase from *Pseudomonas fluorescens* and its relationship to pyrrolnitrin biosynthesis. *Microbiology 142*, 2129–2135.
15. Gasteiger, E., Hoogland, C., Gattiker, A., Duvaud, S., Wilkins, M. R., Appel, R. D., and Bairoch, A. (2005) Protein Identification and Analysis Tools on the ExPASy Server, in The Proteomics Protocols Handbook (Walker, J. M., Ed.) pp 571−607, Humana Press, Totowa, NJ.
16. Morris, D. R., and Hager, L. P. (1966) Chloroperoxidase I. Isolation and properties of the crystalline glycoprotein. *J. Biol. Chem. 241*, 1763–1768.
17. Fersht, A. (1999) Structure and Mechanism in Protein Science, p 172, Freeman, New York.
18. Janes, L. E., Löwendahl, A. C., and Kazlauskas, R. J. (1998) Quantitative screening of hydrolase libraries using pH indicators: identifying active and enantioselective hydrolases. *Chem.—Eur. J. 4*, 2324–2331.
19. Cheeseman, J. D., Tocilj, A., Park, S., Schrag, J. D., and Kazlauskas, R. J. (2004) X-ray crystal structure of an aryl esterase from *Pseudomonas fluorescens*. *Acta Crystallogr. D 60*, 1237–1243.

20. Pflugrath, J. W. (1999) The finer things in X-ray diffraction data collection. *Acta Crystallogr., Sect. D: Biol. Crystallogr. D55*, 1718–1725.
21. Jones, T. A., Zou, J.-Y., Cowan, S. W., and Kjeldgaard, M. (1991) Improved methods for building protein models in electron density maps and the location of errors in these models. *Acta Crystallogr., Sect. A: Found. Crystallogr. A47*, 110–119.
22. Murshudov, G. N., Vagin, A. A., and Dodson, E. J. (1997) Refinement of macromolecular structures by the maximum-likelihood method. *Acta Crystallogr., Sect. D: Biol. Crystallogr. D53*, 240–255.
23. Perrakis, A., Morris, R., and Lamzin, V. S. (1999) Automated protein model building combined with iterative structure refinement. *Nat. Struct. Biol. 6*, 458–463.
24. Read, R. J. (1986) Improved Fourier coefficients for maps using phases from partial structures with errors. *Acta Crystallogr., Sect. A: Found. Crystallogr. A42*, 140–149.
25. Laskowski, R. A. (1993) PROCHECK: a program to check the stereochemical quality of protein structures. *J. Appl. Crystallogr. 26*, 283–291.
26. Pettersen, E. F., Goddard, T. D., Huang, C. C., Couch, G. S., Greenblatt, D. M., Meng, E. C., and Ferrin, T. E. (2004) UCSF Chimera—A visualization system for exploratory research and analysis. *J. Comput. Chem. 25*, 1605–1612.
27. DeLano, W. L. (2008) The PyMOL Molecular Graphics System, DeLano Scientific, Palo Alto, CA (http://www.pymol.org).
28. Vagin, A. A., and Teplyakov, A. J. (1997) MOLREP: an automated program for molecular replacement. *Appl. Crystallogr. 30*, 1022–1025.
29. Emsley, P., and Cowtan, K. (2004) Coot: model-building tools for molecular graphics. *Acta Crystallogr., Sect. D: Biol. Crystallogr. D60*, 2126–2132.
30. Lovell, S. C., Davis, I. W., Arendall, W. B., III, de Bakker, P. I. W., Word, J. M., Prisant, M. G., Richardson, J. S., and Richardson, D. C. (2003) Structure validation by Cα geometry: φ, ψ and Cβ deviation. *Proteins: Struct., Funct., Genet. 50*, 437–450.
31. Jorgensen, W. L., Maxwell, D. S., and Tirado-Rives, J. (1996) Development and testing of the OPLS all-atom force field on conformational energetics and properties of organic liquids. *J. Am. Chem. Soc. 118*, 11225–11236.
32. Wilmouth, R. C., Clifton, I. J., Robinson, C. V., Roach, P. L., Aplin, R. T., Westwood, N. J., Hajdu, J., and Schofield, C. J. (1997) Structure of a specific acyl enzyme complex formed between β-casomorphin-7 and porcine pancreatic elastase. *Nat. Struct. Biol. 4*, 456–462.
33. Wilmouth, R. C., Li, Y.-H., Wright, P. A., Claridge, T. D. W., Aplin, R. T., and Schofield, C. J. (2000) Reaction of clavams with elastase reveals a general method for inhibiting "serine" enzymes. *Tetrahedron 56*, 5729–5733.
34. Everett, A. J., and Minkoff, G. J. (1953) The dissociation constants of some alkyl and acyl hydroperoxides. *Trans. Faraday Soc. 49*, 410–414.
35. Fersht, A. (1999) Structure and Mechanism in Protein Science, pp 117−118, W. H. Freeman, New York.
36. Blacklow, S. C., Raines, R. T., Lim, W. A., Zamore, P. D., and Knowles, J. R. (1988) Triosephosphate isomerase catalysis is diffusion controlled. *Biochemistry 27*, 1158–1165.
37. van Pée, K.-H., Hecht, H.-H., Berkessel, A., Schrapek, T., and Laatsch, H. (1996) Enzymatic, active oxygen-releasing mixture and peracid production, 07/03/96 WOI96066909.
38. Krebsfänger, N., Zocher, F., Altenbuchner, J., and Bornscheuer, U. T. (1998) Characterization and enantioselectivity of a recombinant esterase from *Pseudomonas fluorescens*. *Enzyme Microb. Technol. 22*, 641–646.
39. Kataoka, M., Honda, K., and Shimizu, S. (2000) 3,4-Dihydrocoumarin hydrolase with haloperoxidase activity from *Acinetobacter calcoaceticus* F46. *Eur. J. Biochem. 267*, 3–10.
40. Line, K., Isupov, M. N., and Littlechild, J. A. (2004) The crystal structure of a (−) γ-lactamase from *Aureobacterium* species reveals a tetrahedral intermediate in the active site. *J. Mol. Biol. 338*, 519–532.
41. Friesner, R. A., Banks, J. L., Murphy, R. B., Halgren, T. A., Klicic, J. J., Mainz, D. T., Repasky, M. P., Knoll, E. H., Shaw, D. E., Shelley, M., Perry, J. K., Francis, P., and Shenkin, P. S. (2004) Glide: A new approach for rapid, accurate docking and scoring. 1. Method and assessment of docking accuracy. *J. Med. Chem. 47*, 1739–1749.
42. Li, Z., Sau, A. K., Furdui, C. M., and Anderson, K. S. (2005) Probing the role of tightly bound phosphoenolpyruvate in *Escherichia coli* 3-deoxy-D-manno-octulosonate 8-phosphoate synthase catalysis using quantitative time-resolved electrospray ionization mass spectrometry in the millisecond time range. *Anal. Biochem. 343*, 25–47.
43. Lee, W., Vojcic, L., Despotovic, D., Prodanovic, R., Maurer, K.-H., Schwaneberg, U., and Zacharias, M. (2009) Rationalizing perhydrolase activity of aryl-esterase and subtilisin Carlsberg mutants by molecular dynamics simulations of the second tetrahedral intermediate state, Theor. Chem. Acc. (online doi: 10.1007/s00214-009-0611-3).
44. Li, C., Hassler, M., and Bugg, T. D. H. (2008) Catalytic promiscuity in the α/β-hydrolase superfamily: hydroxamic acid formation, C−C bond formation, ester and thioester hydrolysis in the C−C hydrolase family. *ChemBioChem 9*, 71–76.
45. Caldini, G., Cenci, G., Manenti, R., and Morozzi, G. (1998) The ability of an environmental isolate of *Pseudomonas fluorescens* to utilize chrysene and other four-ring polynuclear aromatic hydrocarbons. *Appl. Microbiol. Biotechnol. 44*, 225–229.
46. Honda, K., Kataoka, M., Sakuradani, E., and Shimizu, S. (2003) Role of *Acinetobacter calcoaceticus* 3,4-dihydrocoumarin hydrolase in oxidative stress defence against peroxoacids. *Eur. J. Biochem. 270*, 486–494.
47. Janković, M., and Sinadinović-Fišer, S. (2005) Prediction of the chemical equilibrium constant for peracetic acid formation by hydrogen peroxide. *J. Am. Oil Chem. Soc. 82*, 301–303. Zhao, X., Zhang, T., Zhou, Y., and Liu, D. (2007) Preparation of peracetic acid from hydrogen peroxide: Part I: Kinetics for peracetic acid synthesis and hydrolysis. *J. Mol. Catal. A: Chem. 271*, 246–252.
48. Chipman, D., Barak, Z., and Schloss, J. (1998) Biosynthesis of 2-aceto-2-hydroxy acids: acetolactate synthases and acetohydroxyacid synthases. *Biochim. Biophys. Acta 2*, 401–419.

Supplemental information

Switching catalysis from hydrolysis to perhydrolysis in *P. fluorescens* esterase

De Lu (Tyler) Yin,[†] Peter Bernhardt,[†] Krista L. Morley,[‡] Yun Jiang,[†] Jeremy D. Cheeseman,[‡] Vincent Purpero,[†] Joseph D. Schrag,*[,§] and Romas J. Kazlauskas *[,†]

Contents

Electrospray mass spectra of acyl enzyme intermediate. Figure S-1 shows the actual spectra showing the multicharged ions observed in the electrospray mass spectra. This figure is the data from which the doconvoluted spectra shown in Figure 3 of the paper are based.

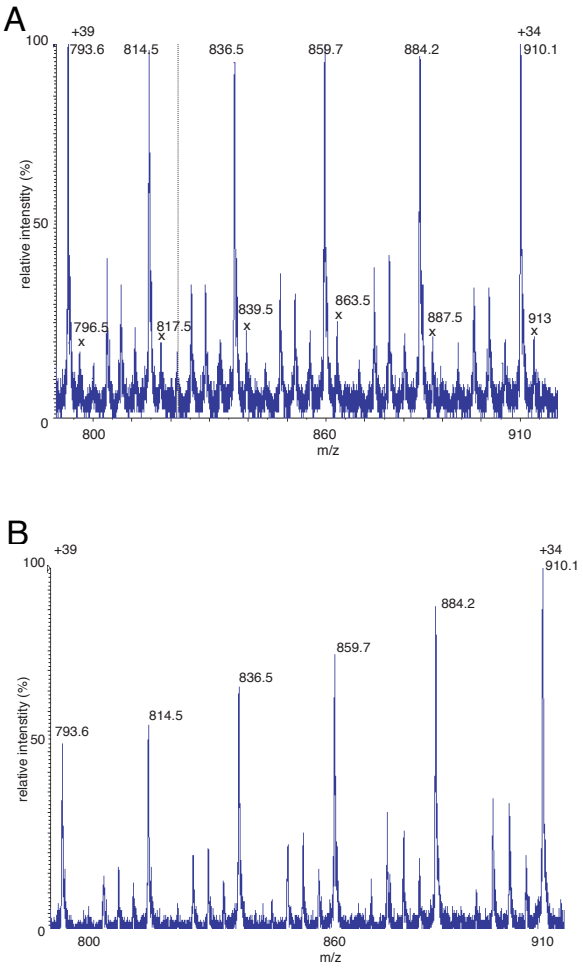

Figure S-1. Electrospray ionization mass spectra for the +34 to +39 charged ions of L29P PFE with and without ε-caprolactone. A) L29P with ε-caprolactone in citrate/formate at pH ~5.5 forms the acyl-enzyme intermediate. The peaks that are assigned to the intermediate are denoted with an "x" and the corresponding m/z. B) L29P PFE only in citrate/formate at pH ~5.5.

pH-rate profile of perhydrolysis catalyzed by mutants and wild-type PFE. The pH rate profile for enzyme-catalyzed perhydrolysis is a bell-shaped curve, Figure S-2, in contrast to a rise at pH 5 and a plateau for hydrolysis of esters (*1*). The bell-shaped curve for perhydrolysis indicates that catalysis requires one group to be deprotonated and another to be deprotonated. We propose that the rise at at pH 4-5 corresponds to the deprotonation of the active site histidine (same as for ester hydrolysis) and the decrease at pH 6-7 corresponds to the ionization of acetic acid. The mechanism requires that the active site histidine act as a base to deprotonate the active site Oγ hydroxyl of serine. The mechanism also requires acetic acid to be in the protonated form because formation of an acetyl enzyme from acetate is unlikely or impossible. There is no corresponding decrease in activity for ester hydrolysis because the ester does not ionize.

The experimental data were fit to a doubly ionizing system giving the curves in Figure S-2. The rise at pH 4-5 corresponded to a pK_a of 5.4 to 6.9 (range for different enzymes), which is similar the 6.5 expected for the imidazoyl moiety of histidine. The decrease at pH 6-7 corresponded to a pK_a of 4.0-5.7 (range for different enzymes), which is similar to the value of 4.8 for free acetic acid. The location of the rise or decrease does not directly indicate the pK_a; it must be calculated from a best fit of the data to a doubly ionizing system. The maximum activity occurs at pH 5.5 where the predominant species are not the catalytically active ones. Most of the imidazoyl side chain is still protonated (inactive form) and most of the acetic acid is deprotonated (inactive form). This pH of 5.5 is value where the largest concentration of both active forms coexist. The pH optimum for perhydrolysis is approximately 5.5 for four enzymes, but one - L29P/F93H PFE - shows a lower pH optimum near 5.3 due to a shift in the rise at pH 5 to lower pH. This shift may be due to a decrease in the pK_a of the active site histidine. The F93H mutation adds another histidine in the active site. Protonation of this histidine adds a positive charge and likely makes it easier to convert the active site histidine to the catalytically active, deprotonated form.

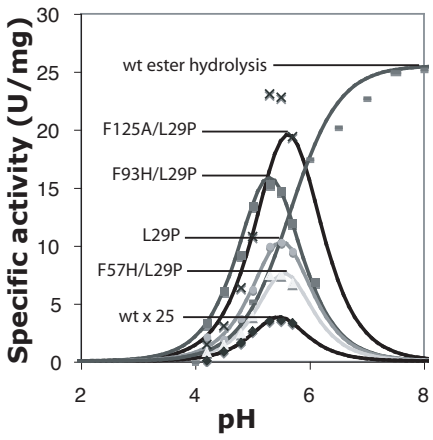

Figure S-2. The pH-rate profile for perhydrolysis of acetic acid is a bell-shaped curve, while the profile for hydrolysis of esters reaches a plateau. Deprotonation of the active site histidine likely accounts for the increase in activity at pH 4-5 for both perhydrolysis and ester hydrolysis, since the mechanism requires the histidine to act as a base. Deprotonation of the perhydrolysis substrate acetic acid likely accounts for the decrease in perhydrolysis activity at pH 5-6. Formation of the acetyl enzyme intermediate is impossible from acetate. The shift in the pH optimum for L29P/F93H PFE may be due to a shift in the pK_a of the active site histidine. The lines are a best fit to a doubly ionizing system using a pKa of 5.4-6.9 for the rise at

pH 4-5 and a pKa of 4.0-5.6 for the decrease at pH 6-7. The location of the rise and decrease does not directly indicate the pK_a. Initial rates for perhydrolysis of acetic acid were measured using the monochlorodimedone assay (1.0 M acetic acid, 9.9 mM H_2O_2, see Experimental Section). Data for hydrolysis of ethyl acetate are from reference 22, which did not report specific activity. Our measured specific activity at pH 7.2 was 18 U/mg, Table 5, so the data are normalized to this value.

Discussion of previous experiments to distinguish acyl enzyme versus a noncovalent mechanisms for PFE.

Previous attempts to distinguish betwen an acyl enzyme mechanism and a non covalent mechanism for PFE (*2*) did not yield a clear answer. Presteady state kinetics of PFE-catalyzed hydrolysis of *p*-nitrophenyl acetate do not show burst kinetics, but this also does not rule out either mechanism. Bugg and coworkers measured the pre-steady-state kinetics for hydrolysis of *p*-nitrophenyl acetate for several enzymes. Two enzymes (CAL-B and acetylcholine esterase) showed burst kinetics – a initial fast release of *p*-nitrophenol ($k = 7\ s^{-1}$) followed by a slow constant release ($k = 0.03\ s^{-1}$ and $0.006\ s^{-1}$, respectively). This observation is consistent with a fast initial formation of an acetyl enzyme intermediate followed by a slower rate-limiting deacylation. Thus, the slow step in these enzymes is the release of the acetyl enzyme intermediate. PFE did not show burst kinetics; *p*-nitrophenol was released at a constant rate of $38\ s^{-1}$, which is 1200 to 6000 faster than the rate for the other two enzymes. This result means either 1) PFE catalyzes this faster hydrolysis of *p*-nitrophenyl acetate without forming an acetyl enzyme intermediate or 2) PFE still forms an acetyl enzyme intermediate, but is faster because both the acetylation step and the deacetylation step are fast. Thus, the observation of burst kinetics demonstrates an acyl enzyme intermediate, but the absence of burst kinetics is an ambiguous result. It may indicate a fast deacylation step.

Bugg and coworkers also measured the Hammett reaction parameter, ρ, for PFE-catalyzed p-nitrophenyl benzoate hydrolysis as 0.0, indicating that substituents on the benzoate do not influence the rate-determining step of the reaction. The transition state for both mechanisms involves nucleophilic attack at the carbonyl by water. Reaction of p-nitrophenyl benzoates with hydroxide shows ρ values of 2.21 indicating that electron withdrawing groups speed up the reaction. Both the non covalent mechanism and the acyl enzyme mechanism predict a positive value for ρ. Indeed, BphD, a C–C hydrolase that likely follows a non covalent mechanism, showed $\rho = +0.98$ and CALB, a hydrolase that follow an acyl enzyme mechanism, showed $\rho = +0.56$. One possible explanation is that an enzyme conformational change may be rate limiting in PFE-catalyzed hydrolysis of p-nitrophenyl benzoates. Previous work showed that benzoates are very poor substrates for PFE and the x-ray structure shows that acyl binding site is too small for the benzoate phenyl group. Thus, we hypothesize that the enzyme conformation must change before the p-nitrophenyl benzoates can react. If this change is rate-determining, it will not change with different substituents on the benzoate.

The pH-activity profiles also do not distinguish the two mechanisms. Both mechanisms require the active site histidine to act as a base to deprotonate the nucleophile hydrogen peroxide. Protonation of this histidine accounts for the drop in activity a low pH. Both mechanisms also involve nucleophilic attack at the carbonyl and thus require the carboxylic acid form of the sub-

strate. Deprotonation of the substrate accounts for the drop in activity at high pH. Nucleophilic attack on the carboxylate form of the substrate is impossible.

References

1. Krebsfänger, N., Zocher, F., Altenbuchner, J., and Bornscheuer, U. T. (1998) Characterization and enantioselectivity of a recombinant esterase from *Pseudomonas fluorescens, Enzyme Microb. Technol. 22*, 641–646.
2. Li, J.-J., Bugg, T. D. H. (2007) Investigation of a general base mechanism for ester hydrolysis in C-C hydrolase enzymes of the α/β-hydrolase superfamily: a novel mechanism for the serine catalytic triad, *Org. Biomol. Chem. 5,* 507-513.

Bioresource Technology 102 (2011) 5183–5192

Contents lists available at ScienceDirect

Bioresource Technology

journal homepage: www.elsevier.com/locate/biortech

Improved pretreatment of lignocellulosic biomass using enzymatically-generated peracetic acid

DeLu (Tyler) Yin [a], Qing Jing [a,1], Waleed Wafa AlDajani [b,2], Shona Duncan [b], Ulrike Tschirner [b], Jonathan Schilling [b], Romas J. Kazlauskas [a,*]

[a] University of Minnesota, Department of Biochemistry, Molecular Biology & Biophysics and The BioTechnology Institute, 1479 Gortner Avenue, Saint Paul, MN 55108-6104, USA
[b] University of Minnesota, Department of Bioproducts and Biosystems Engineering, 2004 Folwell Avenue, Saint Paul, MN 55108-6128, USA

ARTICLE INFO

Article history:
Received 16 November 2010
Received in revised form 24 January 2011
Accepted 25 January 2011
Available online 2 February 2011

Keywords:
Peracetic acid
Perhydrolase
Pretreatment
Lignin
Aspen

ABSTRACT

Release of sugars from lignocellulosic biomass is inefficient because lignin, an aromatic polymer, blocks access of enzymes to the sugar polymers. Pretreatments remove lignin and disrupt its structure, thereby enhancing sugar release. In previous work, enzymatically generated peracetic acid was used to pretreat aspen wood. This pretreatment removed 45% of the lignin and the subsequent saccharification released 97% of the sugars remaining after pretreatment. In this paper, the amount of enzyme needed is reduced tenfold using first, an improved enzyme variant that makes twice as much peracetic acid and second, a two-phase reaction to generate the peracetic acid, which allows enzyme reuse. In addition, the eight pretreatment cycles are reduced to only one by increasing the volume of peracetic acid solution and increasing the temperature to 60 °C and the reaction time to 6 h. For the pretreatment step, the weight ratio of peracetic acid to wood determines the amount of lignin removed.

1. Introduction

Lignocellulosic biomass, such as bioenergy crops and trees (e.g., switchgrass, aspen wood) or agricultural and forestry wastes (e.g., wood residues, corn stover, straw), are potential low cost sources of fermentable sugars. However, the conversion of lignocellulosic biomass into sugars is currently inefficient and expensive. This lignocellulose recalcitrance is one of the primary economic barriers to biofuel and bioproduct synthesis. The sugar polymers are embedded in plant cell walls, which naturally resist chemical, physical and enzymatic degradation. In particular, lignin, an aromatic polymer that is a major component of lignocellulosic biomass, blocks access of enzymes to sugar polymers.

Partial removal of lignin from biomass significantly improves subsequent enzymatic hydrolysis of cellulose and hemicelluloses to fermentable sugars (Duncan et al., 2010; Nakagame et al., 2010). However, natural enzymatic reactions that degrade lignin are slow and require days, weeks or even months. One reason for the slow reaction is that natural enzymatic reactions must use reaction intermediates that are compatible with living microorganisms. Industrial use of lignocellulosics as feedstocks will require faster pretreatment methods.

Most pretreatment methods disrupt cell walls to expose the sugar polymers. For example, dilute acid at high temperatures, ammonia fiber explosion (AFEX), steam explosion or wet oxidation break up the material (Lee et al., 2010; Zheng et al., 2009; Yan et al., 2009), but do not remove much lignin. These pretreatments have limited effectiveness, and can generate side products that inhibit later fermentations (Luo et al., 2002; Lau and Dale, 2010).

Chemical pretreatments that remove lignin are more effective. Pretreatment with ozone (Neely 1984; Vidal and Molinier, 1988), hydrogen peroxide (Azzam, 1989), organic solvents (Chum et al., 1988) or strong caustic (McMillan, 1994) all remove lignin, but only the oxidative reagents are selective for lignin. The other reagents also remove some of the sugars and are therefore undesirable.

A promising lignin-selective reagent is peracetic acid (Sun et al., 2000). Peracetic acid converts lignin to soluble fragments by two different mechanisms. First, peracetic acid reduces the molecular weight of lignin polymers by cleaving β-aryl ether bonds and both carbon–carbon and carbon–oxygen bonds linked to the aromatic rings. (Lawrence et al., 1980). Second, peracetic acid causes other reactions that increase the water solubility of lignin: dealkylation of *O*-methyl groups, introduction of hydroxyl groups to aromatic rings and cleavage of the aromatic rings into muconic acids (Lawrence et al., 1980). These reactions increase the polarity of lignin and create water-soluble lignin fragments that wash away from the lignocellulosic biomass. Peracetic acid-treated biomass can be

* Corresponding author. Tel.: +1 612 624 5904; fax: +1 612 625 5780.
E-mail address: rjk@umn.edu (R.J. Kazlauskas).
[1] Present address: Department of Chemistry, Northwestern University, 2145 Sheridan Road, Evanston, IL 60208–3113, USA.
[2] Present address: FPInnovations, 570 Saint-Jean Blvd., Pointe-Claire QC, Canada H9R 3J9.

0960-8524/$ - see front matter © 2011 Elsevier Ltd. All rights reserved.
doi:10.1016/j.biortech.2011.01.079

efficiently fermented to make ethanol (Teixeira et al., 2000). However, peracetic acid is expensive and can be explosive in concentrated form. This safety hazard increases the cost of storage and transport of peracetic acid.

In-situ generation of peracetic acid eliminates transportation and storage by generating this oxidant as needed. Enzymes are potential catalysts for the synthesis of peracetic acid from hydrogen peroxide and acetate esters such as ethyl acetate, Fig. 1. Although natural enzymes can catalyze this synthesis it is unlikely that their natural role is synthesis of peracetic acid (Yin et al., 2010). Peracetic acid is a highly reactive oxidant that reacts with and inactivates biomolecules. The ability to make peracetic acid is an extra, unexpected reaction of many hydrolases.

Perhydrolysis is the cleavage of an ester by hydrogen peroxide, Fig. 1, and is mechanistically similar to hydrolysis. Many esterases catalyze perhydrolysis, but perhydrolases are a subgroup of esterases that are especially efficient at perhydrolysis. The active site of both esterases and perhydrolases contains a Ser-His-Asp catalytic triad. For example, *Pseudomonas fluorescens* esterase (PFE) is an esterase that catalyzed hydrolysis of a broad range of esters such as ethyl acetate (k_{cat} = 9 s^{-1}). It also catalyzed slow perhydrolysis of acetic acid (k_{cat} = 0.12 s^{-1}) and perhydrolysis of ethyl acetate (k_{cat} = 12 s^{-1}). PFE-catalyzed perhydrolysis of ethyl acetate forms up to 70 mM peracetic acid within 30 min (Duncan et al., 2010).

Duncan et al. (2010) used this perhydrolysis to make peracetic acid and use to pretreat aspen wood, Fig. 1. Without pretreatment, the cellulases released only 22% of the available glucose, but with peracetic acid pretreatment, they released 98% of the available glucose. Although this improvement is dramatic, the procedure was complex and required up to 40 g of enzyme per kilogram of aspen wood. In this paper the complexity and amount of enzyme are reduced. Improving the saccharification step was not a goal of this research; that step uses a modified NREL procedure only to measure the effectiveness of the pretreatment.

2. Methods

2.1. General

Wild-type and F162L PFE were prepared as in Yin et al. (2010). The proteins were purified by nickel affinity chromatography using Ni–NTA resin (Qiagen) and imidazole (80 mM) in the wash buffer to elute a contaminating catalase. The eluted protein was dialyzed

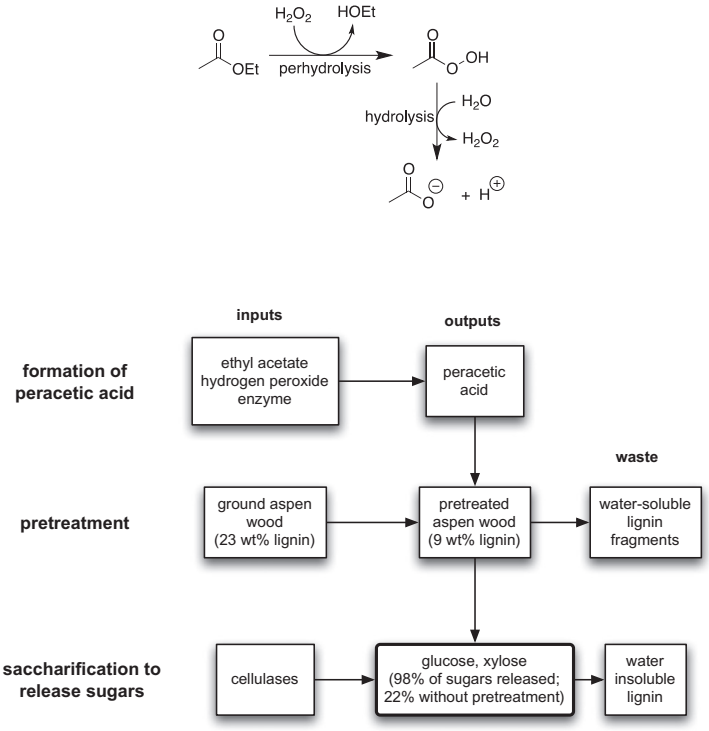

Fig. 1. Enzyme-catalyzed formation of peracetic acid and its use to pretreat aspen wood. Top: Perhydrolysis of ethyl acetate yields peracetic acid. A subsequent undesirable hydrolysis of this peracetic acid yields acetic acid and the starting hydrogen peroxide. Esterase from *Pseudomonas fluorescens* (PFE) catalyzes both reactions. Bottom: Conversion of aspen wood biomass to fermentable sugars involves three steps: formation of peracetic acid, pretreatment of aspen wood with peracetic acid, and saccharification of the pretreated aspen wood. The pretreatment of aspen wood with peracetic acid removed about half of the lignin and made the saccharification more efficient. Without pretreatment, cellulases released only 22% of the available glucose, but released 98% after pretreatment. The lignin fractions also include some sugars due to inefficiencies.

Table 1
Changes in the HPLC mobile phase composition as function of time to measure methyltolylsulfoxide (MTSO) and thus the amount of peracetic acid.

Time (min)	Mobile phase composition[a] water/10%methanol:acetonitrile
0	60:40
3	40:60
3.5	20:80
4.5	20:80
5.5	40:60
6.5	60:40
10	60:40

[a] The first number indicates the volume percentage of water containing 10 vol.% methanol and the second number indicates the percentage of acetonitrile.

and concentrated using Amicon centrifuge filters (Millipore) with a molecular weight cut-off of 10,000 daltons.

2.2. Quantitation of peracetic acid

The amount of peracetic acid was measured using the Karst assay (Pinkernell et al., 1997) where peracetic acid reacts with excess methyltolylsulfide (MTS) to form methyltolylsulfoxide (MTSO). The amount of MTSO was measured by HPLC using a C8 column XDB8 (Agilent) eluted with a gradient of water with 10% methanol and acetonitrile at a flow rate of 1 mL/min, Table 1. MTSO eluted at 2.5 min and the amount was measured by the area of the peak measured at 225 nm and a calibration curve.

2.3. Formation of peracetic acid in aqueous solution

A solution (40 mL) containing buffer (sodium phosphate, pH 7.2, 100 mM) ethyl acetate (500 mM), hydrogen peroxide (1.0 M), and PFE F162L (0.5 mg/mL) in a 50-mL centrifuge tube was incubated for 10 min at 23 °C. HPLC analysis indicated 115 mM of PAA. This solution was used to pretreat aspen wood without further purification.

2.4. Formation of peracetic acid in two-phase reaction

An aqueous solution (200 mL, 1.7 M H_2O_2, 200 mM sodium phosphate pH 7.2, 0.5 mg/mL of F162L PFE) and ethyl acetate (400 mL) was mixed at 23 °C for 30 min at 150 rpm in a 1-L round bottom flask. The ethyl acetate layer containing 130 mM peracetic acid was decanted and used to directly pretreat 13 g of aspen wood.

2.5. Reuse of enzyme in two-phase reaction

Ethyl acetate (0.5 mL) was added to a aqueous solution (0.5 mL) containing sodium phosphate buffer (250 mM, pH 7.2), hydrogen peroxide (1.7 M), and PFE F162L (0.5 mg/mL) in a 1.5-mL centrifuge tube and the mixture was shaken (900 rpm) at room temperature. After 10 min, the reaction tube was centrifuged (30 s at 1000 rpm), the ethyl acetate phase containing peracetic acid was removed with a pipette and replenished with fresh ethyl acetate. The combined ethyl acetate phases were used to pretreat aspen wood. Both wild type (data not shown) and F162L PFE lose ~14% of their activity in each cycle. A control reaction without enzyme formed <10% of the amount of peracetic acid that formed with enzyme. (Data are in Fig. 2.) The conditions used to test other ethyl esters (propionate, butyrate, caproate, heptanoate, decanoate) are identical except the reaction time was extended to 30 min.

2.6. Pretreatment of aspen wood

Bark-free chips of aspen (*Populus tremuloides* Michx.) wood from a Minnesota paper mill were air-dried and milled to 40-mesh in a Wiley mill. The milled aspen wood before pretreatment contained 4.5 wt.% water. Milled aspen wood (1.3 g) was stirred at 300 rpm with a magnetic stir bar in peracetic acid solution (40 mL, 115 mM) in either aqueous buffer (sodium phosphate, 100 mM, pH 7.2) or ethyl acetate in a sealed 100-mL glass bottle for 6 h at 60 °C. The suspension was filtered and the aspen wood was washed with distilled water (40 mL).

As described by Duncan et al. (2010), dry weights were determined by oven drying a sample of the feedstock for 48 h and 100 °C according to NREL protocol for determination of total solids in biomass, LAP-001 (Sluiter et al., 2008). The composition of the aspen was determined before and after each pretreatment. After acid hydrolysis of the feedstock with sulfuric acid, insoluble lignin was determined with the TAPPI method (TAPPI T 222 om-02, 2002). Acid-insoluble lignin removed from the solution by filtering and determined by oven-dry weight of residual lignin on filter paper.

2.7. Saccharification of aspen

Aspen meal was saccharified by treatment with Celluclast 1.5 L (Sigma, St Louis, MO, USA, 60 FPU/g cellulose) and Novozyme 188 (Sigma, 64 pNPGU/g cellulose) for 7 days according to NREL method for the enzymatic saccharification of lignocellulosic biomass, LAP-009 (Brown and Torget, 1996). Celluclast 1.5 L contains, besides cellulase activity, an approximately equal amount of xylanase activity (Rodriguez et al., 2005). The procedure was modified to use 25 mg of cellulose instead of 100 mg previously described by Duncan et al. (2010). The liquids obtained after the saccharification, were analyzed with HPLC with a BIO-RAD Carbo-C Refill Cartridges, 30 × 4.6 mm (guard column) in line with BIO-RAD Aminex HPX-87P, 300 × 7.8 mm (analytical column) eluted at 85 °C with HPLC grade water flowing at 0.6 mL/min or with a BIO-RAD De-Ashing Refill Cartridges, 30 × 4.6 mm (guard column) in line with VARIAN MetaCarb 87P, 300 × 7.8 mm (analytical column) eluted at 80 °C at 0.3 mL/min.

3. Results and discussion

3.1. F162L PFE for generation of peracetic acid

Duncan et al. (2010) used wild-type PFE to catalyze the perhydrolysis of ethyl acetate. Recently, using directed evolution, Yin et al., (in preparation) discovered a variant Phe162Leu PFE that generated about twice as much peracetic acid. This paper uses this improved variant to generate peracetic acid. In a typical procedure, a solution of F162L PFE (0.5 mg/mL) in aqueous hydrogen peroxide (1.7 M, 100 mM sodium phosphate buffer, pH 7.2) containing dissolved ethyl acetate (500 mM) and generated 115 mM peracetic acid in 10 min.

3.2. Reuse of enzyme

The amount of peracetic acid generated increases for 10–30 min and then stays constant. Initially, this behavior was attributed to inactivation of the enzyme by peracetic acid, but further experimentation showed that the enzyme remains active. The constant amount of peracetic acid is a steady state concentration from a balance between enzyme-catalyzed formation of peracetic acid and enzyme-catalyzed hydrolysis to acetic acid and hydrogen peroxide,

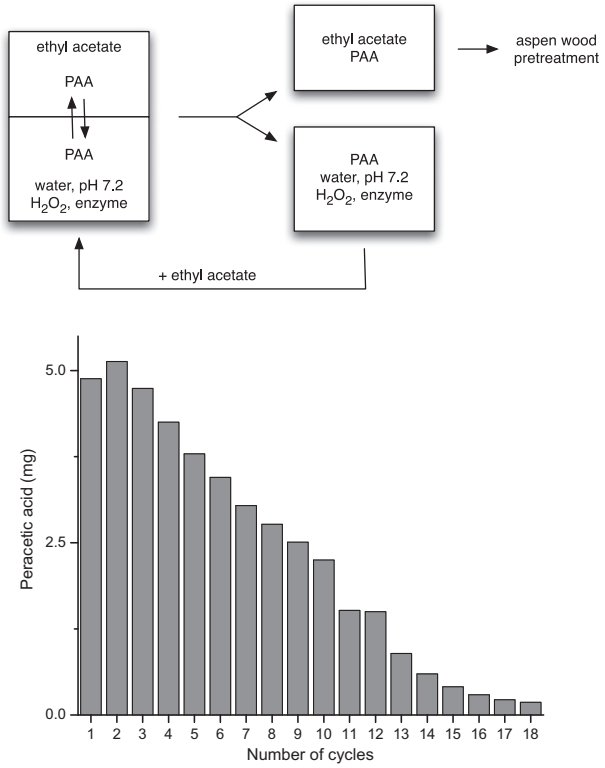

Fig. 2. Multiple reuse of enzyme by decanting the ethyl acetate phase. Top: An aqueous phase containing enzyme, buffer and hydrogen peroxide was stirred with ethyl acetate for 10 min, then the ethyl acetate phase was decanted and fresh ethyl acetate was added for the next cycle. Bottom: The amount of PAA generated decreases in subsequent cycles due to enzyme deactivation. The enzyme activity was measured after cycles 1, 2, 3, 4, 6, and 12, which showed an average 14% decrease in activity per cycle. Reaction conditions: F162L PFE (0.5 mg), 0.5 mL ethyl acetate and 0.5 mL of 250 mM Na phosphate pH 7.2 with 1.7 M H_2O_2. After 18 cycles, the pH of the aqueous solution was at 7. Chemical perhydrolysis of ethyl acetate contributes <10% of enzyme generated peracetic acid.

Fig. 1 (Yin et al., in preparation). This important observation meant that the enzyme could be reused to make more peracetic acid.

A biphasic reaction mixture enabled the separation of the product peracetic acid and the enzyme for reuse. The two-phase reaction contained equal parts of aqueous solution (0.5 mg F162L PFE, 1.7 M H_2O_2, 250 mM sodium phosphate pH 7.2) and a second phase of ethyl acetate. The enzyme remained in the aqueous phase, while the product peracetic acid partitioned approximately equally between the aqueous and ethyl acetate phases. Removal of the ethyl acetate phase containing peracetic acid and replacement with fresh ethyl acetate allowed peracetic acid accumulation to start again. The process could be repeated up to 18 times without adding new enzyme, H_2O_2, or buffer, Fig. 2. In this approach, a total of 42.5 mg of PAA could be generated using only 0.5 mg of enzyme. Compared to aqueous conditions where only 8.74 mg of PAA could be generated with the same amount of enzyme, this represents a fivefold improvement. The amount of peracetic acid generated decreases with each reuse due to ~14% loss of enzyme activity in each cycle and to a decrease in the amount of hydrogen peroxide available. The concentration of hydrogen peroxide after 18 cycles was half of the starting concentration due its removal as peracetic acid. The ethyl acetate phase also extracted a small amount of hydrogen peroxide (1.0–1.4%). Walton and Lewis (1916) reported that ethyl acetate extracted 40% of the hydrogen peroxide from an aqueous solution, but under our conditions (200 mM phosphate, pH 7.2), we found a much smaller amount.

An alternative to the two-phase reaction is immobilization of the enzyme, which would also allow removal and reuse of the enzyme or construction of a flow type reactor to make peracetic acid.

3.3. More hydrophobic peracids

Since the reuse of the enzyme relies on the extraction of the peracid from an aqueous into an organic solution, more hydrophobic peracids could increase the proportion of peracid extracted. Peracetic acid partitions approximately equally between water (56%) and ethyl acetate (44%). The peracetic acid remaining in the aqueous phase lowers the yield and slowly deactivates the enzyme.

Other ethyl esters were tested using the same two-phase procedure, but the reaction time was increased from 10 to 30 min to ensure that the peracid reached a steady state concentration. Ethyl

propionate, butyrate, and valerate, formed the corresponding peracid at about half of the rate as ethyl acetate and after 30 min yielded 219, 160, and 70 mM of peracid, respectively. A larger fraction of these peracids partitioned into the organic layer: 63%, 78%, 80% respectively. The larger esters – heptanoate, caproate, and decanoate – were not substrates for F162L PFE.

Hydrophobic peracids such as perbutyric acid could be more efficient at removal of lignin from lignocellulose because more hydrophobic peracids might react faster or more selectively with the hydrophobic lignin substrate. However, perbutyric and peracetic acid removed similar amounts of lignin. Pretreating aspen with 10 mL of 116 mM perbutyric acid lowered the lignin content to 16.3% and released 35.6% of glucose from cellulose. For comparison, pretreating aspen wood with 10 mL of 115 mM peracetic acid lowered the lignin content to 17% and released 35% of glucose from cellulose. Although perbutyric acid showed ~50% more favorable partitioning into the organic phase than ethyl acetate, the latter was chosen as the substrate because of its lower cost and because the very unpleasant smell of butyric acid also limits its application.

3.4. Optimizing the pretreatment conditions

Previous pretreatment used 70 mM peracetic acid at a ratio with wood of 0.043 g PAA/g dry weight aspen wood powder, repeated for 8 separate cycles (total 0.343 g PAA/g dry weight wood, reacted at 37 °C for 4 h) (Duncan et al., 2010). The improved perhydrolase PFE F162L produced 115 mM PAA, approximately doubling the concentration of PAA used previously. This increase in concentration meant that fewer cycles were needed to remove the same amount of lignin. To further increase the amount of lignin removed using PFE F162L-generated peracetic acid, the temperature and time for the pretreatment of aspen wood was optimized, Fig. 3. Longer times and higher temperatures were better up to the point where high temperatures start to degrade the peracetic acid. A temperature of 60 °C for 6 h removed the most lignin for a given amount of peracetic acid.

Increasing the temperature from 37 to 60 °C removed about 50% more lignin, Fig. 3a. Four pretreatment cycles at 37 °C for 6 h reduced the lignin content from 20.9% to 14.3% using a total peracetic acid loading of 0.282 g PAA/g dry weight aspen wood powder. The lignin content is further reduced to 9.9% by increasing the temperature to 60 °C for 6 h. However, further temperature increase to 80 °C removed less, not more, lignin (20.9–12.2%). The higher temperature may promote decomposition of peracetic acid. Danielewicz and Surma-Ślusarska (2006) reported fast decomposition of peracetic acid during kraft pulp treatment at 70 and 80 °C but not at 50 °C which are consistent with the observation that 80 °C was less effective than 60 °C.

Increasing the pretreatment time from 3 to 6 h also increased the amount of lignin removed. After 3 h the lignin content had reduced to 11.6% compared with 9.9% after 6 h exposure at the same concentration of PAA.

When more lignin was removed, more glucose was released from cellulose in the subsequent enzymatic saccharification of the wood powder, Fig. 3b. Duncan et al. (2010) and others (Gharpuray et al., 1983; Sinitsyn et al., 1991; Chen and Dixon, 2007) previously reported this correlation. In earlier work, the highest glucose release was 98% after 8 cycles at 37 °C and 4 h using 70 mM PAA (total 0.343 g PAA/g dry weight aspen wood powder). By increasing the temperature to 60 °C, the pretreatment time to 6 h, and the PAA concentration to 115 mM, only 4 cycles were needed for a similar glucose release (97%). The total amount of PAA used was 17.8% lower: 0.282 g PAA/g dry aspen powder.

The PAA pretreatment was most effective below pH 5, Fig. 3c. The initial pH of each solution of peracetic acid was adjusted to 2.7, 5.0, 6.0 or 7.0 with 50% w/w NaOH, then the wood suspension was stirred at 60 °C for 6 h. The final pH's of the solutions were 2.9, 4.6, 5.1 and 5.6, respectively. The pH decreases as PAA (pK_a = 8.5) is converted to acetic acid (pK_a = 4.8) and as the oxidation of lignin generates other organic acids. Above pH 5, the same amount of peracetic acid removed less lignin, likely because peracetic acid spontaneously decomposes faster at higher pH (Yuan et al., 1997). This result is similar to the reported optimum pH for a similar reaction – pulp bleaching – using peracetic acid. Peracetic acid bleached pulp most effectively between 49 and 71 °C and pH 4 and 6 Devenyns et al. (1993). For bleaching, pH below 4 was undesirable because it reduced pulp viscosity (Jääskeläinen and Poppius-Levlin, 1999), but for biofuel applications this does not matter.

3.5. Eliminating multiple cycles by increasing the volume of solution

Because F162L PFE generates a maximum of 115 mM peracetic acid, the ratio of PAA-to-wood was increased by increasing the PAA solution volume without increasing the amount of wood added. Higher liquid-to-wood ratios could eliminate multiple pretreatment cycles, Fig. 4. The liquid: wood varied from 10:1 up to 40:1 (v/w) and is plotted according to the total amount of peracetic acid. For example, 4 cycles of a 10:1 liquid: wood reaction gave similar lignin loss and saccharification yields as 2 cycles at 20:1 and as 1 cycle at 40:1. At the 40:1 ratio, this single cycle reduced lignin more than half the original content and resulted in a glucose yield of 99.7%. Lignin content could be reduced further using 3 cycles at 20:1 yielding 4% residual lignin. There is no advantage to remove this much lignin since saccharification already released nearly 100% of the glucose when the wood contained 10% lignin. Thus, the multiple cycles can be replaced by one cycle at 40:1 ratio (40 L PAA solution to 1 kg dry aspen). This simplification would reduce the number of cycles from 4 to 1 and the treatment time from 24 to 6 h.

3.6. Peracetic acid in ethyl acetate

This method of reusing the enzyme generates peracetic acid in ethyl acetate instead of in aqueous solution. This switch in solvent did not affect the efficiency of lignin removal and glucose release, Fig. 4c. Increasing amounts of PAA increased the amount of lignin removed thus increase the amount of glucose released from the remaining cellulose. Using 0.282 g of PAA to pretreat 1 g of aspen wood, 300 g of aspen wood could be pretreated with 1 g of F162L PFE. Under aqueous conditions using wild-type PFE, only 30 g of aspen wood could be pretreated per gram of enzyme. Therefore, 10-fold less enzyme is needed to treat the same amount of wood.

3.7. Material balance

Material balance flow diagrams track the amount of materials used, the outputs and waste as well as the changes in feedstock composition, Fig. 5. The best case aqueous (boxes) and ethyl acetate (rounded, dotted-line boxes) peracetic acid experiments run at 12.4-g dry weight scale were extrapolated to 1 kg dry weight. Each experiment used 0.282 g of peracetic acid per gram of aspen meal, a 40:1 ratio of solution to aspen meal and 60 °C for 6 h for the pretreatment. The subsequent hydrolysis used a scaled down standard NREL LAP-009 procedure for saccharification (Brown and Torget, 1996). The biphasic PAA generation was better because it removed more lignin and less carbohydrates during pretreatment, which lead to increased glucose yield from the enzyme hydrolysis.

The pretreatment with aqueous PAA (rectangular solid-line boxes) removed 151 g of biomass. The majority (115 g) was lignin (57% of total lignin available), but 10% of the cellulose and 13% of the xylose fraction of the hemicellulose were also removed. After saccharification, 473 g of glucose was released, yielding 88.5% cellulose-to-glucose conversion after including glucose lost during

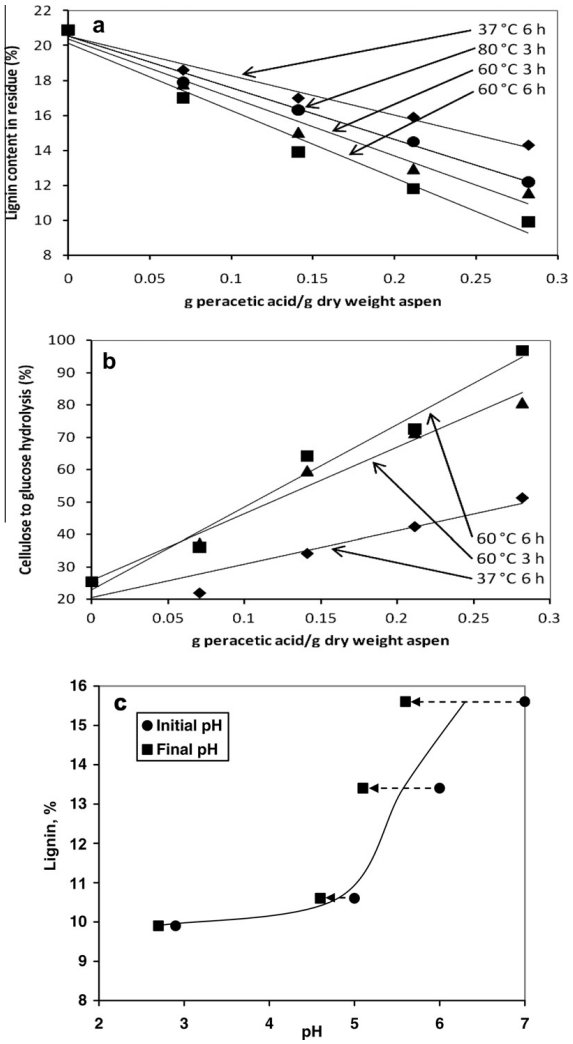

Fig. 3. Changes in lignin content and glucose release with differing amounts of peracetic acid per gram of wood at different temperatures and pH. (a) For a given reaction condition, the total lignin content decreased linearly with the amount of peracetic acid added (R^2 for all lines $\geqslant$0.97). For given amount of peracetic acid, pretreatment at 60 °C for 6 h removed the most lignin, while 37 °C for 6 h removed the least lignin. At the highest loading of peracetic acid (0.282 g/g dry weight aspen wood), the lignin content dropped to 11.6% after 3 h reaction and to 9.9% after 6 h reaction. (b) Percent glucose release from glucan in aspen wood powder rose with increasing amounts of peracetic acid (2 times greater glucose release after pretreatment with the highest peracetic acid loading (0.282 g/g dry weight aspen wood)) (R^2 for all lines $\geqslant$0.89). At the highest peracetic acid loading (0.282 g/g dry weight aspen wood) raising the temperature from 37 to 60 °C reduced lignin content by 4.4% while glucose release increased 41.6%. Increasing the length of the reaction from 3 to 6 h reduced lignin content by 8.3% and glucose release increased by 16.2%. (c) Lignin removal from aspen wood meal with aqueous PAA was most effective below pH 5. A suspension of wood (1.30 g aspen) and PAA (115 mM) in buffer (100 mM $NaHPO_4$, 40 mL total volume) was adjusted to the initial pH (*circles*) with 50% NaOH. After 6 h at 60 °C, the pH had decreased to the final pH (*squares*). The curve passes through average of these two pH values.

pretreatment, 148 g of xylose, yielding 73.2% xylan to xylose after including xylose lost during pretreatment. The fermentable sugar release was 621 g. The polysaccharides in solid biomass gain the weight of a water molecule upon hydrolysis to form sugars. Conversion of glucan to glucose and xylan to xylose increased the mass by a factor of 1.11 and 1.14, respectively. For example, complete hydrolysis of 100 g of cellulose yields 111 g of glucose.

The pretreatment with organic PAA (rounded dotted line boxes), removed a similar amount of biomass, 147 g. The majority (172 g) was lignin (85% of total lignin available), but 5% of the

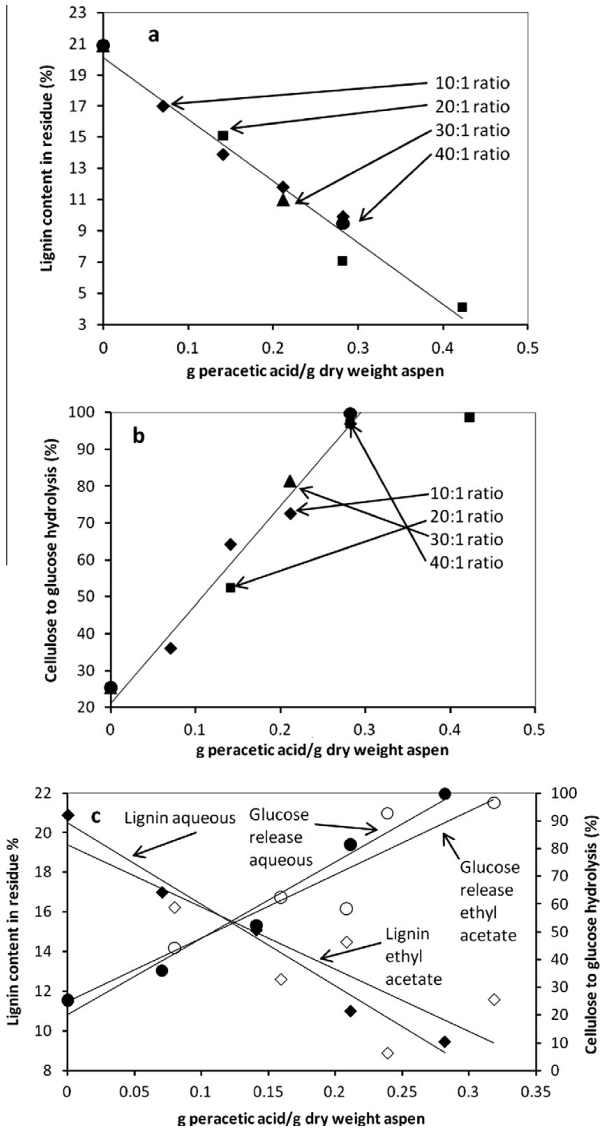

Fig. 4. The effectiveness of the pretreatment depends on the ratio of peracetic acid to aspen wood. The amount of peracetic acid was increased either by repeated treatments (diamonds and squares) or by increasing the ratio of liquid-to-wood (10:1 diamonds, 20:1 squares, 30:1 triangles, 40:1 circles). (a) Lignin content in the aspen wood powder decreased when ratio of total amount of PAA: aspen wood powder was increased (R^2 for line 0.9669). Lignin removal was greatest after 3 cycles of a 20:1 ratio (0.422 g PAA/g dry weight aspen wood powder). (b) Glucose release from cellulose in the aspen wood powder increased when the ratio of PAA: aspen wood powder was increased (R^2 for line 0.95). Glucose release was greatest by either using 2 cycles of a 20:1 ratio (0.282 g PAA/g dry weight aspen wood powder) or 1 cycle of a 40:1 ratio 0.282 g PAA/g dry weight aspen wood powder). (c) Both aqueous solutions of peracetic acid and ethyl acetate solutions of peracetic acid were similarly effective in pretreating aspen wood. Lignin content (diamonds; use left *y*-axis) in pretreated aspen wood decreased with increasing ratios of PAA solution-to-wood. The amount of glucose released (circles; use right *y*-axis) upon subsequent enzymatic saccharification increased with increasing ratios of PAA-to-aspen. Closed symbols are PAA in phosphate buffer and open symbols are PAA in ethyl acetate.

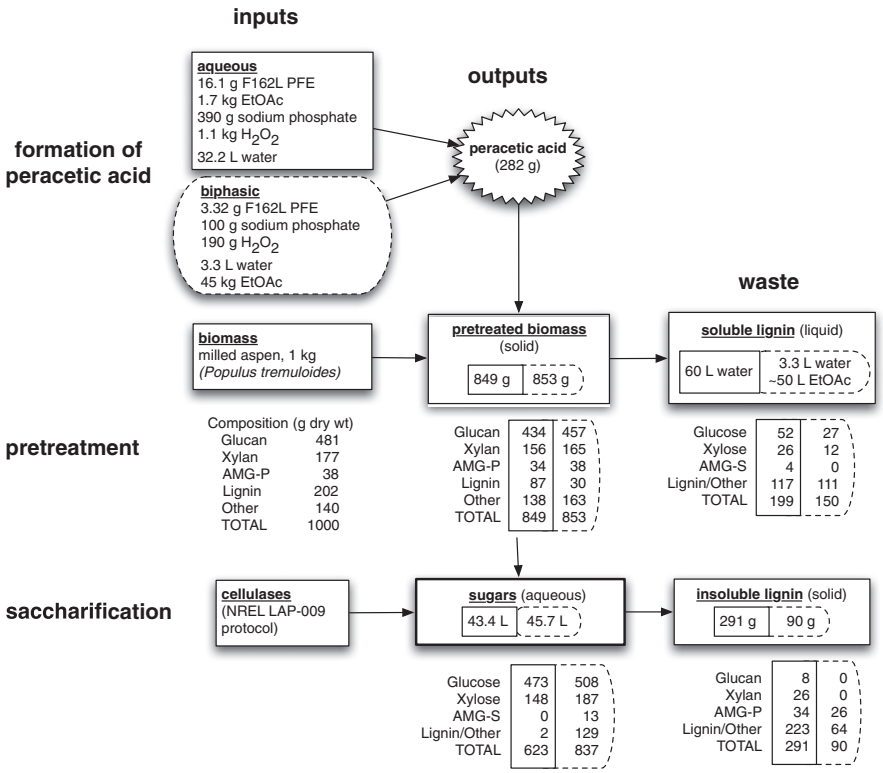

Fig. 5. Material balances for 1 kg of milled aspen wood extrapolated from the results of 12.4-g dry weight scale experiments. Solid line boxes indicate experiments with aqueous peracetic acid, while boxes in dotted lines indicate peracetic acid in ethyl acetate formed in a biphasic reaction. Pretreatment conditions were 60 °C for 6 h and the saccharification used a scaled down standard NREL LAP-009 procedure. Pretreatment with aqueous PAA followed by saccharification yielded 473 g (88.5%) of glucose from the aspen wood powder into the liquid for further processing, with the loss of 151 g biomass (115 g of lignin). Pretreatment with organic PAA (scheme in dotted lines) followed by saccharification yielded 508 g (95.0%) glucose from the aspen wood into the liquid for further processing with the loss of 147 g biomass (172 g lignin). Polysaccharides in the solid are given as glucan or xylan, while the sugars in liquids are given as glucose or xylose. AMG-S: total of arabinose, mannose and galactose sugars. AMG-P: total of arabinan, mannan, and galactan polymers. A given mass of glucan will yield upon hydrolysis a slightly larger mass of glucose due to the gain of the mass of the water. This increase leads to an increase in total mass as more monosaccharides are produced.

cellulose and 6% of the xylose fraction of the hemicellulose were also removed. After saccharification, 508 g of glucose was released, yielding 95.1% cellulose-to-glucose conversion after including glucose lost during pretreatment, 187 g of xylose, yielding 92.5% xylan to xylose after including xylose lost during pretreatment. The fermentable sugar release was 767 g.

During the pretreatment, aqueous generated PAA removed a similar amount of biomass as the organic generated PAA but the composition of the lost biomass was different. Aqueous generated PAA removed less lignin and more carbohydrates compared with the organic generated PAA. Both pretreatment methods reduced the lignin content below the 11% target. The increased amount of carbohydrate in the organic generated PAA treated aspen wood powder meant that more cellulose was available for hydrolysis to glucose by the commercial enzymes than the aqueous generated PAA treated aspen wood. After pretreatment with organic generated PAA and saccharification 767 g fermentable sugars had been released compared with 621 g from aqueous generated PAA pretreatment and saccharification.

Efficient lignin removal depended mostly on the pretreatment time and temperature and on the amount of peracetic acid relative to biomass. The temperature and reaction time increase from 37 to 60 °C and from 4 to 6 h yielded the greatest improvement, nearly doubling saccharification yields to nearly 100% for a given amount of peracetic acid. For a pretreatment of 6 h at 60 °C, aspen wood requires 0.285 g peracetic acid per g of wood. This realization allowed the replacement of a multi-step treatment with a single step treatment by increasing the reaction volume. Either procedure uses the same amount of peracetic acid, but the single step procedure is simpler.

The new procedure reduces enzyme use, chemical use, reaction time, and waste production, Table 2. The amount of enzyme required to make enough PAA to pretreat 1 kg of aspen wood dropped from 32.2 to 16.1 g when using the improved enzyme without recycling. The amount of enzyme dropped another fivefold using the biphasic (ethyl acetate) method to 3.32 g. Optimizing the pretreatment conditions by increasing the amount of liquid to aspen powder reduced the number of cycles from 8 to 1. This

Table 2
Comparison of inputs, waste and pretreatment conditions for generation of peracetic and pretreating 1 kg of aspen wood powder.

	Duncan et al. (2010) aqueous buffer	This work aqueous buffer	This work biphasic (ethyl acetate)
Inputs			
Enzyme	32.2 g	16.1 g	3.32 g[a]
Sodium phosphate	774 g	387 g	99.5 g
Hydrogen peroxide	2100 g	1050 g	192 g
Ethyl acetate	3.78 L	1.89 L	50 L (recycled[b])
PAA generated	343 g	282 g	282 g
Pretreatment conditions	8 cycles, 37 °C, 32 h total	1 cycle, 60 °C, 6 h total	1 cycle, 60 °C, 6 h total
Output			
Liquid	680 L aqueous	60 L aqueous	3.3 L aqueous ~49 L ethyl acetate (recycle[b])
Solid	80 g	291 g	90 g
Fermentable sugar	581 g	588 g	763 g

[a] Based on reuse of the enzymes as in Fig. 5.
[b] Most of the ethyl acetate can be recycled, but this recycling has not been tested.

reduction of cycles reduced the amount of liquid waste produced (680 to 60 L), the amount of chemicals (buffer and hydrogen peroxide) used (2874 to 291.5 g) and the reaction time (32–6 h). The only negative of the optimized procedure is an increase in pretreatment temperature from 37 to 60 °C. Although the biphasic method uses more ethyl acetate, after reaction with the wood, most of the ethyl acetate may be recycled.

Decreasing the lignin content from 22 to 11 wt.% in aspen wood allows nearly complete saccharification of the sugars, Fig. 6. A comparison of the residual lignin content with glucose release for all samples during this research project shows that as lignin content drops, glucose release increases. This enhancement reaches its maximum at around 11% lignin content, giving us a target for lignin removal. Thus, only ~50% of total lignin content needs to be removed to reach maximum gains. Reaction medium selection (phosphate buffer or ethyl acetate) also has no measurable effect, so these variables can be changed to decrease cost and increase convenience without compromising the yield of sugars.

The amount of enzyme needed is still too high for a practical application. Assuming a large-scale enzyme cost of US $100/kg enzyme (Rozzell, 1999), 3 g enzyme/kg aspen wood corresponds to $0.30/kg of wood. Since 1 kg of aspen wood yields 0.1 gal of ethanol (100 gallons of ethanol from 1 ton of hardwood sawdust (US Department of Energy, 2010), this cost corresponds to $3 enzyme/gallon of ethanol, which is approximately 100-fold still too high. (The 3 g of esterase/kg aspen wood is similar to the amount of β-glucosidase used in the saccharification step, also 3 g enzyme/kg aspen wood. Optimization of the saccharification step was not a goal of this research; the NREL procedure uses a large amount of enzyme to ensure that the saccharification is not a limiting step to sugar release.) Immobilization technologies as well as improvements in the catalytic properties of the enzyme have made much larger improvements in other processes (e.g., a >40,000-fold improvement in the catalytic efficiency of a transaminase by directed evolution (Savile et al., 2010), so it is reasonable to expect that the cost of the enzyme can be decreased.

Another way to reduce the amount of enzyme needed is to improve the efficiency of the reaction of peracetic acid with lignin. Using 0.285 g of peracetic acid per gram of aspen wood removed approximately half of the lignin or 10 wt.%, which corresponds to 0.10 g. In mole terms, 0.285 g of peracetic acid is 3.75 mmol, while 0.10 g of lignin corresponds to 0.50 mmol of lignin monomer, assuming an average monomer molecular weight of 200 g/mol. Thus, breaking lignin polymer into soluble fragments required approximately 7.5 mol of peracetic acid for each mole of lignin monomer solubilized. A catalyst or reagent that increases the efficiency of this cleavage would reduce the amount of peracetic acid needed.

The ethyl acetate required also increases the cost of the current method. Most of the ethyl acetate can likely be recycled, but this recycling has not yet been investigated. One way to reduce the amount of ethyl acetate required would be to use acetate esters within the lignocellulose to replace the ethyl acetate. Aspen wood contains 3.5 wt.% acetyl groups, which could generate about one quarter of the peracetic acid (0.062 g PAA/g aspen wood) currently needed for pretreatment.

A preliminary comparison of this approach with the dilute acid pretreatment – the most cost-effective pretreatment option for

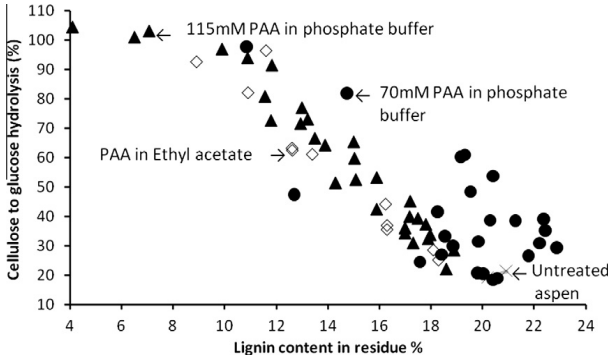

Fig. 6. Cellulose to glucose release (*y*-axis) reaches 100% once about half of the lignin in aspen wood is removed. Removing more than half gives no additional advantage. All pretreatment conditions tested behave similarly.

corn stover by Kazi et al. (2010) and generally well-accepted as a more viable pretreatment alternative – shows two potential cost savings. Assuming fixed upstream feedstock and handling costs and unaffected downstream bioconversion steps like fermentation, the peracid pretreatment (1) eliminates neutralization and conditioning steps, and (2) allows reuse of solvents and peracid-generating enzymes. The neutralization/conditioning steps contributed to 4.27% of a modeled project investment totaling $220.1 M (Aden and Foust, 2009). Removing this step saves $9.4 M. Uncertainties remain about whether milled wood could be replaced by wood chips. A high (87%) recovery of perhydrolase enzyme would lower its cost per run to 13% of total and lower its cost per ethanol gallon from nearly $3 to $0.39. Recovery of ethyl acetate also appears feasible, but was not investigated in this work.

Other potential advantages are higher yields and process integration potential. Nearly 95.1% yield of the original holocellulose fraction was recovered as glucose, which results in a theoretical ethanol yield of 121 gal per dry ton, versus the 89.8 modeled for Aden and Foust (2009). The process is also biologically-based, offering potential for integration with downstream steps, that is, the yeast fermentation might make enzyme and ethyl acetate to further reduce costs.

4. Conclusion

Enzyme-generated peracetic acid is an effective pretreatment for aspen wood that enables release of all of the sugars. The efficiency of the enzyme-generation and pretreatment has been dramatically improved in this work, but further improvements are needed before. Further improvements should focus on reducing the amount of enzyme and ester needed.

Acknowledgements

We thank the Institute for Renewable Energy and the Environment at the University of Minnesota, the National Science Foundation (CBET-0932762) and the Korea Science and Engineering Foundation funded by the Ministry of Education, Science and Technology (WCU program R32-2008-000-10213-0) for financial support.

References

Aden, A., Foust, T., 2009. Technoeconomic analysis of the dilute sulfuric acid and enzymatic hydrolysis process for the conversion of corn stover to ethanol. Cellulose 16, 535–545.

Azzam, M., 1989. Pretreatment of cane bagasse with alkaline hydrogen peroxide for enzymatic hydrolysis of cellulose and ethanol fermentation. J. Environ. Sci. Health B 24, 421–433.

Brown, L., Torget, R., 1996. Enzymatic saccharification of lignocellulosic biomass. NREL Laboratory Analytical Procedure LAP #009, National Renewable Energy Laboratory, Golden, CO, USA.

Chen, F., Dixon, R.A., 2007. Lignin modification improves fermentable sugar yields for biofuel production. Nat. Biotechnol. 25, 759–761.

Chum, H.L., Johnson, D.K., Black, S., 1988. Organosolv pretreatment for enzymatic hydrolysis of poplars: 1. Enzyme hydrolysis of cellulosic residues. Biotechnol. Bioeng. 31, 643–649.

Danielewicz, D., Surma-Ślusarska, B., 2006. Oxygen delignification of high-kappa number pine kraft pulp. Fibre. Text. Eastern Europe 14, 89–93.

Devenyns, J., Desprez, F., Troughton, N., 1993. Peracetic acid as a selective prebleaching agent: an effective option for the production of fully bleached TCF Kraft pulps. TAPPI Non-Chlorine Bleaching Conference, Atlanta, GA, Section 8–1, 341.

Duncan, S., Jing, Q., Katona, A., Kazlauskas, R.J., Schilling, J., Tschirner, U., Wafa AlDajani, W., 2010. Increased saccharification yields from aspen biomass upon treatment with enzymatically generated peracetic acid. Appl. Biochem. Biotechnol. 160, 1637–1652.

Gharpuray, M.M., Lee, Y.-H., Fan, L.T., 1983. Structural modification of lignocellulosics by pretreatments to enhance enzymatic hydrolysis. Biotechnol. Bioeng. 25, 157–172.

Jääskeläinen, A.-S., Poppius-Levlin, K., 1999. Screening of process parameters affecting the kinetics of pine Kraft pulp delignification with peroxyacetic acid. J. Pulp Pap. Sci. 25, 37–41.

Kazi, F.K., Fortman, J.A., Anex, R.P., Hsu, D.D., Aden, A., Dutta, A., Kothandaraman, G., 2010. Techno-economic comparison of process technologies for biochemical ethanol production from corn stover. Fuel 89, S20–S28.

Lau, M.W., Dale, B.E., 2010. Effect of primary degradation-reaction products from Ammonia Fiber Expansion (AFEX)-treated corn stover on the growth and fermentation of *Escherichia coli* KO11. Bioresour. Technol. 101, 7849–7855.

Lawrence, W., McKelvey, R.D., Johnson, D.C., 1980. The peroxyacetic acid oxidation of a lignin-related β-aryl ether. Svensk Papperstidn 83, 11–18.

Lee, J.M., Jameel, H., Venditti, R.A., 2010. A comparison of the autohydrolysis and ammonia fiber explosion (AFEX) pretreatments on the subsequent enzymatic hydrolysis of coastal Bermuda grass. Bioresour. Technol. 101, 5549–5558.

Luo, C.D., Brink, D.L., Blanch, H.W., 2002. Identification of potential fermentation inhibitors in conversion of hybrid poplar hydrolyzate to ethanol. Biomass Bioenerg. 22, 125–138.

McMillan, J.D., 1994. Pretreatment of lignocellulosic biomass. In: Himmel, M.E., Baker, J.O., Overend, R.P. (Eds.), Enzymatic Conversion of Biomass for Fuels Production. American Chemical Society, Washington, DC, pp. 292–324.

Nakagame, S., Chandra, R.P., Saddler, J.N., 2010. The effect of isolated lignins, obtained from a range of pretreated lignocellulosic substrates, on enzymatic hydrolysis. Biotechnol. Bioeng. 105, 871–879.

Neely, W.C., 1984. Factors affecting the pretreatment of biomass with gaseous ozone. Biotechnol. Bioeng. 26, 59–65.

Pinkernell, U., Effkemann, S., Karst, U., 1997. Simultaneous HPLC determination of peroxyacetic acid and hydrogen peroxide. Anal. Chem. 69, 3623–3627.

Rodriguez, C., Hiligsmann, S., Ongena, M., Charlier, R., Thonart, P., 2005. Development of an enzymatic assay for the determination of cellulose bioavailability in municipal solid waste. Biodegradation 16, 415–422.

Rozzell, J.D., 1999. Commercial scale biocatalysis: myths and realities. Bioorg. Med. Chem. 7, 2253–2261.

Savile, C.K., Janey, J.M., Mundorff, E.C., Moore, J.C., Tam, S., Jarvis, W.R., Colbeck, J.C., Krebber, A., Fleitz, F.J., Brands, J., Devine, P.N., Huisman, G.W., Hughes, G.J., 2010. Biocatalytic asymmetric synthesis of chiral amines from ketones applied to sitagliptin manufacture. Science 329, 305–309.

Sinitsyn, A.P., Gusakov, A.V., Vlasenko, E.Y., 1991. Effect of structural and physicochemical features of cellulosic substrates on the efficiency of enzymatic hydrolysis. Appl. Biochem. Biotechnol. 30, 43–59.

Sluiter, A., Hames, B., Hyman, D., Payne, C., Ruiz, R., Scarlata, C., Sluiter, J., Templeton, D., Wolfe, J., 2008. Determination of total solids in biomass and total dissolved solids in liquid process samples. NREL Laboratory Analytical Procedure, National Renewable Energy Laboratory, Golden, CO, USA.

Sun, R.C., Tomkinson, J., Zhu, W., Wang, S.Q., 2000. Delignification of maize stems by peroxymonosulfuric acid, peroxyformic acid, peracetic acid, and hydrogen peroxide. 1. Physicochemical and structural characterization of the solubilized lignins. J. Agric. Food Chem. 48, 1253–1262.

TAPPI T 222 om-02, 2002. TAPPI Test Method: acid-insoluble lignin in wood and pulp.

Teixeira, L.C., Linden, J.C., Schroeder, H.A., 2000. Simultaneous saccharification and cofermentation of peracetic acid-pretreated biomass. Appl. Biochem. Biotechnol. 84, 111–127.

U.S. Department of Energy, www1.eere.energy.gov/biomass/ethanol_yield_calculator.html (accessed Aug 2010).

Vidal, P.F., Molinier, J., 1988. Ozonolysis of lignin. Improvement of in vitro digestibility of poplar sawdust. Biomass 16, 1–17.

Walton, J.H., Lewis, H.A., 1916. The partition coefficients of hydrogen peroxide between water and certain organic solvents. J. Am. Chem. Soc. 38, 633–638.

Yan, W., Acharjee, T.C., Coronella, C.J., Vasquez, V.R., 2009. Thermal pretreatment of lignocellulosic biomass. Environ. Prog. Sustain. Energy 28, 435–440.

Yin, D.T., Bernhardt, P., Morley, K.L., Jiang, Y., Cheeseman, J.D., Purpero, V., Schrag, J.D., Kazlauskas, R.J., 2010. Switching catalysis from hydrolysis to perhydrolysis in *Pseudomonas fluorescens* esterase. Biochemistry 49, 1931–1942.

Yin, D.T., et al. in preparation. Molecular basis of enzyme-catalyzed perhydrolysis of esters.

Yuan, Z., Ni, Y., Van Heiningen, A.R.P., 1997. Kinetics of peracetic acid decomposition: Part I: spontaneous decomposition at typical pulp bleaching conditions. Can. J. Chem. Eng. 75, 37–41.

Zheng, Y., Pan, Z., Zhang, R., 2009. Overview of biomass pretreatment for cellulosic ethanol production. Int. J. Agric. Biol. Eng. 2, 51–68.

DOI: 10.1002/adsc.201100459

Molecular Basis of Chiral Acid Recognition by *Candida rugosa* Lipase: X-Ray Structure of Transition State Analog and Modeling of the Hydrolysis of Methyl 2-Methoxy-2-phenylacetate

Ian J. Colton,[a,d] DeLu (Tyler) Yin,[b] Pawel Grochulski,[c,e,*] and Romas J. Kazlauskas[a,b,*]

[a] McGill University, Department of Chemistry, 801 Sherbrooke Street West, Montréal, Québec H3A 2K6, Canada
[b] University of Minnesota, Department of Biochemistry, Molecular Biology & Biophysics and The BioTechnology Institute, 1479 Gortner Avenue, Saint Paul, MN 55108, USA
Fax: (+1)-612-625-5780; e-mail: rjk@umn.edu
[c] National Research Council of Canada, Biotechnology Research Institute, 6100 Royalmount Avenue, Montréal, Québec H4P 2R2, Canada
[d] Current address: Gowlings, 160 Elgin Street, Suite 2600, Ottawa, Ontario K1P 1C3, Canada
[e] Current address: Canadian Light Source, University of Saskatchewan, 101 Perimeter Road, Saskatoon, SK S7N 0X4, Canada
E-mail: pawel.grochulski@lightsource.ca

Received: June 5, 2011; Revised: August 26, 2011; Published online: September 5, 2011

Supporting information for this article is available on the WWW under http://dx.doi.org/10.1002/adcs.201100459.

Abstract: Lipase from *Candida rugosa* shows high enantioselectivity toward α-substituted chiral acids such as 2-arylpropionic acids. To understand how *Candida rugosa* lipase (CRL) distinguishes between enantiomers of chiral acids, we determined the X-ray crystal structure of a transition-state analog covalently linked to CRL. CRL shows moderate enantioselectivity ($E=23$) toward methyl 2-methoxy-2-phenylacetate, **1**-methyl ester, favoring the (*S*)-enantiomer. We synthesized phosphonate (R_C,R_P,S_P)-**3**, which, upon reaction with CRL, mimics the transition state for hydrolysis of (*S*)-**1**-methyl ester, the fast-reacting enantiomer. An X-ray crystal structure of this complex shows a catalytically productive orientation with the phenyl ring in the hydrophobic tunnel of the lipase. Phe345 crowds the region near the substrate stereocenter. Computer modeling of the slow-reacting enantiomer examined four possible conformations for the corresponding slow-reacting enantiomer: three conformations where two substituents at the stereocenter have been exchanged relative to the fast-reacting enantiomer and one conformation with an umbrella-like inversion orientation. Each of these orientations disrupts the orientation of the catalytic histidine, but the molecular basis for disruption differs in each case showing that multiple mechanisms are required for high enantioselectivity.

Keywords: carboxylic acids; enantioselectivity; enzyme catalysis; hydrolases; molecular dynamics; phosphonates; protein structures; transition-state analogs; X-ray diffraction

Introduction

Lipases often accept unnatural ester substrates and show high enantioselectivity and are therefore useful in organic synthesis. One of the best-studied lipases for its enantioselectivity toward chiral acids is lipase from *Candida rugosa* (CRL). This lipase shows high enantioselectivity toward many carboxylic acids with a stereocenter at the α-position. Examples include 2-arylpropionic acids such as naproxen [aryl=2-(6-methoxy)naphthyl], which are non-steroidal anti-inflammatory drugs and 2-aryloxypropionic acids, such as dichlorprop (aryloxy=2,4-dichlorophenoxy), which are herbicides, and can also reduce blood cholesterol levels.[1,2]

An empirical rule predicts the favored enantiomer of chiral carboxylic acids for *Candida rugosa*-catalyzed reactions[3] (Figure 1). The rule applies to carboxylic acids with a stereocenter at the α-position and relies on the sizes of the substituents at the stereocenter. This rule suggests that CRL distinguishes enantiomers based on the size of the substituents.

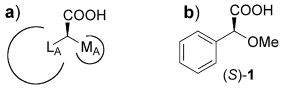

Figure 1. An empirical rule based on substituent size predicts the faster-reacting enantiomer in hydrolyses of esters catalyzed by purified *Candida rugosa* lipase. **a**) Generic structure of the acid predicted to form faster from the corresponding ester. L_A represents a large substituent, while M_A represents a medium substituent. **b**) An example of a carboxylic acid that fits this rule. Hydrolysis of racemic methyl 2-methoxy-2-phenylacetate favors the (*S*)-enantiomer shown by a factor of 23 over the (*R*)-enantiomer.[4]

The molecular details of this enantioselectivity are still unclear. One cannot accurately predict the degree of enantioselectivity, nor can one predict which amino acid substitutions will increase enantioselectivity. An understanding of these details is essential for rational design of enantioselective enzyme-catalyzed reactions. This understanding could also help organic chemists design chemical catalysts with high enantioselectivity.

The compound 2-methoxy-2-phenylacetic acid (*O*-methylmandelic acid, **1**) is the focus of this work. Enantiomerically pure 2-methoxy-2-phenylacetic acid is a useful reagent for NMR analysis of the absolute stereochemistry of amines and alcohols.[5] Lipase from *Aspergillus niger* resolved the corresponding vinyl ester of **1** by transesterification with methanol in isopropyl ether with an enantioselectivity of 25,[6] but this lipase is not considered in this paper. This chiral acid is similar in structure to the 2-arylpropionic acids mentioned above and is a general example for the CRL-catalyzed hydrolysis of esters of chiral acids.

The genome of the yeast *Candida rugosa* contains at least seven lipase isoenzymes named lip1–7. The isoenzymes differ in amino acid sequence ($\geq$80% amino acid sequence identity among lip1–5, $\geq$65% among 1–7), isoelectric point and degree of glycosylation.[7] Commercial samples of *Candida rugosa* lipase are non-recombinant enzymes and contain multiple isozymes. Gel electrophoresis (SDS-PAGE) of commercial samples of CRL shows a major band and minor band. The major band corresponds to lip1, while the minor band is a mixture of isoenzymes lip2–5. In addition, commercial samples of CRL contain a small amount of contaminating protease.[8] The X-ray crystal structures of three isoenzymes have been solved: lip1,[9,10] lip2[11] and lip3.[12]

The isoenzymes differ in their enantioselectivity toward acids and secondary alcohols, but show the same enantiopreference.[13,14] Isoenzyme lip1, the focus of this paper, shows the highest enantioselectivity toward ibuprofen {2-[4-(2-methylpropyl)phenyl]-propanoic acid}, which, among the compounds tested, is closest in structure to compound **1**. Besides isoenzyme composition, the purification procedure can also change the enantioselectivity, but not the enantiopreference, of CRL.[14,15,16] The working hypothesis is that purification steps such as treatment with organic solvents can change the conformation of the lipase, possibly from the closed to the open conformation.

Commercial samples of CRL show low enantioselectivity ($E=8$) toward methyl 2-methoxy-2-phenylacetate (**1**-methyl ester), favoring the (*S*)-enantiomer[4]. Purified CRL (A-form, which likely corresponds to lip1) shows higher enantioselectivity: $E=23$ (*S*).[4] This paper focuses on the molecular basis for this enantioselectivity.

CRL-catalyzed hydrolysis of esters occurs in two steps: acylation of the active site serine followed by deacylation (Figure 2). The acylation step involves the first tetrahedral intermediate, $\mathbf{T_d1}$, while the deacylation step involves the second tetrahedral intermediate, $\mathbf{T_d2}$. The first irreversible step in hydrolysis is the acylation step. (Although in principle, this step is reversible, in practice the concentration of leaving group alcohol is low so it is effectively irreversible.) This acylation step is also likely the rate-determining step because substrates with a better leaving group react faster. Kinetic studies of another lipase showed that acylation was the rate-determining step.[17]

A tetrahedral intermediate exists for only a short time, but a stable phosphonate mimics this intermediate. We synthesized phosphonate inactivators that could react with the active site serine in CRL and make a stable phosphonate. We solved the X-ray crystal structure of the CRL-phosphonate complex corresponding to the tetrahedral intermediate for the fast-reacting enantiomer of **1**-methyl ester. We also synthesized the phosphonochloridate corresponding to the slow-reacting enantiomer, but it did not form a covalent complex with CRL. We investigated the orientations of the slow-reacting enantiomer using molecular modeling and identified the multiple molecular interactions required to prevent its reaction. This understanding is an essential first step to the rational design of higher enantioselectivity, but also shows the complexity and difficulty of the task.

Results

Synthesis of Transition State Analogs

Racemic Inactivators

Two racemic inactivators – the chloro and *p*-nitrophenyl (PNP) derivatives, (±)-**3** and (±)-**4**, were prepared as diastereomeric mixtures (Figure 3). Benzaldehyde and dimethyl phosphite condensed over solid KF to form dimethyl (1-hydroxyphenylmethyl)-phosphonate, (±)-**2**, according to a literature proce-

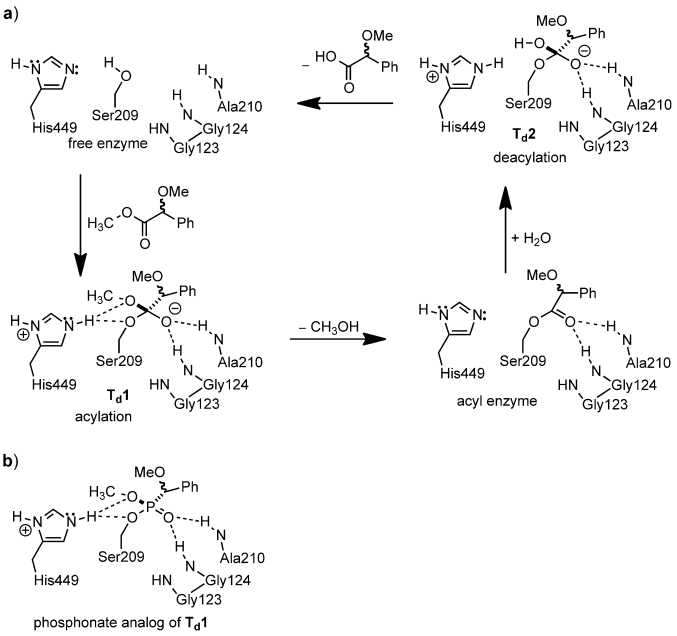

Figure 2. a) Mechanism of CRL-catalyzed hydrolysis of racemic methyl 2-methoxy-2-phenylacetate [(±)-**1**-methyl ester] involves two tetrahedral intermediates and an acyl enzyme intermediate. The rate-determining step is the formation of the acyl enzyme intermediate, which involves formation and collapse of the first tetrahedral intermediate. The transition state for the reaction therefore resembles the first tetrahedral intermediate. For clarity, this Scheme omits the third member of the catalytic triad, Glu341. **b**) A stable phosphonate mimics the first tetrahedral intermediate and the transition state for hydrolysis of (±)-**1**-methyl ester.

dure[18] in 88% yield. Methylation of (±)-**2** using methyl iodide and Ag_2O afforded dimethyl [1-(methoxy)phenylmethyl]phosphonate in 66% isolated yield. This methylation was the most difficult reaction to optimize in this synthesis. Initial trials using basic conditions (MeI/K_2CO_3 in EtOAc or MeI/KOH in DMSO) yielded an uncharacterized decomposition product, likely due to reversion of (±)-**2** back to starting materials under basic conditions[19] and subsequent decomposition. Using the neutral silver oxide to increase the electrophilicity of methyl iodide avoided these problems. A stoichiometric amount of methyl iodide gave inconsistent yields for this methylation step, likely due to evaporation of methyl iodide, but using methyl iodide as the solvent eliminated this problem and was the optimum way to carry out this step. Hydrolysis of dimethyl [1-(methoxy)phenylmethyl]phosphonate using aqueous base afforded the monoacid in 85% yield. Monochlorination, using 1.5 equivalents of oxalyl chloride in refluxing dichloromethane, yielded a 4:1 diastereomeric mixture of mono-

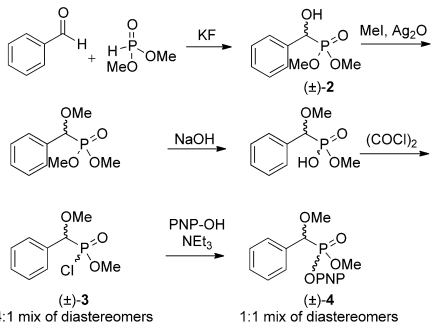

Figure 3. Synthesis of racemic inactivators chloro derivative (±)-**3** and *p*-nitrophenyl derivative (±)-**4**. Only the chloro derivative (±)-**3** inactivated lipase from *Candida rugosa*. PNP = *p*-nitrophenyl

chlorophosphonates, (±)-**3**. Reaction of the monochlorophosphonates with *p*-nitrophenol and triethylamine resulted in a 1:1 mixture of diastereomers, (±)-**4** in 20% overall yield.

Inactivator (±)-**3** inactivated lipase from *Candida rugosa*, but inactivator (±)-**4** did not. Incubation of a 10^3-fold excess of (±)-**3** dissolved in dichloromethane with an aqueous solution of lipase from *Candida rugosa* eliminated >99% of the hydrolytic activity within 8 min. In contrast, overnight incubation of a 10^4-fold excess of (±)-**4** with CRL, eliminated <5% of the hydrolytic activity. Since the chlorophosphonate (±)-**3** was a good inactivator, we prepared compound **3** with a single configuration at the carbon center.

Inactivator 3 Having a Single Configuration at the Carbon Center

The chloro derivative **3** with a single configuration at the carbon center was prepared similarly, but with the addition of a lipase-catalyzed kinetic resolution (Figure 4). Secondary alcohol (±)-**2** was converted to the acetate, (±)-**5**, which was resolved using lipase from *Rhizopus oryzae* (Amano FAP 15) yielding (*S*)-**2** (78% recovery, 68% *ee*) and recovered starting acetate (*R*)-**5** (65% recovery, 88% *ee R*). These enantiomeric purities correspond to an E of 32, significantly lower than the reported E of >100 for this resolution by Li and Hammerschmidt.[20] To increase the enantiomeric purity, the acetate was resolved two more times with the same enzyme. Reincubation of the acetate (68% *ee R*) with lipase for an additional 26.8% conversion, then separation and reincubation for an additional 10.3% conversion yielded the remaining acetate in >98% *ee R*, 0.4 g, 14% overall yield (50% yield is the maximum in a resolution). This acetate was cleaved with triethylamine-methanol to yield (*R*)-**2** for the next step in the synthesis. To prepare enantiomerically pure (*S*)-**2**, we reacetylated enantiomerically enriched (*S*)-**2** to the acetate (*S*)-**5** and carried out a second hydrolysis catalyzed by the lipase until 46% conversion, which yielded (*S*)-**2** in >98% *ee*, 0.11 g (4.4% overall yield).

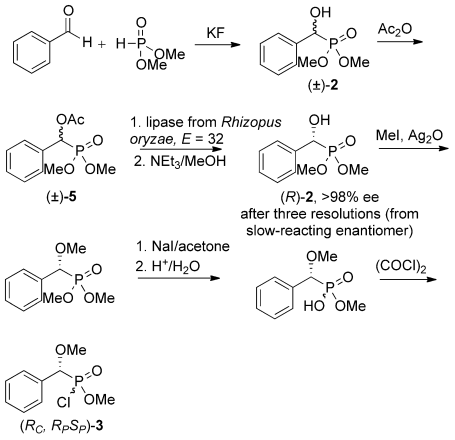

Figure 4. Synthesis of inactivator (R_C,$R_P$$S_P$)-**3**, which, upon reaction with lipase from *Candida rugosa*, mimics the transition state for the CRL-catalyzed hydrolysis of (*S*)-**1** methyl ester (fast-reacting enantiomer). A key step in the synthesis of inactivator (R_C,$R_P$$S_P$)-**3** was a lipase-catalyzed resolution of acetate (±)-**5** by lipase from *Rhizopus oryzae*. An analogous route (not shown) formed phosphonate (S_C,$R_P$$S_P$)-**3**, which mimics hydrolysis of the slow-reacting (*R*)-enantiomer of **1**-methyl ester.

Methylation of (*R*)-**2** used silver oxide and excess methyl iodide as developed for the racemic alcohol, (±)-**2**. The overall yield for the hydrolysis of the acetate and methylation was 50%. Hydrolysis of (*R*)-dimethyl [1-(methoxy)phenylmethyl]phosphonate to the monoacid used 1.5 equivalents of NaI in refluxing acetone, followed by acidification to afford (*R*)-monoacid (83% yield). These milder conditions for the hydrolysis, as compared to the NaOH used to hydrolyze the racemate in Figure 3, minimized the possibility for racemization at the resolved stereocenter. The enantiomeric purity of **2** was measured after reacetylation with acetic anhydride to the acetate **5**, by ^{1}H NMR in the presence of a chiral shift reagent, Eu(hfc)$_3$, but the enantiomeric purity of the subsequent compounds could not be measured.

Finally, chlorination of the monoacid using 100 equivalents of of oxalyl chloride yielded a 4:1 mixture of the two phosphonochloridates, (R_C,$R_P$$S_P$)-**3** as observed by ^{1}H and ^{31}P NMR. Reaction of the monoacid with less oxalyl chloride yielded a substantial amount of pyrophosphonate side product, which did not inactivate CRL.

An analogous route (not shown) formed phosphonate (S_C,$R_P$$S_P$)-**3**, which mimics hydrolysis of the slow-reacting (*R*)-enantiomer of **1**-methyl ester.

X-Ray Crystal Structure

The covalent enzyme-inhibitor complex was prepared by adding excess (R_C,$R_P$$S_P$)-**3** diastereomeric mixture dissolved in 2-methyl-2,4-pentanediol to the purified CRL solution. The inhibited protein crystallized under conditions similar to those for the open form CRL.[9] The crystal structure was solved by isomorphous replacement with the open form CRL structure. As expected from the synthesis, the configuration at the carbon stereocenter was *R* (Figure 5). The

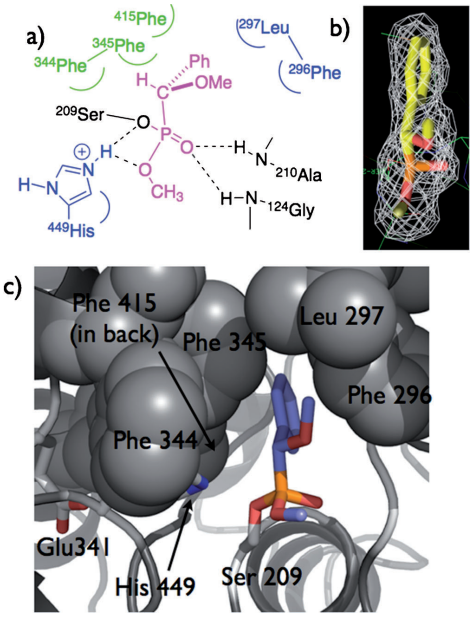

Figure 5. Phosphonate transition state analog for hydrolysis of (*S*)-**2** in the active site of CRL. **a**) Schematic diagram. **b**) The model of the phosphonate fits well in the observed electron density. The mesh represents the difference simulated annealing omit map at the 3 sigma level. The inhibitor and all protein atoms within a 3.5 Å sphere from the inhibitor were excluded from calculations. **c**) X-ray crystal structure. The analog mimics a catalytically productive orientation because the phosphorus links covalently to the catalytic serine (Ser209) and the analog makes good hydrogen bonds (O–N distances <3.2 Å) to the catalytic histidine (His449; shown as sticks for clarity) and the oxyanion hole (Ala210, Gly124). The carbon stereocenter lies at the entrance to a tunnel with the phenyl group pointing inside the tunnel. Residues Phe344, Phe345, and Phe415 (mostly hidden by Phe344 and Phe345) block the left side of the tunnel entrance. A hydrogen substituent can fit here, but not an OMe substituent. Residues Leu297 and Phe296 form the right side of the tunnel entrance. Site-directed mutagenesis experiments previously identified Phe344 and Phe345 as important for the enantioselectivity of CRL toward 2-arylpropionic acids.

configuration at phosphorus was also a single configuration (S_P) although the inhibitor was a mixture of both configurations at phosphorus. Presumably, the inhibitor with one phosphorus configuration reacted much faster that the other leading to only the fast-reacting phosphorus configuration bound to the lipase.

The overall structure is identical to the open form of *Candida rugosa* lipase.[9] The lipase adopts the α/β hydrolase fold. The protein scaffold is formed by a central 11-stranded mixed β-sheet and an N-terminal 3-stranded β-sheet. The flap is in its open conformation and is stabilized by Glu66 which is preceded by a proline at one hinge and by the Pro92 *cis-trans* isomerization at the other hinge. The X-ray structure of the closed form of CRL[10a] was solved previously using different crystallization conditions and without a phosphonate inhibitor. The transition state analog in the current structure is well defined in the electron density. There are 3 sugar molecules and 175 water molecules identified in the electron density. The overall geometry of the molecule is very good (Table 1) with the final $R/R_{free}=17/21\%$, average B-factor of 22.6 Å^2 and good stereochemistry.

Table 1. Data collection and refinement statistics for x-ray structure of the complex of inactivator (R_C,R_P,S_P)-**2** with *Candida rugosa* lipase, which mimics reaction of the fast-reacting enantiomer (*S*)-**1**.

Crystal parameters and diffraction data	
X-ray source	CuK_α
Space group	$C222_1$
Unit cell dimensions (Å)	$a=65.0$
	$b=97.5$
	$c=176.1$
Data collection statistics	
Total number of accepted reflections	51,648
Total number of unique reflections[a]	23,670 (2,716)
Resolution range (Å)	54.1–2.2
Highest shell (Å)[a]	2.3–2.2
R_{merge} (%)[b]	9.2 (23.0)
Mean I/σI	10.5 (3.1)
Completeness (%)	81.0 (62.5)
Refinement statistics	
Protein molecules in asymmetric units	1
Number of water molecules	175
Number of sugar molecules	3
Number of Ca^{2+}	2
Final R/R_{free} factors[c]	17/21
Average B-factor (Å^2)	22.6
r.m.s deviations bond lengths (Å)	0.006
r.m.s deviations bond angles (°)	1.3
Ramachandran statistics: favored (%), allowed (%), outlier (%)	93.4, 5.1, 1.5

[a] Data for the highest resolution shell are given in parentheses.

[b] $R_{merge}=|\Sigma_{hkl}\ \Sigma_i|I_i(hkl)-<I(hkl)>|/\Sigma_{hkl}\ \Sigma_i|I_i\ (hkl)$, where I(hkl) is the observed intensity and $<I(hkl)>$ is the average intensity obtained from multiple observations of symmetry-related reflections after rejection.

[c] $R=\Sigma||Fo|-|Fc||/\Sigma|Fo|$, where Fo and Fc are the observed and calculated structure factors, respectively. R_{free} is calculated using 9.9% of the reflections randomly excluded from refinement.

The crystal structure of the transition state analog confirms that the stereocenter matches the fast-reacting enantiomer because of the good fit of this stereoisomer with the measured electron density (Figure 5). The electron density was obtained by running a simulated annealing refinement with the analog and nearby protein atoms (within 3.5 Å) omitted. The calculated unbiased difference map confirms the selected enantiomer.

The carbon stereocenter of the inhibitor lies at the mouth of a tunnel with the phenyl ring pointing inside the hydrophobic tunnel (Figure 5). This tunnel accommodates the fatty acyl chains of other inhibitors. The methoxy substituent at the carbon stereocenter points toward Phe296, while the hydrogen at the carbon stereocenter points toward Phe344.

Similar crystals formed using the phosphonochloridate mimicking the slow-reacting enantiomer showed no inhibitor in the active site. Presumably the slow reacting enantiomer fits so poorly that this inhibitor did not react with the lipase.

Modeling to Find Possible Orientations of the Slow-Reacting Enantiomer

To identify the orientation of the slow enantiomer, we used molecular modeling. There are four ways that the slow enantiomer can bind in the same place in CRL as the fast enantiomer. Three of these possibilities involve an exchange of two substituents at the stereocenter and one possibility involves an umbrella-like inversion orientation[21] (Figure 6). An analogy to these different possibilities is the two different ways that you can overlay your right and left hand, Figure 6 (**b**). In one way the two palms face in the same direction, but the finger do not align, which is similar to one of the exchange of substituents possibilities. In the second way, the palms face in opposite directions, but fingers line up correctly, which is similar to the umbrella-like inversion. High enantioselectivity requires the lipase to prevent reaction of the slow enantiomer in any of these four orientations.

To identify how CRL prevents hydrolysis of (*R*)-**1** in all four possible orientations, we modeled tetrahe-

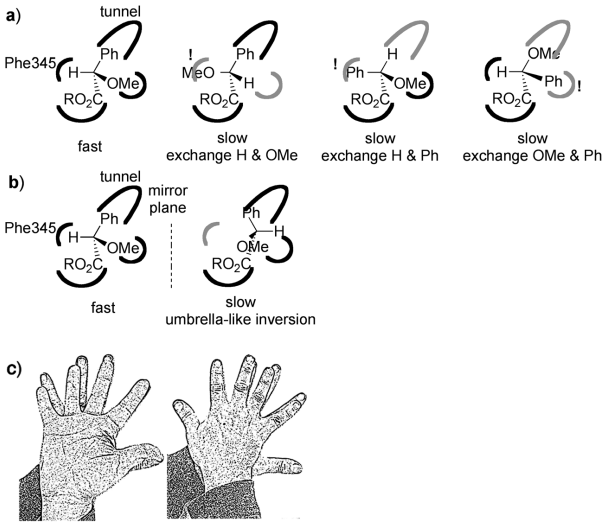

Figure 6. Possible orientations of the slow enantiomer of **1** in the active site of *Candida rugosa* lipase. **a**) Schematic of the fast-reacting enantiomer of methyl 2-methoxy-2-phenylacetate [(*S*)-**1**, left] and three possible exchange-of-substituents orientations for the slow enantiomer [(*R*)-**1**, right three structures]. The curves lines represent the active site; gray curves indicate the two positions that have mismatched substituents for the slow enantiomer. The exclamation points mark points where steric interactions disfavor the three orientations for the slow enantiomer. **b**) Schematic of the fast-reacting enantiomer (*S*, *left*) and an umbrella-like inversion orientation of the slow enantiomer (*R*, *right*) in the same site. The mirror plane shown relates the two substrate molecules. This reflection places the hydrogen substituent of the slow enantiomer in a new location leaving the original site empty (gray curve). **c**) An analogy to these different possible orientations is the two ways to overlay your right hand on top of your left hand. On the left panel, the fingers match with each other, but the palms face in opposite directions: bottom hand palm faces down, while top hand palm faces up. On the right panel, the fingers do not overlay correctly, but both palms face down.

dral intermediates corresponding to these four possibilities. These tetrahedral intermediates were built using the crystal structure of the phosphonate analog for hydrolysis of (*S*)-**1** as the model. The modeling used the OPLS 2005 force field[24] for the lipase and tetrahedral intermediate and a TIP3P model[25] for the water solvent. A molecular dynamics simulation generated multiple conformations of each possible orientation to mimic the multiple conformations possible during the reaction.

The tetrahedral intermediate must form four catalytically important hydrogen bonds with the lipase: from the two N–H bonds of the oxyanion hole (Ala124, Gly210) to the oxyanion oxygen of the tetrahedral intermediate and from N_ε–H of the catalytic histidine to the alcohol oxygen of the tetrahedral intermediate and to O_γ of active site serine, see Figure 3 above. Conformations containing all five catalytically essential hydrogen bonds were considered catalytically productive, while those missing one or more hydrogen bonds were considered non-productive. The fraction of catalytically productive conformations among all the conformations generated by molecular dynamics in each case indicates the likelihood that the reaction can occur. Since the enantioselectivity of CRL lip1 toward **1** is 23, we expect the fraction of catalytically productive conformations to be 23-fold lower for (*R*)-**1** as compared to (*S*)-**1**.

This modeling approach is similar to the near-attack-complex modeling developed by Bruice and co-workers.[22] A near attack complex is not an intermediate, but a fleeting structure where the distances and angles are close to those needed for the reaction. Our approach differs by not modeling a near attack complex, but the tetrahedral intermediate. Lipase-catalyzed hydrolysis of an ester involves the formation and collapse of a tetrahedral intermediate. The structures of the transition states for formation and collapse of the tetrahedral intermediate are similar to the tetrahedral intermediate, so this modeling approach models the reactivity of each case.

Modeling correctly predicts that the tetrahedral intermediate for hydrolysis of (*S*)-**1**-methyl ester adopts a catalytically productive orientation (Table 2). The geometry of the 250 structures generated by the molecular dynamic simulation were measured to identify hydrogen bonds between the lipase and the tetrahedral intermediate. Hydrogen bonds were defined as an O–N distance of <3.55 Å and an O–H–N angle $>120°$ (180° is ideal). These criteria are permissive to include the entire range of hydrogen bond distances observed in proteins.[23] The (*S*)-enantiomer formed all four catalytically essential hydrogen bonds to the protein in 51% of the structures, which is consistent with the experimental result that (*S*)-**1**-methyl ester is a good substrate. The structures of the modeled tetrahedral intermediate were similar to the phosphonate X-ray crystal structure; Figure 7 shows a typical structure.

Modeling also correctly predicts that the slow enantiomer reacts very slowly because it only rarely adopts a catalytically productive orientation (Table 1). Almost all orientations disrupt at least one of the two hydrogen bonds to the catalytic histidine. The exception is the (*R*)-exchange H/OMe orientation where one of the 250 modeled conformations (0.4%) showed intact catalytic hydrogen bonds. The rarity of this catalytically productive conformation indicates that reaction of the (*R*)-enantiomer is much slower than for the (*S*)-enantiomer.

The (*R*)-exchange H/Ph orientation disrupts three key hydrogen bonds in most conformations: two from

Table 2. Percentage of conformations that contain a hydrogen bond between the partners indicated.[a]

	Oxyanion oxygen of tetrahedral intermediate			His449-N_ε-H		
Conformation	Ala124-*N*-H, %	Gly210-*N*-H, %	Ser209-Oγ, %	Me-O, %	All four productive H-bonds, %	Glu208-O (non-productive), %[b]
(*S*)	82 (100)	100 (100)	93 (89)	78 (88)	51	7.5 (59)
(*R*)-exchange H/Ph	100 (100)	12 (100)	0.79 (0)	87 (0)	0	100 (100)
(*R*)-exchange OMe/Ph	100 (100)	100 (100)	60 (1.6)	0.40 (2.8)	0	99 (98)
(*R*)-exchange H/OMe	100 (100)	100 (100)	100 (99)	0.39 (99)	0.39	25 (0.40)
(*R*)-umbrella	98 (100)	100 (100)	0.39 (0)	65 (0)	0	100 (100)

[a] Percentage of the structures where the N–O distance is <3.55 Å. The numbers in parentheses indicate the percentage of the structures where the N–H–O angle is $>120°$. The data is in Figure S-1, Figure S-2, and Figure S-3 in the Supporting Information.

[b] In some non-productive structures a catalytically non-productive hydrogen bond formed between the catalytic histidine and the side chain of Glu208.

the catalytic histidine to the catalytic serine O_γ and to the substrate's ester oxygen and one from Ala124 N–H to the oxyanion oxygen. The side chains of Phe415 and Phe345 restrict the space available for the phenyl group, so it bumps into the catalytic histidine and moves the imidazole ring (Figure 7). The hydrogen

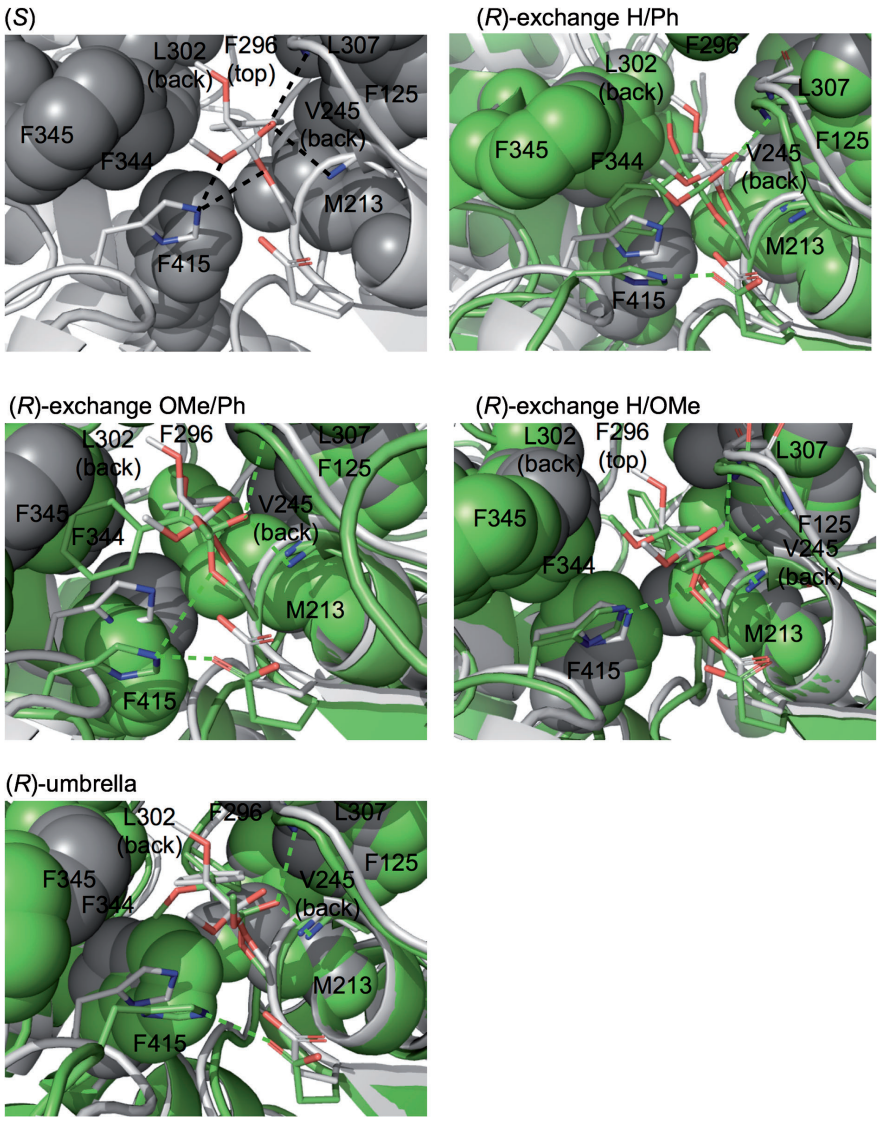

Figure 7. Representative structures from molecular dynamics modeling of tetrahedral intermediates for hydrolysis of (*S*)- and (*R*)-**1**. For (*S*)-**1** (gray), all four catalytically important hydrogen bonds are present (dotted lines). In all four orientations of (*R*)-**1** [green overlaid on the gray structure of (*S*)-**1**], one or both of the hydrogen bonds from the catalytic histidine to either the catalytic serine O_γ or the substrate's ester oxygen are missing.

bond donor atom, N_ε moves by 3.3 Å as compared to the (S) enantiomer and thus breaks the two hydrogen bonds between His-N_ε the tetrahedral intermediate. The overall tetrahedral intermediate moves by 1.0 Å towards the reader's left, which disrupts a key hydrogen bond between the oxyanion and main-chain amide of Ala210. None of the conformations identified by molecular dynamics contain all four essential hydrogen bonds; thus, none were catalytically productive.

The (*R*)-exchange OMe/Ph orientation disrupts the two key hydrogen bonds between the catalytic histidine and the catalytic serine O_γ and the substrate's ester oxygen. The initial model for this orientation places the phenyl group point upward where it clashes with Phe296. During geometry optimization, the substrates phenyl group moves, bumps into the catalytic histidine and moves the imidazole ring (Figure 7). The hydrogen bond donor atom, N_ε moves by 3.6 Å as compared to the (S) enantiomer and thus breaks the two hydrogen bonds between His-N_ε the tetrahedral intermediate.

The (*R*)-exchange H/OMe orientation disrupts only one hydrogen bond – between the catalytic histidine and the substrate's ester oxygen. The methoxy group at the stereocenter bumps into Phe344 causing the entire tetrahedral intermediate to shift 0.7 Å to the reader's right. The shift breaks a key hydrogen bond between His449 and the ester oxygen. In one conformation out of 250 (0.40%) all catalytically essential hydrogen bonds are present.

The (*R*)-umbrella orientation disrupts only one hydrogen bond – between the catalytic histidine and the catalytic serine O_γ. As the phenyl group moves to a position similar to the (*S*)-enantiomer, the methoxy group at the stereocenter bumps into the catalytic histidine and moves the imidazole ring (Figure 7). The hydrogen bond donor atom, N_ε moves by 3.0 Å as compared to the (*S*) enantiomer and thus breaks the hydrogen bonds between His-N_ε and the catalytic serine O_γ.

In place of the disrupted hydrogen bonds between the catalytic histidine and either the catalytic serine or substrate ester OMe, a new hydrogen bond forms between His-Nε and Glu-O (Table 2). This hydrogen bond is not catalytically productive because it does not stabilize the tetrahedral intermediate. The fast-reacting enantiomer (*S*)-**1**-methyl ester forms this hydrogen bond only rarely, 7.5% of the time. In contrast, the slow-reacting enantiomer orientations usually make this non-productive hydrogen bond. Three orientations – exchange H/Ph, exchange OMe/Ph, and umbrella – make it nearly all the time. The (*R*)-exchange H/OMe orientation make this hydrogen bond only 25% of the time, but it also forms another non-productive hydrogen bond between the ester oxygen and the main-chain amide of Gly123 – this hydrogen bond forms 31% of the time. This hydrogen bond is non-productive because the N–H cannot donate a proton to leaving group OMe because the pK_a of an amide N–H (~17) is higher than the pK_a of methanol (15).

The slow enantiomer most likely reacts *via* either the (*R*)-exchange H/OMe orientation or the (*R*)-umbrella orientation. These orientations are closest to a catalytically productive orientation because they lack only one hydrogen bond as compared to three for (*R*)-exchange H/Ph and two for (*R*)-exchange OMe/Ph. The other three orientations also make a non-productive hydrogen bond with the catalytic histidine all the time, but this exchange H/OMe orientation makes non-productive hydrogen bonds only 56% of the time. This non-productive hydrogen bond occupies the histidine and prevents reaction. We hypothesize that protein engineering efforts to increase enantioselectivity should focus on further destabilizing the (*R*)-exchange H/OMe orientation and the (*R*)-umbrella orientation.

The modeling does not quantitatively match the experimental results. We identified only one out of 1000 modeled conformations (0.1%) for the slow reacting enantiomer that were catalytically productive. Since 51% of the conformations were catalytically productive for the fast-reacting enantiomer and the slow-reacting enantiomer reacts 23-fold slower, quantitative agreement requires ~2% of the conformation for the slow-reacting enantiomer to be catalytically productive. The reason for the lack of agreement is unknown and could be due to imperfect modeling or due to an underestimate of the enantioselectivity; for example, if the enzyme contained a contaminating less enantioselective isozyme.

Discussion

Orientation of the Fast-Reacting Enantiomer

Previous computer modeling and extrapolation from X-ray crystal structures indicated that chiral acids with an α-stereocenter bind to CRL with the stereocenter positioned at the mouth of the tunnel and the large substituent extending into the tunnel. The X-ray structure reported in this paper confirms this hypothesis. The phenyl group lies inside the tunnel, while the medium substituent (methoxy) points upward near Phe296 and Leu297 residues, while the hydrogen points toward Phe344, Phe345 and Phe415. The binding site for chiral secondary alcohols overlaps with this region. The hydrophobic region consisting of Phe296, Phe344, Phe345 and Leu297 also corresponds to the 'large pocket' for secondary alcohols.

Orientation of the Slow-Reacting Enantiomer

Previous modeling and experiments with chiral acids proposed differing orientations of the slow-reacting enantiomer, likely because the researchers studied different chiral acids. Both the proposed orientations are exchange-of-substituents conformations, while our proposed umbrella-like inversion orientation is a new proposal.

Molecular modeling of the CRL-catalyzed resolution 2-arylpropionic acids suggested that the slow enantiomer reacts *via* a hydrogen/medium (methyl) exchange-of-substituents orientation.[24,25,26] Modeling naproxen (aryl = 6-methoxy-2-naphthyl) in the active site of CRL placed the aryl group in the tunnel. For the fast-reacting enantiomer, the methyl group at the stereocenter pointed toward Phe296, as does the methoxy group in the phosphonate structure in this paper. For the slow reacting enantiomer, the hydrogen and methyl group at the stereocenter exchange positions (Figure 8). This is the same conclusion that we came to for **1**-methyl ester, whose structure is closest to the 2-arylpropionic acids. Modeling of 2-(4-substituted phenoxy)propionic acid also suggested that the methyl and hydrogen exchange locations when the slow enantiomer reacts.[27]

The enantioselectivity of CRL toward naproxen increases at higher temperatures indicating that entropic effects favor the fast reacting enantiomer.[28] The fast enantiomer may be more flexible in the active site, while the slow enantiomer can only react *via* a rarely reached conformation.

In contrast, the slow enantiomer of 2-methylalkanoic acids, where the large group is *n*-alkyl, likely reacts in reacts *via* a medium (methyl)/large (*n*-alkyl) exchange-of-substituents orientation.[29] The experimental evidence is that adding long-chain alcohols decreases the enantioselectivity of the CRL-catalyzed esterification of 2-methyldecanoic acid from $E = 83$ (90 mM n-heptanol) to $E = 37$ (900 mM *n*-heptanol).[30] The decreased enantioselectivity stems from slower reaction of the fast enantiomer, but no change in the reaction rate of the slow enantiomer. To fit the slow-reacting enantiomer, Holmquist and co-workers first exchanged the locations of the hydrogen and methyl group, but found that this orientation displaced the catalytic histidine and was therefore not catalytically productive. Next, they exchanged the methyl and *n*-alkyl groups. The methyl group pointed into the tunnel, while the alkyl group was near Phe296 and extended toward the solvent. Enantioselective inhibition by the long-chain alcohols occurs when the alcohol binds in the tunnel. This binding does not affect the binding of the slow-reacting enantiomer, but it blocks the fast-reacting enantiomer, resulting in lower enantioselectivity.

Further support for this exchange of medium and large group locations came from a reversal of enantioselectivity for substrates that do not fit into the tunnel.[31] The CRL-catalyzed hydrolysis of ethyl 2-methyl-6-(2-thienyl)hexanoate favored the (*R*)-enantiomer, in contrast to (*S*)-2-methyldecanoate. The 2-thienyl group made the alkyl chain too large to fit in the tunnel, so it binds near Phe 296 and extends toward the solvent. This reversal supports the notion that the methyl/*n*-alkyl exchange is a catalytically productive orientation and can account for the reaction of the slow enantiomer of 2-methyldecanoic acid. (The experiments in refs.[34–37] mentioned above used crude CRL so minor isozymes may contribute to the results. The major isozyme lip1 is most likely the main contributor.)

Increasing the enantioselectivity of CRL toward chiral acids is difficult for two reasons. First, different orientations of the slow enantiomer are possible. High enantioselectivity requires preventing reaction

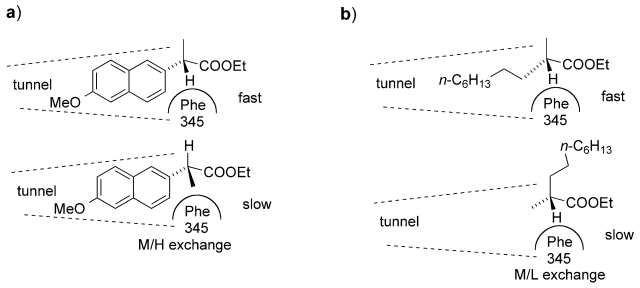

Figure 8. Different proposed orientations of the slow enantiomer in CRL-catalyzed resolutions of chiral acids. **a**) For 2-arylpropionic acids, the slow enantiomer likely reacts *via* a medium (methyl)/hydrogen exchange. **b**) For 2-methylalkanoic acids, where the large group (*n*-alkyl) is more flexible, the slow enantiomer likely reacts *via* a medium (methyl)/large (*n*-alkyl) exchange.

via all of them, which is complex since changes that hinder one orientation may help another orientation. Second, exchanging amino acids near the substrate is a gigantic change on a molecular scale. Changing one amino acid, for example, Phe to Leu, removes several atoms; assuming no addition rearrangements, the side chain is now at least 2 Å further from the substrate. This is a large distance on a molecular scale. Contrast this change to the ability to increase the cylinder size in an engine by a millimeter, which is a much more subtle change. The alternative in protein engineering is to change not the amino acids directly in contact with the substrate, but the next sphere so that the large changes in structure are more distributed and effect on the substrate-binding site is more subtle.

Site-directed mutagenesis experiments and a comparison of isoenzymes identified Phe345 and Phe296, but not Phe344, as important to the high enantioselectivity of CRL (lip1) toward 2-arylpropionic acids, but did not identify substitutions to increase the enantioselectvity of CRL (lip1) (Table 3). Site-directed mutagenesis indicates that Phe345 is essential for high enantioselectivity toward naproxen, a 2-arylpropionic acid, but that Phe344 is not essential. Substitution of Phe345 with valine decreased the enantioselectivity of CRL (lip1 isozyme, same as the one in this paper) from 32 to 2.6.[30] Substitution of Phe344 with valine had no significant effect on enantioselectivity. The enantioselectivity changes with ketoprofen, another 2-arylpropionic acid, were similar.[30] Comparison of the enantioselectivity of CRL isoenzymes[7] also indicates that Phe344 is not essential for enantioselectivity and further identifies Phe296 as essential for high enantioselectivity toward ibuprofen, also a 2-arylpropionic acid. Three lipase isoenzymes (lip1–3) have 80% of the amino acids identical, but two amino acids differ in the tunnel entrance region where the α-steroecenter of a carboxylic acid binds (Table 3). Isoenzymes lip1 and lip3 showed high enantioselectivity toward ibuprofen.[14] Since these isoenzymes differ at position 344 (Phe in lip1 *versus* Ile in lip3), the similar enantioselectivity indicates that this position is not essential for enantioselectivity. In contrast, lip2, which has a valine at 296 instead of phenylalanine in lip1 and lip3, has lower enantioselectivity toward ibuprofen ($E=15$). Isoenzyme lip2 also has a leucine at 344, but this is unlikely to affect enantioselectivity because valine or isoleucine at this position did not affect enantioselectivity.

Table 3. Effect of amino acid substitutions near the mouth of the tunnel on the enantioselectivity of CRL toward 2-arylpropionic acids. Substitutions in bold decrease the enantioselectivity strongly, while the other substitutions have little effect.

Isozyme	296	344	345	E	Refs.
lip1	Phe	Phe	Phe	>50; ibuprofen 32; naproxen	[14,30]
lip1 - Phe344Val	Phe	Val	Phe	29; naproxen	[30]
lip1 - Phe345Val	Phe	Phe	**Val**	2.6; naproxen	[30]
lip1 - Phe344,345Val	Phe	Val	**Val**	7.6; naproxen	[30]
lip2	**Val**	Leu	Phe	15; ibuprofen	[14]
lip3	Phe	Ile	Phe	>50; ibuprofen	[14]

Mutations in the lid region, which is far from the substrate binding site, had minor effects on enantioselectivity, most likely by altering the proportion of open and closed forms.[32] Researchers replaced the lid region (residues 66–93) in lip1 with the corresponding sequence in lip3 to create lip1lid3. This replacement introduced six changes in the amino acids sequence at positions 69, 74, 76, 88, 91, and 93. The changed amino acids do not contact the substrate and the closest one lies >15 Å from the phosphonate. Under some conditions, the enantioselectivity of lip1lid3 was slightly lower than the enantioselectivity of lip1 toward the 2-chloroethyl ester of 2-hydroxycaproic acid. The reaction was a transesterification with methanol in isooctane. The enantioselectivities were similar ($E=10$ for lip1, 8 for lip1lid3) with a water activity of 0.06, but differed slightly ($E=20$ for lip1, 13 for lip1lid3) at a water activity of 0.53. The authors suggested that catalysis occurs in the closed form of the lipase with low enantioselectivity and in the open form of the lipase with higher enantioselectivity. The substitutions on the lid alter the proportion of open and closed forms. These experiments do not help much in identifying key residues.

Mutations within the tunnel of a related lipase, lipase from *Geotrichum candidum*, which also contains a tunnel, could increase the enantioselectivity toward 2-methylalkanoic acids from $E=32$ to 54, a moderate increase.[33] These amino acids were far from the stereocenter and the molecular basis for this change is unknown.

Conclusions

In spite of these extensive and detailed studies of the enantioselectivity of CRL toward chiral α-substituted carboxylic acids, researchers still cannot predict which amino acid substitutions will increase enantioselectivity. The problem is difficult because all possible orientations of the slow enantiomer must be considered. In particular, the umbrella-like inversion orientation has not been previously considered, but the computer modeling in this paper suggests that the slow enantiomer can react *via* this orientation. The molecular dynamics showed that all four possible orientations of the slow enantiomer were stable conformations and

identified the ones most likely to react, thereby lowering the enantioselectivity. Extending this approach to test possible amino acid substitutions may enable rational design of more enantioselective lipases.

Experimental Section

General

Chemicals and lipase from *Candida rugosa* (L-1754) was purchased from Sigma Aldrich. FAP 15 lipase (*Rhizopus oryzae*) was purchased from Amano International Enzyme Co. (Troy, VA). ^{1}H NMR spectra were recorded in $CHCl_3$ at 200 MHz with $CHCl_3$ as an internal standard ($\delta = 7.26$). ^{13}C NMR spectra were recorded in $CHCl_3$ at 50 MHz with $CHCl_3$ as an internal standard ($\delta = 66.5$) and were proton decoupled. ^{31}P NMR spectra were recorded in $CHCl_3$ at 121 MHz with 85% phosphoric acid (0 ppm) as an external standard.

(±)-Dimethyl (1-Hydroxyphenylmethyl)phosphonate [(±)-2]

Following a literature procedure,[19] benzaldehyde (0.53 g, 0.51 mL, 5 mmol) and dimethyl phosphite (0.55 g, 0.46 mL, 5 mmol) were consecutively added to anhydrous potassium fluoride (25.8 mmol, 1.50 g). The reaction mixture was manually stirred until it thickened and then solidified within 5 min. Twenty-five mL of CH_2Cl_2 were added and the solid was extracted for 5 min. The suspension was filtered and the filtrate evaporated under vacuum to afford (±)-**2** as a white solid; yield: 0.95 g (4.39 mmol, 88%). ^{1}H NMR: $\delta = 7.51$–7.27 (m, 5H), 5.05 (d, $J_{H,P} = 11.$ 1 Hz), 4.68 (br s, 1H), 3.68 (d, 3H, $^3J_{H,P} = 10.5$ Hz), 3.66 (d, 3H, $^3J_{H,P} = 10.3$ Hz) [lit.[18]: ^{1}H NMR ($CDCl_3$, 400 MHz): $\delta = 7.50$–7.29 (m, 5H, C_6H_5), 5.05 (d, 1H, $J = 10.8$ Hz, PhCH), 4.11 (br s, 1H, OH), 3.70, 3.67 (2×d, 2×3H, $J = 10.3$ Hz, $P(OMe)_2$)]; ^{13}C NMR: $\delta =$ 136.5, 128.3 (d, $J = 2.0$ Hz), 128.1 (d, $J = 3.1$ Hz), 127.0 (d, $J = 6.0$ Hz), 70.5 (d, $^1J_{C,P} = 160$ Hz), 53.9 (d, $^2J_{C,P} = 7.1$ Hz), 53.6 (d, $^2J_{C,P}$ 7.3 Hz); ^{31}P NMR: $\delta = 24.3$ (s).

(±)-Dimethyl [1-(Methoxy)phenylmethyl]-phosphonate

(±)-**2** (1 g, 4.6 mmol), silver(I) oxide (2.14 g, 9.2 mmol), acetic acid (0.53 mL, 0.55 g, 9.2 mmol) and methyl iodide (15 mL, 241 mmol) were combined and stirred in the dark for 22 h. The reaction mixture was diluted with CH_2Cl_2, filtered, and washed with 50 mL water. The CH_2Cl_2 layer was separated, dried and filtered. Purification by flash chromatography using 5:1 CH_2Cl_2/EtOAc ($R_f = 0.32$) afforded the product; yield: 0.70 g (3.0 mmol, 66%). ^{1}H NMR: $\delta = 7.46$–7.36 (m, 5H), 4.56 (d, 1H, $^2J_{H,P} = 15.8$ Hz), 3.72 (d, 3H, $^3J_{H,P} = 9.0$ Hz), 3.67 (d, 3H, $^3J_{H,P} = 8.8$ Hz), 3.40 (s, 3H); ^{13}C NMR: $\delta = 133.9$, 128.4–128.2 (m), 127.7 (d, $J = 6.0$ Hz), 80.0 (d, $^1J_{C,P} = 168.9$ Hz), 58.4 (d, $^3J_{C,P} = 14.8$ Hz), 53.5 (d, $^2J_{C,P} = 7.0$ Hz), 53.3 (d, $^2J_{C,P} = 6.9$ Hz); ^{31}P NMR: $\delta = 21.9$ (s); MS (CI/NH_3): m/z (rel. intensity) = 231 (27, $M+H^+$), 121 (100).

(±)-Methyl [1-(Methoxy)phenylmethyl]phosphonic Acid

The above (±)-dimethyl [1-(methoxy)phenylmethyl]phosphonate (0.60 g, 2.6 mmol) was hydrolyzed to the mono acid by refluxing in aqueous sodium hydroxide (2.7 M) for 5 h. The solution was acidified to pH 1 with 1 N HCI and then extracted with CH_2Cl_2 (2×50 mL) and ether (2×50 mL). Further extractions with CH_2Cl_2 (2×50 mL) and EtOAc (1×50 mL) did not remove the majority of the product, so the water was evaporated off under reduced pressure and the residue was extracted with CH_2Cl_2 (3×50 mL). The combined organic extracts were dried with magnesium sulfate, filtered and evaporated under reduced pressure affording the mono acid; yield. 0.46 g 82.2 mmol, 85%): ^{1}H NMR. δ09.91 (br s, 1H), 7.40–7.31 (m, 5H), 4.42 (d, 1H, $^2J_{H,P} =$ 15.8 Hz), 3.60 (d, 3H, $^3J_{H;P} = 10.6$ Hz), 3.38 (s, 3H); ^{13}C NMR: $\delta = 134.0$, 128.2, 127.9 (d, $J = 5.2$ Hz), 79.8 (d, $^1J_{C,P}$ 171.0 Hz), 58.6 (d, $^3J_{C,P} = 14.2$ Hz), 53.1 (d, $^2J_{C,P} = 6.7$ Hz); ^{31}P NMR: $\delta = 23.3$ (s); MS (CI/NH_3): m/z (rel. intensity) = 217 (16, $M+H^+$), 121 (100).

(±)-Methyl [1-(Methoxy)phenylmethyl]phosphono-chloridate [(±)-3]

Oxalyl chloride (0.80 g, 0.55 mL, 6.3 mmol) was added to a solution of (±)-methyl [1-(methoxy)phenylmethyllphosphonic acid (0.0136 g, 0.063 mmol) in dichloromethane (13 mL) and the mixture was refluxed for 18.5 h under N_2. Evaporation of the solvent under reduced pressure yielded (±)-3 as a mixture of diastereomers of the phosphonochloridate (yield: 70%) and pyrophosphonate derivatives [yield: 30%, ^{31}P NMR: $\delta = 13.3$ (app t)] as determined by ^{31}P NMR. ^{1}H NMR: $\delta = 7.51$–7.39 (in, 5H), 4.74 (d, 1H, $^2J_{H,P} =$ 11.4 Hz), 3.87 (d, 3H, $^3J_{H,P} = 12.8$ Hz), 3.86 (d, 3H, $^3J_{H,P} =$ 12.8 Hz), 3.49 (s, 3H); ^{31}P NMR: $\delta = 36.7$ (s), 36.6 (s).

(±)-Methyl *p*-Nitrophenyl[1-(methoxy)phenylmethyl]-phosphonate [(±)-4]

Oxalyl chloride (78 μL, 0.113 g, 0.89 mmol) was added to a solution of (±)-methyl [1-(methoxy)phenylmethyl]phosphonic acid (0.128 g, 0.59 mmol) in dichloromethane (7 mL) and the mixture was refluxed for 14 h under N_2. The solvent and excess oxalyl chloride were removed under reduced pressure and the chlorophosphonate was redissolved in dichloromethane (7 mL). *p*-Nitrophenol (0.092 g, 0.65 mmol) was added followed by triethylamine (91 μL, 0.066 g, 0.65 mmol) and the mixture was stirred overnight under N_2. The mixture was purified by column chromatography using 20:1 CH_2Cl_2/EtOAc ($R_f = 0.17$) to afford a 1:1 mixture of diastereomers (±)-**4**; overall yield: 0.040 g (1.2 mmol, 20%). ^{1}H NMR: $\delta = 8.17$ (d, 2H, $^3J = 9.2$ Hz), 7.52–7.34 (m, 5H), 7.24 (d, 2H, $^3J = 9.4$ Hz), 4.74 (d, 1H, $^2J_{H,P} = 15.4$ Hz), 4.72 (d, 1H, $^2J_{H,P} = 15.0$ Hz), 3.84 (d, 3H, $^3J_{H,P} = 11.0$ Hz), 3.77 (d, 3H, $^3J_{H,P} = 11.0$ Hz), 3.43 (s, 3H); ^{31}P NMR: $\delta = 17.8$ (s); MS (CI/NH_3): m/z (rel. intensity) = 338 (4.6, $M+H^+$), 121 (100).

(±)-Dimethyl [1-(Acetyloxy)phenylmethyl]-phosphonate [(±)-5]

(±)-**2** (0.200 g, 0.92 mmol), K_2CO_3 (0.26 g, 1.9 mmol), *N*,*N*-dimethylaminopyridine (6 mg, 0.05 mmol) and acetic anhydride (0.130 mL, 1.4 mmol) were added to ethyl acetate (20 mL) and the mixture was stirred at room temperature overnight. The mixture was filtered to remove K_2CO_3, and the filtrate was washed with water (1×20 mL). The water layer was extracted with EtOAc (2×25 mL), and the combined organic extracts were dried with magnesium sulfate. Evaporation of the solvent under vacuum afforded a clear oil; yield: 0. 19 g (0.75 mmol, 81%). ^{1}H NMR: δ = 7.51–7.33 (m, 5H), 6.17 (d, 1H, $^2J_{H,P}$ = 13.5 Hz), 3.73 (d, 3H, $^3J_{H,P}$ = 10.7 Hz), 3.65 (d, 3H, $^3J_{H,P}$ = 10.6 Hz), 2.19 (s, 3H) [lit.[20]: ^{1}H NMR ($CDCl_3$, 400 MHz): δ = 7.50–7.32 (m, 5H, C_6H_5), 6.17 (d, 1H, *J* = 13.3 Hz, PhCH), 3.72, 3.65 (2×d, 2×3H, *J* = 10.3 Hz, $P(OMe)_2$), 2.18 (3H, s, MeCO).]

Kinetic Resolution of (±)-Dimethyl [1-(Acetyloxy)-phenylmethyl]phosphonate [(±)-5]

(±)-**5** (2.8 g, 10.8 mmol) was added to an Erlenmeyer flask (500 mL) followed by a 3/1 mixture of hexanes/*tert*-butyl methyl ether (20 mL) and phosphate buffer (10 mM, pH 7.00, 100 mL). Lipase F-AP 15 (509 mg), dissolved in phosphate buffer (50 mM, pH 7.00, 60 mL) and adjusted to pH 7.00, was added to the phosphonate mixture. The pH was maintained at 7.00 with 0.50 N NaOH by automatic titration using a pH stat. The reaction was stopped at 43.8% conversion by acidifying the reaction mixture to pH 4 with 1 N HCl. The mixture was extracted with CH_2Cl_2 (1× 100 mL), EtOAc (1×50 mL) and again with CH_2Cl_2 (1× 100 mL). The combined organic extracts were filtered through a pad of diatomaceous earth. The aqueous layer was also filtered through a pad of diatomaceous earth and the filtrate was further extracted with CH_2Cl_2 (1×100 mL). The organic extracts were combined, dried with $MgSO_4$, filtered and the solvent evaporated under reduced pressure. The remaining starting material acetate and product alcohol were separated by flash chromatography using 5:1 CH_2Cl_2/EtOAc to elute the acetate (*R*)-**5** [yield: 1.22 g, 4.7 mmol, 78% recovery, 68% *ee* by Eu(hfc)$_3$ chiral shift reagent] and then 100% EtOAc to elute the product alcohol (*S*)-**2** [yield: 0.66 g, 3.1 mmol, 65% recovery, 88% *ee* by Eu(hfc)$_3$ chiral shift reagent following reacetylation].

To increase the enantiomeric purity of the product alcohol, (*S*)-**2**, a sample was resolved a second time. (*S*)-**2** (0.504 g, 2.3 mmol, 88% *ee*) was reacetylated with acetic anhydride (0.357 g, 0.330 mL, 3.5 mmol) and K_2CO_3 (0.650 g, 4.7 mmol) using *N*,*N*-4-dimethylaminopyridine (0.0156 g) as catalyst in EtOAc (20 mL). The reaction mixture was filtered, washed with dd H_2O (50 mL), dried with $MgSO_4$ and the solvent evaporated under reduced pressure to afford (*S*)-**5**; yield: 0.54 g (2.1 mmol, 90%). A sample of (*S*)-**5** (0.49 g, 1.9 mmol, 88% *ee*) was dissolved with 3/1 hexanes/*tert*-butyl methyl ether (10 mL) and added to phosphate buffer (50 mM, pH 7.0, 100 mL). Lipase FAP-15 [220 mg dissolved in phosphate buffer (50 mM, pH 7.00, 50 mL)] was added and the pH was maintained at 7.00 with 0.50 N NaOH by automatic titration using a pH stat. The reaction was stopped at 46% conversion by acidifying the reaction mixture to pH 3.9 with 1 N HCl. The reaction mixture was filtered through a pad of diatomaceous earth. The filtrate was extracted with CH_2Cl_2 (3×100 mL). A small portion of emulsion which remained throughout the extractions was separately filtered through a small pad of diatomaceous earth and washed with CH_2Cl_2. The filtrate of this filtered emulsion was combined with the original CH_2Cl_2 extracts. The starting material was separated from the product alcohol by column chromatography using 5:1 CH_2Cl_2/EtOAc in order to elute the remaining substrate, (*S*)-**5** (0.233 g, 0.90 mmol, 88% recovery), then 100% EtOAc to elute the product alcohol, (*S*)-**2** [0.112 g, 0.52 mmol, 59% recovery, >98% *ee* by Eu(hfc)$_3$ chiral shift reagent following reacetylation].

To increase the enantiomeric purity of the acetate, (*R*)-**5**, a sample (1.00 g, 3.9 mmol, 68% *ee*) was resolved a second time. The sample was mixed with 3/1 hexanes/*tert*-butyl methyl ether (20 mL) and phosphate buffer (50 mM, pH 7.00, 130 mL). Lipase FAP 15 (505 mg dissolved in phosphate buffer, 50 mM, pH 7.00, 50 mL) and adjusted to pH 7.00, was added and the pH was maintained at 7.00 with 0.50 N NaOH by automatic titration using a pH stat. The reaction was stopped after 16.5% conversion by adjusting the reaction mixture to pH 4 using 1 N HCl. The top organic layer was separated. The aqueous layer was filtered through a pad of diatomaceous earth and extracted with CH_2Cl_2 (3× 100 mL). The original organic layer from the enzyme reaction and the combined CH_2Cl_2 extracts were filtered through a fresh pad of diatomaceous earth and dried with $MgSO_4$. The acetate was purified by flash chromatography using 5:1 CH_2Cl_2/EtOAc to afford enantiomerically enriched (*R*)-**5** [0.75 g, 2.9 mmol, 90% recovery based on the pH stat percent conversion, 92.7% *ee* by Eu(hfc)$_3$ chiral shift reagent]. A sample of this material (0.5 g, 1.9 mmol) was hydrolyzed for an additional 10.3% conversion in the same manner to afford (*R*)-**5** [0.40 g, 1.6 mmol, >98% *ee* by Eu(hfc)$_3$ chiral shift reagent].

(*R*)-Dimethyl [1-(Methoxy)phenylmethyl]-phosphonate

(*R*)-**5** (0.34 g, 1.33 mmol) was reacted with dry MeOH (15 mL) and freshly distilled triethylamine (2 mL) for 18.5 h at room temperature. The solvent and amine were removed under reduced pressure and finally under high vacuum. To this crude product was added Ag_2O (0.62 g, 2.7 mmol), MeI (15 mL) and acetic acid (0. 160 g, 0. 152 mL, 2.7 mmol) and the mixture was stirred in the dark overnight. The methyl iodide was then evaporated off with a stream of air. The product was redissolved in CH_2Cl_2, filtered, concentrated under reduced pressure, and purified by flash chromatography using 5:1 CH_2Cl_2/EtOAc to afford (*R*)-**2**; overall yield: 0.157 g (0.68 mmol, 50%). The ^{1}H NMR spectrum was identical to that of the racemic standard.

(R_C,R_P,S_P)-Methyl [1-(Methoxy)phenylmethyl]-phosphonic Acid

The above (*R*)-dimethyl [1-(methoxy)phenylmethyl]phosphonate (0.047 g, 0.21 mmol) was refluxed in freshly distilled acetone with NaI (0.046 g, 0.31 mmol) for 22 h. The fine product salt was filtered and rinsed with absolute ethyl ether. The salt was dissolved in water, acidified to pH 1 and

the water was evaporated off under reduced pressure. The residue was extracted with dichloromethane (25 mL), dried with $MgSO_4$, filtered and the solvent removed under reduced pressure to afford the monoacid; yield: 0.036 g (0.17 mmol, 81.3%). The ^{1}H NMR spectrum was identical to that of the racemic standard.

(R_C,$R_P$$S_P$)-Methyl [1-(Methoxy)phenylmethyl]-phosphonochloridate [(R_C,$R_P$$S_P$)-3]

Oxalyl chloride (1.59 g, 1.09 mL, 12.5 mmol) was added to a solution of (*R*)-methyl [1-(methoxy)phenylmethyl]phosphonic acid (0.027 g, 0.125 mmol) in dichloromethane (15 mL) and the mixture was refluxed for 18.5 h under N_2. Evaporation of the solvent under reduced pressure yielded (R_C,$R_P$$S_P$)-**3** as a mixture of diastereomers according to ^{31}P NMR. The ^{1}H NMR spectrum was identical to that of the racemic standard.

(*S*)-Dimethyl [l-(Methoxy)phenylmethyl]phosphonate

To (*S*)-**2** (0.108 g, 0.50 mmol, >98% *ee*) were added Ag_2O (0.232 g, 1.0 mmol), MeI (10 mL) and acetic acid (0.060 g, 0.057 mL, 1.0 mmol). The mixture was stirred in the dark for 24 h. The MeI was then evaporated off with a stream of air. The product was redissolved in CH_2Cl_2, filtered and concentrated under reduced pressure. The product was purified by flash chromatography using 5/1 CH_2Cl_2/EtOAc to afford (*S*)-dimethyl [l-(methoxy)phenylmethyl]phosphonate; yield: 0.058 g (0.25 mmol, 50%). This compound had an identical ^{1}H NMR spectrum to the racemic standard.

(S_C,R_P,S_P)-Methyl [1-(methoxy)phenylmethyl]phosphonic acid was made starting with (*S*)-dimethyl [1-(methoxy)phenylmethyl]phosphonate and subsequently converted to (S_C,R_P,S_P)-methyl [1-(methoxy)phenylmethyl]phosphonochloridate using the same reaction conditions as described above to prpeare the corresponding diastereomers that mimic the slow-reacting enantiomer of **1**.

Inactivation of Purified CRL using (±)-3

An aqueous solution of purified CRL (0.55 mg, 0.0092 μmol in MES buffer, 10 mM, pH 6, 1 mL) was added to a dichloromethane solution of freshly synthesized chlorophosphonate, (±)-**3** (9.2 μmol in 1 mL) and vigorously stirred for eight minutes. The aqueous phase was removed, centrifuged for 1 min and tested for activity using the enzyme assay described below.

Enzyme Assay

An aliquot (5 μL) of enzyme solution followed by an aliquot of *p*-nitrophenyl acetate (5 μL of a 50 mM solution in acetonitrile) were added to phosphate buffer (1.0 mL, pH 7.5, 10 mM) at 25 °C. The initial rate of formation of *p*-nitrophenolate was monitored at 404 nm for 30 s. An extinction coefficient of 11600 $M^{-1}cm^{-1}$, which accounts for the incomplete ionization of *p*-nitrophenolate at pH 7.5 was used to calculate activity. Crude CRL showed 30 U/g solid (1 U/mg protein) with this assay. U = 1 μmol of ester hydrolyzed per minute.

X-ray Crystal Structure

The covalent enzyme-inhibitor complex was prepared by adding the inhibitor dissolved in 2-methyl-2,4-pentanediol (MPD) to the protein solution. The inhibited protein was crystallized under conditions similar to those used for native protein.[9] The crystals are isomorphous with the native crystals of CRL in the open form, Table 1. Diffraction data were collected at 23 °C on an R-AXIS II image plate area detector and all refinements were done with CNS[34] and all modeling was done using O[35] and COOT.[36] Coordinates were deposited with the Protein Data Bank (www.pdb.org) and have the code 3RAR.

Molecular Modeling

Hydrogen atoms were added to the CRL-phosphonate X-ray crystal structure using the software Maestro (Schrödinger, Portland OR; www.schrodinger.com) to correspond to a pH of 7.0, except for the catalytic histidine, which was protonated. The sugars attached to CRL and the bound calcium ions in the crystal structures were included in the simulation. Water molecules far from heteroatoms (>5 Å) were removed. The geometry was optimized using the program Macromodel v. 9.0 (Schrödinger) using the OPLS 2005 force field[37] until an rmsd (root mean square deviation) of <0.3 Å was reached. Atomic partial charges were calculated using the bond increment method.[38] To model the tetrahedral intermediate for hydrolysis of (*S*)-**1**, the phosphorus atom was replaced by a carbon atom, the oxygen corresponding to the oxyanion was assigned a formal negative charge, and the geometry of the structure was optimized to an rmsd of <0.05 Å. To model the four different conformations of the tetrahedral intermediate for hydrolysis of (*R*)-**1**, the substituents at the stereocenter were exchanged as indicated in Figure 1 and the umbrella structure was generated by moving the hydrogen atom to form the (*R*) enantiomer without moving the other functional groups. Each conformation was modeled independently and was geometry optimized to an rmsd of <0.05 Å. Molecular dynamics simulations used the software Desmond (D.E. Shaw Research, New York, NY). The protein surrounded by 33885 water molecules (TIP3P model[39]) to create a box sized 109 Å × 109 Å × 95 Å. Seventeen sodium ions were added to neutralize the negative charge of the protein. The charge of −17 was verified using PROPKA 3.1,[40] which predicted a −17.5 charge at pH 7. This negative charge is about twice a large as that for a typical protein because CRL is about twice the size as a typical protein: 62 kDa versus 30 kDa for a typical protein. Sixty-two additional sodium and chloride ions were added to correspond to an ionic strength of 0.10 M. The system was equilibrated to 300 K and 1 atm pressure by using Berendsen thermostat and barstat method[41] in six separate stages. First, the solvent only was minimized; next the solvent and protein were minimized. Stage 3 was a short MD simulation (12 ps, velocity resampling every 1 ps) at constant volume, moles and temperature (10 K), while stage 4 was a short MD simulation (12 ps, velocity resampling every 1 ps) at constant pressure (1 atm), moles and temperature (10 K). Stage 5 was a slightly longer MD simulation (24 ps) where the temperature is increased to 300 K and the non-hydrogen atoms of the protein were fixed, while stage 6 was an MD simulation (24 ps) at 300 K, 1 atm with all atoms

free to move. The molecular dynamics simulation was for 1.2 ns with a step time of 1 fs and recorded every 4.8 ps yielding 250 structures. Long-range electrostatic interactions were calculated with particle mesh Ewald method and cut off at 15 Å, while the Lennard–Jones interactions were cut off at 9.0 Å. The root mean square deviations of the structures during the MD simulation were no more than 2 Å, (see Supporting Information, Figure S5. The four catalytically essential hydrogen bonds, His449 to SerOγ and ester oxygen, the two hydrogen bonds to the oxyanion, and the catalytically non-productive hydrogen bond His449 to Glu208 were deemed present if the N−O distance was <3.5 Å and the N−H−O angle was $>120°$. A catalytically productive conformation was one that contained all four catalytically essential hydrogen bonds and did not contain the non-productive hydrogen bond. Table 2 lists the fraction of catalytically productive conformation out of the 250 total conformations.

Acknowledgements

We thank the Natural Sciences and Engineering Research Council of Canada for funding, the Minnesota Supercomputing Institute for access to computer modeling hardware and software, and Dr. Peter Bernhardt for initial molecular modeling.

References

[1] D. R. Feller, V. S. Kamanna, H. A. I. Newman, K. J. Romstedt, D. T. Witiak, G. Bettoni, S. H. Bryant, D. Conte-Camerino, F. Loiodice, V. Tortorella, *J. Med. Chem.* **1987**, *30*, 1265–1267.

[2] G. Bettoni, F. Loiodice, V. Tortorelia, D. Conte-Camerino, M. Mambri, E. Ferrannini, S. H. Bryant, *J. Med. Chem.* **1987**, *30*, 1267–1270.

[3] S. N. Ahmed, R. J. Kazlauskas, A. H. Morinville, P. Grochulski, J. D. Schrag, M. Cygler, *Biocatalysis* **1994**, *9*, 209–225.

[4] S.-H. Wu, *PhD thesis*, University of Wisconsin, Madison, USA, **1987**, p 120.

[5] S. K. Latypov, J. M. Seco, E. Quiñoá, R. Riguera, *J. Org. Chem.* **1995**, *60*, 1538–1545; S. K. Latypov, J. M. Seco, E. Quiñoá, R. Riguera, *J. Am. Chem. Soc.* **1998**, *120*, 877–882.

[6] T. Miyazawa, S. Kurita, M. Shimaoka, S. Ueji, T. Yamada, *Chirality* **1999**, *11*, 554–560.

[7] Review: P. D. de Maria, J. M. Sanchez-Montero, J. V. Sinisterra, A. R. Alcantara, *Biotechnol. Adv.* **2006**, *24*, 178–194.

[8] J. J. Lalonde, C. Govardhan, N. Khalaf, A. G. Martinez, K. Visuri, A. L. Margolin, *J. Am. Chem. Soc.* **1995**, *117*, 6845–6852.

[9] P. Grochulski, Y. Li, J. D. Schrag, F. Bouthillier, P. Smith, D. Harrison, B. Rubin, M. Cygler, *J. Biol. Chem.* **1993**, *268*, 12843–12847.

[10] P. Grochulski, Y. Li, J. D. Schrag, M. Cygler, *Protein Sci.* **1994**, *3*, 82–91; P. Grochulski, F. Bouthillier, R. J. Kazlauskas, A. N. Serreqi, J. D. Schrag, E. Ziomek, M. Cygler, *Biochemistry* **1994**, *33*, 3494–3500.

[11] J. M. Mancheño, M. A. Pernas, M. J. Martínez, B. Ochoa, M. L. Rúa, J. A. Hermoso, *J. Mol. Biol.* **2003**, *332*, 1059–1069.

[12] D. Ghosh, Z. Wawrzak, V. Z. Pletnev, N. Li, R. Kaiser, W. Pangborn, H. Jörnvall, M. Erman, W. L. Duax, *Structure* **1995**, *3*, 279–288; V. Pletnev, A. Addlagatta, Z. Wawrzak, W. Duax, *Acta Crystallogr. D: Biol. Crystallogr.* **2003**, *59*, 50–56.

[13] K. Lundell, T. Raijola, L. T. Kanerva, *Enzyme Microb. Technol.* **1998**, *22*, 86–93.

[14] N. López, M. A. Pernas, L. M. Pastrana, A. Sánchez, F. Valero, M. L. Rúa, *Biotechnol. Prog.* **2004**, *20*, 65–73.

[15] S. H. Wu, Z. W. Guo, C. J. Sih, *J. Am. Chem. Soc.* **1990**, *112*, 1990–1995.

[16] I. J. Colton, S. N. Ahmed, R. J. Kazlauskas, *J. Org. Chem.* **1995**, *60*, 212–217.

[17] K. Nishizawa, Y. Ohgami, N. Matsuo, H. Kisida, H. Hirohara, *J. Chem. Soc. Perkin Trans. 2* **1997**, 1293–1298.

[18] F. Texier-Boullet, A. Foucaud, *Synthesis* **1982**, 165–166.

[19] M. S. Kharasch, R. A. Mosher, I. S. Bengelsdorf, *J. Org. Chem.* **1960**, *25*, 1000–1006.

[20] Y.-F. Li, F. Hammerschmidt, *Tetrahedron: Asymmetry* **1993**, *4*, 109–120.

[21] A. Mezzetti, J. D. Schrag, C. S. Cheong, R. J. Kazlauskas, *Chem. Biol.* **2005**, *12*, 427–437.

[22] S. Hur, T. C. Bruice, *Proc. Natl. Acad. Sci. USA* **2003**, *100*, 12015–12020.

[23] D. F. Sticke, L. G. Presta, K. A. Dill, G. D. Rose, *J. Mol. Biol.* **1992**, *226*, 1143–1159.

[24] M. Botta, E. Cernia, F. Corelli, F. Manetti, S. Soro, *Biochim. Biophys. Acta* **1997**, *1337*, 302–310.

[25] F. Manetti, D. Mileto, F. Corelli, S. Soro, C. Palocci, E. Cernia, I. D′Acquarica, M. Lotti, L. Alberghina, M. Botta, *Biochim. Biophys. Acta* **2000**, *1543*, 146–158.

[26] S. Mittal, S. Khanna, A. Roy, P. V. Bharatam, H. P. S. Chawla, *Enzyme Microb. Technol.* **2005**, *36*, 232–238.

[27] K. Watanabe, T. Uno, T. Koshiba, T. Okamoto, Y. Ebara, S. Ueji, *Bull. Chem. Soc. Jpn.* **2004**, *77*, 543–548.

[28] A. C. Sehgal, R. M. Kelly, *J. Am. Chem. Soc.* **2002**, *124*, 8190–8191.

[29] M. Holmquist, F. Haeffner, T. Norin, K. Hult, *Protein Sci.* **1996**, *5*, 83–88.

[30] P. Berglund, M. Holmquist, K. Hult, H. E. Högberg, *Biotechnol. Lett.* **1995**, *17*, 55–60.

[31] P. Berglund, M. Holmquist, K. Hult, *J. Mol. Catal. B: Enzym.* **1998**, *5*, 283–287.

[32] F. Secundo, G. Carrea, C. Tarabiono, P. Gatti-Lafranconi, S. Brocca, M. Lotti, K.-E. Jaeger, M. Puls, T. Eggert, *J. Mol. Catal. B: Enzym.* **2006**, *39*, 166–170.

[33] M. Holmquist, P. Berglund, *Org. Lett.* **1999**, *1*, 763–765.

[34] A. T. Brünger, P. D. Adams, G. M. Clore, W. L. DeLano, P. Gros, R. W. Grosse-Kunstleve, J.-S. Jiang, J. Kuszewski, M. Nilges, N. S. Pannu, R. J. Read, L. M. Rice, T. Simonson, G. L. Warren, *Acta Crystallogr. D: Biol. Crystallogr.* **1998**, *54*, 905–921.

[35] T. A. Jones, J.-Y. Zou, S. W. Cowan, *Acta Crystallogr. A: Crys.* **1991**, *47*, 110–119.

[36] P. Emsley, B. Lohkamp, W. G. Scott, K. Cowtan, *Acta Crystallogr. D: Biol. Crystallogr.* **2010**, *66*, 486–501.

[37] G. A. Kaminski, R. A. Friesner, J. Tirado-Rives, W. L. Jorgensen, *J. Phys. Chem. B* **2001**, *105*, 6474–6487.
[38] J. R. Maple, M. J. Hwang, T. P. Stockfisch, U. Dinur, M. Waldman, G. S. Ewig, A. T. Hagler, *J. Comput. Chem.* **1994**, *15*, 162–182.
[39] W. L. Jorgensen, J. Chandrasekhar, J. D. Madura, R. W. Impey, M. L. Klein, *J. Chem. Phys.* **1983**, *79*, 926–935.
[40] M. Rostkowski, M. H. M. Olsson, C. R. Søndergaard, J. H. Jensen, *BMC Struct. Biol.* **2011**, *11*, 6.
[41] H. J. C. Berendsen, J. P. M. Postma, W. F. van Gunsteren, A. Dinola, J. R. Haak, *J. Chem. Phys.* **1984**, *81*, 3684–3690.

Supporting information

Molecular basis of chiral acid recognition by Candida rugosa lipase. X-Ray structure of transition state analog and modeling of the hydrolysis of methyl 2-methoxy-2-phenylacetate.

Ian J. Colton, DeLu(Tyler) Yin, Pawel Grochulski*, Romas J. Kazlauskas*

Contents

MD trajectories of catalytically essential hydrogen bonds for (S)-1 and the four (R)-1 orientations

Molecular dynamics simulates the multiple conformations possible for each orientation of the transition state analog. Here we measure which of these conformations contains all four catalytically essential hydrogen bonds between the transition state analog and the enzyme. The reasoning is that orientations that allow formation of the catalytically essential hydrogen bonds are reactive conformations, while orientations that lack these hydrogen bonds do not react.

The first two catalytically essential hydrogen bonds are between the oxyanion oxygen of the transition state analog and two main chain N–H from the enzyme (Ala124, Gly210), Figure S1. The (S)-1 orientation and three of the four (R)-orientations contain these two hydrogen bonds most of the time. The (R)-exchange H/Ph is missing one of the hydrogen bond (to Ala124) most of the time since the O–N distance is >3.55 Å most of the time. Hydrogen bond angles (N-H-O) are >120° (180° is ideal) all the time. (Data not shown.)

The next two hydrogen bonds are between His449-Ne and Ser209-O? and methyl ester oxygen, Figure S2. For (S)-1, the distance for both pairs of atoms are less than 3.55 Å most of the time. However, for all four (R)-1 orientations, one or both hydrogen bond distances are >3.55 Å and are therefore missing. The bond angles (N-H-O) for these hydrogen bonds correspond to an angle that is <120° when the distances are >3.55 Å. However, bond angles >120° do not always correspond to bond distances <3.55 Å, therefore both angle and distance had to be measured to determine whether a hydrogen bond is present, Figure S3.

The results of Figures S1, S2, and S3 are summarized in Table 1 of the main text.

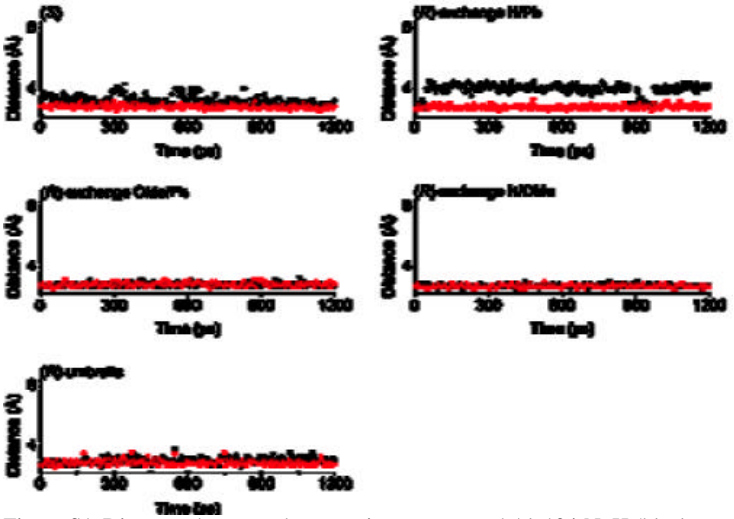

Figure S1. Distances between the oxyanion oxygen and Ala124-N–H (black squares) and between the oxyanion oxygen and Gly210 N–H (red circles) over the course of the molecular dynamics simulation (250 structures). Distances <3.55 Å indicate a hydrogen bond.

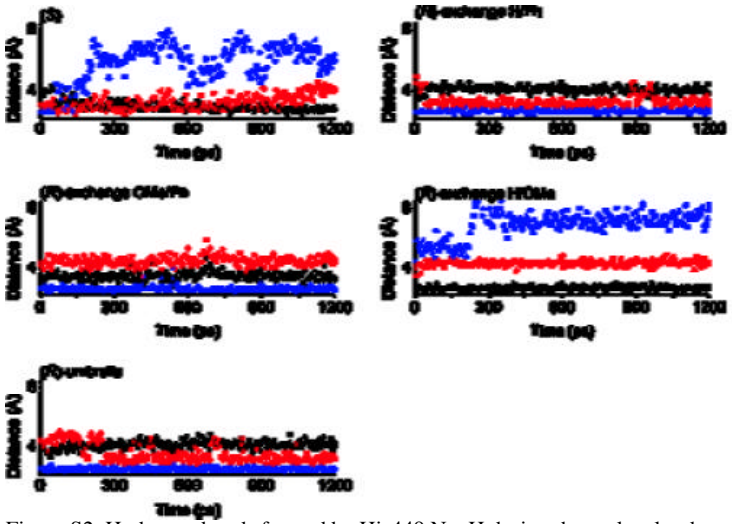

Figure S2. Hydrogen bonds formed by His449 Ne–H during the molecular dynamics simulation (250 structures). The distance to Ser209-O? (black squares) and the substrate's methyl ester oxygen (red circles) identify catalytically essential hydrogen bonds, while the distance to Glu208-Oe (blue triangles) identifies a catalytically nonproductive hydrogen bond. Distances <3.55 Å indicate a hydrogen bond. The fast reacting enantiomer (S)-1 forms the two catalytically productive hydrogen bonds, but not the catalytically nonproductive hydrogen bond. In contrast, the different orientations of (R)-1 break at least one of the catalytically productive hydrogen bonds and usually replace it with the catalytically nonproductive hydrogen bond.

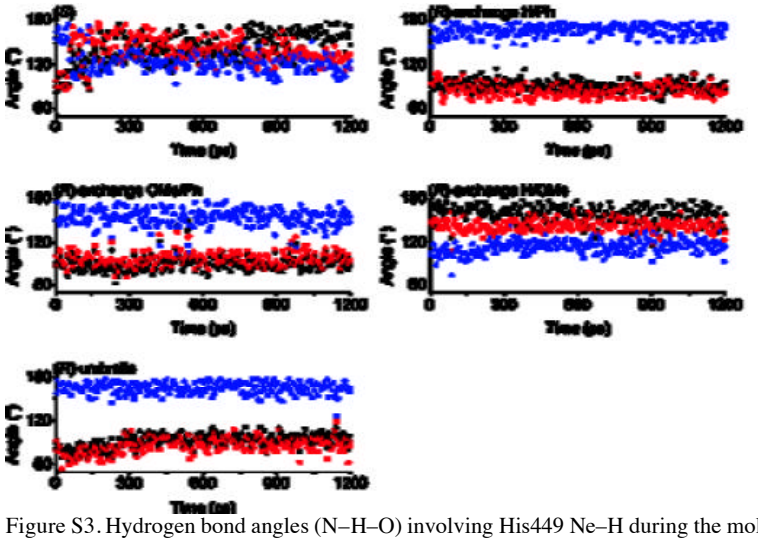

Figure S3. Hydrogen bond angles (N–H–O) involving His449 Ne–H during the molecular dynamics simulation (250 structures). The angle to Ser209-O? (red circles) and the substrate's ester oxygen (black squares) identify catalytically essential hydrogen bonds, while the angle to Glu208 Oe (blue triangles) identifies a catalytically nonproductive hydrogen bond. Angles >120° (180° is ideal) indicate a hydrogen bond. The fast reacting enantiomer (S)-1 forms the two catalytically productive hydrogen bonds, but not the catalytically nonproductive hydrogen bond. Although the angles for the catalytically nonproductive hydrogen bond are often in the acceptable range, Figure S2 above shows that the distances are too long to be a hydrogen bond. In contrast, the different orientations of (R)-1 break at least one of the catalytically productive hydrogen bonds and usually replace it with the catalytically nonproductive hydrogen bond. The (R)-exchange H/OMe orientation has suitable bond angles to make hydrogen bonds, but Figure S2 above shows that distance for one of them (to the substrate's ester oxygen) is too long to form a hydrogen bond.

MD trajectories of new, nonproductive hydrogen bonds for the (R)-exchange H/OMe orientation

In some orientations, new, catalytically nonproductive hydrogen bonds formed. The most common nonproductive hydrogen bond was between His449-Ne and MeO at the stereocenter found in 5.2% of the structures and between methyl ester oxygen to the main-chain amide of Gly123 found in 31% of the structures. The results of Figure S4 are summarized in the results section of the main manuscript.
With the exception of (R)-exchange H/Ph, the His449-Ne makes a new hydrogen bond with Glu208-Oe instead of the methyl ester oxygen.

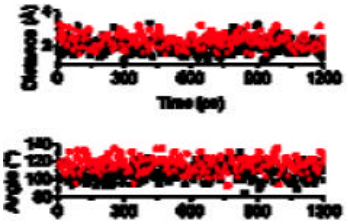

Figure S4. Catalytically nonproductive hydrogen bond distances and angles during the molecular dynamics simulation (250 structures) of the (R)-exchange H/OMe conformation. The distance from His449 Ne to MeO (square) and the hydrogen bond angle from N-H-O (square) occur 5.2% of the time to form a catalytically nonproductive hydrogen bond. The distance from Gly123 main-chain amide to the methyl ester oxygen (circle) and the hydrogen bond angle from N-H-O (circle) occur 31% of the time to form a catalytically nonproductive hydrogen bond.

Quality of the molecular dynamics simulations

To gauge the quality of the molecular dynamics simulations, we measured the deviation of the structures from their initial position during the simulation. The root mean square deviation (R.M.S.D) of the protein backbone initially increased from its initial state during the molecular dynamics simulation as the protein found a stable group of conformations, Figure S5. The CRL structure with the (S)-enantiomer reached a constant deviation within 200 ps, while the structures with the (R)-enantiomer required up to 800 ps. This difference is consistent with the notion that the (R)-enantiomer fits poorly in the active site and requires a longer time to find a stable set of conformations. After this initial adjustment, the protein backbone fluctuated no more than 2 Å from the starting structure in all five MD simulations. This low value indicates that the structures are stable and retain their protein fold.

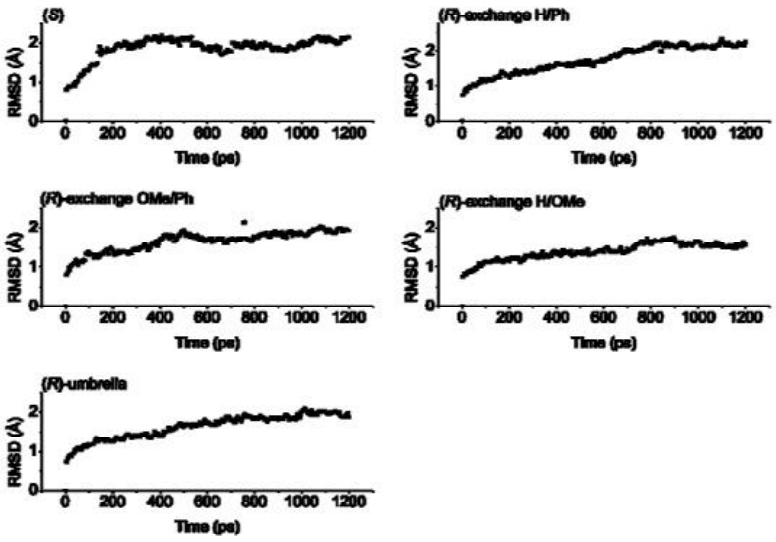

Figure S5. Root-mean-square deviation of the protein backbone for (S) and (R)-exchange structures during the molecular dynamics simulation. The stabilization of the R.M.S.D. values in the first 200-800 ps shows that structures have equilibrated and the small values of R.M.S.D. after equilibration show that the structures are stable and retain their initial protein fold. The structure (frame = 0) before the simulation starts is the reference structure.